Department of Electronic & Electrical Engineering

Investigation and Optimisation of Pulsed 405 nm LEDs and their use in a Blended Environmental Decontamination System.

A thesis presented in fulfillment of the requirement for the degree of

Doctor of Philosophy

Jonathan Bernard Gillespie (MEng)

2020

Department of Electronic & Electrical Engineering

University of Strathclyde

Glasgow, UK

DECLARATION OF ORIGINALITY

This thesis is the result of the author's original research. It has been composed by the author and has not been previously submitted for examination, which has led to the award of a degree.

Signed: 

Date: 29th July 2020

ACKNOWLEDGEMENTS

I would first and foremost like to thank my primary supervisor Dr Michelle Maclean who provided endless time, support and motivation throughout my PhD. I would also like to acknowledge other supervisory academics, Dr Martin Judd and Dr Martin Given for their support and assistance. I would furthermore like to thank Professor John Anderson and Dr Mark Wilson who provided much time and assistance throughout my research.

I would also like to thank Frank Cox for his time, assistance and expertise and further thanks goes to the workshop technicians for their assistance. Additional thanks go to Maureen Cooper for all of her administrative help.

I would like to acknowledge the Engineering and Physical Sciences Research Council (EPSRC) for their support through a Doctoral Training Grant (EP/L505080/1; EP/K503174/1) allowing me to undertake my PhD.

My PhD tenure was undoubtedly made by the students I studied with. A big thanks to my good friends Rach, Sian, Dan, Karen, Michael, Burhan, Caron, Laura and Justine – who provided many a required distraction and brightened my days in university.

I'd finally like to thank my parents – Pat and Johnny – and my two sisters – Sarah and Emma – for their continual love, patience and support throughout my PhD research.

ABSTRACT

With the rise in strains of antibiotic resistant bacteria, and with that, the rising rates of hospital infection, there is a drive for new antimicrobial infection control technologies. One such technology is the use of narrow spectrum light with a central wavelength in the region of 405 nm – henceforth referred to as '405 nm light' - which has been developed for continuous environmental decontamination applications. This study investigates the use of this pulsed 405 nm light, to evaluate potential operational advantages that this delivery method may provide when compared with continuous 405 nm light.

The initial part of the study investigates the fundamental effects of pulsed operation of light emitting diodes (LEDs), by altering a range of parameters including the frequency of the pulsing, the peak irradiance, the duty cycle and the exposure time, and the resulting effects on the antimicrobial action. Results using pulsed 405 nm light demonstrated more efficient bacterial inactivation, yielding a higher electrical energy efficiency and optical efficiency, suggesting beneficial results in using pulsed 405 nm light over continuous 405 nm light.

The study then investigates, more specifically, the application of pulsed 405 nm light to the area of continuous environmental decontamination. The study documents the design, build and testing of a prototype blended pulsed antimicrobial white light based on pulsed 405 nm LEDs – supplemented by red, green and yellow/amber wavelengths to produce the blended white light. The pulsed blended white light prototype demonstrated an improved colour quality with the supplementary colours when compared with the 405 nm light alone whilst demonstrating effective antimicrobial action.

Overall, this study provides the first evidence of the use of pulsed 405 nm LEDs and the operational advantages over continuously run 405 nm LEDs in terms of antimicrobial action. The study then utilises this pulsed delivery system to develop a pulsed blended white light prototype system, a possible viable future design option for continuous environmental decontamination systems.

TABLE OF CONTENTS

CHAPTER 1
INTRODUCTION

In recent years, environmental decontamination has been highlighted as an increasingly important area of infection control, particularly within the healthcare environment. The continued increase of antibiotic resistant strains of bacteria, and also highly transmissible viruses, has emphasised the need for novel decontamination technologies to control the levels of environmental contamination and consequently, reduce infections.

One such technology, which has been extensively tested and documented for decontamination applications, is ultraviolet (UV) radiation (Reed, 2010; Kowalski, 2014; Santos *et al.*, 2012; Bohrerova *et al.*, 2008). There are however some limitations to the technology, including levels of optical penetration and its physically degrading effects on materials. However, the major issue, particularly for environmental decontamination applications, is that of human safety, as UV exposure among other gaseous exposures used for decontamination can pose significant risk to humans. Therefore visible light, which can be used in the presence of humans, would be preferential for certain applications.

The antimicrobial action of 405 nm violet light have been well documented (Guffey and Wilborn, 2006; Enwemeka *et al.,* 2008; Maclean *et al.,* 2008; Murdoch *et al.,* 2013) and although its germicidal efficacy is lower than that of UV light, it can be used to inactivate bacteria at levels which have no significant effect on mammalian cell viability, function or proliferation rate (Ramakrishnan *et al.,* 2014).

In terms of optical germicidal efficiency, studies have shown that pulsed UV light can produce more efficient microbial inactivation when compared to that of continuous UV light (McDonald *et al.*, 2000). This has been generally through the use of high irradiance broadband flash lamps, with a limited number of recent studies demonstrating the concept using UV light-emitting diodes (LEDs) (Li *et al.,* 2010;

Wengraitis *et al.,* 2012). Conclusions from this literature then pose the question; if pulsed UV light can be more efficient than continuous; could similar operational advantages be achieved with pulsed 405 nm light? This idea is where the main focus of this thesis lies.

Initial work in this study (Chapter 4) looks at the characterization of LEDs, and specifically LEDs under varying pulsed regimes; investigating effects of temperature, levels of current, frequency, and pulse width. Additionally, the chapter looks at the design and testing of the pulsing circuit to be used for the rest of the study.

The next phase of work (Chapter 5) provides 'proof-of-concept' testing to investigate whether pulsed 405 nm light provided any beneficial outcomes in terms of electrical, optical or antimicrobial efficacy when compared with continuously run 405 nm LEDs. Parameters investigated included: the pulsing frequency; the duty cycle; the peak irradiance; and the overall germicidal dose. Analysis of the comparative optical and electrical efficiencies was also conducted.

The final investigative stages of the study (Chapters 6 and 7) look specifically at the extension of results from the proof-of-concept pulsed 405 nm work towards practical application. This involved the design, construction, testing and scale-up of a pulsed, blended antimicrobial white light, inherently containing pulsed 405 nm light, in an effort to demonstrate a means of deploying the 405 nm light technology in a more, energy efficient and aesthetically acceptable form.

This thesis concludes (Chapter 8) with a discussion of the major findings and key conclusions from the experimental and analytical work conducted, proposes future work and additional ideas for further study.

CHAPTER 2
LITERATURE REVIEW

2.0 OVERVIEW

This section will review the background literature pertaining to the problem of environmental contamination and its significant role in the transmission of infection, particularly within healthcare settings. It will also discuss the different technologies currently being used to combat the problem of environmental contamination. The chapter will then focus on the use of visible 405 nm violet light as a method for continuous environmental decontamination - reviewing the literature on the clinical evidence of its efficacy, and also its mechanism of action. Finally, means of enhancing the antimicrobial efficacy of the 405 nm light will be discussed; one of which is the concept of pulsing, thus introducing the central research idea behind this study.

2.1 ENVIRONMENTAL CONTAMINATION & ITS ROLE IN INFECTION TRANSMISSION

The motivation for this study stems from the problem of infection control and the need for improved methods of environmental decontamination. Healthcare associated infections (HAIs) were an increasing problem over a decade ago (Dancer, 2009) however in the 2018 Health Protection Scotland annual report (NHS, Health Protection Scotland, 2019) observed most infection rates demonstrating no change over that past few years whilst a US study between 2011-2015 demonstrated a reduction in HAIs (Haque *et al.*, 2018) suggesting the reduction is due to the national initiative to counter HAIs. Either way, HAIs are still currently a hot topic and there are a variety of ways the causative organisms can be spread, particularly in the healthcare environment – and whilst they are still occurring within the healthcare setting, there must be an effort made to reduce or eradicate HAIs.

HAIs, also referred to as nosocomial infections, are defined as 'an infection occurring in a patient in a hospital or other healthcare facility in whom the infection was not present or incubating at the time of admission' (Ducel *et al.*, 2002). It was found during a 2016 survey in Scotland that about 1 in 9 ICU patients (11.4%) had an HAI at the time of the survey along with 6.5% of patients in surgical wards and 4% in medical wards (NHS, Heath Protection Scotland, 2017). HAIs can prove fatal to patients admitted who are already seriously unwell and additionally, HAIs are estimated to cost the UK NHS (National Health Service) an excess of £1 billion with some 300,000 cases each year (Mackley *et al.,* 2018). On a larger scale, it is estimated that in the EU, over 4 million patients acquire HAIs annually and this is thought to contribute to approximately 110,000 fatalities per year (OECD/EU, 2016). It is in the global interest to reduce the levels of HAIs being transmitted.

An additional complication and global issue is that of the emergence of antibiotic or multi-drug resistance – i.e. bacteria, viruses and fungi which become resistant to standard treatments. Resistance is a natural occurrence but is being accelerated mainly due to the misuse and overuse of antibiotics in combination with the failure to develop or discover new antibiotics (Aslam *et al.,* 2018). For example, in 2016, it is thought that globally, 490,000 people developed multi-drug resistant Tuberculosis (TB), and this increasing resistance is also beginning to complicate the treatment of conditions like pneumonia, gonorrhea, salmonellosis, HIV and malaria (WHO, 2018A; WHO, 2018B).

The organisms which lead to HAIs can be both endogenous and exogenous i.e. agents from the patient themselves or from an external source. A few sites of the body which typically carry organisms are the skin, nose, mouth and gastrointestinal tract – these represent endogenous sources of HAIs. External or exogenous sources include health care worker, visitors, healthcare equipment and devices as well as the environment itself (Horan *et al.*, 2008).

A wide variety of organisms can cause HAIs; however, a study has shown that 80-87% of HAIs are predominantly caused by a relatively small number of microbial

species (Haque *et al.*, 2018). *Table 2.1* lists some of the most common bacteria, viruses and fungi which lead to HAIs.

Table 2.1: List of common bacteria, viruses and fungi which lead to HAIs. (Khan *et al.*, 2017; European Centre for Disease Prevention and Control, 2012; Endarko, 2012; Tomb, 2017)

Bacteria	***Viruses***	***Fungi***
Staphylococcus aureus *(Including methicillin-resistant* S. aureus *(MRSA))*	*Hepatitis B*	*Candida albicans*
Pseudomonas aeruginosa	*Hepatitis C*	*Aspergillus* species
Escherichia coli	*Herpes simplex*	*Cryptococcus neoformans*
Clostridium difficile	*Human Immunodeficiency Viruses (HIV)*	
Acinetobacter baumannii	*Norovirus*	
Klebsiella pneumoniae	*Influenza*	
Enterococcus species		

The microorganisms causing these HAIs are transmitted in a number of ways. They can be transmitted through droplets (>5-10 or particles suspended in air (Memarzadeh *et al.*, 2010); food or water; contact with visitors, patients or healthcare workers; or contact with the environment – e.g. furniture, medical devices or fixtures like switches or taps (Meena *et al.,* 2019*).*

Airborne transmission is when droplets are produced, for example through a patient sneezing or coughing, and so infectious particles are released into the environment (Memarzadeh *et al.*, 2010). These particles are generally split into two types – droplet (particles with diameter>5µm), or airborne particles or aerosols (particles with diameter<5µm) (Siegel *et al.,* 2007). The droplets tend to travel much less distance due to their size and so you generally have to be close enough, within 3 feet, to allow the droplet to make contact to allow for infection. Airborne transmission however, with smaller particles, means the particles and infectious organisms can remain airborne for up to and longer than a week depending on the environment – and so airborne particles can easily be found 20 m from the infectious source (Fernstrom and Goldblatt, 2013). Droplets however are prone to evaporation

and a study by Wells (Wells, 1934) suggested a droplet of diameter 50μm could evaporate in 0.4s which could very easily mean that a droplet this size could evaporate and become airborne before it comes in contact with a surface. It is easy to see that airborne particles are a common occurrence and could travel sizable distances depending on air currents, and thus a person could inhale, ingest or otherwise come into contact with infectious organisms without coming into direct contact with the source (Fernstrom and Goldblatt, 2013). Other sources of airborne particles include vomiting, bowel evacuation, flushing the toilet and even talking – however sneezing produces the most particles producing approximately 40,000 particles per sneeze, with talking only producing 36 per 100 words (Fernstrom and Goldblatt, 2013). Another study by Sergent (Sergent *et al.*, 2012) demonstrated significant increase in airborne and surface contamination after wound dressing changes.

The most common means of infection transmission, in the healthcare setting, is however healthcare workers (HCW) hands (Allegranzi and Pittet, 2009). It is very easy to touch a contaminated surface or patient and then subsequently come into contact with another patient, leading to transmission of infection. Frequently touched surfaces – things like bed rails, light switches, overbed tables, beside locker and door handles - can become a significant source of contamination if hand hygiene standards are not properly adhered to. Reductions in HAIs have been demonstrated with improved hand hygiene: a study by Pittet (Pittet *et al.*, 2000) demonstrated the overall number of nosocomial infections reduced from 16.9% to 9.9% between 1994-1998 with a significant improvement in the hand hygiene of nurses and nursing assistants (Pittet *et al.*, 2000). Although hand hygiene offers an effective means of reducing infection - the main issue appears to be with compliance. The aforementioned study by Pittet (Pittet *et al.*, 2000), noted that doctor compliance was poor and a study by Randle (Randle *et al.*, 2010) demonstrated compliance of 75% and 78% for nurses and allied health professionals respectively however only 59% for ancillary and other staff, and 47% doctors. The downfall appeared to be hand hygiene after contact with

surrounding environment – leading to the point of transmission of organisms from the environment.

Although routine environmental cleaning is undertaken in the clinical environment, it is hard to clean everywhere all the time and pathogens can survive on dry surfaces for a significant amount of time if not disinfected. A review paper, by Boyce (Boyce, 2007), stated that pathogens such as methicillin resistant *Staphylococcus aureus* (MRSA), vancomycin resistant *Enterococcus* (VRE) and *Clostridium difficile* can remain viable on dry surfaces for anything from days up to months. The study also demonstrated 36% of the surfaces cultured in a room accommodating a patient with MRSA present in a wound or urine were contaminated; whilst only 6% of surfaces demonstrated contamination in a room accommodating a patient with MRSA on other body sites.

A further study demonstrated that in a room with 8 patients who had diarrhoea that yielded heavy growth of MRSA, almost 60% of the 80 surfaces in the room were contaminated compared to 23.3% in a room with 6 MRSA positive-patients whose stool tested negative for MRSA (Boyce *et al.*, 2007). The study showed the most commonly contaminated surfaces were the bedside rail, blood pressure cuff, television remote control, overbed table, and toilet seat. The studies demonstrate how easily the environment is contaminated – even with standard cleaning practice in place - and the study by Boyce (Boyce, 2007) is one of many demonstrating how long organisms can survive on surfaces.

Additionally, a study by Johnson (Johnston *et al.,* 2006) documented a case of 2 healthcare workers being infected with community-associated MRSA (CA-MRSA) – one being in direct contact with patients and the other being administrative staff with no direct patient contact. If healthy healthcare staff can be infected – then compromised patients are also very much at risk. The study suggests that inanimate environmental surfaces most likely had a role in the transmission of the infection and demonstrates how environmental transmission of infectious agents is an issue.

2.2 CONVENTIONAL CLEANING

With the problem of environmental contamination playing a big part in the transmission of infectious organisms, methods and practices of cleaning must be examined. It is standard practice for environmental surfaces within patients' rooms to be regularly cleaned or disinfected. Cleaning three times a week, if not daily, is recommended specifically when patients are discharged or when areas or surfaces are visibly dirty or soiled (Rutala and Weber, 2013).

Cleaning and disinfection are slightly different and both important. Cleaning physically removes causative organisms and any organic matter that may provide a breeding ground for the organisms. Disinfection, however, tends to mean inactivation of pathogenic organisms (Veerabadran and Parkinson, 2010). A combination of both is required to stop the transmission of pathogenic organisms and resulting HAIs.

There are several parties responsible for the cleaning and decontamination of the environment as well as reusable non-invasive care equipment. These include nurses (trained and untrained), domestic cleaning staff, porters, housekeeping, and Allied Health Professionals (AHP), however there can be confusion over who is responsible for what. There is also a lack of clarity when moving between departments as to which department is responsible – for example for decontamination of the trolley for moving patients (NHS, HPS, 2017).

General rules suggest domestic cleaning staff clean the general environment – floors, surfaces, tables, under the bed – up to bumper level; and nursing staff are responsible for the immediate patient environment (e.g. bed from the bumper up, bed rails and mattresses) along with reusable care equipment (NHS GGC, 2016). Generally, domestic cleaning staff clean the toilets however - dependent on staff training – this is often referred to a nursing team or domestic supervisor when blood of bodily fluids are present (NHS, HPS, 2017).

Current cleaning recommendations – prescribed by the NHS in the National Infection Prevention and Control Manual (NIPCM) – for reusable non-invasive care equipment (commode, blood pressure cuff etc.) is that they are decontaminated:

- between each use;
- after blood or bodily fluid contamination;
- at regular pre-defined intervals as part of an equipment cleaning protocol;
- before inspection servicing and repair.

All equipment, after decontamination, must be rinsed and dried and then stored.

In terms of the clinical environment – decontamination of patient isolation and cohort rooms/areas is recommended at least daily, and this can increase on advice from a Health Protection Team (HPT) if there is an increase in environmental contamination rate e.g. if patients have diarrhoea (NHS, HPS, 2018). For decontamination, recommended methods are,

- a combined detergent/disinfectant solution at a dilution of 1,000 parts per million available chlorine (ppm av.cl.); or
- a general-purpose neutral detergent in a solution of warm water followed by disinfection solution of 1,000ppm av.cl.

Detergents contain liquid or water-soluble chemical compounds, the key disinfection compounds being surfactants, i.e. surface-active agents (Ramm *et al.*, 2015). Detergents are used in conjunction with water and a microfiber cloth, to clean surfaces however, according to a study carried out by Wren (Wren *et al.,* 2008), Ultra Microfiber Cloths (UMF) can remove most of the bacteria on surfaces with water, without the aid of biocides or detergents. However, this does pose the issue that these cloths can then become a source of pathogens. Detergent wipes however are becoming a more popular alternative to reusing clothes, and are advocated in the UK (Ramm *et al.*, 2015)

It is also advised that cleaning and/or decontamination equipment must be single use or completely dedicated to cleaning or decontaminating that specific area. The NICPM also recommends terminal decontamination of patient rooms after

patient transfer, discharge or if the patient is deemed no longer infectious. The vacated room or cohort area is cleared of healthcare waste; bedding, screens and linens; and reusable non-invasive care equipment. The waste and bedding, screens and linens are bagged before removal from the room and the care equipment should be decontaminated in the room prior to removal. The room/area and all remaining equipment must then be decontaminated using the same method as described above for environmental decontamination (NHS, HPS, 2016).

Thorough cleaning is one key part in reducing the number of HAIs as demonstrated in a study by Denton (Denton, 2004) - showing decreased levels of *Acinetobacter baumannii* when a new cleaning protocol, using hypochlorite solution in an intensive care unit, was introduced. Consequently, a significant correlation was demonstrated via the reduced number of patients which contracted an *A. baumannii* infection.

However, there are limitations with current physical cleaning methods. There will always be elements of human error, missing surfaces and then the problem of the continuous airborne production and transmission from patients as mentioned, and the healthcare staff themselves inadvertently spreading pathogens as discussed (Duckro, 2005; Hayden *et al.*, 2008). Therefore, other cleaning procedures/methods of terminal cleaning can be utilized in order to target decontamination of the 'whole room'. Examples of these terminal 'whole room' decontamination strategies will now be discussed.

2.3 WHOLE-ROOM TERMINAL CLEANING TECHNOLOGIES

As mentioned in the preceding section, the terminal clean – also termed a 'deep clean' – is carried out when patients are transferred, discharged, or deemed no longer infectious and so the room is vacated and completely decontaminated. The standard recommendation for a terminal clean is the same as the decontamination method in general, just using a detergent to clean all surfaces and equipment and then a

disinfectant to decontaminate the area. There are however other methods of full room decontamination. These methods to date have generally been gaseous disinfection or ultraviolet disinfection. These methods can only be used for terminal cleans are they use gases and/or UV light which are harmful to humans, and so these procedures are designed to decontaminate a full room whilst vacant (no patients or staff present). These terminal cleaning procedures are not a replacement for conventional cleaning, they are designed to provide a supplementary measure of environmental decontamination.

2.3.1 GASEOUS DISINFECTION TECHNOLOGIES

The method of terminal or deep cleans described in *Section 2.3*, in which the room and equipment is hand cleaned with detergent and then disinfectant, is very time consuming and labour intensive - requiring the cleaner to apply disinfectant to a large number of high touch surfaces and equipment in rooms to ensure proper decontamination. However, it is impractical to clean the entire room (e.g. walls, high ledges and other environmental sites that are inaccessible or not easily cleaned), therefore the use of gaseous disinfectants, such as chlorine dioxide (ClO_2) or hydrogen peroxide (H_2O_2), for full room decontamination provides benefits. Gaseous delivery of these disinfectants has demonstrated superior antimicrobial effects when compared with other applications of the chemicals in aqueous forms (Montazeri *et al.*, 2017). This is due to the gases being more diffusible and penetrable making it easier for the gas to reach areas which are difficult to access and hard-to-clean sites. For this reason, gaseous disinfection or 'fogging' is sometimes used for terminal or deep cleans – and there are various different gases that can be used for this purpose.

2.3.1.1 Hydrogen Peroxide (H_2O_2)

Hydrogen peroxide (H_2O_2) is a chemical, which can be used in aerosol form or deployed as a vapour and can be used as a supplementary cleaning method for terminal or deep clean of empty hospital room. Hydrogen peroxide is an oxidizing

agent and has been demonstrated to be effective against a wide range of pathogens, including Mycobacterium *tuberculosis* (Hall *et al.,* 2007), MRSA (Mitchell *et al.*, 2014), and *C. difficile* (Falagas *et al.,* 2011). The antimicrobial effects of hydrogen peroxide are induced as a result of the production of free hydroxyl radicals which cause oxidative damage to the DNA, proteins and membrane lipids of the target organisms (Linley *et al.,* 2012). Hydrogen peroxide can also be harmful to humans, however once decomposed poses no threat to humans or the environment, with only water and oxygen as the products.

There are in general two types of hydrogen peroxide systems – one using aerosol hydrogen peroxide (AHP) and the second using hydrogen peroxide vapour (HPV). AHP systems generate an aerosol from a solution typically containing 5-6% hydrogen peroxide along with silver ions (<50 ppm) whilst the HPV systems generate a vapour with 30-35% hydrogen peroxide. One difference apart from the concentration of hydrogen peroxide is the fact that HPV is a vapour, which is a gas, whereas AHP is small droplets which have evaporated and so are smaller than droplet and can remain suspended in the air easier. Furthermore, upon completion of the HPV dispersal and disinfection phase, an active aeration system breaks down all the vapour into oxygen and water vapour. The AHP relies on passive breakdown of the hydrogen peroxide over time – and so the level must be monitored, and the room left until the hydrogen peroxide level reduces to sufficiently safe levels (Bioquell, 2015; Fu *et al.*, 2012). It should be noted that there is debate on the definition of aerosols and droplets and their sizes and differentiation.

Bioquell are a major producer of the HPV technology and have various systems including built in wall decontamination units (Bioquell SeQure); full custom integrated building decontamination systems; portable systems for decontaminating emergency medical transport (Bioquell BQ-EMS); and Portable full room decontamination systems (Bioquell BQ-50) – all employing the HPV approach. Shown in *Figure 2.1 (a)* & *(b)* are illustrations of the wall mounted systems and the portable full room decontamination systems, respectively.

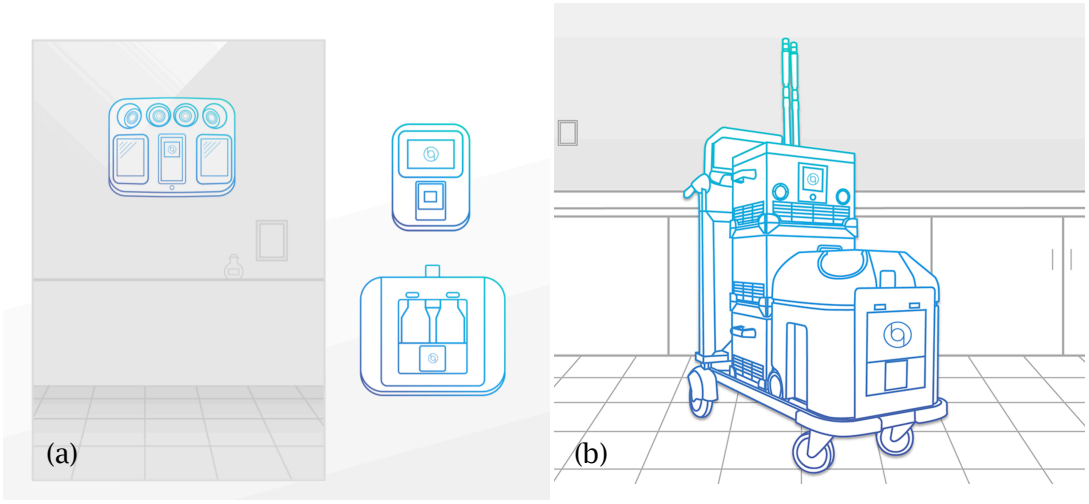

Figure 2.1: Illustrations of the Bioquell HPV decontamination systems commercially available. (a) Wall Mounted Decontamination System (BQ-SeQure) (b) Portable Full Room Decontamination System (BQ-50). Illustrations adapted from pictures from www.bioquell.com/healthcare/systems-for-healthcare/

OxyPharm are another commercial company which supply systems using the aerosol Hydrogen peroxide method of decontamination. They also offer a range of different systems including the 'Nocospray' for small room decontamination; the 'Wall Mounted Nocospray'; and the 'Nocomax Easy' for decontamination of much bigger areas, up to 20000m^3. Pictures of the 'Nocospray' and 'Nocomax Easy' are shown in *Figure 2.2 (a)* & *(b).*

The Glosair aHP is another system made by the same company (OxyPharm) but employs aerosol hydrogen peroxide for full room decontamination. Comparing the Bioquell HPV system and the Glosair aHP system (also made by OxyPharm for full room disinfection with HP), the HPV system can complete the disinfection of a single occupancy room in 1.5-2hrs with the aHP system taking longer at 2-3hrs (Bioquell, 2015). In a study by Fu (Fu *et al.*, 2012), HPV and aHP systems were tested and compared, and the HPV system inactivated more than 90% of the 6-log$_{10}$ *Geobacillus stearothermophilus* biological indicators in the decontamination process compared to <10% inactivation achieved with the aHP system. Similarly, a study by Holmdahl (Holmdahl *et al.,* 2011) compared HPV and aHP technologies and demonstrated complete inactivation of 6-log$_{10}$ *G. stearothermophilus* with the HPV technology in

three separate tests: while the aHP technology demonstrated only 10% inactivation in the first test and 79% for the subsequent two tests. Both studies seem to suggest that the HPV performs better in terms of disinfection and the Bioquell white paper (Bioquell, 2015) suggests it takes less time to perform the disinfection cycle.

(a) (b)

Figure 2.2: Pictures of the OxyPharm AHP decontamination systems commercially available. (a) 'Nocospray' – for small room decontamination. (b) 'Nocomax Easy' – for larger area decontamination. Pictures sourced from https://www.oxypharm.net/en/products/machine/

2.3.1.2 Ozone (O_3)

Similar to hydrogen peroxide, ozone is an oxidizing agent and has been demonstrated to be effective for the inactivation of vegetative bacterial cells (Boer *et al.,* 2006) however it has a limited impact on bacterial spores and fungi (Dancer, 2014). Ozone is a strong oxidizing agent and when in the presence of water generates an array of oxidizing radicals including hydrogen peroxide (H_2O_2), singlet oxygen ($^1O_2$), and hydroxyl radicals (OH^-), which then target the organisms causing membrane and DNA damage (Murray *et al.,* 2008). Ozone is however toxic to humans in large doses. The UK and USA deem <0.1ppm to be a safe exposure level, with the hydrogen peroxide exposure limit is <1ppm (Otter *et al.,* 2013). For this reason, containment of the ozone when decontaminating a room is a key safety concern. Furthermore – it is

documented that ozone can cause damage to materials, including rubber (Masaoka *et al.*, 1982) so care should be taken in terms of the materials in the room and their condition monitored if ozone was repeatedly used.

A study by Sharma and Hudson (2008) demonstrated that a 20-minute period of treatment with 25 ppm ozone was able to inactivate an excess of 3-$\log_{10}$ CFU of a range of bacteria including MRSA, *A. baumannii* and *C. difficile* of populations of approximately 6×10^{8} CFU/ml. The system used was a commercially available system, the Vitroforce 1000 (Vitroforce systems, Omega Environmental, CA, USA) shown in *Figure 2.3.*

Figure 2.3: The Vitroforce 1000 ozone generator (Vitroforce systems, Omega Environmental, CA, USA) used for environmental decontamination. Image adapted from: *https://www.omegaenv.com/environmental-consulting-firm-services/disinfection-odor-elimination-viroforce/technology/*

The system fills the room with ozone upon start up, killing 99.9% of viruses and/or bacteria and upon completion, the ozone is drawn into a catalytic converter speeding up the process of decomposing the ozone to standard oxygen, so the room is once again safe to occupy. The study by Sharma (Sharma and Hudson, 2008) states a 20-minute period of treatment: this was 20 minutes with the room filled with ozone, so with the inclusion of the additional steps i.e. time for the room to fill with ozone, the activation of the rapid humidifying device, and the conversion of the ozone to oxygen, the full process was closer to 60 minutes before the doors of the room could be opened and the room entered.

2.3.1.3 Chlorine Dioxide (ClO_2)

Chlorine dioxide is another oxidizing agent used in gaseous form as a method of environmental decontamination. It demonstrates effective bactericidal, sporicidal and fungicidal properties, and chlorine dioxide demonstrates 2.5x the oxidising power of chlorine (Davies *et al.*, 2011). The inactivation mechanism of chlorine dioxide is oxidative stress, which results in the degradation of protein structure and genomic RNA (Yeap *et al.*, 2015).

Studies with chlorine dioxide in the clinical environment are limited. A study carried out by Lowe *et al.* (2013) investigated the use of chlorine dioxide on a variety of nosocomial organisms within a hospital room. Pathogens, including *A. baumannii, E. coli* and *S. aureus,* were placed on various surfaces and sites in the room and exposed to chlorine dioxide gas. The study demonstrated more than a 6-$\log_{10}$ inactivation of each organism on the sites. The system used was the Minidox-M Decontamination System (Clordisys Solutions, Inc. Lebanon, NJ, USA) which is a commercially available system – however the description does not mention the use in a clinical setting. A picture of the system is shown in *Figure 2.4.* The study did not provide a time however the company states that full rooms, can be decontaminated in under 3.5 hours (Clordisys.com, 2014). Chlorine dioxide is toxic to humans, the exposure limit being 0.1ppm as a Time Weighted Average (Osha.gov, 1991) so the room must be sealed appropriately for application of this method of decontamination.

In addition to the danger posed to human health by exposure to chlorine dioxide: it is also explosive at concentrations higher than the 10% in air, so storage of the gas and even use of the gas raises safety concerns; a by-product of incomplete production of chlorine dioxide is toxic gaseous chlorine, and it can degrade and discolour certain materials within rooms (Davies *et al.,* 2011). Chlorine dioxide can however be smelled at harmful levels – making it easier to detect when humans are

present. It is also, unlike hydrogen peroxide, is not carcinogenic so does have some aspects which make it advantageous.

Figure 2.4: The Minidox-M Decontamination System (Clordisys Solutions, Inc. Lebanon, NJ, USA) used for environmental decontamination.
Image adapted from: *https://www.clordisys.com/minidoxm.php*

2.3.2 Ultraviolet Light Technologies

Another method of whole room environmental decontamination or terminal cleans is that of ultraviolet (UV) light. This technology can avoid the use of potentially harmful chemicals - however UV light in itself is harmful to humans so the room must be again unoccupied for UV decontamination to take place. The antimicrobial properties of UV light were discovered in the 1870s and have been researched, developed and deployed over the last century to inactivate microbes (Reed, 2010). This specific section will look at the application of UV as a terminal clean technology.

The antimicrobial effects of UV radiation are well established. UV radiation is a part of the electromagnetic spectrum with wavelengths just shorter than that of visible light, and spans from approx. 10 nm up to around 400 nm. There are 3 main wavelength bands of UV radiation of interest:

- UV-A, which is the longest wavelength region of UV radiation, between 315-400 nm;
- UV-B is between 280-315 nm; and
- UV-C which is the shortest wavelength of UV radiation between 200-280nm (Reed, 2010; World Health Organization, 2020).

UV-C is it the most commonly used type of UV radiation for disinfection due to the higher energy in this lower wavelength region (Yang *et al.*, 2019). There is however a problem with penetrability of UV-C, and this can limit its effectiveness for decontamination applications (Memarzadeh *et al.,* 2010).

The inactivation mechanism of UV-C, with max germicidal efficiency around 260-265nm, targets DNA and RNA molecules. The UV-C around 260-265 nm matches the peak absorption by bacterial DNA making it very effective. UV-C radiation is directly absorbed by RNA and DNA causing the formation of covalent bonding between neighbouring pyrimidine nucleotides which results in mutagenic lesions. These mutations inhibit the transcription and thus replication of the molecules resulting in cellular functions being compromised and can ultimately lead to death of the cell (Maclean *et al.*, 2008; Kowalski, 2014). UV-B, which includes wavelengths from 280 nm up to around 315nm, causes inactivation the same way, but as the wavelength moves further away from the peak germicidal efficiency at 265nm, the amount direct DNA damage reduces and more oxidative damage is achieved (Nyangaresi *et al.,* 2018).

UV-A radiation has a lower germicidal efficacy when compared to UV-C. UV-A photons generate reactive oxygen species, such as hydrogen peroxide (H_2O_2) and Hydroxyl radicals (OH^-), within exposed cells, which then cause indirect oxidative damage to cells and proteins, and can result in single strand DNA breaks (Li. *et al.,* 2010).

In terms of environmental decontamination applications, the use of UV light means no potentially dangerous chemicals are required for the decontamination process, unlike H_2O_2 or ozone. UV-C is most commonly used because of its high antimicrobial efficacy and UV can be deployed in continuous or a pulsed form.

2.3.2.1 Continuous Ultraviolet Light Technology

Continuous UV decontamination uses a source, such as mercury lamps, that produces continuous UV output, which have a peak output in the region of 254 nm, or more recently UV-LED technology has presented a different option for sources (Livingston *et al.*, 2020). As discussed, most studies use UV-C, and continuous UV-C technology is widely used for disinfection (Kim *et al.*, 2015).

There have been various studies carried out using continuous UV-C for environmental decontamination in a clinical setting. A recent study by Yang (Yang *et al.,* 2019) demonstrated inactivation of a variety of multi-drug resistant, mycobacteria and fungi that are commonly found in the hospital environment. The source used was the Hyper Light Disinfection Robot (Model: Hyper Light P3, Mediland). The system consists of 6 amalgam lamps, pictures shown in *Figure 2.5,* and produces continuous UV-C at 254 nm for disinfection and claims 99.99% reduction of organisms including bacteria, viruses and pathogens in 15 minutes within a 3-metre radius (Mediland.com, 2019).

The UV-C source was placed in 3 different locations - 2 locations in the bedroom (on either side of the bed in opposite corners of the room) and 1 in the adjoining toilet - and the machine was run for 5 minutes in each location (15 minutes in total). Samples were taken from 20 high touch sites around the room and incubated for control values and the room was then exposed to UV-C and further samples taken and incubated for 24hrs with the control. In the control samples, 3 showed no growth; however, of the 17 remaining sample sites demonstrated between 10^1 and 10^3 CFU of pathogens. After 15 minutes of exposure and 24 hours incubation of plates – 16 of the 20 sites demonstrated 100% inactivation and only four sites demonstrated growth

of in the region of $1x10^1$ CFU. Statistical analysis demonstrated a significant reduction ($p=0.0005$) in the median bacterial population comparing sites before and after UV-C exposure.

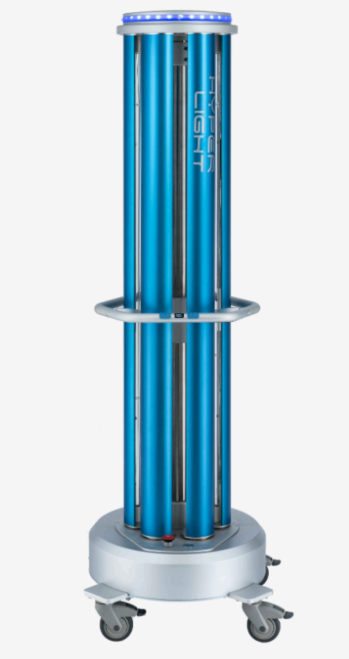

Figure 2.5: The Hyper Light P3 disinfection robot by Mediland. This disinfection robot produces 254nm UV-C for environmental decontamination. Image sourced from (Mediland.com, 2019).

Other commercially available continuous UV systems include the Surfacide Helios (Bates Group, Rayne, UK), Tru-D SmartUVC (RDS, UK) and the Ultra-V (Hygiene Solutions, King's Lynn, UK) – most of these continuous UV systems employ a low-pressure mercury vapour lamp to produce the mercury peak at 254nm (Boyce, 2016).

In terms of human exposure – UV-B and UV-C is known to cause acute and chronic eye and skin damage (Trevisan *et al.*, 2006). The UV decontamination can only be used in an unoccupied room and so, as with the other technologies, is used as a terminal clean alongside conventional cleaning.

A recent study (Livingston *et al.,* 2020) investigates continuous UV-A LED radiation – this however is not a terminal clean solution but more for continuous decontamination. The study by Livingston (Livingston *et al.*, 2020) used a UV-A LED

based system, emitting 365 nm and visible light, mounted in the ceiling, provided by Current (powered by GE, Cleveland, OH, USA). Medical devices were then placed under the unit and left for 4 hours for decontamination. The results demonstrated a significant reduction ($p<0.01$) in the aerobic bacteria from non-selective plates and MRSA. A commercial system for use in the healthcare setting is currently under development however the study concludes that efficacy of the deployment of UV-A in healthcare setting requires further investigation. The study addresses the safety issues of using UV-A in the presence of human but suggests that the levels could be below the damage threshold for humans – however this remains a key safety concern.

2.3.2.2 Pulsed Ultraviolet Light Technology

Pulsed UV is when the UV radiation is delivery in high irradiance pulses opposed to continuous delivery. For many pulsed UV disinfection applications, the source used is a type of Xenon lamp (McDonald *et al.*, 2000; Luksiene *et al.,* 2007; Elmnasser *et al.*, 2007), however with the emergence of more efficient UV-LEDs, UV-LEDs are becoming more commonly used sources. Studies have shown that pulsed UV can demonstrate better performance than continuous UV, with both UV-C (McDonald *et al.*, 2000; Wengraitis *et al.*, 2012) and UV-A output (Li *et al.*, 2010).

A study by Stibich (Stibich *et al.*, 2011) compared a standard terminal clean (manual cleaning for approx. 30 minutes using germicide (Wexcide; Wexford Labs)) with a terminal clean using a pulsed UV system, on Vancomycin-resistant Enterococcus (VRE) infected rooms in a cancer centre. The results demonstrated that 23.3% of the samples tested positive for VRE before cleaning, and after a terminal clean the positive VRE samples were 8.2% and 0% for standard terminal clean and Pulse UV terminal clean, respectively. Similarly with the heterotrophic plate counts (HPC), before cleaning the positive samples were 78.1% (Mean plate count: 33 CFU/cm^2) and the post clean samples were 63.7% (Mean plate count: 27.4 CFU/cm^2) and 36% (Mean plate count: 1.2 CFU/cm^2) for standard terminal clean and pulsed UV

terminal clean respectively. A positive sample in each case is defined as the growth on any microbe on the HPC and as specifically a VRE colony on the VRE samples. The study demonstrated Pulsed UV provided better terminal cleans, which was run for 4 minutes in each of the three locations within the room, when compared with the standard terminal clean protocol, which was carried out by hand using Wexcide and took 30 minutes. The Pulsed UV system used was the LightStrike Germ-Zapping robot (Xenex Disinfection Services, USA), which is a commercially available pulsed UV system for environmental decontamination (*Figure 2.6*).

Figure 2.6: The pulsed UV-C light system, the LightStrike Germ-Zapping robot (Xenex Disinfection Services, USA).

This system has also been demonstrated in a study by Hosein (Hosein *et al.*, 2016) where it was deployed for terminal cleans in isolation rooms in a hospital in London and resulted in 5-$\log_{10}$ reduction in multidrug resistant organisms with a turnaround time of 1 hour. The process demonstrated a decrease to the bioburden in the room and was well received by the hospital staff causing minimal disruption of patient flow. A further study by Jinadatha (Jinadatha *et al.*, 2015) investigated the use of UV decontamination without manual cleaning. Results showed a statistically significant ($p<0.01$) reduction in MRSA in 5 high-touch sites in 14 rooms previously

occupied by an MRSA patient. There was a reduction from 393 MRSA colonies down to 100 colonies after UV decontamination. This demonstrates a good result however it possibly suggests that although a reduction in colonies was observed, a better outcome would have been achieved if manual cleaning had been carried out prior to the UV exposure.

2.3.2.3 Comparison of Pulsed and Continuous UV

Both methods of UV delivery have been demonstrated to be effective for inactivating microorganisms, and studies demonstrate both UV-C and UV-A are both capable of environmental disinfection. Still to date – the most common type system is the continuous UV-C low-pressure mercury vapour decontamination system. However with LED technology on the rise there could be a change in this. In general, UV offers a decontamination option with shorter decontamination times, in the region of minutes up to 1 hour, when compared with H_2O_2, Chlorine Dioxide and Ozone which tend to be more in the region of 1-4 hours decontamination. UV also removes the added hazard of working with and storing hazardous chemicals. UV however can result in degradation of certain materials, specifically polymers which can be used in the hospital envirnment (Dancer, 2014; Yousif and Haddad, 2013).

2.3.3 Summary of Terminal Clean Technologies

As discussed, each of these methods of disinfection demonstrate significant antimicrobial efficacy in addition to being effective against a wide range of pathogens. There is no denying the efficacy of the methods however the application of environmental decontamination poses more than a few obstacles, the first and foremost being room occupation.

For each of these whole-room treatments, the rooms must be unoccupied for any of these technologies to be employed. In shared hospital rooms, it could be a very long time before all patients are discharged; and the room is empty and even in single occupancy rooms, the patient could be there for a number of weeks and after

discharge the fastest turn around possible is required so the shortest and most efficient method of decontamination is key. These terminal or deep clean technologies will not replace conventional cleaning however do provide further reduction of the bioburden when they can be deployed.

The length of time required for a full disinfection cycle varies for each of the technologies. Of the example systems discussed the Chlorine Dioxide has the longest turnaround at around 3.5 hours with UV and Ozone demonstrating the shortest turnaround at around an hour. In the terminal clean as discussed, the faster the better.

Furthermore, the toxicity poses another practical issue for the Hydrogen Peroxide (HP), Ozone and Chlorine dioxide gases. The rooms have to be unoccupied when populated with the gas, but the rooms also have to be airtight in order to ensure containment of the toxic gas. Cost will be further driven up by the need for specialist training and operators for the gaseous and UV decontamination equipment in order to adhere with safety regulations. A further issue as discussed is that ozone and UV can cause material degradation, in plastics and rubber respectively, in rooms.

This section has detailed the antimicrobial effectiveness of several technologies however has not discussed how infection rates have been affected when these technologies are used in the required environments. Various studies have detail that there is a demonstrated improvement in infection rates when using UV, HP and chlorine dioxide for example in conjunction with existing manual cleaning methods. A study by Passaretti (Passaretti *et al.,* 2013) demonstrated that patients admitted to rooms decontaminated with HPV were 64% less likely to acquire a Multi Drug Resistant Organism. An additional study (McCord *et al.*, 2016) using hydrogen peroxide demonstrated a reduction in *C. difficile* infections from 1 case per 1000 patient-days in the 24 months before the use of HPV down 0.4 cases in the 24 months when HPV was used.

Furthermore, a study by Conlon-Bingham (Conlon-Bingham *et al.*, 2016) demonstrates a decrease in the hospital infection rate of MRSA on average of four

cases per month with the use of chlorine dioxide decontamination along with manual cleaning. Similar studies with UV demonstrate a drop of 57% in *C. difficile* infection rates in an acute care facility after the introduction of pulsed UV decontamination (Miller *et al.*, 2015); and demonstrated hospital facility-wide and ICU infection rates significantly decreased upon the use of pulsed UV decontamination (Vianna *et al.,* 2016). These studies demonstrate the strong link between bacterial reduction in the environment and the infection rate.

All of these terminal clean methods demonstrate effective inactivation properties against a wide variety of problematic bacteria, fungi and viruses and so can help in reducing the environmental contaminants. They can provide high levels of decontamination in the region of a few hours and can reach places that standard cleaning might not reach.

2.4 Whole Room Continuous Decontamination using 405 nm Light

A method of environmental decontamination that has recently been developed is the use of antimicrobial visible violet light in the region of 405 nm. This technology uses narrow spectrum light with a central wavelength around 405 nm light – henceforth referred to as '405 nm light'. This violet light has demonstrated significant antimicrobial action against a wide variety of problematic pathogens and can be used in doses lethal to microbes with no effect on mammalian cells. This means the 405 nm light technology can be deployed safely in the presence of patients/staff (Ramakrishnan *et al.,* 2014) therefore these systems have the benefit of being able to be utilized to provide continuous decontamination (unlike the previously discussed technologies which are restricted to terminal clean). The 405 nm light technology is discussed in more detail in *Section 2.5.*

The concept and development of environmental decontamination systems which utilise antimicrobial 405 nm light was established through work by

researchers at The Robertson Trust Laboratory for Electronic Sterilisation Technology (ROLEST), at the University of Strathclyde (Maclean *et al.*, 2010). The system is a patented design (Anderson *et al.,* 2013). This system, known as the high-irradiance narrow-spectrum light environmental decontamination system (HINS-light EDS), is a ceiling-mounted light source designed to provide continuous decontamination in illuminated areas.

The system itself emits a blend of white light with a high output of antimicrobial 405 nm light and can be seen in *Figure 2.7*. 405 nm light has demonstrated broad-spectrum antimicrobial efficacy, (Maclean *et al.,* 2009) and due to the photons being part of the visible light spectrum, the light can be used at levels that are antimicrobial but not harmful to mammalian cells (Ramakrishnan *et al.*, 2016), thus facilitating its use for continuous decontamination. Although 405 nm light is less germicidally efficient than UV light, it can be used continuously opposed to the episodic use of UV. Once installed the system is easy to use (just a simple matter of switching it on) and requires no specialist training.

(a) **(b)**

Figure 2.7: Ceiling-mounted HINS-light Environmental Decontamination System. (a) System in-situ mounted in the ceiling (b) Close up photo of HINS light system. (Bache, 2013).

In terms of clinical evaluation of the technology, there have been a number of studies demonstrating its efficacy for decontamination of healthcare environments, with most studies conducted in patient-occupied isolation rooms. Maclean *et al.* (2010) conducted a study using the ceiling-mounted HINS-light EDS in a hospital isolation room used to treat burns patients. All standard cleaning procedures were left in place throughout the study to ensure the effects were only that of the EDS unit, and the EDS was operated continuously between 8am – 10 pm (in tandem with the standard room lighting.

The study demonstrated a 91% reduction in surface bacterial levels around the unoccupied room with a 92% reduction in presumptive *S. aureus.* In the room occupied with a MRSA-infected patient, the study was run for a longer time over 6 days showing a maximum reduction in total bacterial contaminants of 86% and a reduction of 76% of presumptive *S. aureus.* The antimicrobial effect of the EDS was further confirmed by the increase in bacterial contamination back to the pre-treatment levels, within 2 days after the HINS light EDS was switched off.

A further study by (Bache *et al.,* 2012) investigated the effects of the HINS-light EDS on an inpatient isolation room in addition to an outpatient clinic. After the use of the HINS-light EDS, there was a significant bacterial reduction in the inpatients room of between 24-75% and again demonstrated an increase in the bacterial levels 2 days after the HINS-light EDS units had been switched off. In the outpatient clinic, use of the EDS significantly reduced the degree to which environmental contamination rose over the 8-hr clinic day, achieving the equivalent of a 61% reduction in bacterial contaminants.

A third study by Maclean (Maclean *et al.,* 2013) deployed the ceiling-mounted HINS-light EDS in an intensive care unit isolation room, with results demonstrating a significant reduction in bacterial contamination across a range of surfaces, showing up to a 66.8% reduction in staphylococcal-type organisms and a 53.3% reduction in total bacterial contamination.

In all three studies discussed, the existing cleaning methods were maintained to ensure the only change was the introduction of the HINS-light EDS. This would be the case in reality as the HINS-light, even though a continuous method of decontamination, is still supplementary to conventional cleaning.

The technology has been licensed in the USA by Kenall Lighting and is commercially available under the brand name 'Indigo-Clean', with various 405 nm light-based units for different clinical applications. Examples of these ceiling mounted continuous environmental decontamination systems can be seen in *Figure 2.8.*

Figure 2.8: A example of one of the surgical suite lights (Model: M4SEDIC22) developed by Kenall. Image taken from: https://kenall.com/M4SEDIC22.htm.

A recent case study published in 2018 used the Indigo-Clean technology in a surgical theatre and demonstrated a 56-88% reduction in bacterial contamination 2 weeks after the installation of the violet light unit. Significantly, the study also demonstrated that use of the decontamination system in the theatre over a 1-year period resulted in a 73% reduction in surgical site infections (SSIs) (Murrell *et al.*, 2018).

A further study by Murrell (Murrell *et al.*, 2019) used the Kenall Continuous Environmental Decontamination (CED) system in an operating theatre. Upon

sampling the results demonstrated an average 81% bacterial reduction from sample plates taken before and after the installation of the CED system. The adjacent operating theatre, which shared heating, ventilation and air-conditioning systems also seen an average of 49% bacterial reduction without the CED in that operating theatre. Additionally, the percentage of Surgical Site Infections reduced from 1.4% the year prior to the installation of the CED to 0.4% the year after the installation of the CED demonstrating the tangible effect the CED system has on specifically infection control and not just bacterial reduction.

Demonstration of the impact of this system for reducing infections is a significant achievement, both for this technology specifically, but also for providing more evidence in the literature of the direct link between environmental contamination and risk of infection.

2.5 ANTIMICROBIAL VIOLET 405 NM LIGHT

The use of 405 nm light as a method of environmental decontamination is the central concept of this thesis, and as such, this section provides a detailed overview of its broad-spectrum efficacy, the mechanism of action, and its benefits and limitations.

2.5.1 405 NM LIGHT ANTIMICROBIAL INACTIVATION PROCESS

Exposure of microorganisms to violet light induces inactivation through oxidative damage, and this inactivation process has three main steps: (i) the photoexcitation of endogenous porphyrin molecules within the microbial cells; (ii) the generation of highly active oxidative species (reactive oxygen species, singlet oxygen); and (iii) oxidative damage leading to cell death. These steps are described in detail in the following sections.

2.5.1.1 Photoexcitation of Porphyrins

The antimicrobial effects of violet light are due to the absorption of photons in this wavelength region by endogenous porphyrins within the microorganisms, thought to be primarily coproporphyrin III and uroporphyrin III (Dai *et al.*, 2012). The porphyrins have an absorption maxima, termed the Soret band, that generally lies in the region of 400 nm (Shkirman *et al.*, 1999). When unexposed the electrons of interest within the molecules are said to be at singlet ground state, meaning the electrons are paired with one having an upward spin and the other a downward, both at the same energy level as shown in *Figure 2.9*.

A section of the molecule will have an energy band gap corresponding with the energy in the region of 400-420nm light photons and so the electrons in this portion of the molecule will absorb photons in this region. The photons will cause electron pairs at singlet ground state to be excited to singlet excited state electron pairs, a pair in which each electron still has opposing spin but has a different orientation, as shown in *Figure 2.9.*

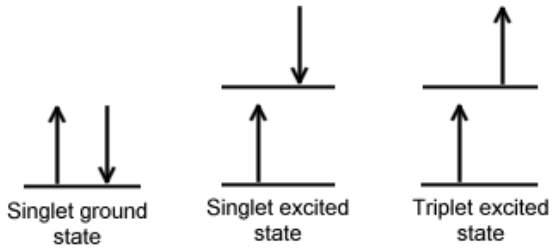

Figure 2.9: Illustration of the electrons spins and energy levels in the different ground and excited states of molecules. For instance, in the singlet ground state oxygen molecule the electron spins are paired and on the same level – however in the triplet excited oxygen molecule, the electron spins are unpaired and in different energy levels.
Image adapted from: **https://www.wikiwand.com/en/Intersystem_crossing**

From the singlet excited state, the electron pairs can either undergo vibrational relaxation until it reaches the local minima and then return to singlet ground state through a radiative transfer; or can undergo vibrational relaxation followed by a transition to the triplet excited state, as can be seen in *Figure 2.10*. The triplet excited state is when the electron spins become unpaired, for example with

both electrons having an upward spin and different energy levels *(Figure 2.9).* This transformation from the singlet excited state to the triplet excited state is known as an Intersystem Crossing as illustrated in *Figure 2.10*. It should be noted that *Figure 2.10* is an illustration of a general case of excitation and is not specific to the porphyrins in the case of the use of 405 nm light – it is purely illustrative.

The triplet excited state electron pair, which has a longer lifetime than the singlet state because of the unpaired electron spins, may consequently react in one of two ways (Type I and Type II photo-processes) leading to cytotoxicity (Lukšienė, 2003; Dai *et al.*, 2012; Hamblin and Hasan, 2004; Wainwright, 1998).

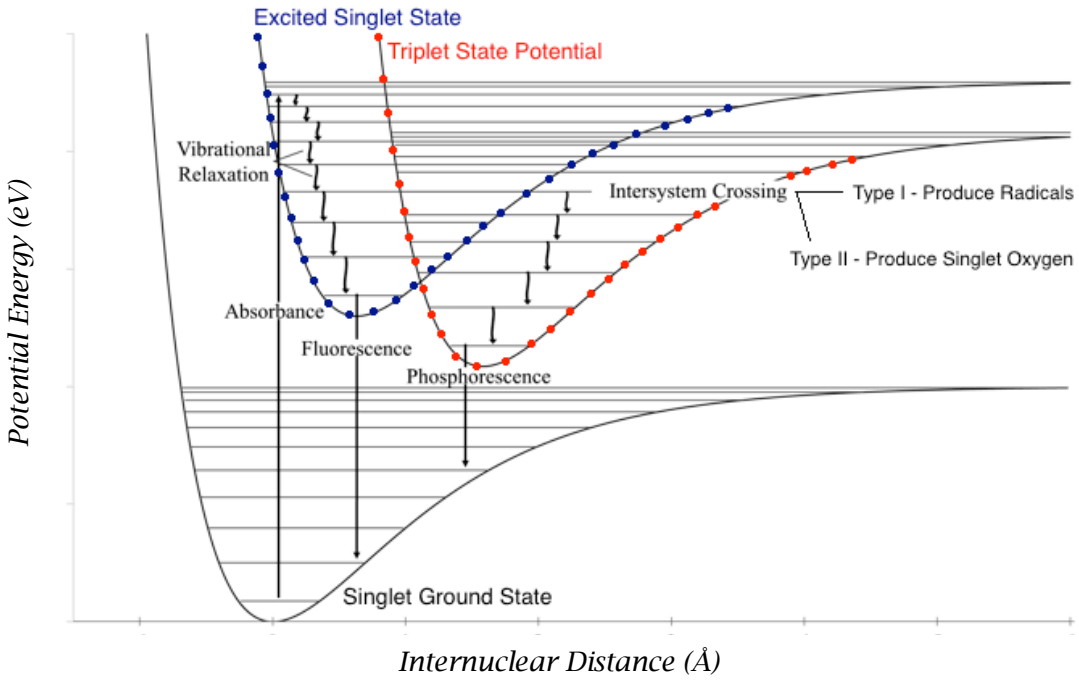

Figure 2.10: Illustration of the energy levels and the transitions that occur between the singlet, triplet and ground state energy levels in the production of radicals and oxidising agents. Image adapted from (Atkins *et al.*, 2014)

2.5.1.2 Generation of oxidising molecules

In the first case, the ***Type I photo-process***, the triplet state porphyrin molecules react with organic substrates resulting in the production of radical ions

like superoxide, hydrogen peroxide and hydroxyl radicals, which can then react with ground state triplet molecular oxygen ($^3\Sigma_g^-$) to produce toxic species which can, in turn, lead to damage and even death of biological cells. In the second case, the ***Type II photo-process***, the triplet state porphyrin molecules react directly with ground state triplet molecular oxygen ($^3\Sigma_g^-$) resulting in the production of singlet oxygen species $^1\Delta_g$. The singlet oxygen molecule has the ability to oxidise cellular components, such as proteins and nucleic acids, which can then lead to cell death (Lukšienė, 2003; Amin *et al.*, 2016).

2.5.1.3 Inactivation Mechanism

At present, there are varying hypotheses on the exact inactivation mechanism. Some studies have suggested that 405 nm light indirectly causes damage to the DNA molecules. Enwemeka (Enwemeka *et al.*, 2008) suggests that, although their study wasn't directly investigating the inactivation mechanism, 405 nm has similar effects on DNA compared with that of UV light, with the capacity to denature DNA molecules. Findings in a recent study by Kim (Kim and Yuk, 2016) support this view suggesting that the antibacterial mechanism is mostly attributed to the oxidation of DNA although a loss of membrane function was also evidenced. Other studies have suggested that DNA is not damaged, but that the cell death is due to membrane damage. A study by Kim (Kim *et al.,* 2016) using *Escherichia coli, Salmonella typhimurium* and *Shigella sonnei*, found no more DNA damage than normal with the application of violet light, and results indicate loss of function and possible damage to the outer and cytoplasmic membranes of the bacteria. In addition, a study by Dai (Dai *et al.*, 2012) indicates the application of violet light caused significant cytoplasmic disruption within *Pseudomonas aeruginosa*. Findings from Zhang (Zhang *et al.*, 2014) demonstrated during a study looking at the susceptibility of *Acinetobacter baumannii,* that after exposure to a dose of 195 Jcm^{-2} of violet light (415 nm±10 nm), that severe cell wall damage was done with leakage of intracellular substances; with a further study by Zhang (Zhang *et al.*, 2016) indicating that after

exposure to violet light, *Candida albicans* showed complete decomposition of organelles, with again disrupted cell walls with some cells showing almost complete loss of cytoplasmic components. Due to the light exposure initiating the formation of highly reactive oxygen species, it is likely that inactivation in exposed organisms will be a result of a combination of the above, with non-specific oxidative damage occurring to all components of the cell (nuclear material, cell membrane, organelles), with maximum damage exerted closest to the site of ROS production within the cell.

2.5.2 BENEFITS & LIMITATIONS OF THE TECHNOLOGY

Although, UV light has a much higher antimicrobial efficacy than 405 nm light, UV light has significant limitations in terms of its potential for carcinogenicity, its depth of penetration, and its potential for material degradation, and so there are restrictions in where and how it can be safely deployed. 405 nm light, however, has advantages in these areas, which make it suitable for certain decontamination applications, in particular applications where mammalian tissue needs to be exposed during treatment – for example, during continuous environmental decontamination.

In terms of its compatibility with mammalian cells, studies have shown that it can be used at levels which induce microbial inactivation without causing damage to mammalian cells. A study carried out by (McDonald *et al.,* 2011), investigating the potential of 405 nm light for wound decontamination, looked at the effects on fibroblast cells, which are critical in the wound healing process, under exposure to violet light. Significant reductions in *Staphylococcus epidermidis* bacterial populations were achieved with 405 nm light exposure whilst no inhibitory effect on the function of the 3T3 fibroblast cells was observed. This difference in sensitivity between bacteria and mammalian cells demonstrates the potential for 405 nm light to be a viable option for wound disinfection. Further studies looked at the effects of 415nm light exposure on mouse abrasions. Dai (Dai *et al.*, 2013B) exposed mouse abrasions infected with MRSA and applied the same dose to human keratinocytes (HaCaT) to observe the impact on the mammalian cells. The study demonstrated a

significant 4.75-log_{10} reduction in the MRSA with only 0.29-log_{10} reduction in the HaCaT cells for the same dose of 168 Jcm^{-2} – 25-fold slower inactivation, again demonstrating the increased susceptibility of microbial cells compared to mammalian cells. Similar studies by Dai (Dai *et al.*, 2013A) and Zhang (Zhang *et al.,* 2014) using other bacterial species (*P. aeruginosa* and *A. baumannii*) demonstrated similar results with significant bacterial inactivation being observed with minimal impact on the mammalian cells.

In addition, 405 nm light has better penetrability than UV light. Penetrability is dependent on the wavelength of UV: UVB and UVC cannot penetrate glass or plastic although as the wavelength of UV increases to UVA its penetrability begins to increase, although still to a lesser degree than visible light wavelengths. However, 405 nm light, which is part of the visible spectrum, can pass through both glass and transparent plastics effectively, with a study by McKenzie (McKenzie *et al.*, 2013) showed successful inactivation of *Escherichia coli* biofilms indirectly on the underside of glass and clear acrylic surfaces. Another study demonstrated the ability of 405 nm light to decontaminate blood plasma whilst held *in situ* in blood transfusion bags (Maclean *et al.*, 2016), again highlighting the potential for 405 nm light to penetrate through materials and achieve decontamination efficacy.

An additional benefit to 405 nm light is the reduced potential for degradation of materials. A study by Irving (Irving *et al.*, 2016) investigated the use of UV-C and 405 nm light for endoscope storage and the degradation of the plastic over time with each optical decontamination method. The results demonstrated an increase in average surface roughness from 2.34nm to 68.7nm, along with visible cracking, with the use of UV-C. The same dose of 405 nm light demonstrated little to no changes in the material surface. This is a major advantage of 405 nm light, particularly for the application of environmental decontamination where objects, equipment and surfaces in treated rooms will be continuously exposed to low-level 405 nm light. The effects of material degradation by UV-light is an aspect that requires

consideration in areas where there is routine use of UV-C terminal clean technologies (as described in *Section 2.3.2*).

As with all decontamination technologies, 405 nm light has limitations - the main one being its decreased germicidal efficacy when compared to UV-light, as already mentioned (Maclean *et al.*, 2014). When compared with UV light, 405 nm light requires a much larger dose for the same degree of inactivation to be achieved. This means either exposure over a much longer time, or exposure to very high irradiances, either way this means there is a requirement for more optical energy and thus higher power. For certain applications, for instance time-sensitive applications this could render 405 nm non-viable however, for the application of safe, continuous environmental decontamination, it is a good technological fit.

Another drawback, only really relevant for the application of continuous decontamination of occupied environments, is that of the use of narrow-band visible violet light. As mentioned above (and in more depth in *Section 2.6)* the main safety benefit of 405 nm light is that it can be used, at certain levels, in the presence of humans; however for continuous use in occupied environments, the violet light needs to be appropriately blended in order to produce an optical output which is overall white light, in order to ensure acceptability of the technology in terms of both aesthetics and comfort.

If not blended correctly, there can be a light imbalance. Due to the high degree of light scattering, light with a dominant violet output can be uncomfortable to work under, and can also distort peoples 'real' colour perception – which in a clinical environment is a major consideration due to the need for high quality lighting in order to conduct routine medical tasks such as monitoring of patient's complexion/coloration, and locating veins for injection. This can be used deliberately in some cases – for example, light sources with higher wavelengths of violet light are used in some public washrooms to discourage people from injecting themselves due to the light making it harder to find veins (Crabtree *et al.*, 2013) – however this would not be acceptable in the clinical environment.

Also, 405 nm light, similar to UVA (known as Blacklight), can cause white colours to fluoresce (e.g. paper, bed sheets etc.) which for instance in the hospital environment could be uncomfortable for long periods. Therefore, it is of great importance that appropriate optical blending is incorporated into any violet-light technology being developed for use for environmental decontamination in occupied environments.

2.5.3 ANTIMICROBIAL EFFICACY OF 405 NM LIGHT

Work carried out by Maclean (Maclean, 2006; Maclean *et al.,* 2008) investigated the bactericidal properties of high-irradiance narrow-band wavelengths of visible light against *Staphylococcus aureus*. The study used a broadband Mercury-Xenon lamp in conjunction with bandpass filters to look at specific narrow bandwidths of visible light. The results highlighted the potential for successful inactivation using photons in the violet range (400-420 nm), with a significant increase in the bacterial inactivation around the 405 nm wavelength, with 405 nm light achieving an increased inactivation of almost a 1-$\log_{10}$ when compared with 400 nm light; and at a wavelength of 410 nm – in improvement excess of 1-$\log_{10}$ reduction when compared with 400 nm light exposures. These antimicrobial wavelengths in the region of 405 nm was termed HINS (High Irradiance Narrow Spectrum) light by the team at Strathclyde.

Following identification of the antimicrobial efficacy of light in the region of 405 nm, the majority of subsequent studies used narrowband light sources, such as light emitting diodes (LEDs), as the antimicrobial light source. LEDs have various benefits including the compact size, electrical efficiency and narrowband wavelength spread.

Various studies have now been carried out demonstrating the broad-spectrum efficacy of violet light, against problematic bacterial and fungal organisms. Pathogens such as *Acinetobacter baumannii*, *Bacillus cereus, Candida albicans, Clostridium difficile, Escherichia coli, Pseudomonas aeruginosa, Staphylococcus aureus,*

Staphylococcus epidermidis, Enterobacter cloacae, Stenotrophomonas maltophilia, Enterococcus faecium, Klebsiella pneumoniae, Elizabethkingia meningoseptica, Streptococcus pneumoniae, Porphyromonas gingivalis and Listeria monocytogenes) are all susceptible to 405 nm light (Maclean *et al.*, 2009; Murdoch *et al.*, 2013; Maclean *et al.*, 2013; Halstead *et al.,* 2016; Barneck *et al.,* 2016; Hope *et al.,* 2013; O'Donoghue *et al,* 2016).

Many pathogens are known to produce problematic biofilms – where organisms can secrete a protective slime layer which promotes microbial replication and survival in adverse conditions. Because of this slime layer, bacteria in biofilms are generally much harder to inactivate than planktonic organisms (Gebreyohannes *et al.*, 2019), however 405 nm light has shown to be effective for successful inactivation of bacterial biofilms of organisms including *A. baumannii, P. aeruginosa, E. coli, Listeria monocytogenes* and *S. aureus* (Halstead *et al.,* 2019; Halstead *et al.,* 2016; McKenzie *et al.*, 2013). The study by Halstead (Halstead *et al.,* 2016) demonstrated an array of 34 different organisms – a few of which are detailed in the previous paragraph – were all susceptible to violet light with 71% of the organisms demonstrating over a 5-$\log_{10}$ reduction in populations with a dose of 54-108 Jcm^{-2}.

405 nm light has also been shown to be effective against strains of pathogens, which are demonstrating resistance to antibiotics, such as methicillin-resistant *S. aureus* (MRSA) and β-lactam-resistant *E. coli (*Enwemeka *et al.,* 2008; Rhodes *et al.*, 2016). The same study mentioned above by Halstead (Halstead *et al.,* 2016) demonstrated bacterial inactivation of MRSA using 400 nm light and observed between a 6-7-$\log_{10}$ reduction in MRSA bacterial populations with a dose between 54-108 Jcm^{-2}. Ramakrishnan (Ramakrishnan *et al.*, 2014) suggests that the reason it is effective against antibiotic resistant strains is that the damage mechanism is not site specific and the reactive oxygen species (ROS) - generated by 405 nm light exposure - cause widespread damage unlike antibiotic inactivation.

Additionally, 405 nm light has been shown effective against spores and endospores which are notoriously resistant to common treatments. Maclean (Maclean

et al., 2012) demonstrated the successful inactivation of *B. cereus* and *C. difficile* endospores achieving up to 4-$\log_{10}$ reduction of spore population in suspension with a dose of 1.73 kJcm^{-2}. The study also compared this with vegetative cells of *B. cereus* and *C. difficile* and demonstrated up to a 4-$\log_{10}$ reduction in populations with a dose of 108 Jcm^{-2} and 48 Jcm^{-2} respectively. The study successfully highlighted the much higher doses required to inactivate endospores when compared with vegetative bacterial cells – but did demonstrate that violet light can successfully inactivate both. Additionally, Murdoch (Murdoch *et al.*, 2013) has demonstrated the inactivation of dormant and germinating *Aspegillus niger* spores – this required a dose of 2.3 kJcm^{-2} to achieve the 5-$\log_{10}$ reduction in the spore population.

Finally, viruses – which lack the endogenous porphyrins involved in the inactivation mechanism (discussed in *Section 2.5.1*) have displayed some degree of susceptibility to inactivation by 405 nm light. Previous studies have shown that viral inactivation, when suspended in minimal media (e.g. simple salt solutions), is minimal, however significant inactivation can be achieved when viruses are exposed when suspended in nutrient-rich suspending media – such as faecal matter and saliva – demonstrating that the inactivation of viruses can be enhanced with the involvement of exogenous photosensitive components (Tomb *et al.,* 2016; Tomb *et al.*, 2014; Tomb, 2017). The study by Tomb (Tomb *et al.,* 2016) demonstrated the inactivation of feline calicivirus in PBS suspension – demonstrating a 4-$\log_{10}$ reduction in Plaque Forming Units (PFU) with an applied dose of 2.8 kJcm^{-2}. The study also demonstrated that in nutrient rich environments (i.e. using artificial saliva, faeces etc.) the required dose is dramatically reduced to between 50-85%. This study demonstrates that 405 nm light does have some viricidal action although it has not been as well established as other types of pathogen to date.

Over the last 10 year since the research on 405 nm light for disinfection began – studies have well established the significant antimicrobial effects of 405 nm light. It has proven very effective against bacteria, fungi and spores and some very promising work has demonstrated some amount of viricidal actions. 405 nm light

has to work with the disadvantage of requiring high doses and longer exposure times than UV – but the advantage of safe use around humans means it can deployed in a completely different way, as a continuous means of decontamination and this is what gives the technology so much potential. This has been demonstrated by the fact it has been licensed by US companies Hubbell Lighting (https://www.hubbell.com/hubbelllightingcomponents/en/spectraclean)and Kenall Lighting (https://kenall.com/Indigo-Clean) who both now sell commercial units and Kenall have published studies demonstrating successful reduction of infection rates.

2.6 Comparison of UV and 405 nm Light Technologies

Both UV and 405 nm light are both part of the electromagnetic spectrum and both have significant antimicrobial properties. The antimicrobial properties or UV however have been demonstrated as early as 1877 when sunlight was found to prevent microbial growth (Reed, 2010). Ultraviolet is very widely used now with various commercial system for terminal or whole room cleans as discussed in *Section 3.2.3,* in addition to the use in air and water filtration systems. The main drawback with UV is safety. It may be very effective at inactivating pathogens, but it also causes damage to humans.

405 nm light as a method of disinfection emerged just over 10 years ago (Maclean *et al.,* 2008) and has since been extensively researched, and the technology commercialised in the USA by Kenall and Hubbell – as detailed in *Section 2.4*. One of the technologies biggest advantages is that it is visible light and thus can be used in the presence of humans and so can provide continuous decontamination (Maclean *et al.,* 2010).

Both technologies have been proven against a wide variety of common and problematic pathogens – however 405 nm light is not fully established against viruses unlike UV (Maclean *et al.,* 2014). Shown in *Table 2.2* is some of the common organisms that these technologies can be used to combat. Although both technologies pose significant antimicrobial action – UV is much more germicidal than

405 nm. Also shown in *Table 2.2* is a selection of studies comparing doses and exposure times required to achieve different levels of inactivation of some common pathogens with both 405 nm light and UV.

Table 2.2: Table comparing the inactivation achieved and dose required for the inactivation of 3 common pathogens (in liquid suspensions) of 405 nm light and UV-C. Data is taken from studies by Maclean (Maclean *et al.,* 2009), Chang (Chang *et al.,* 1985) and Garvey (Garvey *et al.,* 2014).

Organism	***Type of Radiation***	***Inactivation (Log reduction)***	***Dose (Jcm^{-2})***
S. aureus	*UVC*	*4 log_{10}*	*13 $\times 10^{-3}$*
	405 nm	*5 log_{10}*	*36*
E. coli	*UVC*	*5 log_{10}*	*11 $\times 10^{-3}$*
	405 nm	*3.1 log_{10}*	*180*
P. aeruginosa	*UVC*	*5.6 log_{10}*	*4.32 $\times 10^{-6}$*
	405 nm	*4.1 log_{10}*	*180*

As can be seen from the comparison in *Table 2.2*, the UV far outperforms the 405 nm light in terms of dose required for inactivation of the 3 pathogens. For instance, looking at *S. aureus* – the 405 nm light achieves a 1-log_{10} higher inactivation than UV; however, the comparative doses are very different with the UVC dose over 1000x less than the 405 nm. Both the *E. coli* and *P. aeruginosa* demonstrate higher levels of inactivation with UV than with 405 nm light for significantly lower doses.

This is a limited comparison with three studies and 3 pathogens. Depending on the study – the doses and inactivation can vary substantially however the still demonstrate UV as requiring a lower dose. This is dependent on a number of factors including: the means of exposure i.e. suspension, seeded agar plates or in the environment; the starting population; the type of organism; the type of UV. Only UV-

C was discussed in this section as it tends to be the most commonly used however UV-B and UV-A will have different doses and different inactivation mechanisms as discussed in the earlier section – however should still demonstrate more germicidal efficacy than the 405 nm light.

2.7 Safety Considerations of 405 nm Light Technology

Although 405 nm light is part of the visible spectrum and can be used at levels which are not damaging to mammalian cells, as with all light sources, there are safety considerations that must be taken into account, particularly when developing a system for continuous environmental decontamination to which room occupants will be exposed. Previous work carried out in the ROLEST research group by Endarko (Endarko, 2011) analysed the safety aspects of the HINS light EDS system developed at the University. When using 405 nm for environmental decontamination:

- the UV-A tail of the 405 nm LED spectra have to be within eye and skin exposure limits;
- levels of blue light have to be within exposure limits; and,
- retinal thermal hazards must be addressed.

There are accepted threshold levels for each of these – recognized by the World Health Organisation (WHO) – set by the International Commission on Non-Ionizing Radiation Protection (ICNIRP). The ICNIRP have guidelines on the upper threshold limits for different wavelengths of light and document all equations necessary to calculate Threshold Limit Values (TLV) depending on the wavelength of the radiation; associated type of damage; length of exposure; and type of exposure i.e. direct/indirect/intermittent (ICNIRP, 1997).

In general, the skin is less sensitive to injury from visible and infrared (IR) radiation than the eye, and so exposure limits calculated for the eye are in general more restrictive. Additionally, overexposure injuries of the eye tend to be more serious than those of the skin (ICNIRP, 1997).

It is then pertinent to discuss the sensitivity of the human eye and how it perceives colour. The eye has a different response to different wavelengths – most obviously seen by the fact that UV and IR cannot be detected. Across the visible region of light, the eye demonstrates different levels of sensitivity based on the incident wavelengths of light. This sensitivity curve is known as a luminous efficiency function – or more specifically with visible light, the eye sensitivity function or Photopic curve – shown in *Figure 2.11*.

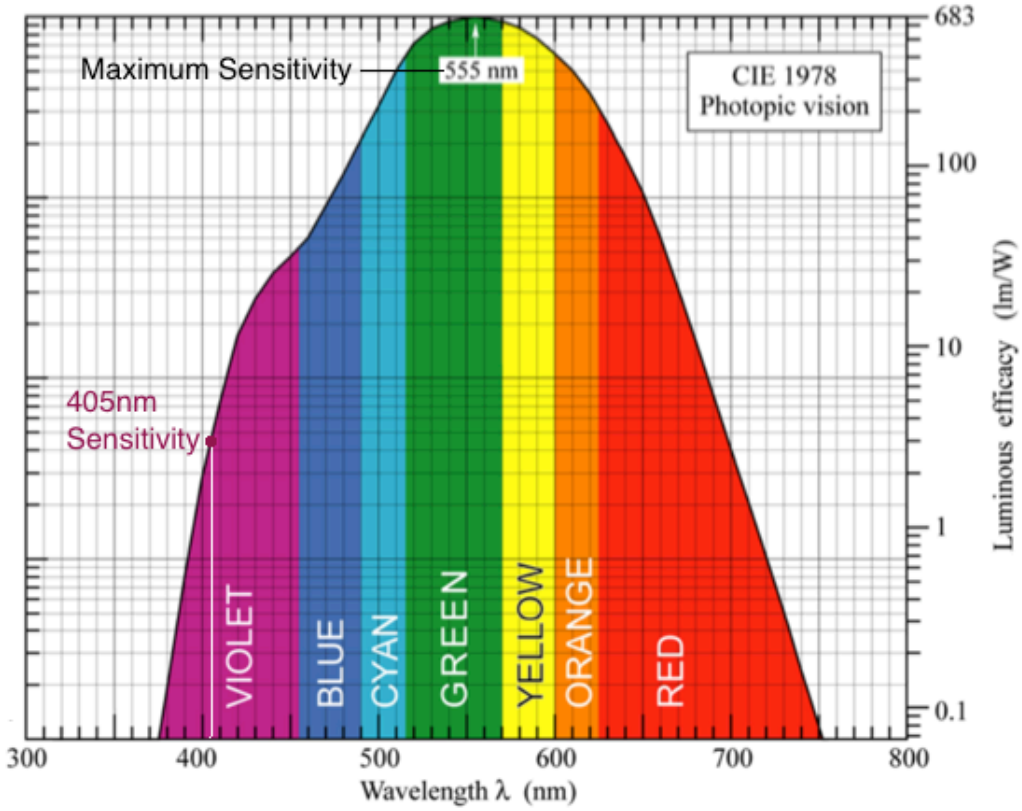

Figure 2.11: The eye sensitivity function of Photopic curve – demonstrating the human eye's differing sensitivity to different wavelengths of light across the visible spectrum. *Adapted from Schubert, 2006.*

As can be seen, the eye is most sensitive to green light with peak sensitivity at 555 nm. The 405 nm violet light is between 3-4 lm/W in terms of luminous efficacy so more than 2-$\log_{10}$ less than the 683 lm/W of 555 nm.

There are two main ways in which the incident radiation can cause damage to the human eye: photothermal means or photochemical means. Photothermal damage

is caused when the incident radiation is absorbed by the eye tissue and is converted to vibrational, rotational or translational energy, leading to an increase in temperature. If this rate of temperature increase is larger than the rate of heat dissipation – then the overall temperature of the tissue will increase and so photothermal damage can result. With photochemical damage, the absorbed optical energy causes electron excitation and can lead to the production of radicals and ROS, which then can cause photochemical damage to cells, proteins, enzymes and/or nucleic acids (Behar-Cohen *et al.,* 2011). The exact mechanisms of this were discussed in depth in *Section 2.6.2*, although this was in reference to organisms rather than human tissue, although the general mechanism is the same. There are various components of the eye that can be damaged with different wavelengths, and a summary of examples is shown in *Table 2.3.*

Table 2.3: Summary of the ocular tissues; the wavelengths absorbed by each; and the damage mechanism triggered by the absorption of the radiation. **Adapted from Behar-Cohen et al., 2011)**

Ocular Tissues	***Damage Inducing Wavelengths (nm)***	***Damage Mechanism***
Cornea	UVA/B/C (100-400) & IR (780-1400)	Photothermal
Iris (melanin)	300-700	Photothermal
Lens	365 Peak @ 8 years old. 450 Peak @ 65 years old. (Peak absorption increases with age)	Photothermal
Retina	400-700	Photochemical
RPE (Retina Pigment Epithelium) (melanin)	400-700	Photothermal & Photochemical
Lipofuscin	355-450	Photodynamic effect – Photochemical

There are various parts of the eye which can be injured, and by an array of different wavelengths of visible light as demonstrated by information in *Table 2.3.*

Photokeratitis, a painful inflammation of the outer corneal layer, can be caused by exposure to UV light, so when working with 405 nm LEDs it is important to

consider the spectral output of the LEDs and ensure that the tail region of their emission spectrum does not contain too much UV-A content, or extend to far into the UV-A region (Bullough, 2000).

Blue-light hazard is arguably the most important to consider when developing technologies which use 405 nm light sources. Blue light hazard is the photochemical damage caused mostly to the retina as a result of exposure to blue light (Bullough *et al.*, 2017; Bache, 2013). Blue light hazard, or Photoretinitis, has a peak absorption at 450 nm *in vivo* (Behar-Cohen *et al.,* 2011). Although the narrowband 405 nm LEDs used for antimicrobial efficacy will have minimal output in the region of 450nm, when developing an antimicrobial blended white light source, as is the case in the present study (Chapters 6 & 7), it will be important to ensure the light output at 450nm of the blended source is in line with optical safety limits.

2.8 Enhancing 405 nm Light Technology

Despite the advantages of 405 nm light for environmental decontamination applications, as mentioned, the technology is less germicidally efficient than UV light decontamination, and so any means of improving the efficacy of the antimicrobial action would be highly beneficial.

2.8.1 Mechanisms of Enhancing 405 nm Light Antimicrobial Efficacy

A number of studies have investigated various methods of enhancing the antimicrobial efficacy of 405 nm light. These have included the use of additional photosensitizers and photocatalysts, and synergistic activity with chemicals and sub-lethal stresses (McKenzie, 2014; Moorhead *et al.*, 2016; Tomb, 2017).

As discussed in *Section 2.6.2*, the inactivation mechanism of 405 nm light involves the absorption of photons in the region 405 nm by endogenous porphyrin molecules within the exposed microorganisms, which results in photoexcitation and

the production of reactive oxygen species (ROS). The incorporation of titanium dioxide (TiO_2), a photocatalyst, into the reaction has been shown to enhance the antimicrobial efficacy of 405 nm light. A study by McKenzie (McKenzie, 2014) investigated the photo-catalytic inactivation effects of 405 nm light used in conjunction with TiO_2-nanoparticles and demonstrated a significant increase in the inactivation rates, with a 1% concentration of TiO_2 reducing the required antimicrobial dose by 50%. Use of nitrogen-doped (N-doped) TiO_2 has also shown to provide further enhancement of the antimicrobial efficacy of 405 nm light (Chen *et al.,* 2012).

In addition to photosensitizer/photocatalytic enhancement, a number of studies have investigated the potential for the antimicrobial effects of 405 nm light to be enhanced through synergistic effects with already used decontamination strategies. A study by Moorhead (Moorhead *et al.*, 2016) set out to look at the synergistic effects of 405 nm light and chlorinated disinfectants for inactivation of highly resilient *Clostridium difficile* spores. Results demonstrated that when spores were exposed to 405 nm light in the presence of sub-lethal levels of chlorinated disinfectants (as may be the case on soiled environmental surfaces), a 33% reduction in sporicidal dose was achieved, demonstrating that the sporicidal properties of 405 nm light could be improved with the concurrent use of low-strength chlorinated disinfectants.

In addition to synergy with the oxidative effects of disinfectants, another study investigated the potential for synergy with sub-lethal stresses typically used in the food industry. McKenzie (McKenzie *et al.*, 2014) investigated the effects of sub-lethal temperatures, salt and acid conditions on the antimicrobial efficacy of 405 nm light and found that inactivation was significantly enhanced when bacteria were exposed at high (45 ˚C) and low (4 ˚C) temperatures, at low pH (3-3.5), and high salt concentrations (up to 15%) - with up to 50% less dose required to achieve to inactivation when compared to non-stressed bacteria. These are interesting findings, it is important to note that these experiments are carried out under lab conditions and demonstrate potential for enhanced inactivation; however, are more applicable

in the food industry opposed to the clinical environment. The results are however still of interest when discussing mean of enhancing 405 nm light performance.

2.8.2 PULSING FOR ENHANCED PERFORMANCE?

In addition to looking at mechanisms to enhance the germicidal efficacy of 405 nm light by means of additional photosensitizers, and/or synergy, consideration should be given to investigating potential methods by which the delivery of the optical energy can be enhanced. Use of higher power light sources, or a greater number of sources, can help achieve higher irradiance outputs but this is unlikely to be a feasible solution for all applications due to prohibitive costs and energy efficiency requirements. It is important therefore to consider other means by which this can be achieved.

As discussed in *Section 3.4.2.2,* pulsed UV-light is a mechanism for delivering short rapid pulses of high energy UV-light for rapid decontamination, and studies have demonstrated improved performance with pulsed UV when compared with continuous UV (McDonald *et al.,* 2000). This is typically done using xenon flashlamp sources, and this principle has been used to develop the Xenex LightStrike Germ-zapping Robot, a commercially available technology for environmental decontamination applications (*Figure 2.6*).

Two recent publications have investigated the potential to operate UV-LEDs using pulsing, with interesting results. A study by Li (Li *et al.*, 2010) demonstrated the inactivation of *Candida albicans* and *E. coli* biofilms using UV-A LEDs under pulsed operation at different frequencies. The study demonstrated superior performance of the pulsed UV-A LEDs with over 99% inactivation (over a 2-$\log_{10}$ reduction), compared with the continuous UV-A exposure which achieved closer to 95% (over a 1.3-$\log_{10}$ reduction) inactivation for the *C. albicans*. The frequency was also altered between 0.1-1000 Hz – and the performance increased until peak performance at 100Hz where *E. coli* and *C. albicans* demonstrated over a 97% and 99% reduction respectively. Upwards of 100 Hz, the performance decreased, and this was

the case for both organisms. This study demonstrated pulsing, and the pulsing frequency, could have an effect on the antimicrobial efficacy.

Similarly, a study by Wengraitis (Wengraitis *et al.*, 2013) which used UV-C LEDs, demonstrated comparable results demonstrating a change in inactivation rate in terms of dose with different pulsing frequencies and duty cycles; with some of the pulsed exposures demonstrating a higher inactivation rate in terms of dose than the continuous exposure. The lowest duty cycle of 10% and frequency of 1Hz demonstrated the highest inactivation rate in terms of dose of almost 11 log kills/mJcm^{-2}. This study also demonstrates that pulsing can have a significant effect on the antimicrobial effects of UV radiation.

The findings from these publications highlighted the possibility that UV-LEDs could be operated under pulsed conditions in order to achieve enhanced antimicrobial efficacy, therefore this then raised the question as to whether pulsed operation could be beneficial for enhancing the antimicrobial efficacy of 405 nm LEDs.

2.9 Aims and Focus of Study

As discussed in this chapter, the antimicrobial properties of 405 nm light have been of growing interest over the last number of years, and research by the University of Strathclyde has led to the development of a 405 nm light system for continuous environmental decontamination. This technology has now been commercialised in the United States by Kenall Lighting, under the brand name Indigo-Clean (Kenall Lighting, USA).

There is however still much to be investigated about this fundamental antimicrobial technology and means of enhancing performance both germicidally and operationally. Benefits of the pulsed operation of LEDs compared to continuous operation have been demonstrated with UV LEDs (Wengraitis *et al.,* 2013; Li *et al.*, 2010) and therefore a major focus of the present study will investigate whether the same principle can be applied to 405 nm LEDs.

The study will investigate the fundamental effects that pulsing might have on the LEDs, both in terms of the optical output of the light sources, and any effects on the germicidal efficacy. Tests will seek to determine whether pulsed 405 nm LEDs could deliver higher levels of bacterial inactivation; better energy efficiencies; and/or better inactivation efficacies.

Furthermore, the study will focus on the practicalities of whether the pulsed LED concept can be used to create a prototype light source for environmental decontamination. The study will investigate the development of a pulsed LED system, where the 405 nm antimicrobial LEDs will be pulsed and blended with supplementary colours LEDs (Red, Yellow and Green) – all under differing pulsing regimes – with the objective of developing a blended white light source for the application of continuous environmental decontamination, using pulsing as a method of control.

CHAPTER 3
GENERAL MATERIALS & METHODS

3.0 OVERVIEW

This chapter will provide details of the general methodologies and equipment used for, the culture and handling of microorganisms and for the measurement and capture of light emissions. Specific methodologies related to the experimental arrangements used in this study will be described in later chapters.

3.1 MICROBIOLOGICAL MATERIALS & METHODS

This section details the bacterial strains and the methods of cultivation used as standard throughout the study.

3.1.1 BACTERIAL STRAINS

During this study, two strains of bacteria were used, both obtained from the National Collection of Type Cultures (NCTC), Collindale, UK:

- *Staphylococcus aureus* (NCTC 4135)
- *Pseudomonas aeruginosa* (NCTC 9009)

These particular organisms where chosen for a number of reasons. Firstly, they are commonly found organisms and are problematic in the healthcare environment for causing infection. They are very commonly found as surface contaminants making them appropriate for this study. One is gram positive and the other is gram negative allowing comparison of any potential differences between the two types of organism. Finally, they are commonly used in other studies both within and out with the research group making comparison of results to other studies easier.

3.1.2 MEDIA & PREPARATION

Nutrient broth (Oxoid, UK) was used for liquid cultivation of both bacterial strains. 100 ml volumes of nutrient broth, (13 gL^{-1}) were prepared in conical flasks, with cotton wool bungs, and autoclaved prior to inoculation with bacteria.

Nutrient agar (Oxoid, UK) was used for cultivation and enumeration of bacterial samples. Nutrient agar was prepared at a concentration of 28 gL^{-1}, and autoclaved, before pouring into sterile petri dishes to prepare nutrient agar plates.

Phosphate Buffered-Saline (PBS) was used to prepare bacterial suspensions, and it was made with 1 tablet per 100 ml of distilled water and autoclaved prior to use.

As mentioned, all growth media was autoclaved (Kestral Automatic Autoclave, LTE Scientific, UK) for 15 minutes at a temperature of 121 °C at a pressure of approximately 1 bar (gauge pressure) to ensure no contamination during microbial experiments.

3.1.3 STORAGE & CULTIVATION OF BACTERIA

3.1.3.1 Storage of Bacteria

For long-term storage, bacteria were stored at -20 °C on microbank beads. For short-term storage, the bacterial culture was streaked on the surface of a nutrient agar slope and incubated at 37 °C. After incubation, the slope was stored at 4 °C in a refrigerator and used as the stock culture. This slope was replaced every month in order to ensure it was free from contamination. In order to check purity, the bacterial culture was also streak-plated, to visualize single colonies from the inoculum *(Figure 3.1)*, and Gram stained (*Section 3.1.4*) to microscopically check the Gram status and cell morphology.

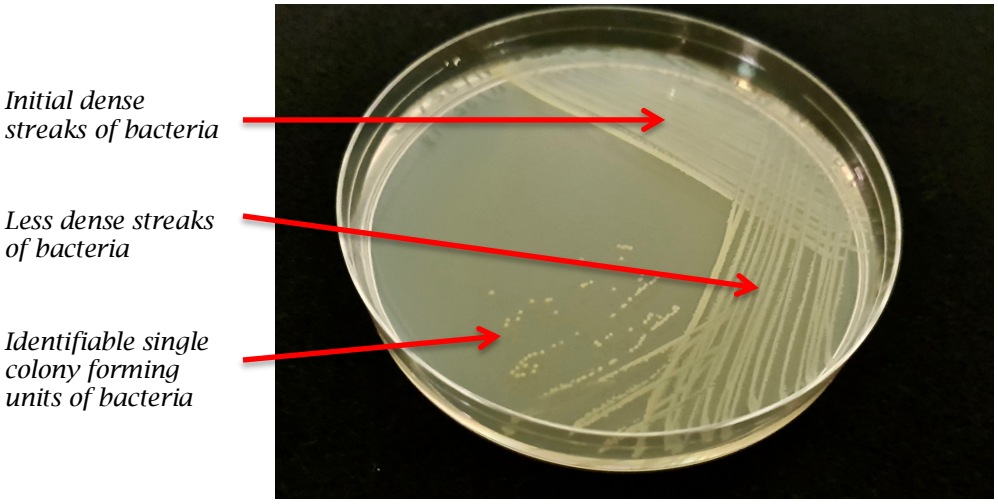

Figure 3.1: Single colonies grown on an agar streak plate. Streak plates are a method of diluting bacterial cells by systematically streaking them across an agar surface in order to obtain isolated colonies. As can be seen there are 3 defined levels of populations: the top right, with very dense CFU of bacteria; the lower left where the density drops and the streak lines are more defined; and finally the bottom towards the left, where the CFU begin to spread out such that single colony forming units are identifiable.

3.1.3.2 Cultivation of Bacteria

In order to cultivate bacteria for experimental purposes, a sterile loop was used to transfer bacterial cells from the refrigerated stock culture (on the agar slope) into nutrient broth. The inoculated nutrient broth was then placed in a rotary incubator at 37 ˚C for 18 hours at 120 rpm.

After incubation, the broth was decanted into sterile centrifuge tubes and centrifuged at 3939 ×g for 10 minutes at 20 ˚C (Labofuge 400R, Heraeus, Germany). The resultant bacterial pellet was then re-suspended in 100 ml PBS, giving a 'neat' bacterial population of 10^9 $CFUml^{-1}$ (Colony Forming Units per millilitre). The suspension was then serially diluted by pipetting 1 ml of the starting suspension into 9 ml PBS resulting in a 10-fold dilution. After each dilution, the suspension was mixed using a vortex (Whirlimixer, Fisherbrand UK) to ensure uniform distribution of the bacteria. The 'neat' suspension underwent serial dilution to obtain a population of 10^3 $CFUml^{-1}$, which was the cell density used for all experiments in this study.

During this study, various experiments and exposures were undertaken using a range of setups and parameters. There were two main types of bacterial exposures: exposure of bacteria in suspension (Chapter 5); and exposure of bacteria seeded onto agar plate surfaces (Chapters 6 and 7). The specific methodologies for the light-treatment and enumeration of these bacterial samples are provided in the relevant chapters.

3.1.4 GRAM STAIN PROCEDURE

Bacterial species are categorized into two groups: Gram positive and Gram negative. Due to the structural differences of the two, they stain differently, with Gram positive bacteria staining purple, and Gram-negative bacteria staining pink. Through use of a microscope, the stain colour and morphology of a bacterial cell can then be determined.

As discussed earlier, Gram stains were carried out on a regular basis to ensure the stock bacterial culture was pure and uncontaminated.

To carry out the Gram stain, the first step was to prepare a bacterial smear (of the bacteria of interest) on a glass slide, and then use this smear for the staining procedure. The steps of this are as follows:

1. Place a drop of distilled water on a clean glass slide.
2. Using a sterile inoculation loop, remove a small amount of bacterial culture from the agar plate or slope, and mix it into the drop of water on the slide to create a smear.
3. Allow the smear to air dry, and then heat fix the bacteria to the slide, by quickly passing the slide through a Bunsen burner flame a few times.
4. The slide should then be flooded with crystal violet (Sigma Aldrich, UK) and left to sit for ~1 minute.
5. Gently rinse the slide with distilled water (dH_2O).
6. The side should then be flooded with Iodine (Sigma Aldrich, UK) and left to sit for ~1 minute.

7. Again, after the minute, gently rinse the slide with dH_2O.
8. Using ethanol, rinse the slide gently (rocking side-to-side) until the ethanol runs almost clear.
9. Rinse the ethanol off the slide with dH_2O.
10. The slide should then be flooded with safranin (Sigma Aldrich, UK) and left to sit for ~45 seconds.
11. Gently rinse the slide with dH_2O and blot dry the slide.
12. The slide is then viewed using a Nikon Eclipse E400 microscope at ×1000 magnification to confirm the Gram status (Gram positive = purple; Gram negative = pink) and morphology of the bacterial sample.

Figure 3.2(a) and *(b)* show microscopic images of *S. aureus*, a Gram-positive coccus, and *P. aeruginosa*, Gram negative, rod-shaped bacterium respectively.

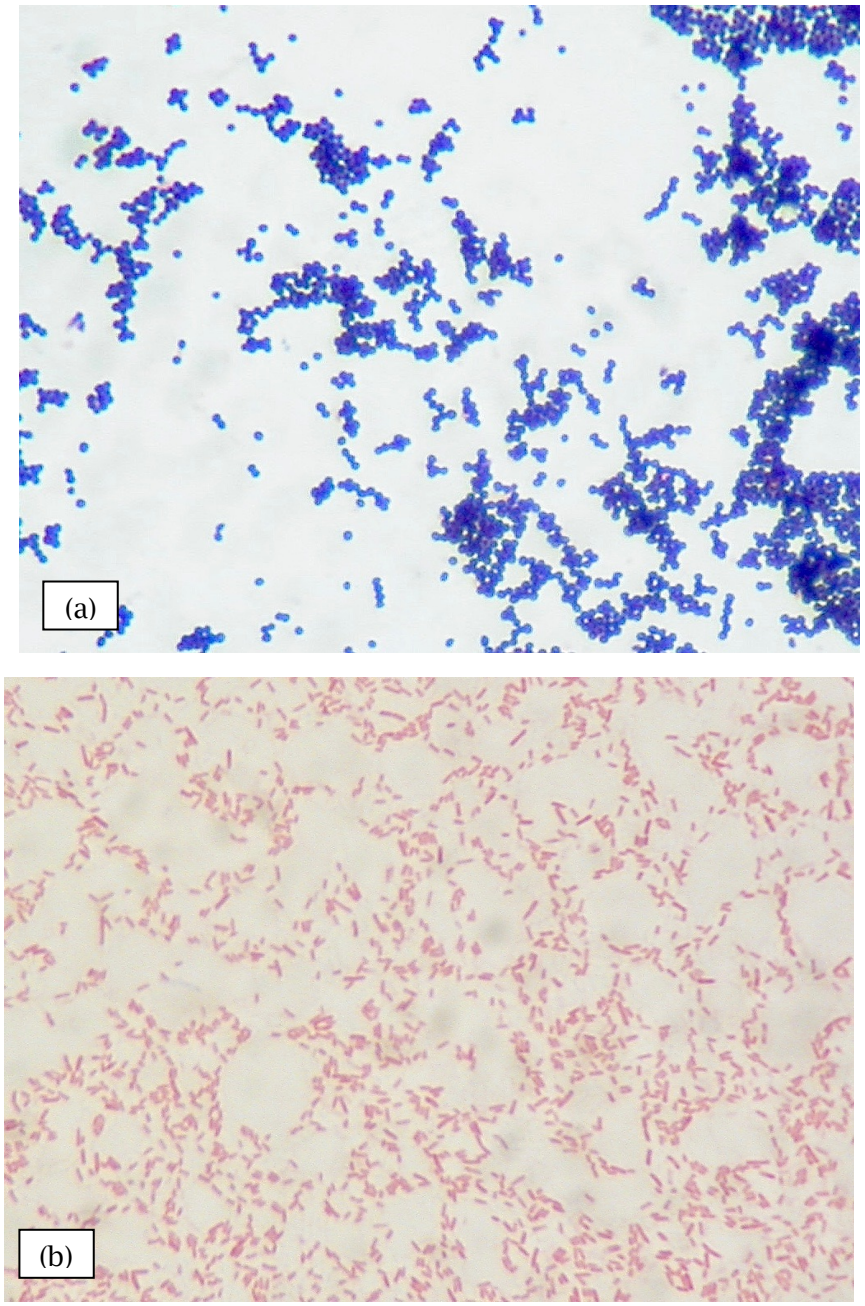

Figure 3.2: Examples of the results of a Gram Stain of (a) *S. aureus*. – Gram-positive organism meaning the stain comes out as purple colour and as it is a *Staphylococcus*, the bacteria present as purple cocci or spheres. (b) *P. aeruginosa* – Gram-negative organism meaning the stain comes out as a red/pink colour and *P. aeruginosa* is a rod-shaped bacterium so the bacteria presents as pink rods.

3.2 Optical Measurement Equipment

This section details the three methods of optical measurement used throughout this study. The three methods are the use of the radiant optical power meter, the spectrometer and the use of a photodiode. Each is described in more detail in the proceeding sections.

3.2.1 Radiant Optical Power Meter

The optical power meter used throughout the study was the Model-70260, Oriel Instruments, UK, used with a photodiode detector, Model-1Z02413, Ophir. The photodetector head was an area of 1 cm^2 and the output of the power meter was given in $mWcm^{-2}$. The power meter sensitivity could be adjusted to a specific wavelength on the console and was set to 405 nm for all experiments throughout this study. It should be noted that the irradiance measured was not solely 405 nm light; the system measured all light but was calibrated to measure 405 nm light accurately and so measurements were made in low background light or darkness to ensure an accurate measurement of the 405 nm light.

The response time of the optical power meter was in the region of 0.1 s and given that most of the experiments in the study involved pulsing with the majority of pulsing around 1 kHz, the power meter could only provide an average irradiance reading. The average reading will be lower than the peak irradiance of each pulse and a parameter known as the duty cycle was used to calculate the peak irradiance from the average.

The duty cycle is defined as the percentage of a period of a waveform during which the signal is high, or in this case, the LED array is on; e.g. a 50% duty cycle is illustrated in *Figure 3.3,* in which the voltage level is high 50% of the period. Duty cycle is given by *Equation 3.1*, with τ being the pulse width and T being the pulse period.

$$Duty\ Cycle = \frac{\tau}{T} \times 100\% \qquad (Equation\ 3.1)$$

Shown in *Figure 3.3* is an illustration of two pulsed waveforms with differing duty cycles and the average amplitudes of the waveforms illustrating the effects of duty cycle on average irradiance.

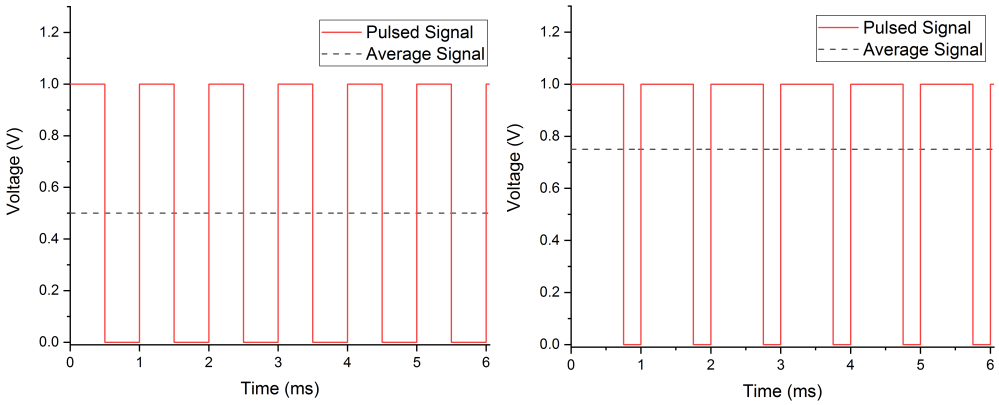

Figure 3.3: An illustration showing a pulsed voltage signal and associated average voltage signal, for (a) a 50% duty cycle and (b) a 75% duty cycle. The increase in duty cycle of the voltage signal results in an increase in the average voltage signal.

The duty cycle is how the average irradiance and peak irradiance are related. The peak can be discovered mathematically with the duty cycle and the reading of average irradiance using the relationship shown in *Equation 3.2*.

$$Peak\ Intensity = \frac{Average\ Intensity}{Duty\ Cycle} \qquad (Equation\ 3.2)$$

(Where the duty cycle is represented as a decimal)

The power meter had to be tested in order to be sure that the average would be as expected since the pulses were out with the response time of the power meter. This was verified by measuring the 100% duty cycle irradiance – then pulsing at a 50% duty cycle and over a range of frequencies, and the output of the power meter displayed 50% of the continuous irradiance as expected confirming that the power meter displayed an accurate average irradiance.

3.2.2 SPECTROMETER

The spectrometer was used to capture the spectral output of the light sources used. The model used was the Ocean Optics HR4000, with Ocean Optics SpectraSuite software, which measures broadband light from 200 nm up to 1100 nm.

The spectrometer was used in two configurations depending on the requirement of the experiment. The first configuration used the spectrometer and an optical fibre and allowed capture of an optical spectrum with arbitrary irradiance readings, wavelength resolution of 0.28 nm. This provided the shape and spread of radiation and was used to compare peaks relatively.

For an absolutely irradiance reading, the spectrometer and optical fibre were used in combination with a cosine corrector (CC3-UV-T, Ocean Optics, USA), which was connected to the end of the optical fibre. A calibrated light source (DH2000, Ocean Optics, USA) was first used to ensure calibration and accuracy of the spectrometer, and following this, absolute irradiance spectral data could be captured, again with a wavelength resolution of 0.28 nm.

A major focus of this study was to investigate the efficacy of pulsed 405 nm light, and the majority of experiments used pulsing at 1 kHz frequencies. The response time of the spectrometer made it difficult to catch the spectrum of a single pulse given the pulse duration was <1 ms. This meant that all spectra from pulsed sources recorded in this study were taken as an average. The average spectral reading will only differ in the measured height of irradiance due to the 'off' time of the pulses – with the relative spectral peaks remaining unchanged by the pulsing. The correct irradiance peak could be found using the same equation discussed at the end of *section 3.2.1.*

3.2.3 PHOTODIODE

A photodiode was used as a method of capturing the pulse waveforms and as a measure of consistency during most experiments throughout this study. The benefit of the photodiode was the response time, which was in the region of 25 ns. This facilitated capture of the optical pulse waveforms, and enabled verification of the shape, pulse width, time periods and relative irradiances of the pulses. The photodiode was operated in photovoltaic mode with the setup shown in *Figure 3.4*.

The model of photodiode used (OSRAM BPW34 B) had a blue sensitive diode with peak sensitivity in the violet-blue region of the spectrum. It was not calibrated in any way and so could not be used to take readings of absolute irradiance; however, it was used to monitor any changes in the peak irradiance and the optical pulse width and period.

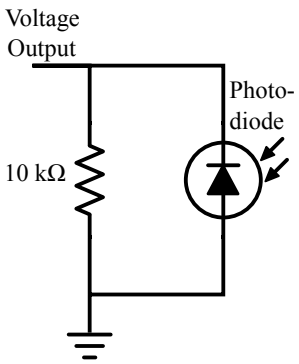

Figure 3.4: The circuit of the photodiode set up in photovoltaic mode and used throughout the study to capture optical pulse waveforms, and enable verification of the shape, pulse width, time periods and relative irradiances of the pulses of light being measured.

3.2.4 SUMMARY OF OPTICAL MEASUREMENT METHODS

Three different methods have been described for the capture of light and each has a different application which will be summarised here.

1. Radiant Optical Power meter – used for average irradiance readings ($mWcm^{-2}$) to check the irradiance before and after exposures, as well as to set the irradiance of the LEDs prior to bacterial exposures.
2. Spectrometer – fundamentally used for the capture of the light spectra. Relative irradiance spectra of the 405 nm LEDs were captured. Additionally, calibrated spectra from the blended prototype was captured to quantify and help tune the quality of the light output from the LEDs.
3. Photodiode – used with an oscilloscope to monitor real time optical pulsing throughout the duration of the experiments to ensure consistency. The high response time allowed for capture of the optical pulses to check duty cycle and monitor peak irradiance.

Each of the three methods had a specific task which it was used. The Spectrometer could have been used to carry out all of the optical measurement tasks – however the power meter and photodiode were much easier to use in terms of setup and complexity with no real drawbacks when compared with the spectrometer, so for this reason each of the three methods was used for the most suited tasks.

CHAPTER 4
OPERATION & CHARACTERISATION OF LEDS UNDER PULSED CONDITIONS

4.0 OVERVIEW

This chapter provides an introduction to LEDs as the source of light that will be used throughout the study. Literature will be examined relating to how LEDs operate; as well as the effects pulsed operation can have on the performance and output of the LEDs. The chapter will then detail experiments undertaken to ascertain a suitable electronic circuit for pulsing the LEDs throughout the study; and finally, it will detail the rudimentary experiments carried out with LEDs to investigate their behaviour under pulsed conditions.

4.1 LED BACKGROUND, UNDERLYING PRINCIPLES & OPERATION

Light generation has always been of significant interest however it was only the late 1800s when the first electrical light source, the incandescent lamp, was commercialised. Since then other more efficient electrical sources have been realized the most common and well known being the fluorescent lamp, including the compact fluorescent lamp (CFL). The most recent option, becoming increasing popular for electrical light, is the LED. LEDs were first commercialised in the early 1960s (Cole *et al.*, 2015). It wasn't however until the breakthrough with blue LEDs using InGaN to overcome inefficiency problems over the last 20-30 years, which won I. Akasaki, H. Amano and S. Nakamura the Nobel Prize in Physics in 2014, that LEDs really became common place (Gayral, 2017). With the introduction of blue LEDs, a combination of colours could be used to produce white LEDs allowing for the realisation of a new alternative white light source. These LEDs will also be the focus of this study, which will focus specifically on 405 nm LEDs.

An LED is a discrete semiconductor device, which is designed to emit light when subject to a forward current. As the name suggests, it is a diode, and so allows current to flow through it in one direction, the forward direction, but not in the opposite, or reverse direction. This is accomplished through the combination of two different types of doped semiconductor: an n-type and a p-type.

Semiconductors are materials that have a measure of conductivity somewhere between metals and insulators. There are two general classifications of semiconductor: an elemental semiconductor, i.e. a group IV element such as silicon; or a compound semiconductor, commonly a compound of a group III and group V element e.g. GaAs. (Neamen, 2012, pp. 1-2) In the case of LEDs, we are concerned with the latter, the compound semiconductors.

Semiconductors by nature form a crystalline structure; and at a temperature of absolute zero, in the lowest energy state, each electron is in the valence energy band and is part of a covalent bond. In this arrangement, the semiconductor will not conduct. However, if the temperature is increased a few degrees above 0 K, some electrons in the highest unoccupied molecular orbit (HOMO) may gain enough thermal energy to make the jump across the band gap (E_g) from the valence band up to the conduction band (Neamen, 2012, pp. 72-73), as demonstrated in *Figure 4.1*.

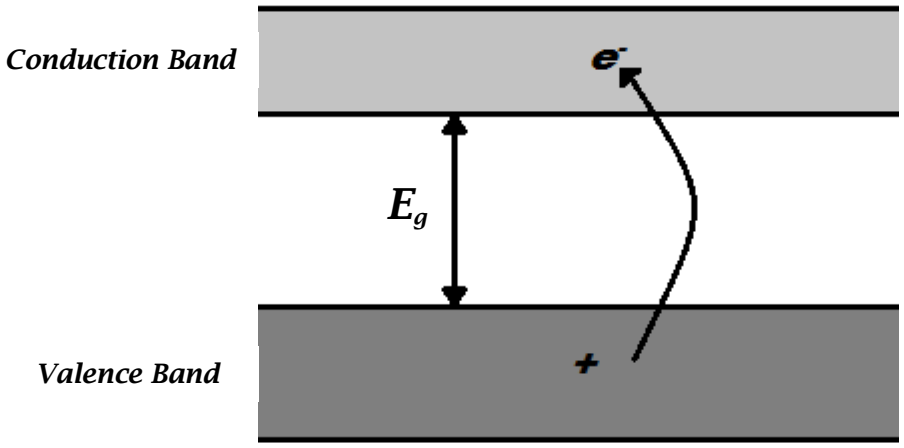

Figure 4.1: An illustration of an excited electron moving from the valence band up to the conduction band by jumping across the band gap (E_g).

Electrons in the conduction band are free to move about the crystal lattice of the semiconductor between atoms. When an electron is elevated to the conduction band, the covalent bond it was part of is broken and as the electron moves around the lattice it leaves behind a hole for another electron to fill, as shown in Figure 4.2. These are the two charge carriers in a semiconductor, the negative electrons, which travel in the conduction band, and the positive holes, which effectively travel in the valence band. (Neamen, 2012, pp.78)

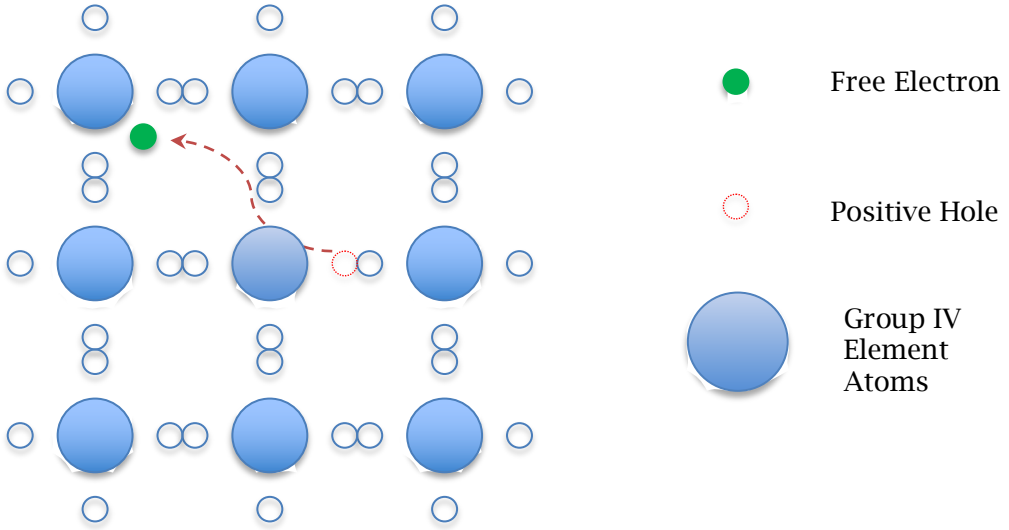

Figure 4.2: A 2D illustration of the generation of a positive hole by the excitation of a bonded electron from the valence band to the conduction band, in a group IV elemental semiconductor crystal lattice.

When an electron recombines with a positive hole, it drops back down to the valence band to form a covalent bond and as it falls through the band gap; the band gap energy is released. The semiconductor material determines the band gap and so different materials will have different band gaps and thus release different amounts and types of energy. The interest of this study is materials that have band gap energy, which corresponds to the wavelengths of visible light, i.e. light emitting semiconductors.

Common light emitting diodes, are compound semiconductors – group III-V compounds and more complex ternary compounds which include 3 elements, for example Indium Gallium Nitride (InGaN). In the case of these compound

semiconductors, they also form large covalent network lattice structures (Neamen, 2012, pp.2).

Pure silicon, in its crystalline form, at a temperature of absolute zero will have all electrons constrained within covalent bonding and with an increase in temperature some electrons are released and are able to jump to the conduction band. However, the electrical conductivity of a semiconductor can be improved through the process known as doping. This process is when impurity atoms (atoms of a different element) are added to the semiconductor. (Neamen, 2012, pp.16)

If we consider a group III element, Boron for example, used as a dopant; there will be an inherent positive hole in the semiconductor lattice because the group III element will only have 3 valence electrons for bonding, whilst the semiconductor structure will be looking to bond with 4 valence electrons. (Neamen, 2012, pp.119) This is an example of a p-type semiconductor, as it has more positive charge carriers (positive holes) than negative (electrons). A 2D illustration is shown in *Figure 4.3.*

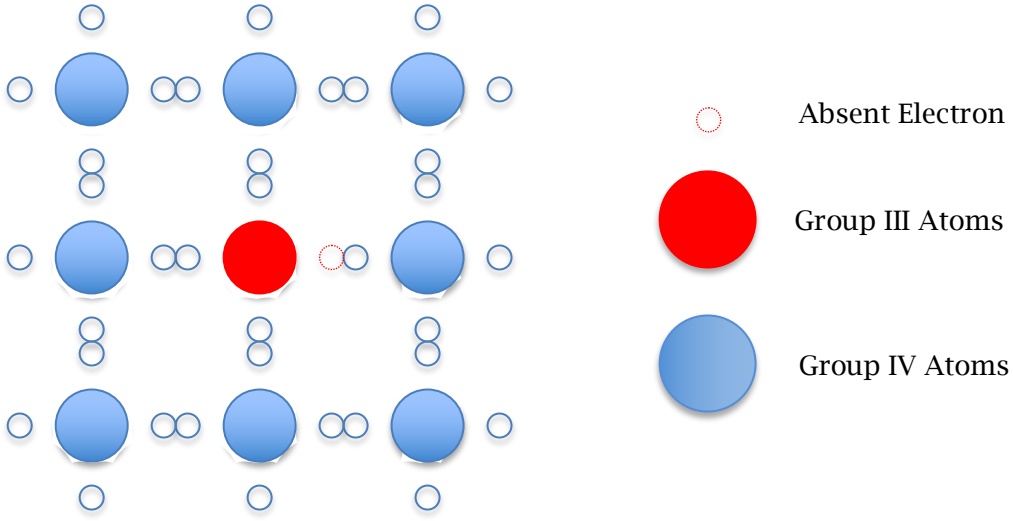

Figure 4.3: A 2D illustration of a semiconductor structure doped with a group III element, resulting the in the generation of a positive hole (positive charge carrier) in the valence band. An example of a p-type semiconductor.

With the generation of positive charge carriers in the semiconductor by adding a dopant, the electrical conductivity of the semiconductor can be drastically improved. Likewise, if the dopant has more than 4 valence electrons - for instance

Phosphorus (Group V), which has 5 valence electrons – then the lattice will have extra electrons in the structure as the group 4 lattice only required 4 valence electrons to bond with, whilst the dopant atoms have 5 (Neamen, 2012, pp. 118). This forms an n-type semiconductor with more negative charge carriers. A 2D illustration of the lattice is shown in *Figure 4.4*.

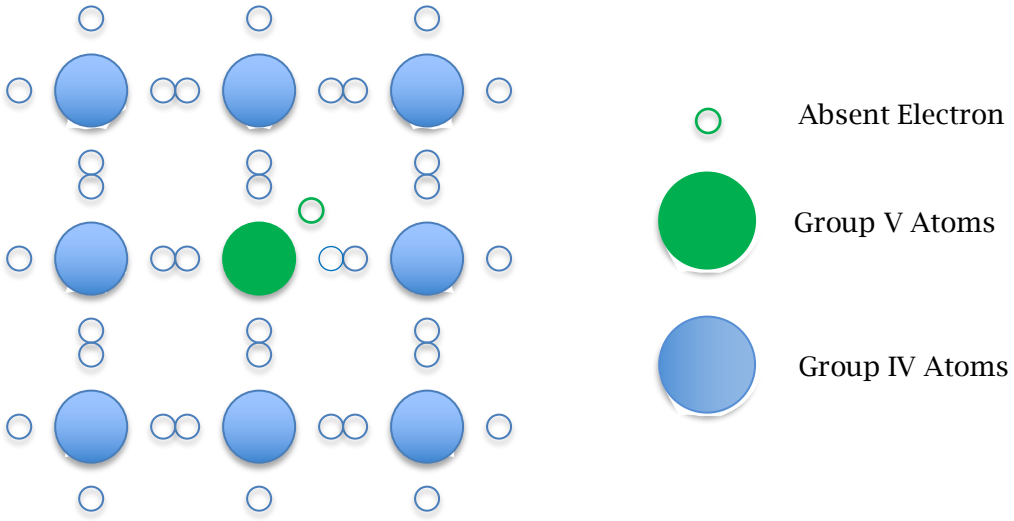

Figure 4.4: A 2D illustration of a semiconductor structure doped with a group V element, resulting the in the generation of a free electron (negative charge carrier) in the conduction band. An example of an n-type semiconductor.

This doping process can also be carried out with other element out with group II and V to change the electrical conduction of the semiconductor.

With knowledge of p-type and n-type semiconductors, the idea of a diode can be introduced, also known as a p-n junction. As the name suggests, a p-n junction is when a p-type semiconductor is combined with an n-type semiconductor. Where the n-type and p-type meet, what is known as depletion layer forms: where the positive holes from the p-type and the free electrons from the n-type combine (Schubert, 2006, pp.59). This can be seen in *Figure 4.5*.

When the p-n junction is subject to a forward bias voltage – i.e. positive to the p-type region and negative to the n-type region – the p-n junction will conduct, assuming there is enough voltage to overcome the built-in potential barrier – which in effect is the energy required to move electrons and holes across and out of the

depletion layer thus reducing its size (shown in *Figure 4.5*). The positive voltage potential will repel the positive holes from the p-type region across the depletion layer to the negative voltage potential which attracts them: and vice versa, the free electrons from the n-type region are repelled in the opposite direction and attracted to the positive voltage potential. This results in admittance of a continuous flow of current through the semiconductor (Schubert, 2006, pp.60).

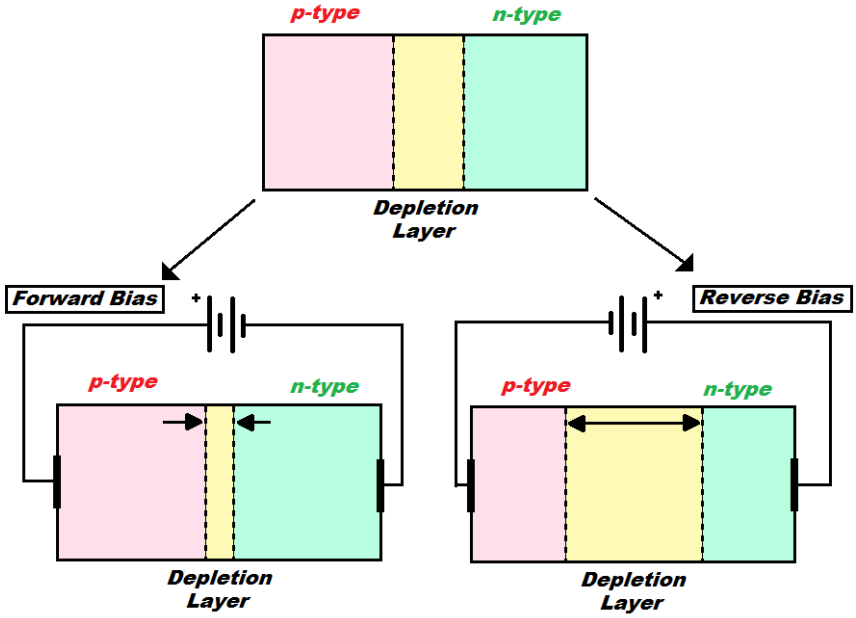

Figure 4.5: An illustration of the formation of a depletion layer in a p-n junction and the effects of the application of a forward and reverse bias on the size of the depletion layer and thus the conductivity of the semiconductor.

Alternatively, if the p-n junction is subject to a reverse bias voltage – i.e. positive to the n-type region and negative to the p-type region – the p-n junction will cease to conduct. The positive voltage potential will draw the free electrons to the n-type region and likewise the negative voltage potential will attract the positive holes to the p-type region causing the width of the depletion layer and thus the potential barrier to increase (shown in *Figure 4.5*). This greatly reduces the conductivity of semiconductor to virtually a non-conductive state. (Neamen, 2012, pp.281)

When a p-n junction is subject to forward bias voltage and thus conducting, the recombination of electron hole pairs across the junction, as the charge carriers

move, result in a release of energy – equal to the size on the energy band gap. In diodes, the energy released varies with the band gap, which is dependent on the composition material. Standard electrical diodes are usually made from materials that have an indirect band gap. This means the electrons in the lowest energy level in the conduction band and the highest in the valence band do not sit at the same momentum – and this makes radiative recombinations very unlikely, as momentum must be conserved (Neamen, 2012, pp.84). Most of the recombinations are non-radiative meaning the energy is dissipated into the lattice as vibration energy - effectively dissipated in the diode as heat (Schubert, 2006, pp.35).

However, there are certain materials where the energy band gap corresponds to the energy of photons of visible light and the momentum of electrons in the lowest energy level in the conduction band and the highest in the valence band are the same (direct band gap). These materials have far higher probabilities for radiative recombinations because the recombinations can occur with just a photon release with no need for phonon release for momentum conservation (Neamen, 2006, pp.85). The wavelength of the photon is again determined by the energy band gap, as dictated by the Planck-Einstein Relation, *Equation 4.1*.

$$E = \frac{hc}{\lambda} \qquad \textit{(Equation 4.1)}$$

Where E is the photon energy in Joules (J); h is Planck's constant, 6.626×10^{-34} with the unit Joule-seconds (Js); c is the speed of light in metres per second (ms^{-1}); and λ is the wavelength of the photon in metres (m). This photon energy or band gap energy is dependent on the elemental makeup of the semiconductors used to create the p-n junction. (Neamen, 2012, pp.648)

The material of main interest in this study is Indium Gallium Nitride (InGaN), which produces violet light, and can be used to create 405 nm light emitting semiconductors.

This section explains on the simplest level the workings of light emitting semiconductors however; LEDs come in many different shapes, sizes and layouts. A sizable number of LEDs are built up of multiple layers, with a combination of differing n-type and p-type material in different shapes combined to produce the most efficient light output however the principles remain the same.

4.2 PULSING LEDS: BASICS & EXISTING LITERATURE

One of the main focal points of this study is to investigate the effects of pulsing LEDs and so this section (4.2) will look at the existing literature on pulsing LEDs and detail the effects and implications of pulsing LEDs.

Pulsing a device is when, instead of being provided with a continuous electrical supply, the device is subject to short bursts of electrical energy punctuated by periods of no energy. Depending on the response time of the device and the frequency of the pulsing, the device could switch on and off with the energy pulses, as in this study; or the device could act as if subject to a continuous supply (if there is a slow response and a high frequency of pulsing) with a magnitude of the average electrical input. As mentioned, in this study the interest lies in pulsing the LEDs and so the aim is to have the LEDs switch on and off. Semiconductors typically have very fast response times so can be pulsed a high frequencies whilst still turning off and on.

A study carried out by Willert (Willert *et al.,* 2010), demonstrated that, when compared to the Xenon flash lamp, which can be used with a filter to produce near monochromatic light, the LED has a better response with less of a delay and a sharper drop off at the end of the pulse, as demonstrated in *Figure 4.6*.

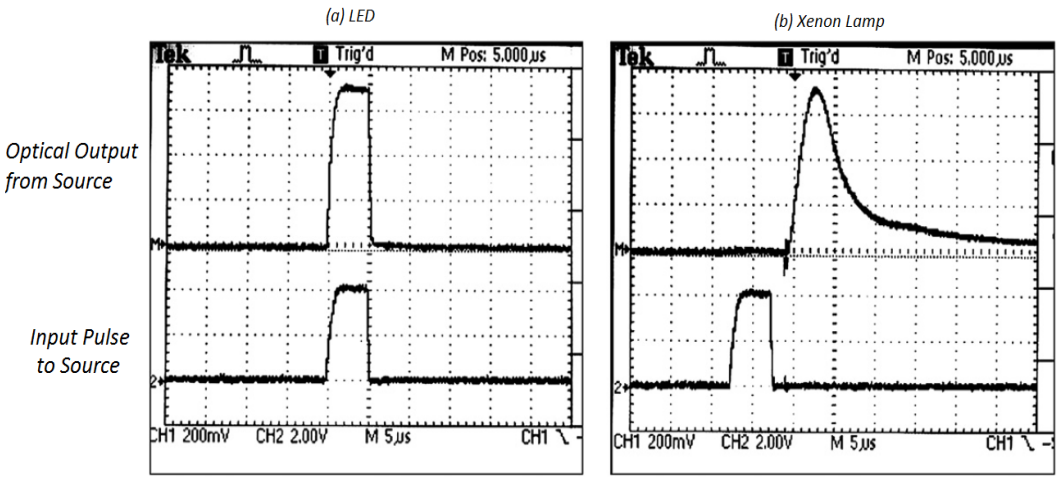

Figure 4.6: Labelled extract from study by Willert (Willert *et al.,* 2010) demonstrating the output optical response of an (a) LED compared with a (b) Xenon lamp when subject to an electrical input pulse of 5 µs.

When discussing pulsing, the most common application tends to be Pulsed Width Modulation or PWM. When a voltage source is pulsed fast enough, the output can appear as a DC voltage with an magnitude of the average voltage across the pulses; and so with PWM, the width of the pulse, or length of the 'on' time, will increase or decrease the average voltage, or effective magnitude, seen at the output. For example, a voltage source supplying 1 V, could be run through a pulsing circuit set to run at a 1 kHz frequency with a pulse width of 0.5 ms, meaning the source is on for 50% of the time and off for 50% of the time, i.e. 50% duty cycle. The average voltage would thus be 0.5 V as illustrated in *Figure 4.7(a).*

If the pulsing frequency is high enough, the pulsed signal can be thought of as a DC voltage signal with a magnitude identical to that of average. With this in mind, pulse width – or duty cycle- could then be either increased or reduced to alter the average output voltage achieved (as shown in *Figure 4.7(b)*), and thus the level of apparent DC voltage.

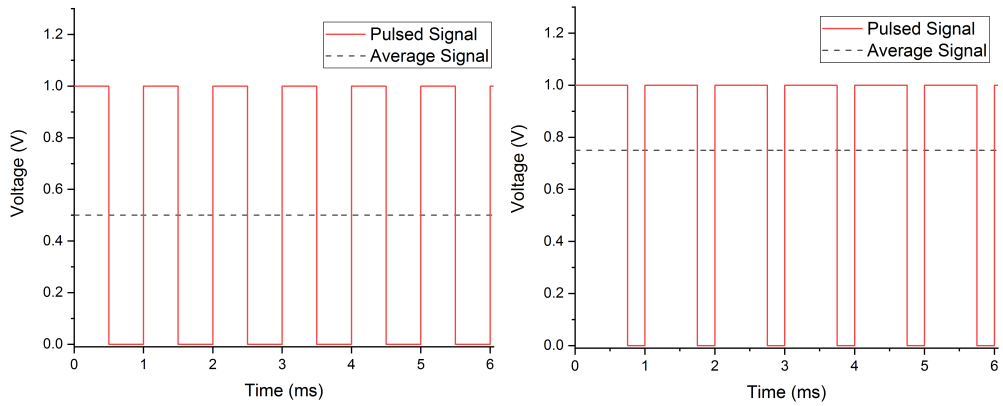

Figure 4.7: An illustration of PWM, showing a pulsed voltage signal and associated average voltage signal, for (a) a 50% duty cycle and (b) a 75% duty cycle. The idea being that if the pulsing frequency of the voltage signal is high enough, the pulsed signal can be thought of as a DC voltage signal like that of the average voltage signal demonstrated.

With this application allowing easy control of the average voltage, PWM is widely used as a method of controlling input power. It is more efficient than using variable resistors to control the amplitude of voltages produced since the resistor would just dissipate the excess power, whereas PWM allows you to supply only the power required.

PWM is also a useful way of reducing the operating temperature of LEDs. Due to the 'off' time during the pulsing, the LED has a short period to cool down and this can be highly beneficial in terms of performance.

There are two main efficiencies when discussing LED performance: Internal Quantum Efficiency; and External Quantum Efficiency. Internal Quantum efficiency is the fraction of the diode current that results in luminescence – i.e. how much of the current injected actually results in radiative electron-hole recombinations. External Quantum Efficiency pertains to how much of the light radiated actually leaves the semiconductor – with some recombinations being non-radiative meaning the electron energy is converted to vibration energy in the lattice atoms – effectively the energy is realised as heat (Schubert, 2006, pp.35). Photons from radiative recombinations however do not always leave the semiconductor with photons being reabsorbed by

the semiconductor or losses at the semiconductor-air boundary (Neamen, 2012, pp.650).

In LEDs, the temperature is a key parameter affecting the optical output. As the p-n junction of the LED increases in temperature the LED will become less efficient and the optical output will suffer. This is down to the recombination probability, which is related to temperature. Equal momentum for electrons and holes is required for a recombination producing a photon – however an increase in temperature results in momentum change of the electrons and thus less available electrons and holes for recombination. This leads to less radiative recombinations, more non-radiative recombinations effectively meaning that an increase in temperature results in a decreased optical output (Schubert, 2006, pp.54).

There are issues when pulsing an LED at high current. The first and main issue remains the same, increasing temperature of the p-n junction. This causes diminished output irradiance; too much heat can cause damage to the semiconductor junction itself in addition to output spectral shift (a change in output wavelength), as demonstrated by Serawiratne (Senawirante *et al.*, 2010) and Lin (Lin *et al.*, 2012) among others.

Research carried out Keppens (Keppens et al., 2010) demonstrated that a change in junction temperature of an LED, by as little as 40 K, can have a large effect on the spectral output. A graph shown in *Figure 4.8* shows the effects on spectral output both in terms of wavelength and flux density.

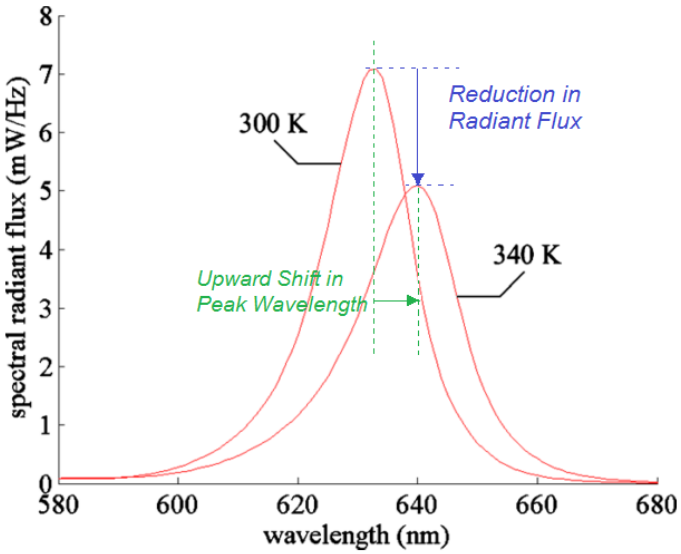

Figure 4.8: Graph comparing the spectral output of a single colour LED at two different temperatures demonstrating the effect temperature has on the peak dominant wavelength and the maximum output radiant flux produced. Extract from a study conducted by Keppens *(Keppens et al., 2010).*

At the higher temperature of 340K, the LED demonstrates a much lower radiant flux showing roughly a 30% decrease from approximately 7 $mWHz^{-1}$ to 5 $mWHz^{-1}$. Furthermore, an increase in temperature causes a shift upwards of approximately 10 nm in the peak dominant wavelength of the LED spectral output from approximately 630nm up to 640nm.

A similar type of wavelength shift is also demonstrated in the study previously referenced by Willert (Willert *et al.,* 2010), albeit with a change in forward current opposed to a direct change in temperature. The dominant wavelength of the spectral output is increased by almost 30nm with an increase in forward current from 50 mA to 55A and a decrease in pulse width from continuous to 1 μs, as demonstrated in *Figure 4.9*. Unfortunately, the variation has been carried out at the same time, so although the total charge ($Q = I \times t$) is kept the same for each pulse, there are still two variables changing, the magnitude of the forward current and the width of the pulse delivered.

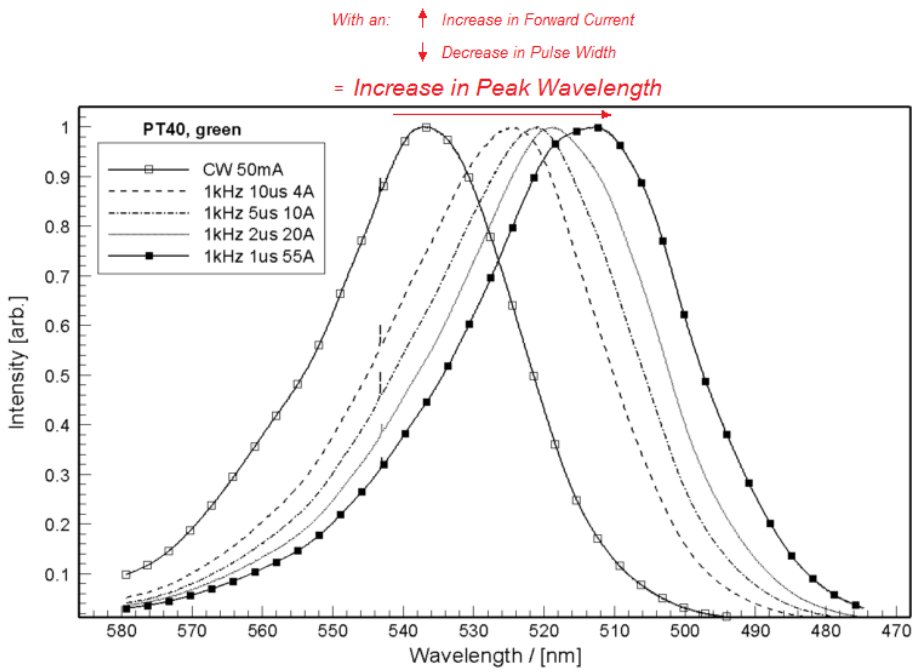

Figure 4.9: Graph of the spectral outputs of a green LED subject to increasingly short pulses of increasing levels of current demonstrating a shift in the peak dominant wavelength with the variations. Extract from a study conducted by Willert *(Willert et al., 2010).*

This means it cannot be completely deduced whether it was: current alone; pulse width alone; or the combination of both which caused the wavelength shift. Furthermore, the combinations of current and pulse width were chosen to be of similar integral power so as to assume a consistent average junction temperature, but this may not be the case, and if the temperature is varying this could also have an effect on the wavelength shift. The paper does however show that wavelength shift is possible, in particular when overdriving (applying more than the rated current) LEDs. It should be noted that Willert's study is not directly comparable to the present study as it looks at single pulses – opposed to longer duration periodic waveforms used to continually pulse used in this study. It remains, however of interest.

The paper additionally highlights how different colour LEDs, or technically speaking the different semiconductor materials, can be affected differently: where the orange LED demonstrated a wavelength shift of about 2 nm (Orange and red LEDs

are typically GaAsP or AlInGaP) opposed to the 30 nm wavelength shift of the green LED (Green and blue LEDs are typically InGaN).

These papers highlight possible issues working with LEDs in controlling predominantly the peak dominant wavelength which will be key in the 405 nm work undertaken in this study so temperature and rated current values will have to be carefully considered.

This study will be the first to undertake pulsed LED work specifically using 405 nm LED with several existing studies looking at pulsed UV LEDs or flashlamps.

4.3 FUNDAMENTAL PULSING LED EXPERIMENTS

This section will detail some rudimentary experiments looking at the effects of varying temperature, forward current and duty cycle on the peak irradiance as well as the spectral output of the LED(s) being used. These experiments are split into three main sections: The first looking at the design and build of the circuitry required to pulse the LEDs; the second focusing on experiments with a single 405 nm through-hole LED; and the third then moving onto to use a 405 nm 5x5 array of LEDs.

The experiments in the subsequent section (4.3) are mainly scoping experiments with a big emphasis on getting practical experience in working with LEDs the circuitry and the methods of control and optical capture. For this reason, each of the three means of optical capture (Photodiode, Power meter and Spectrometer) are used at different points as the requirement dictates. Whilst the results from each may not be directly compatible, they are still fit for purpose in each experiment.

4.3.1 PULSING ELECTRONICS

One of the mains objectives of this research is to investigate whether pulsing 405 nm LEDs could results in any advantageous results; either in terms of electrical efficiency or antimicrobial performance in comparison to continuous 405 nm light. Logically, the first step in being able to investigate this is to physically realise a method of periodically pulsing LEDs i.e. electronics to control the pulsing of LEDs for

experimentation. To do this a switch is required to switch the power to the LED on and off – and the transistor is the electrical component used which is driven by an input pulsing signal allowing for the power to be switch on and off to the light source.

The TTL (Transistor-Transistor Logic) input can be easily generated from a pulse generator (TGP110 model - 10MHz Pulse Generator; Thurlby Thander Instruments, UK), however this is the control signal. TTL is a simple logic signal either to indicate either 1 or 0 (on or off; High or Low) – effectively a square wave signal. This signal will then be used to control the switching on and off of a dedicated power supply that will match the power requirements of the LED(s) being used, thus providing sufficient power to operate the LED(s). The system should have a fast response time such that pulsing periodically up to the low kHz (0.1-5kHz) region is possible.

A study undertaken by Willert (Willert *et al.,* 2010) investigated pulsed delivery of light and illustrates the circuit used, which was able to produce periodic 1kHz signals with pulse widths down to 1µs. This circuit is shown in *Figure 4.10.*

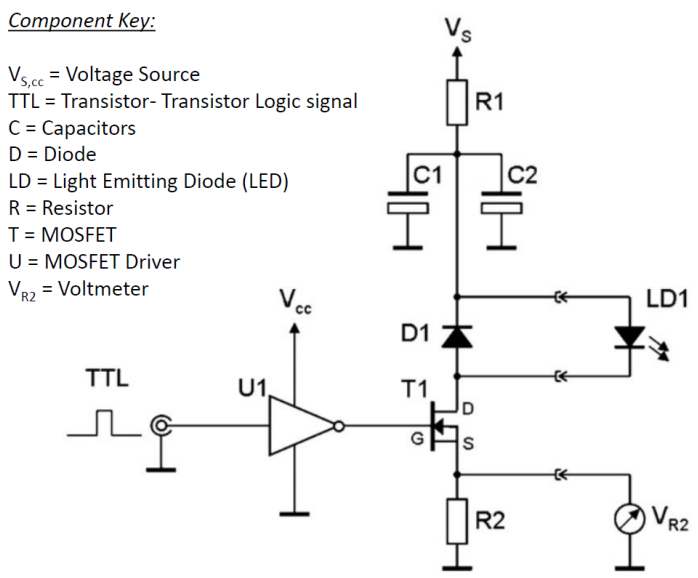

Figure 4.10: Extract from a study by Willert (Willert *et al.,* 2010) showing the Pulsing Circuit used to pulse high currents through LEDs with pulse width in the region of microseconds.

This circuit was used as a basis from which to work, however it was altered as required to suit the application to this study. Changes made were as follows;

- Only one capacitor was required so C1 was removed. This was because the power requirements and pulsing speeds were much lower than that of the Willert study and so the capacitor was not required to provide the initial level of power quickly.
- The diode D1 was removed because arrays have built in reverse protection – so this was removed as an element – albeit the reverse diode was present as part of the LED array.
- The Transistor was changed from a MOSFET (Metal-Oxide-Semiconductor Field-Effect Transistor) to a high-power capacity NPN BJT (Bipolar Junction Transistor). This change was one of convenience, due to the availability of suitable BJTs in the lab.
- The MOSFET driver circuit, U1, was removed and replaced by a resistor due to the replacement of the MOSFET – this section of the circuit was no longer required.
- The variable resistor V_{R2} was removed and the R2 was kept and used as a shunt resistor. R2 was very small and purely used as a means of electrical measurement to avoid the grounding effect cause by connecting the oscilloscope across the transistor.

This resulting circuit is shown in *Figure 4.11*.

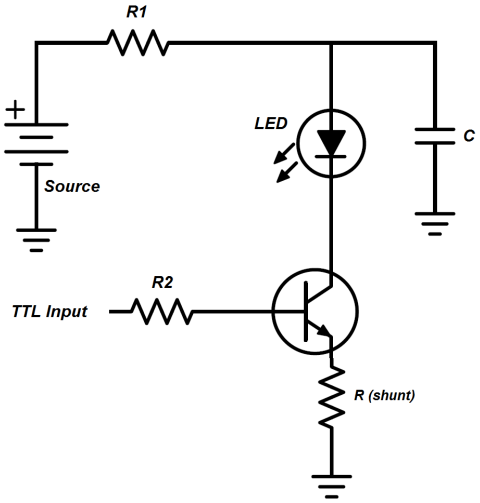

Figure 4.11: The resulting circuit after the changes were implemented to the circuit used in the study by Willert (Willert *et al.,* 2010). This is the circuit used for pulsing LED(s) throughout the study.

This worked as intended with the transistor acting as the on off switch for the LED. The capacitor charged up while the transistor was off, not conducting, and then when a high TTL was input to the base of the transistor, the transistor switched on and began conducting and so the current then flowed through the LED. The TTL signal thus controlled the LED switch on and off.

The components of the circuit then had to be tailored to the BJT and specific LED requirements. The voltage source initially used was a 30V – 1A bench power supply (Farnell Inst. Ltd. L30, UK). The resistor, R1, served two purposes: the charging resistor for the capacitor, C, allowing control of the time constant, τ, i.e. charging time; but more importantly a means of controlling the power through the LED itself.

A set voltage is dropped across the transistor when it is conducting, the rest of the voltage is split across the LED and R1, assuming for the moment R(shunt) drops a negligible amount of voltage. Depending on the I-V characteristic of the LED, a value for R1 can be calculated using Ohm's law to ensure the LED isn't drawing too much current.

The capacitor was left as is from the Willert *(*Willert *et al.,* 2010*)* study. The resistor, R2, ensures the current level is sufficient, such that the TTL input provides enough current to switch the transistor on and off. This was set as 1kΩ.

Finally, the shunt resistor, R(shunt), has a very small resistance of 1Ω and this is so the oscilloscope can be connected for electrical measurements. If the oscilloscope is connected directly into the circuit it has a grounding effect and alters the way to circuit operates so to counter this, the shunt resistor is introduced between the ground and component immediately before ground. This reading can then be used to monitor the voltage levels and used to calculate current through this branch of the circuit.

4.3.2 Effects on Peak Irradiance with Current & Duty Cycle Variations using Single 405 nm Through-Hole LED with no Temperature Control

This section uses the circuitry from *Section 4.3.1* and looks at the effects on the LED output when the duty cycle of the pulsing signal is changed.

4.3.2.1 Experimental Method

As stated, the circuit used in this experiment to pulse the LED is detailed in *Section 4.3.1* and again illustrated below in *Figure 4.12*. The LED used for this set of experiments is a single through-hole LED (LUMEX Quasarbrite 405 nm model) – specifically a 405 nm mode shown in *Figure 4.13.*

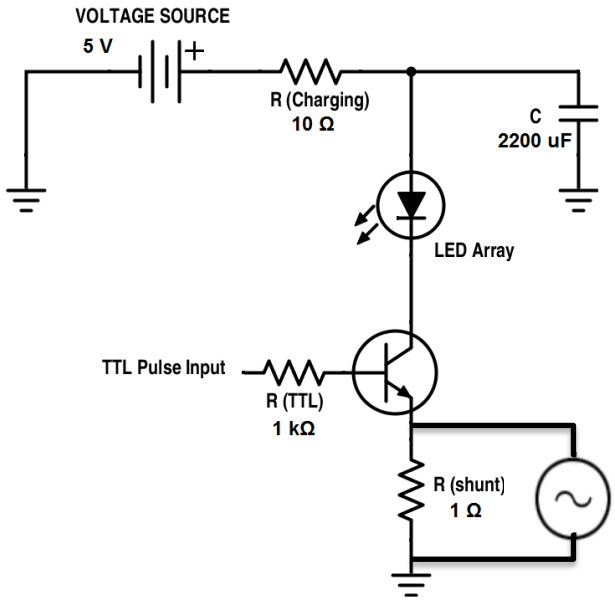

Figure 4.12: An Illustration of the circuit, detailing component values, used in this set of experiment for pulsing an LED or LED array.

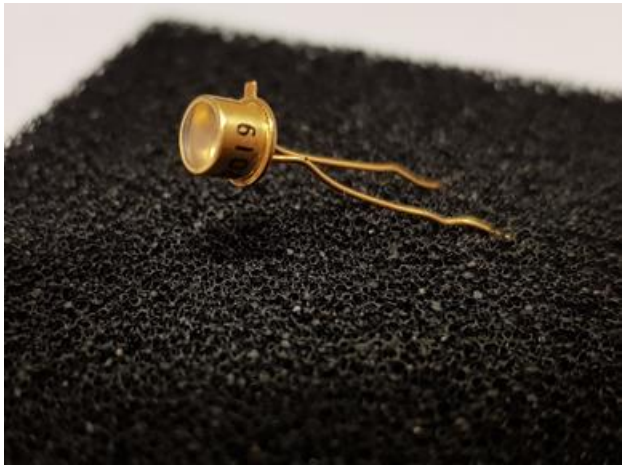

Figure 4.13: A photograph of the single through-hole LUMEX 405 nm LED used for experiments in *Sections 4.3.2 to 4.3.4.*

The Bench power supply was set at 5 V. The calculation had to then be carried out determine the resistance require for R1. The circuit is simplified for the calculation to 4 elements in series to look at the power draw of each component: the charging resistor; the LED; the transistor; and the shunt resistor.

From the LED datasheet, the typical draw is 50 mA at 3.7 V – meaning 50 mA is the total current required to flow through the circuit and will flow through all

components since they are in series. The transistor will see a 0.7 V drop and the LED will see a 3.7 V drop. From this, it can be deduce that the remaining 0.6 V, of the 5 V supplied from the source (Farnell Inst. Ltd. L30, UK), will be dropped across the shunt resistor and the resistor R1, the resistance value being calculated. Since the resistance and current of the shunt resistor are known, the voltage drop can be calculated using Ohm's Law.

$$V_{Shunt} = IR_{Shunt} = (0.05)(1) = 0.05V \qquad \textit{Equation 4.2}$$

Thus, the remaining voltage, V_{R1} = 0.55 V, is the voltage dropped across R1. With this, the resistance of the R1 can be solved for via a voltage divider calculation (a derivative of Ohm's Law) as shown below,

$$\frac{V_1}{R_1} = \frac{V_2}{R_2} \qquad \textit{Equation 4.3}$$

Where V_1 and V_2 are the voltage drops across resistor R_1 and R_2 respectively. When rearranged and V_{Shunt}, V_{R1} and R_{Shunt} values input, the value of the resistance require for R_1 was calculated as 11 Ω. This was rounded and R1 was chosen to be a 10 Ω resistor as displayed on *Figure 4.12.* The typical voltage and current were used to calculate an approximate value for resistor R_1 – because, the forward current will be altered by increasing and decreasing the voltage of the power supply and it would be unreasonable to recalculate a new resistance for every current reading.

With the circuit built and ready for operation, the photodiode circuit was employed, as described in Chapter 3, and aligned with LED as shown in *Figure 4.14.* The oscilloscope was used to observe the light captured by the photodiode from the pulsing LED, allowing for pulse width, amplitude and frequency to be read.

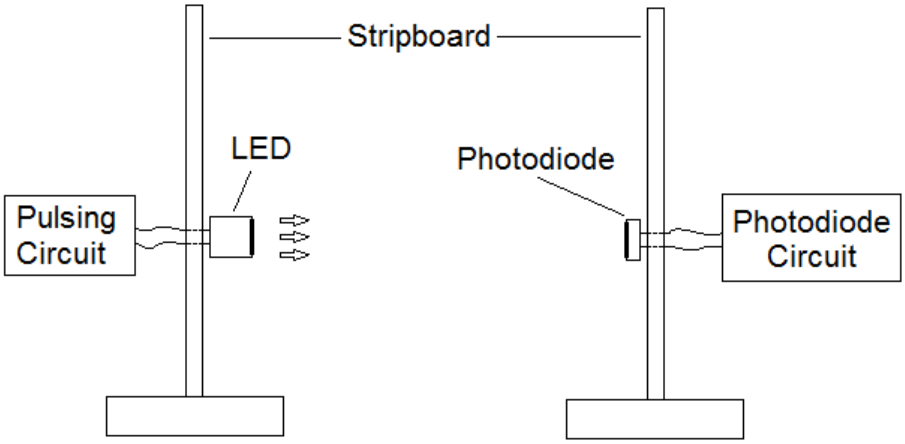

Figure 4.14: Illustration of the experimental setup in which the photodiode is aligned with the LED for capturing light pulses.

With the experimental setup in place, the input current sweep experiment was undertaken. There were 4 different runs of the experiment. Each run consisted of applying an incrementally increasing current to the LED (from 15 mA, in increments of 5 mA, up to 80 mA (60 mA for continuous)) and to monitor the peak output irradiance of the LED, captured by the photodiode. In the first run, the LED was run continuously at each current iteration and in the subsequent 3 runs the LED was pulsed at a duty cycle of 25%, 50% and 75% respectively, at a frequency of 1 kHz, at each current iteration.

4.3.2.2 Experimental Results

The experiment was carried out once using the photodiode to capture the output on the oscilloscope and from this the peak voltage could be measured which was directly related to the peak irradiance. The specific calibration for the relationship between voltage output and intensity was not carried out – however the relationship was stated to be linear with the rated bounds on the data sheet. The results are shown in *Figure 4.15.*

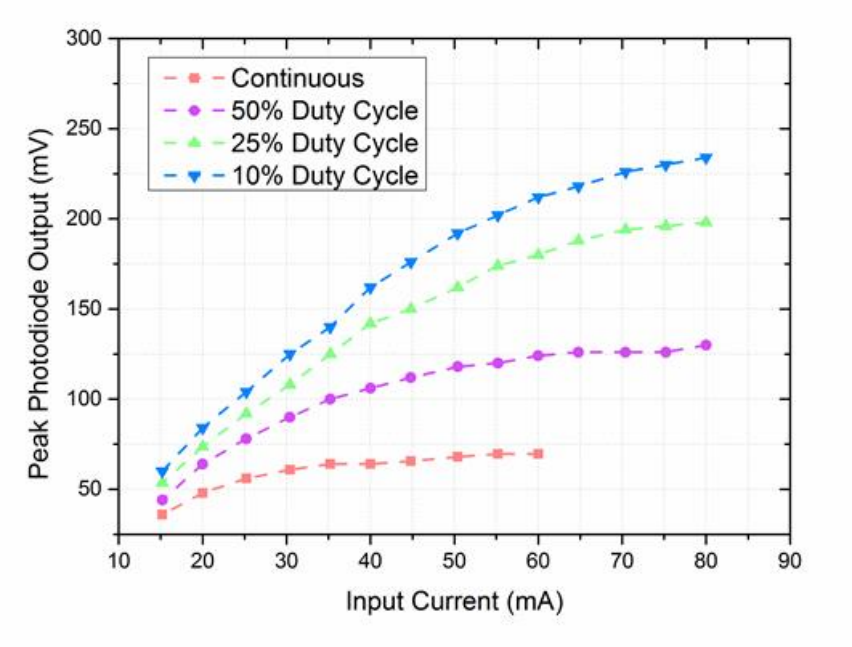

Figure 4.15: A Comparison of the peak irradiance of the 405 nm LED (LUMEX Quasarbrite) photodiode output, measured from the photodiode, at 4 different duty cycles across a range of currents. Lines are for visual guidance.

As can be seen from the graph, the 10% duty cycle demonstrates much higher peak output irradiance than the other three duty cycles. In reality, the 10% duty cycle pulsed LED is much dimmer than the other two duty cycles because it is off 90% of the time, however the experiment demonstrates that it actually produces the highest optical peaks. The oscilloscope displayed the periodic square wave and the peak was read using the measurement feature on the scope.

However, the temperature was not controlled in this experiment, and the legs of the LED were tangibly hotter when operated continuously, so much so that it was decided that after the 60 mA input current, it felt too hot to increase the current any further. It was clear that temperature differential across the experiments had to be addressed to ensure fair testing; and so, an experiment was carried out to quantify the significance of temperature variance on the LED output. This temperature variance was most likely the reason for the differences in peak optical output.

4.3.3 Investigating the Consistency of the LED Output from Switch On

The previous experiment in *Section 4.3.2* demonstrated sizable differences in the output irradiance between the different duty cycles when pulsed; however, the temperature was not controlled. This experiment was undertaken to investigate whether there is a settling time, due to the increase in the operating temperature, before the LED output, or peak irradiance, becomes consistent at a single level.

The hypothesis was; the first pulse in any case would produce higher peak irradiance before the temperature began to increase – which would in turn reduce the peak irradiance. After a number of pulse repetitions, the temperature, and thus the peak irradiance, would then reach a consistent value – however there would be a region of change from switch on, until the equilibrium point, or consistent temperature/peak irradiance, was reached.

4.3.3.1 Experimental Method

To investigate this, the photodiode and oscilloscope apparatus was set to capture a large number of pulses from the switch on of the power. The system was switched on pulsing at 100 Hz, as opposed to the 1 kHz in order to make it easier to capture the waveforms, at a 50% duty cycle, with the photodiode placed to capture the output purely to observe any settling time for the output to reach a consistent level.

4.3.3.2 Experimental Results

The experiment required multiple attempts in order to capture the waveforms from switch on. The waveform was capture manually on the oscilloscope, so the first graph, *Figure 4.16(a)* was easily captured, however the capture of the second figure, *Figure 4.16(b)*, over a much shorter time was more difficult.

(a)

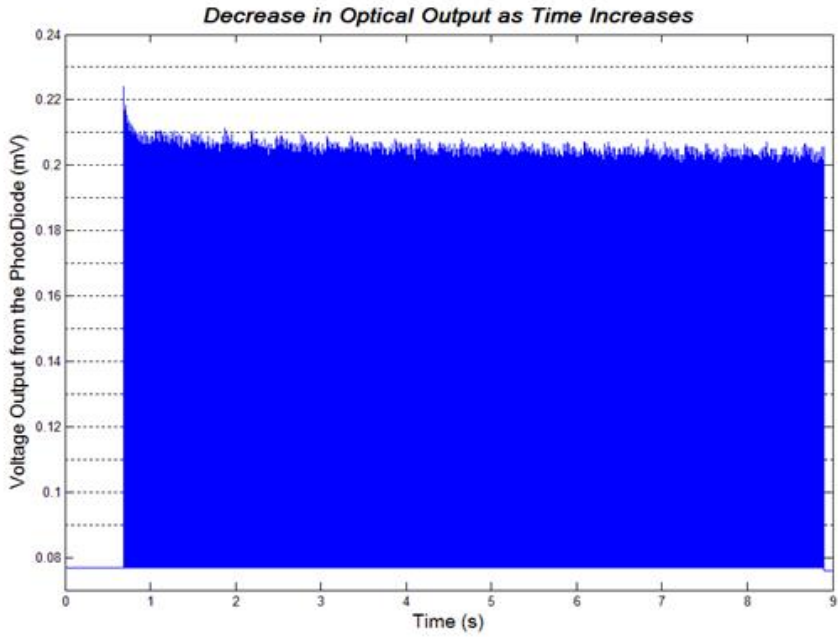

(b)

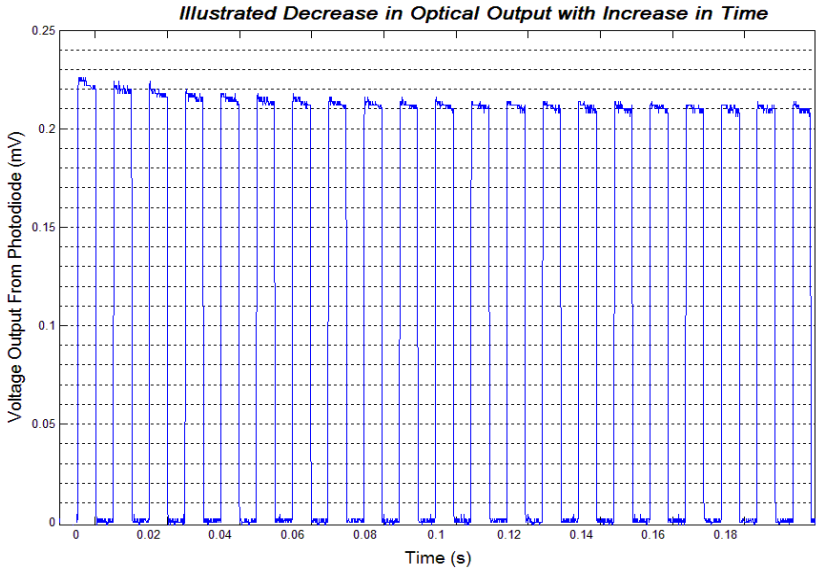

Figure 4.16: Photodiode Capture of the initial higher peak pulse before the optical output reaches equilibrium: (a) Zoomed out capture showing peak from initial switch on to reduced equilibrium; (b) Zoomed in capture showing individual pulses and the reducing peak irradiance.

Figure 4.16(a) shows the photodiode output over the first 8 /9 seconds from switch on and as can be seen, the highest peak irradiance for the pulsing is at the start and then reduces to an equilibrium point where the optical output appears at a

consistent level. *Figure 4.16(b)* shows an oscilloscope capture over a much smaller time frame and again demonstrates the reduction in peak irradiance with time.

The assumption is that this apparent reduction in the peak irradiance is due to the increasing temperature of the junction. The temperature increases after each pulse and the output level appears to drop until it reaches an equilibrium point and an average temperature is maintained – and thus a consistent peak irradiance. However, it can even be seen on each pulse itself in *Figure 4.16(b)*, that during the on time the output drops slightly from the start to the end of the pulse. This explanation appears to fit the results and the idea that high temperatures reduce the efficiency of LED operation (Schubert, 2006, pp.98).

Following this, the next question to be addressed was whether the 10% duty cycle would still outperform the continuous run, in terms of peak optical output, if the temperature was kept constant?

4.3.4 Effects on Peak Irradiance with Current & Duty Cycle Variations using Single Through-Hole LED with Temperature Control

This section repeats the experiment from *Section 4.3.2*; except in this instance, the temperature of the LED is monitored and controlled to ensure an adequate level of consistency.

4.3.4.1 Experimental Method

There was significant difficulty in attempting to monitor and control the temperature of the LED, specifically because the p-n junction is not accessible due to the housing, as can be seen in *Figure 4.13*. This meant the thermocouple (Kane-May KM340, UK) could only be placed on the leg of the LED as close to the junction as possible. Additionally, the temperature could only be controlled by cooling the legs under the assumption that the heat would conduct down the legs away from the

junction. For the active cooling, the Peltier module (GM200, European Thermodynamics Ltd, UK) was used. The Peltier module is a flat unit that transfers heat from one surface of one side to the opposite side effectively cooling one side, the rate being dependent on the input current. Reverse current will result in the opposite, i.e. heating. The LED legs were interfaced with thermal paste to allow maximum surface area contact, thus providing a large heat sink. In addition, the power meter was used to measure an average irradiance of 405 nm light output and then, with the duty cycle, the peak irradiance could be calculated, as discussed in *Section 3.2.1* in chapter 3. Again, the LED was pulsed at 1 kHz and the temperature was kept constant at 20 ˚C. The experiment was repeated in triplicate.

4.3.4.2 Experimental Results

The experiment was run, as in *Section 4.3.2*, across the 4 duty cycles and a range of currents and results are shown in *Figure 4.17*.

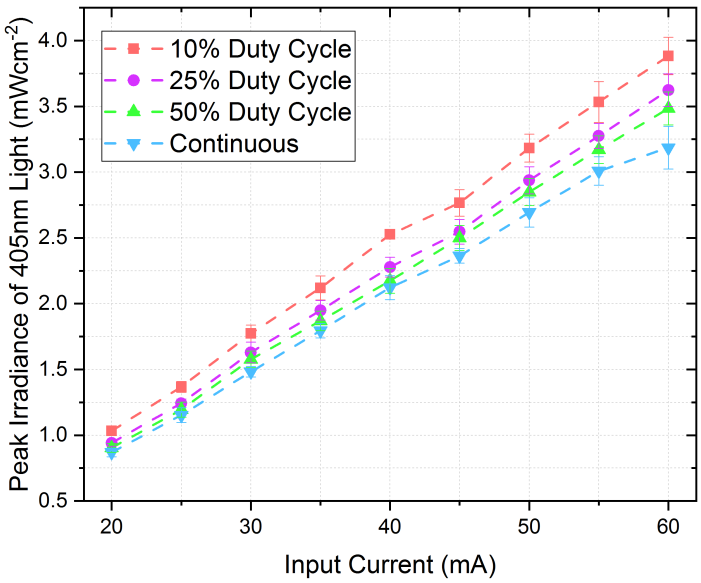

Figure 4.17: Comparison of the peak photodiode output, directly related to the irradiance, from a 405 nm LED pulsed at 1 kHz at 4 different duty cycles across a range of currents at a constant temperature of 20 ˚C. Each data point is the average of 3 data point with standard deviation error bars (n=3±SD). Lines are for visual guidance.

The results show quite a difference when compared with the previous experiment in *Section 4.3.2* (*Figure 4.15*). There appears to be a much more a linear

relationship with peak irradiance and forward current. There is however still a higher peak irradiance with the pulsed runs than the continuous run, and this difference increases with the forward current. From the graph, with 60 mA of forward current at the 10% duty cycle, the peak irradiance is roughly 0.7 $mWcm^{-2}$ higher (which is roughly 22% higher) than that of the continuous run at 60 mA.

This apparent increase in output however could still be attributed to a temperature differential between the continuous and pulsed experiments. There was difficulty in monitoring and controlling the temperature of the LED because of the shape of the LED housing, and so the only way to monitor and control temperature was via the LED legs. Although the temperature monitoring and control is not ideal, the experiments still illustrates the effect temperature can have on the LED output. There is a notable change in the LED output graphs, with the temperature controlled experiment showing values of irradiance across the range of duty cycles much closer together. Additionally, a more linear relationship seems apparent between current and irradiance can also be observed. For this reason, it was decided to repeat the experiment using a flat LED array, allowing the temperature to be monitored and controlled more easily.

4.3.5 Effects on Peak Irradiance with Current & Duty Cycle Variations using 5x5 LED Array with Temperature Control

The decision was made to repeat the experiment carried out in *Section 4.3.4*, using a flat, higher power 5×5 405 nm LED array (ENFIS UNO Tag array, ENFIS Ltd, UK).

4.3.5.1 Experimental Method

During this experiment, the same pulsing circuitry was used as described in *Section 4.3.1*. The LED used this time was a 5x5 array of 405 nm LEDs, ENFIS UNO

Tag array. This came as a flat square array, as can be seen in *Figure 4.18*, allowing for easier contact for more efficient and effective thermal management from the back.

Figure 4.18: The ENFIS UNO 405 nm 5x5 LED Tag array.

The LED array was mounted on the Peltier module and then subsequently onto an aluminium heat sink attached to a fan (with the LED array, Peltier module and heatsink all interfaced with thermal adhesive), with a thermocouple positioned for *in situ* temperature measurements. The full schematic is shown in *Figure 4.19*.

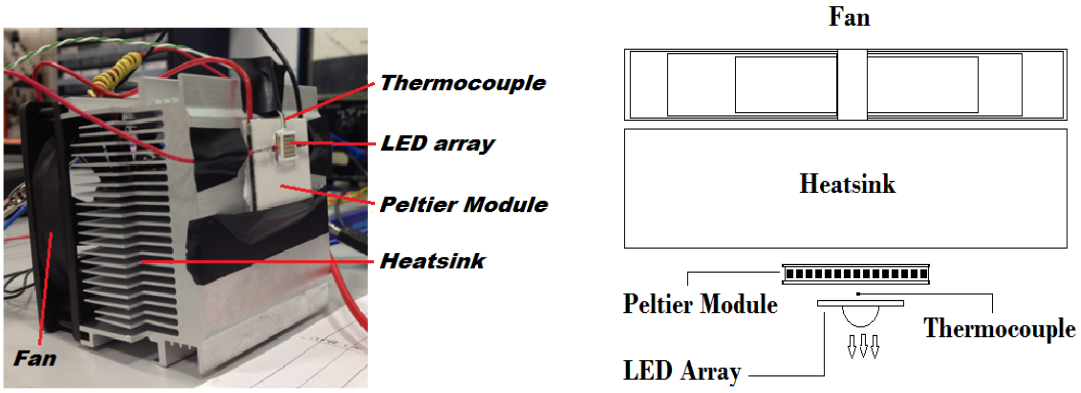

Figure 4.19: Picture of the experimental setup of the ENFIS 5x5 405 nm LED array mounted on the thermal management setup (left) and the schematic of the setup (right).

This LED configuration would permit easier measurement of the bulk temperature, and active cooling closer to the LEDs p-n junctions (as can be seen in *Figure 4.19*).

During the experiment, the array was subject to 3 input currents (20 mA, 40 mA & 60 mA) and this was repeated with each of the four duty cycles (10%, 25%, 50%, 100%) all at a frequency of 1 kHz. During each of these iterations, the temperature was monitored via the thermocouple and adjusted using the Peltier module to maintain a consistent temperature of 20 ˚C throughout the experiments.

Furthermore, it was decided that the calibrated spectrometer would be used during this experiment, Ocean Optic HR4000. In this setup the optical fibre captures the spectral output, and then upon analysis, the content of 405 nm ± 0.3 nm can be obtained, in units of $\mu Wcm^{-2}nm^{-1}$. However, as discussed in the chapter 3, *Section 3.2.2*, with the spectrometer it would be very difficult to capture single optical pulses at 1 kHz, and would require extra apparatus to do so, so the average spectral output was captured and then used to calculate the actual value of peak output, as detailed in *Section 3.2.2*.

Figure 4.20 shows this experimental set-up with the optical fibre and spectrometer set up to capture the optical readings this time. The distance between the LED array and the optical fibre was minimised such that the high current level of 60 mA did not cause saturation but was close enough in order to maximize the optical irradiance resolution achieved.

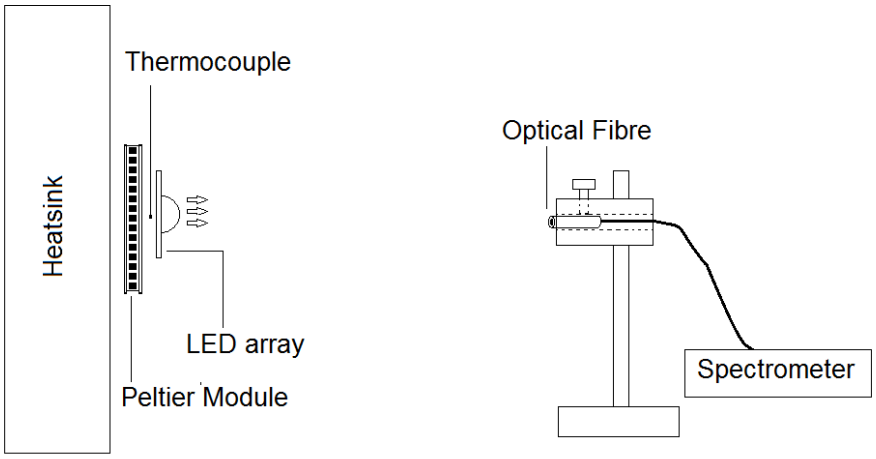

Figure 4.20: Experimental setup using the optical fibre and spectrometer to capture the output spectrum of the 5×5 ENFIS 405 nm LED array.

4.3.5.2 Experimental Results

The experiment was carried out with the array pulsed at the 4 duty cycles; at the 3 different current levels; with the temperature maintained at 20 ˚C; and the optical output capture by the spectrometer for each case. The results are shown in *Figure 4.21*.

As can be seen, there is a minor disparity between the different duty cycles with a maximum difference of approx. 6 $\mu Wcm^{-2}nm^{-1}$, at 60 mA between the 10% and continuous run. This experiment suggests that with this LED array, with the maintenance of constant temperature, the duty cycle appears to have little effect on the optical output. This could arguably be due to the maintenance of a consistent temperature throughout the experiment.

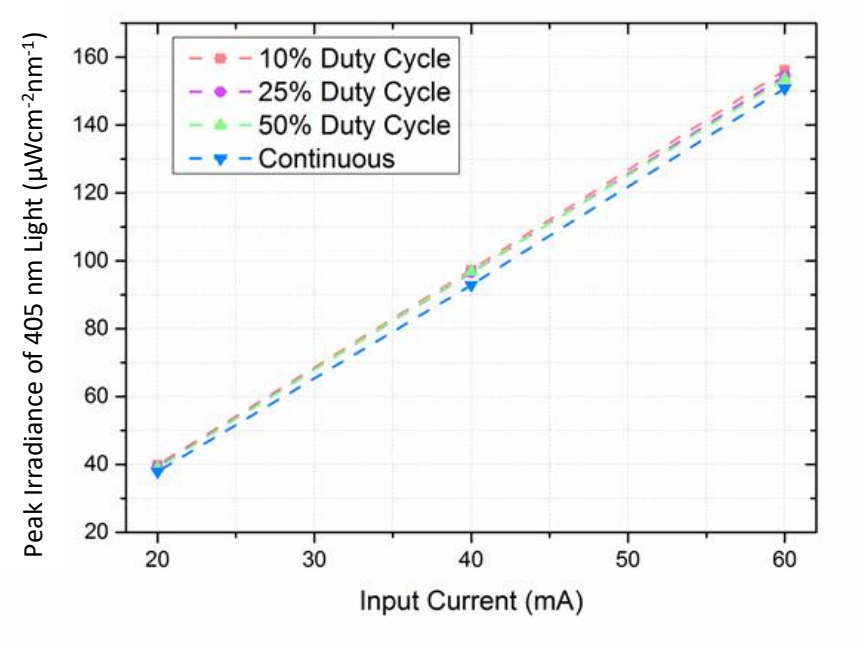

Figure 4.21: Experimental results showing the peak 405 nm light content at different duty cycles across a range of currents at a constant temperature of 20 ˚C. Lines are for visual guidance.

4.3.6 Investigation of Spectral Shift in the LED output; with varying temperature, input current & Duty Cycle

The output irradiance measurements collected by the spectrometer in the experimental system (*Figure 4.20*) are focused on the 405 nm light content at the specific peak in the spectrum. There is the possibility that if there was any spectral shift experienced as a result of increased temperatures, this may have an impact on optical measurements. Additionally, a study by Maclean (Maclean *et al.,* 2008) demonstrated that the antimicrobial efficacy is greatly affected by a shift in output wavelength out with the 400-420 nm range. To investigate this, an experiment was set up which measured the effect that temperature, forward current and duty cycle had on the wavelength output of the LED, i.e. the Full Width Half Maximum (FWHM) and the lowest wavelength of the FWHM (a measure of wavelength shift) emitted.

4.3.6.1 Experimental Method for Temperature Sweep

This experiment used the same LED array and test setup as that described in *Section 4.3.5.1*, using the ENFIS UNO tag array along with the thermal management apparatus and the spectrometer setup to capture the optical output. The pulsing frequency was 1 kHz for all experiments. The FWHM and lowest wavelength of the FWHM were used as measurement to deduce any spectral shift.

The Full Width Half Maximum is a measure of the spread of the spectrum. It is calculated by,

- First finding the peak or maximum optical output reading
- Calculate half of the peak
- Locate the 2 cross-over wavelengths of the spectrum at the half maximum
- The FWHM is the difference between the high and low cross-over wavelengths

The FWHM and lowest wavelength of FWHM are illustrated in *Figure 4.22.*

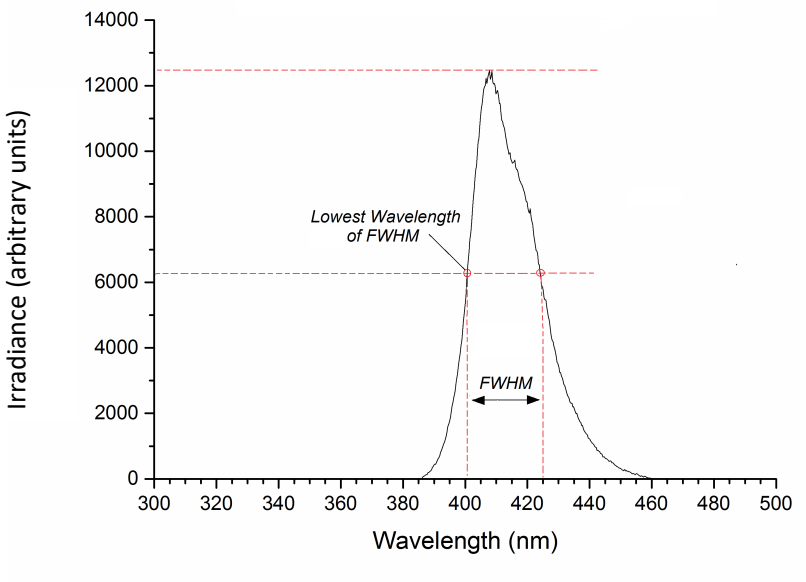

Figure 4.22: A visual representation of the Full Width Half Maximum (FWHM) and the lowest wavelength of the FWHM as used for Spectral comparison.

The first experiment was a temperature sweep, during which the current was set at 40 mA, the frequency at 1 k Hz and the duty cycle at 50%. The Peltier module

was used to alter the temperature incrementally from 6 ˚C up to 42 ˚C, looking at the effect on the FWHM and the lowest wavelength at every 4 ˚C increment.

4.3.6.2 Experimental Results for Temperature Sweep

The experiment was set up and a spectrum was captured at increments of 4 ˚C and the experiments were carried out in triplicate. The FWHM and lowest wavelength of FWHM were then extracted from the spectra. The results are presented in *Table 4.1*, with data being the average of three experimental readings with the accompanying standard deviation.

Table 4.1: Results of the temperature sweep on the FWHM and lowest wavelength of the FWHM. Each data point is the average of 3 data points and is presented with the standard deviation (n=3±std dev.).

Temperature (°C)	FWHM (nm) ± Std Dev	Lowest Wavelength at FWHM (nm) ± Std Dev
6	14.93 ± 0.78	400.63 ± 0.40
10	15.00 ± 0.53	400.67 ± 0.35
14	15.17 ± 0.57	400.67 ± 0.35
18	15.40 ± 0.53	400.67 ± 0.35
22	15.43 ± 0.35	400.77 ± 0.21
26	15.60 ± 0.20	400.80 ± 0.17
30	15.60 ± 0.26	400.93 ± 0.21
34	15.67 ± 0.31	401.00 ± 0.30
38	15.60 ± 0.40	401.17 ± 0.31
42	15.43 ± 0.49	401.53 ± 0.46

The results demonstrate an upward trend in both FWHM and lowest wavelength at FWHM suggesting that temperature does have an effect on the spectral output of the LED albeit a very small effect in this case. This is not to say that over a wider temperature range and with a different LED array, that the variation could not be more significant.

As discussed earlier in the chapter in *Section 4.2*, the study by Keppens (Keppens *et al.,* 2010), looked at this kind of work subjecting an LED to varying temperatures within an oven and the results agree - demonstrating an increased FWHM and a red shift in the wavelength albeit in a more substantial change. The

results are further confirmed by the study carried out by Senawiratne (Senawirante *et al.*, 2010) who also demonstrated that a red shift was experienced when the temperature of the LED was increased, via thermal heating and not through self-heating induced by increased current injection.

The temperature appeared to have less of an effect over the Spectral output than over the irradiance. The maximum shift in FWHM or lowest wavelength at FWHM was just over 1 nm. The application in the remainder of this study looks at 405 nm light as a means on inactivating bacteria based on a specific range of wavelengths, between 400-420 nm with maximum inactivation around 405 nm ± 5 nm (Maclean *et al.,* 2008).

The thermal management setup successfully provides the ability to monitor and control the LED bulk temperature to ensure as consistent a temperature as possible – however the results show minor fluctuations in the temperature should not have a major effect on the spectral output of the LED.

4.3.6.3 Experimental Method for Forward Current and Duty Cycle variations

This experiment used the same setup as that described in *Section 4.3.6.1*, the difference this time that instead of the temperature being varied it was kept constant at 20 ˚C. This experiment varied the input current and duty cycle of the pulsed LEDs. For each increment of forward current between 20 mA and 60 mA, the duty cycle varied across the four chosen values, 10%, 25%, 50% & 100%. At each of the specific current and duty cycle iterations the spectrum was captured using the spectrometer (Ocean optics HR4000, UK) and the FWHM and lowest wavelength of the FWHM were found.

4.3.6.4 Experimental Results for Forward Current and Duty Cycle variations

The full experiment was carried out in triplicate. The results and standard deviations of the FWHM are shown in *Table 4.2*.

Table 4.2: The results of the forward current sweep at different duty cycles on the FWHM. Each data point is the average of 3 data points followed by the standard deviation. (n=3±std dev.).

Input Current (mA)	FWHM (nm)			
Duty Cycle-	*10%*	*25%*	*50%*	*100%*
20	15.20 ± 0.17	15.16 ± 0.22	15.09 ± 0.12	15.19 ± 0.15
25	15.07 ± 0.06	15.20 ± 0.20	15.20 ± 0.17	15.23 ± 0.15
30	15.13 ± 0.06	15.07 ± 0.06	15.13 ± 0.06	15.27 ± 0.23
35	15.20 ± 0.17	15.07 ± 0.06	15.13 ± 0.06	15.30 ± 0.17
40	15.10 ± 0.10	15.10 ± 0.10	15.33 ± 0.12	15.43 ± 0.06
45	15.13 ± 0.12	15.10 ± 0.10	15.33 ± 0.12	15.47 ± 0.12
50	15.10 ± 0.10	15.13 ± 0.12	15.33 ± 0.12	15.53 ± 0.12
55	15.13 ± 0.12	15.13 ± 0.12	15.23 ± 0.15	15.53 ± 0.12
60	15.00 ± 0.00	15.10 ± 0.00	15.27 ± 0.12	15.60 ± 0.20

The trends for the FWHM in *Table 4.2* are much harder to discern. For the most part, the FWHM appears to increase with an increasing duty cycle, with a few exceptions in several of the intermediate points and the 20 mA iterations. With the current increase, the trends again are less consistent – it appears that for the 10% and 25% duty cycles, the FWHM decreases as forward current increases and the opposite for the 50% and 100% duty cycles. With this LED, the variation is very small however as before there is some variation and over a wider range and with a different colour or array, the variation could be more significant.

Holc (Holc *et al.,* 2010) undertook a study in temperature dependence of superluminescent LEDs (SLEDs), as discussed in *Section 4.2*. This experiment demonstrated a decrease in FWHM with an increasing forward current, which appears to match the trend observed in the 10% and 25% duty cycles. The study however uses SLEDs and does not pulse the SLEDs, so the results are not directly comparable.

Another study by Lin (Lin *et al.,* 2012) investigated temperature sensitivity of optical parameters in LED and one experiment appears to demonstrate that with an increasing forward current the FWHM also increases. This matches the trend for the 50% and 100% duty cycles however this experiment again did not use pulsed LEDs, so it is not directly comparable.

The results showing the effect on the lowest wavelength at FWHM with varying input current and duty cycle are shown in *Table 4.3.*

Table 4.3: Results of the forward current sweep at different duty cycles on the Lowest wavelength of the FWHM.

Input Current (mA)	Lowest Wavelength at FWHM (nm)			
Duty Cycle-	***10%***	***25%***	***50%***	***100%***
20	401.00 ± 0.00	400.99 ± 0.01	400.99 ± 0.01	401.08 ± 0.15
25	401.00 ± 0.00	401.00 ± 0.00	400.97 ± 0.01	401.03 ± 0.06
30	400.90 ± 0.17	400.97 ± 0.06	400.90 ± 0.17	401.00 ± 0.00
35	400.77 ± 0.12	400.90 ± 0.17	400.90 ± 0.17	400.97 ± 0.06
40	400.77 ± 0.12	400.80 ± 0.17	400.70 ± 0.00	400.87 ± 0.15
45	400.70 ± 0.00	400.77 ± 0.12	400.70 ± 0.00	400.80 ± 0.17
50	400.70 ± 0.00	400.70 ± 0.00	400.70 ± 0.00	400.70 ± 0.00
55	400.70 ± 0.00	400.70 ± 0.00	400.70 ± 0.00	400.70 ± 0.00
60	400.70 ± 0.00	400.67 ± 0.06	400.70 ± 0.00	400.70 ± 0.00

The numerical changes in the lowest wavelengths at FWHM in *Table 4.3* are small, however there appears to be a trend. The lowest wavelength at FWHM appears to decrease with an increasing current forward current for all duty cycles – suggesting movement in the spectra with increasing forward current. The duty cycle however doesn't appear to have a sizable effect on the lowest wavelength at FWHM – implying little movement in the output spectra. There is a very small redshift in the lower currents with an increase in duty cycle, however higher currents demonstrate no shift at all over the range of duty cycles.

A study by Bęczkowski (Beczkowski and Munk-Nielsen, 2010) investigated effects on spectral characteristics of PWM, when used as a light control strategy, and his results show that with an increase in duty cycle (or average current of PWM) the

wavelength undergoes a slight redshift, agreeing with the results in *Table 4.3*. The study by Bęczkowski (Beczkowski and Munk-Nielsen, 2010) however uses a different current range and green LEDs and the different colour LEDs have different material composition and thus behave differently.

Another study by Willert (Willert *et al.*, 2010), as discussed in *Section 4.2*, demonstrates a sizable spectral blueshift with an increasing forward current. The current range however is much bigger than that of the results in *Table 4.3 & 4.4* with a range of 50 mA to 55 A, opposed to the 20 mA to 60 mA range in this study. Furthermore, this is a green LED and the study itself demonstrates the difference in behaviour of different colour LEDs with an orange LED showing a much less dramatic shift over the current range.

As discussed, the remainder of this study requires wavelengths between 400-420 nm for bacterial inactivation (Maclean *et al.,* 2008). Therefore, any spectral shift caused by temperature or pulsing could be problematic. The results however demonstrate very small spectral shifts, all less than 1 nm, with changing duty cycle and forward current; and likewise, very small shifts with the implemented temperature control - so the LED output should be within the 400-420 nm range required for bacterial inactivation.

4.4 CONCLUSION

This chapter has detailed the basic operating principles of LEDs and has reviewed the issues surrounding their operation using continuous and pulsed input power. Initial work developed and tested a suitable LED pulsing circuit, which was then used in conjunction with different LED configurations (single through-hole LEDs and LED arrays), to conduct a range of fundamental experiments to establish key operating parameters. The experiments worked across a range of currents, and looked specifically at 10%, 25%, 50% and 100% duty cycles and the effects on LED behaviour for each. This study is the first investigate pulsed 405 nm LED, with

previous studies looking at PWM in differing colours of LED, pulsed UV LEDs but mainly pulsed UV using flash lamps.

The main objective of this chapter was to investigate how LEDs behave, specifically any change to the irradiance and output spectra, under pulsed conditions. The pulsing appears to have little effect on the irradiance, the major influencing factor being temperature. Likewise, there were minor amounts of spectral shift with temperature variation and even less with duty cycle and forward current variation – almost undiscernible from noise.

This suggests that with the thermal management in place to maintain a consistent temperature for all future experiments, the irradiance and spectral output of the LEDs should only undergo very minor and manageable changes so an acceptable level of consistency should be achievable.

CHAPTER 5
INVESTIGATING THE EFFECTS OF PULSED 405 NM LIGHT ON ANTIMICROBIAL EFFICACY

5.0 OVERVIEW

As discussed in the *Section 3.4*, 405 nm light has significant antimicrobial properties. Whilst Chapter 4 looked primarily at 405 nm LEDs and their behaviour: This chapter investigates the comparative antimicrobial efficacy of pulsed and continuous 405 nm light. The common bacterium *Staphylococcus aureus* is used throughout the chapter; and this bacterium is subject to 405 nm light in various different arrangements observing inactivation achieved in each case. The main objective of this chapter is to look for any benefits, either electrically or in terms of antimicrobial efficacy, of using pulsed 405 nm light for bacterial inactivation as opposed to continuous.

5.1 MATERIALS & METHODS

This section will provide details of the experimental set-up and protocols for microbial inactivation testing used in this chapter.

5.1.1 405-NM LIGHT SOURCE ARRANGEMENT

The light source used in this chapter was a 405-nm ENFIS Innovate UNO 24 (Photonstar Technology, UK), which is an array of 24 × 405-nm LEDs (*Figure 5.3(b)*). This LED array had a typical peak wavelength at 405 nm and a typical spectral spread of 16 nm, producing 5100 mW of radiant flux (over the spectral output). A graph of the spectral output is shown in *Figure 5.2*. The LED array was mounted on a PCB and on a heatsink with a fan, as can be seen in *Figure 5.1(a).*

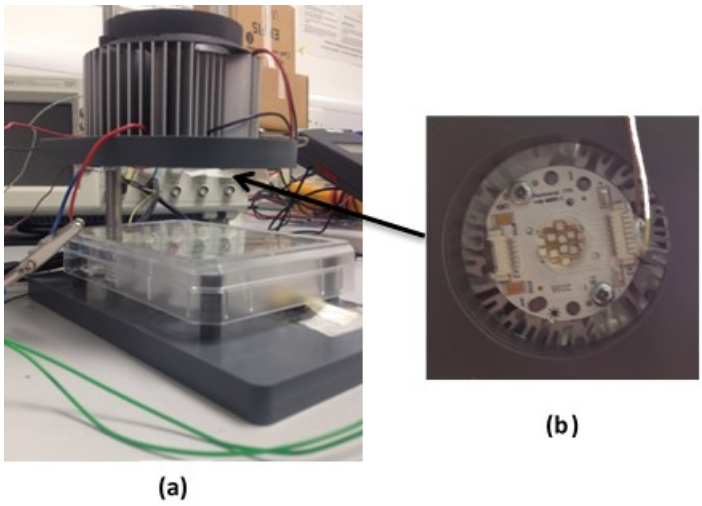

Figure 5.1: Experimental setup used to expose bacterial suspensions to 405 nm light. (a) Photograph of the LED within the experimental setup and (b) the LED array mounted on the PCB.

Due to this fixed arrangement, it was difficult, particularly with the thickness of the PCB, on which the LED array was mounted, to measure the temperature to monitor for any changes. For this reason, a photodiode (OSRAM, UK. Model: BPW34 B) was employed to monitor the level of 405 nm light irradiance throughout the experiment to ensure consistency.

For bacterial exposures, the array was mounted in a PVC housing, which held the array in a 10 cm above the sample plate (*Figure 5.3(a)*). The setup used is shown in *Figure 5.1(a),* with a closer look at the LED array mounted on the PCB in *Figure 5.1(b).*

As discussed in *Section 4.2* and demonstrated in *Section 4.3* in the previous chapter – temperature can have significant effects the operation of LEDs. As the temperature changes, the I-V characteristic of the LEDs also changes meaning that with a constant voltage, a change in temperature would cause a change in current drawn, which is directly related to the light output. For this reason, a means of monitoring and controlling the temperature of the LED array was required.

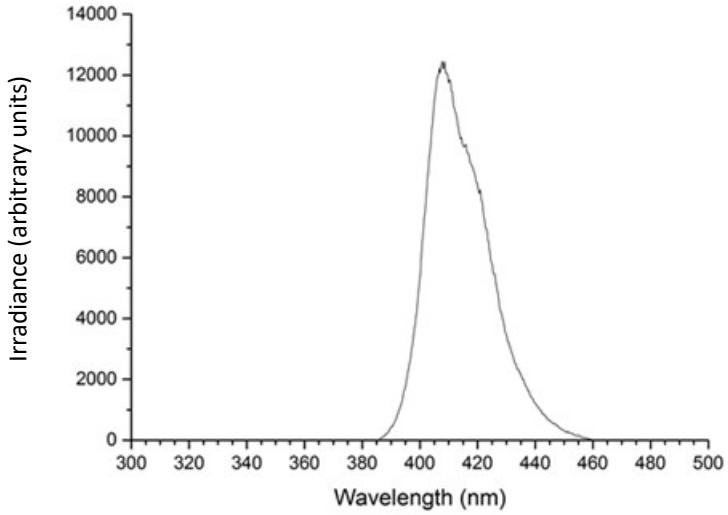

Figure 5.2: Output spectrum of the ENFIS Innovate UNO 24 as captured by the HR4000 Ocean Optics spectrometer setup (described in *Section 3.2.2*).

Consequently, the LED array was used in conjunction with a range of thermal management components, shown in *Figure 5.3*, in order to maintain a constant temperature throughout the experiments:

- A heatsink was attached to a 5V fan to aid with heat ejection.
- A Peltier module (which employs the Peltier effect whereby a heat is given out or absorbed as a current is passed across a junction between two materials), was used for active cooling, or heating depending on the polarity of the current. To do this, one side was attached to the LED array and the other attached to the heatsink.
- A thermocouple was positioned between the Peltier module and the LED array in order to monitor the bulk temperature of the LED array.

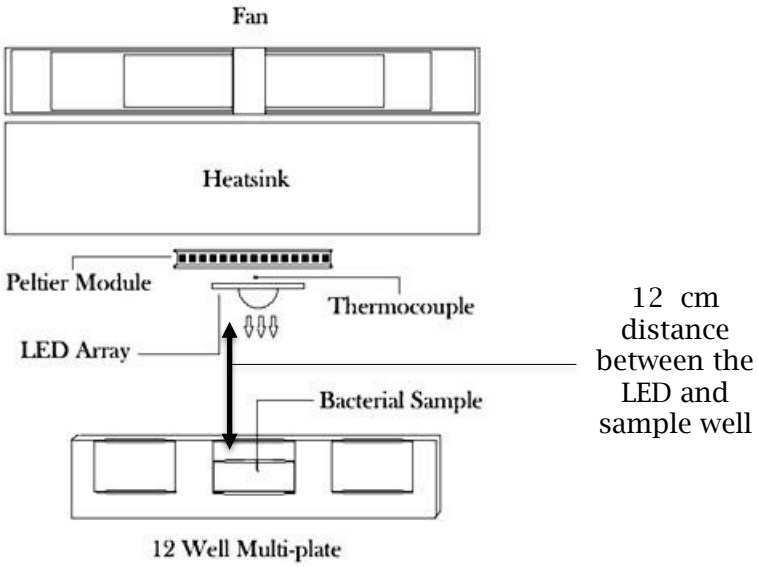

Figure 5.3: Cross-sectional view of the experimental setup showing the LED array system, and the layout of the thermal management components, used for the exposure of bacterial samples.

As the light source was an array of LEDs, they were inherently mounted in position on a PCB meaning that direct LED temperature could not be measured. However, in this case, the bulk temperature was sufficient to provide an indicator of the temperature and allow for some element of control via the Peltier module. The power input to the Peltier module was set at the start of each experiment to achieve the set temperature (24 ˚C), and the temperature was monitored throughout the experiment using the thermocouple, and the current input to Peltier module adjusted to ensure temperature consistency throughout the duration of each experiment. A thermal adhesive was used to uniformly interface the heat sink, Peltier module, LED array and thermocouple, ensuring good thermal conductivity (*Figure 5.3*). The temperature 24 ˚C was chosen to represent a common room temperature value.

5.1.2 ELECTRONIC CIRCUITS

As described in the previous chapter in *Section 4.3.1*, the pulsing circuit, shown in *Figure 5.4(a),* was used throughout this chapter to power the LED array.

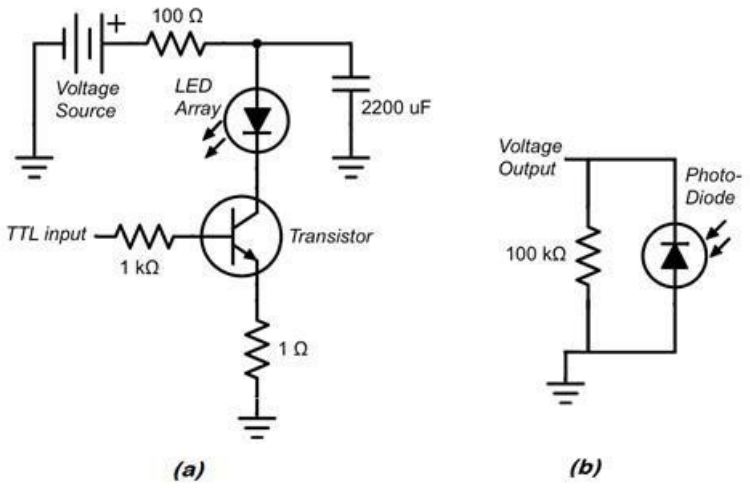

Figure 5.4: The electronic circuits used for pulsing and light measurement. (a) Circuit used to provide the input power, pulsed or continuous, to the LED array for bacterial exposures. (b) Circuit used to measure the voltage output from the photodiode to monitor the optical output of the LED array.

The electronic driving circuit took its input from a pulse generator that provided a 5 V transistor-transistor-logic (TTL) signal. An example of the pulsed TTL signal used to activate the transistor is shown in *Figure 5.5*.

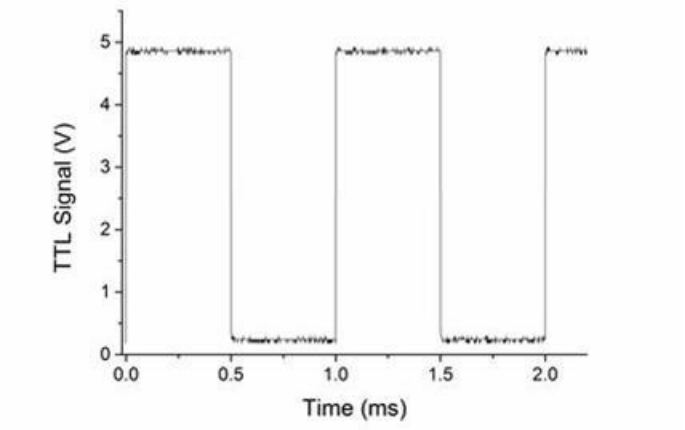

Figure 5.5: Illustration of the pulsed TTL signal used to control the switching operation of the LED array.

The frequency and duty cycle of this signal could be set from the signal generator. This signal is delivered to the base of the transistor which acts as a switch; when the signal voltage is high, the switch is closed, the transistor conducts and power is delivered to the LED array: and when the voltage is low, the switch is open, the transistor ceases to conduct and the LED array is disconnected from the power source. Thus, this TTL voltage signal determines when the LED source is on and off and therefore also determines the frequency and duty cycle of the optical pulses produced by the LED array.

The circuit in *Figure 5.4(a)* was used to operate the LED array either: continuously, by setting the signal generator to output a 100% duty cycle (effectively a 5V DC signal); or pulsed, by setting the generator to output a periodic square wave signal with 25%, 50% or 75% duty cycles. The system did not change for continuous and pulsed operation; the signal generator was just set accordingly to either the periodic square wave for pulsed operation or a DC signal for continuous operation.

For the voltage source, two L30 sources (Farnell Inst. Ltd.) were connected in series to supply a voltage in the range of 0-40 V. As mentioned previously, the setup was altered throughout the experiments in this chapter, and details are provided in the subsequent sections.

The optical output, as discussed in chapter 3 in *Section 3.2*, was captured through use of 3 methods:

- a photodiode (Model - BPW34 B, OSRAM), as shown in *Figure 5.4(b)* was used to capture the shape of the optical pulses.
- a radiant power meter (Model 70260, Oriel Instruments) and photodiode detector (Model 1Z02413, Ophir), calibrated at 405 nm, was used to measure the average irradiance in $mWcm^{-2}$.
- a spectrometer (Ocean Optics HR4000) was used to capture the light output spectrum.

The photodiode was used in conjunction with the oscilloscope (Tektronix TDS 2024) and because the modest size of the photodiode PCB, it was easily incorporated into the apparatus such that the output signal could be monitored continuously throughout all experiments to ensure that the duty cycle and irradiances of the optical pulses did not change over the course of an experiment.

Finally, voltage and current waveforms at different parts of the pulsing circuit could be monitored using the oscilloscope (Tektronix TDS 2024). The current through the LED array was indirectly measured by measuring the current across the 1 Ω shunt resistor connected between the transistor emitter and ground. The voltage across the shunt resistor was measured, and then using the known value of the resistance in conjunction with Ohm's Law (V=IR), the current being drawn through the shunt resistor and the LED array was calculated.

5.1.3 PREPARATION OF BACTERIAL SAMPLES

S. aureus was the bacteria used for all experiments in this chapter. As detailed in *Section 3.1.3.2*, bacterial suspensions were prepared at a density of approximately $1\text{-}3\times10^{3}$ $CFUml^{-1}$, and suspensions with this cell density were used for exposure experiments.

For all experiments (described in *Sections 5.1.4.1 - 5.1.4.4*), samples were taken at the start, during, and at the end of the treatment periods. In each experiment, 4 ml volumes of bacterial suspension (suspended in PBS solution) were pipetted into the well of a 12-well multi-plate, and placed directly under the light source, as shown in *Figure 5.3*. The bacterial test suspensions were then subjected to prescribed light treatment (as described in *Sections 5.1.4.1 - 5.1.4.4*). Non-exposed control suspensions were left under standard laboratory lighting conditions and sampled at identical time points.

After light exposure, samples were spread plated onto 90 mm nutrient agar plates in order to enumerate the surviving populations. Agar plates were incubated

for 18-24 hours at 37 ˚C After incubation, colonies were enumerated, and results converted to $CFUml^{-1}$.

All experimental data are an average of a minimum of triplicate independent experimental results, measured in duplicate ($n \geq 6$). Each sample was taken and plated in duplicate and the experiments repeated three times. Standard deviation (SD) was calculated and used for all data and graphical representation. Data sets were analysed using one-way ANOVA and Tukey tests with OriginPro 9.0.0 statistical software, with significant differences accepted at $P \leq 0.05$.

5.1.4 BACTERIAL INACTIVATION PROTOCOLS

A series of experimental protocols were established in order to investigate important aspects related to the use of pulsing as a delivery method for 405 nm light. These included:

- Investigating the effects of duty cycle and peak irradiance variation.
- Investigating how the frequency of the optical pulses affected the antimicrobial efficacy of 405 nm light.
- Investigating the effects of varying exposure length and duty cycle.
- Investigating pulsed-delivered dose and resulting bacterial inactivation.

Generation of this data allowed comparison of the efficacy of pulsed, compared to continuous, 405 nm light in terms of antimicrobial efficacy, and any electrical or optical efficiency improvements. Details of each of these protocols are provided in the following sections. It should be noted that for all the recorded doses – this is calculated from the power meter reading of the 405 nm light and so it the dose of all light around the 405 nm region produced by the LED array.

5.1.4.1 Investigating the effects of duty cycle and peak irradiance variation

This experiment investigated how the peak irradiance of pulsed 405 nm light affects the antimicrobial efficacy of the 405 nm light. The peak irradiance and duty cycle of the optical impulses were varied, in order to determine their effect on bacterial inactivation. The duty cycles used in this experiment were 25%, 50%, 75% and 100% (or continuous). The peak irradiance increased with the smaller duty cycles simultaneously to keep the overall dose and exposure time the same. The exposure length was chosen to achieve a significant amount of inactivation but still have a small count of CFU at the end of each exposure. The 24 ˚C temperature was chosen as a representative stand room temperature. The parameters and variables for this particular experiment are shown in *Table 5.1*.

During exposure, bacterial samples were taken at 30-minute intervals - 0, 30, 60, 90 and 120 minutes. Experiments were conducted in triplicate, with two samples plated at each of the sample time point (n=6).

Table 5.1: The parameters and variables concerning the operation of the LED array for the duty cycle and peak irradiance variation experiments detailed in *Section 5.1.4.1*.

Duty Cycle (%)	Peak Irradiance ($mWcm^{-2}$)	Pulsing Frequency (kHz)	Bulk LED Temperature (˚C)	Exposure Time (minutes)	Dose (Jcm^{-2})
25	64	1	24	120	115
50	32				
75	21				
100	16				

5.1.4.2 Investigating the effects of frequency variation

This experimental protocol was aimed to establish the effects of varying the pulse frequency of the light on the antimicrobial efficacy. The initial run of the experiment was carried out pulsing at 1 kHz, at a duty cycle of 50%, and at an average irradiance of 24 $mWcm^{-2}$ (48 $mWcm^{-2}$ peak irradiance) over a 60-minute exposure time. The 50% duty cycle was chosen as a middle ground between a lower duty cycle and continuous.

Over the course of the experiment the frequency was the only parameter varied across 5 different values. The experimental parameters for the experiments are shown in *Table 5.2*.

Table 5.2: The parameters and variables concerning the operation of the LED array for the pulsing frequency variation experiments detailed in *Section 5.1.4.2*.

Pulsing Frequency (kHz)	Pulse Width (ms)	Duty Cycle (%)	Exposure Time (minutes)	Bulk LED Temperature (°C)	Peak Irradiance ($mWcm^{-2}$)	Dose (Jcm^{-2})
0.1	**10**	50	60	24	48	86.4
0.5	**2**					
1	**1**					
5	**0.2**					
10	**0.1**					

The exposure time for this set of experiments was reduced to 60 minutes, compared to the 120-minute exposure in *Section 5.1.4.1* as the peak intensity required was lower, at 48 $mWcm^{-2}$ as opposed to 64 $mWcm^{-2}$, so the experimental time could be reduced. Bacterial samples were taken at 15-minute intervals – at 0, 15, 30, 45 and 60-minute time points at each of the given frequencies. The experiment was carried out in triplicate, with two samples taken at each sample time point (n=6).

5.1.4.3 Investigating the effects of varying exposure length and duty cycle

This experiment was undertaken to investigate what effect the length of the exposure has on the antimicrobial efficacy, with a constant overall constant dose and varying duty cycles. The experimental methodology was adapted from that used in a study by Li (Li *et al.*, 2010) who carried out a similar experiment using pulsed UV LEDs.

The duty cycle was altered over the four experiments, and the exposure length was then increased with the reducing duty cycle in order to keep the overall dose constant. All other parameters remained constant. The experimental parameters for the 4 iterations are shown in *Table 5.3*.

Table 5.3: The parameters and variables concerning the operation of the LED array for the exposure length experiments detailed in *Section 5.1.4.3*.

Duty Cycle (%)	Exposure Time (minutes)	Pulsing Frequency (kHz)	Bulk LED Temperature (°C)	Peak Irradiance ($mWcm^{-2}$)	Dose (Jcm^{-2})
25	80	1	24	30	36
50	40				
75	27				
100	20				

During the experiment, bacterial samples were taken at four equidistant points over the length of the exposure. Experiments were conducted in triplicate, with two samples plated at each sample time point (n=6).

Following this, it was decided that the experiments would be run again to achieve more bacterial inactivation and to assess if a larger disparity in the exposure

times would have any effects. This was done because the results were quite mixed and were hard to draw any trends or conclusions from so it was decided that a longer exposure might provide a clearer trend or conclusion. Everything was kept the same with the exception of the length of the exposures, which directly affected the dose. The new parameter values are shown in *Table 5.4.*

During the experiment, bacterial samples were taken at four equidistant points over the duration of the exposures. Experiments were conducted in triplicate, with two samples plated at each sample time point (n=6).

Table 5.4: The parameters and variables concerning the operation of the LED array for the second iteration of longer exposure length experiments detailed in *Section 5.1.4.3.*

Duty Cycle (%)	Exposure Time (minutes)	Pulsing Frequency (kHz)	Bulk LED Temperature (˚C)	Peak Irradiance ($mWcm^{-2}$)	Dose (Jcm^{-2})
25	120	1	24	30	54
50	60				
75	40				
100	30				

5.1.4.4 Investigating pulsed-delivered dose and resulting bacterial inactivation

This experiment was undertaken to investigate whether the bacterial inactivation achieved by pulsed light was proportional to the dose delivered, i.e. with a constant peak irradiance and exposure time, to investigate whether a duty cycle of 25% would result in 25% of the bacterial inactivation achieved with continuous exposure (100% duty cycle).

In this set of experiments, the exposure time was shortened to 40 minutes because the peak irradiance is lower than that of the experiments in *Section 5.1.4.1-5.1.4.3* with a peak irradiance of 29 $mWcm^{-2}$. All parameters for the four iterations of the experiment are shown in *Table 5.5.*

Table 5.5: The parameters and variables concerning the operation of the LED array for the pulsed-delivered dose variation experiments detailed in *Section 5.1.4.4*.

Duty Cycle (%)	Dose (Jcm^{-2})	Pulsing Frequency (kHz)	Bulk LED Temperature (˚C)	Peak Irradiance ($mWcm^{-2}$)	Exposure Time (minutes)
25	17.4	1	24	29	54
50	34.8				
75	52.5				
100	69.9				

Bacterial samples were taken at 0, 10, 20, 30 and 40-minute time points. Experiments were conducted in triplicate, with two samples plated at each sample time points (n=6).

During this set of experiments (detailed in *Section 5.1.4.4*), optical efficiencies were used to measure performance: optical efficiency being the *bacterial inactivation in* $CFUml^{-1}$ *achieved per unit of optical energy applied per* cm^{-2}. The electrical readings were used to measure the power consumption of the LED array, in addition to power consumption of the thermal management unit attached to the array and were measured using a VIVID power meter (model: GT-PM-04). This was then used in conjunction with the length of the exposure, to calculate the overall energy consumption.

5.2 RESULTS & DISCUSSION

This section details the results from the experiments outlined in *Section 5.1.4*. The results are either graphed or tabulated and any trends or conclusions to be drawn are outlined and discussed.

5.2.1 INVESTIGATING THE EFFECTS OF DUTY CYCLE AND PEAK IRRADIANCE VARIATION

This experiment investigated the effect of peak irradiance on the antimicrobial efficacy of the 405 nm light. The duty cycle was altered accordingly to maintain a consistent dose throughout the experiments. Four duty cycles and peak irradiances were tried as detailed in *Section 5.1.4.1*. Shown in *Figure 5.6* & *5.7* are the results from the 4 different duty cycles.

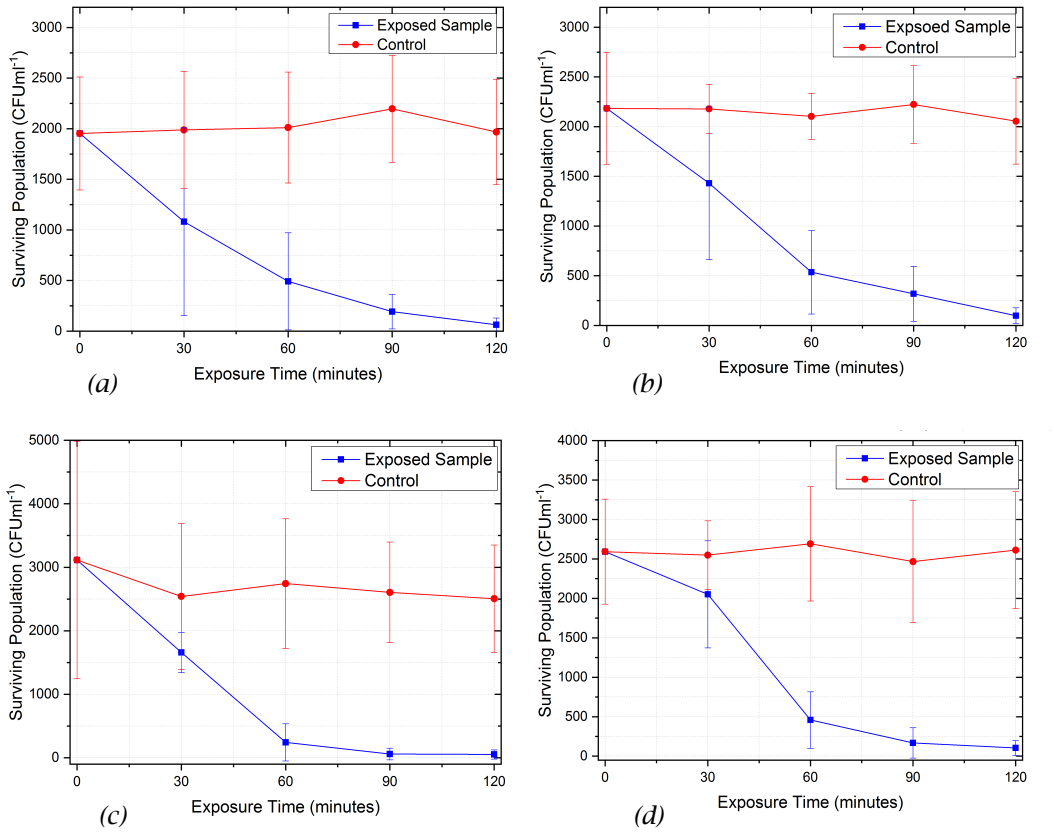

Figure 5.6: Graphs demonstrating the effect of peak irradiance and duty cycle variation on the inactivation of S. aureus when subject to pulsed 405 nm light. Bacterial suspensions were exposed to an average irradiance of 16 mWcm^{-2} over a 2 hour period using duty cycles of (a) 25%, (b) 50%, (c) 75%, and (d) 100%/continuous exposure. Data

points represent the mean values (n=6) of surviving population ± SD, standard deviation. Lines are for visual guidance.

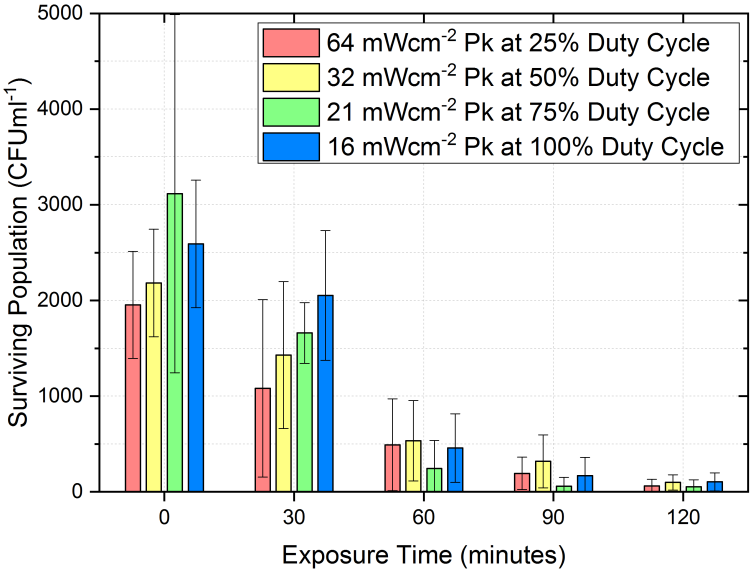

Figure 5.7: Comparison of the inactivation effects of pulsed 405-nm LED-light exposures with varying duty cycles (25%/50%/75% duty cycles) and continuous LED-light exposures (100% duty cycle) on bacterial suspensions of *S. aureus*. Irradiance was held constant at 16 mWcm^{-2}. Each data point is a mean value (n=6) ± SD, Standard Deviation.

For each of 120-minute exposures to the 405-nm light, the results showed just under a 2-log$_{10}$ reduction in the bacterial population from start to finish with all duty cycles. This represents a significant reduction in bacterial population ($p<0.05$) from the starting populations to the post exposure populations. The percentage reductions from start to finish - as demonstrated in *Figures 5.6(a), (b), (c) & (d)* - were approximately 97%, 94%, 98% and 96% for the 25%, 50%, 75% and 100% duty cycles respectively. The 75% appears to provide the highest level of inactivation at approximately 98% with 50% showing the lowest at approximately 94%. Subsequent statistical analysis showed that the difference between all the final post exposure bacterial populations is not significant, $p=0.6$. The graphs in *Figure 5.6* demonstrate the gradual reduction of the bacterial population over the exposure time, as expected, with each of the four duty cycles. The only apparent anomaly appeared at the 30-

minute time point with the 100% duty cycle exposure (*Figure 5.6 (d)*). There appeared to be a slower inactivation than the others at this point however by the 60-minute time point – all duty cycles appeared to show similar levels of inactivation. After statistical analysis however, no significant statistical difference ($p \geq 0.05$, ANOVA) was demonstrated between the bacterial populations of the different duty cycle exposures at the 30-minute time point. Additionally – as observed - no significant difference in bacterial populations was found between any of the duty cycles at any of the given time point. The non-exposed control samples showed no significant change in bacterial populations over the course of the experiments ($p \geq 0.05$).

These results suggest that with the same dose applied over the same time, with varying duty cycles and peak irradiances, antimicrobial efficacy does not appear to be affected, either beneficially or adversely, when applied in a pulsed regime or continuously.

Similar studies using pulsed UV LEDs have found differing results demonstrating advantageous effects when using pulsed UV LEDs compared with continuous (Wengraitis *et al.*, 2012; Li *et al.*, 2010). These studies, however, are not directly comparable with the experiments carried out in this study, due to the use of differing microbial strains and compositions; differing methods of pulsed radiation delivery; and importantly, different light wavelengths (UV and 405 nm), and consequently, differing inactivation mechanisms. Nonetheless, it is still of interest to discuss the results with respect to the potential benefits of pulsed light regimes and possible similarities.

In a study by Wengraitis (Wengraitis *et al.*, 2012*), Escherichia coli* biofilms were exposed to pulsed UV-C LED light, which varied in duty cycle, from 10%-100%, and frequency from 0.1-100 Hz. Results demonstrated a changes in sensitivity, defined by the authors as log kill per energy per unit area, log kills/mJcm^{-2}, between certain duty cycle. A 25% duty cycle pulse regime showed approximately a 2-fold increase in sensitivity over 50%, 75% and 90% duty cycles, with an increase from the approximate average of 2.5 log kills/mJcm^{-2} to 5 log kills/mJcm^{-2}. A further approximate 2-fold

increase in sensitivity was found with a 10% duty cycle pulse regime compared with the 25% regime with an increase from the approximate average of 5 log kills/mJcm^{-2} to 9 log kills/mJcm^{-2}. The continuous exposure result appears somewhere in-between the 25% result and the 50%, 75% and 90% results, but the authors stated that there were not a sufficient number of continuous wave samples to include these results in the statistical analysis. The results are not directly comparable with this study due to:

- the focus of the study being UV-C opposed to 405 nm light exposures;
- the use of biofilms compared to bacterial suspensions;
- the parameter variation was not identical to that of the experiment in this section (*5.2.1*) – with the lower duty cycles 10%, 25% & 50% being subjected to 250 µJcm^{-2}, 500 µJcm^{-2} and 1 mJcm^{-2} respectively and the remaining 3 duty cycles subject to 1.3 mJcm^{-2}. The dose was however kept consistent in the experiment in this section (*5.2.1*); and,
- the time of exposures was varied, with constant peak irradiance.

Nonetheless, the overall results of Wengraitis' study (Wengraitis *et al.*, 2012) show an inverse relationship with sensitivity versus duty cycle. Most inactivation per unit optical dose was achieved at lower duty cycles. This indicates that the inactivation or at least the efficacy of inactivation may not be entirely dose dependent. The results in this section (*5.2.1)* however show little difference in inactivation with a consistent dose suggesting a dose dependency relationship. From this result – dose dependency was further researched with 405 nm light and the investigation results are detailed in *Section 5.2.4.*

Another study by Li *(*Li *et al.*, 2010) demonstrated increased inactivation of *E. coli* (bacterium) and *Candida albicans* (yeast) biofilms with pulsed application of UV-A LEDs (Li *et al.*, 2010). The results indicated an improvement in performance whilst altering the duty cycle, with all duty cycles (25%,50%,75%) yielding significantly different ($p<0.05$) levels of inactivation. The continuous exposure demonstrated

91.5% reduction in the *C. albicans* population whilst the three pulsed exposures demonstrated significantly ($P<0.05$) higher population reductions all in excess of 99%. Similarly, with the *E. coli*, the pulsed exposures demonstrated inactivation of over 90% of the bacterial population with the continuous exposure demonstrating lower inactivation at about 85%. As mentioned, the results shown in *Figure 5.6 & 5.7* demonstrate over 90% reduction of bacterial populations however none reach an excess of 99% as demonstrated by Li (Li *et al.,* 2010) with the *C. albicans.* That being said, the statistical analysis suggested no significant difference ($p<0.05$) between any of the population reductions demonstrated in this study, i.e. *Figure 5.6 & 5.7* – whereas the study by Li (Li *et al.,* 2010) demonstrates significant differences in the percentage reductions. The paper illustrates error bars on the graphical representation of the data however fails to give a value for n so it is unclear how many repeats the experiment had – whereas the n=6 value for this study gave a high degree of variability leading to statistical analysis showing no significant differences.

While these results are not directly comparable with the present study since the focus is on UV-A and non-identical methods, they are indicative of the improved antimicrobial efficacy that may be achieved via pulsed UV light delivery.

As mentioned, the methodologies used in these UV-based studies (Wengraitis *et al.*, 2012; Li *et al.*, 2010) were different from the present experiment in that the exposure time and dose were varied in each experiment with constant peak irradiance.

5.2.2 INVESTIGATION INTO THE EFFECTS OF FREQUENCY VARIATION

In this experiment the frequency of optical impulses was altered. The bacterial inactivation achieved with five frequencies, ranging from 100 Hz-10 kHz, each with a 50% duty cycle, was compared; the results are shown in *Figure 5.8* & *5.9*. The average irradiance for each of the frequencies was 24 $mWcm^{-2}$ and each exposure was run for 60 minutes.

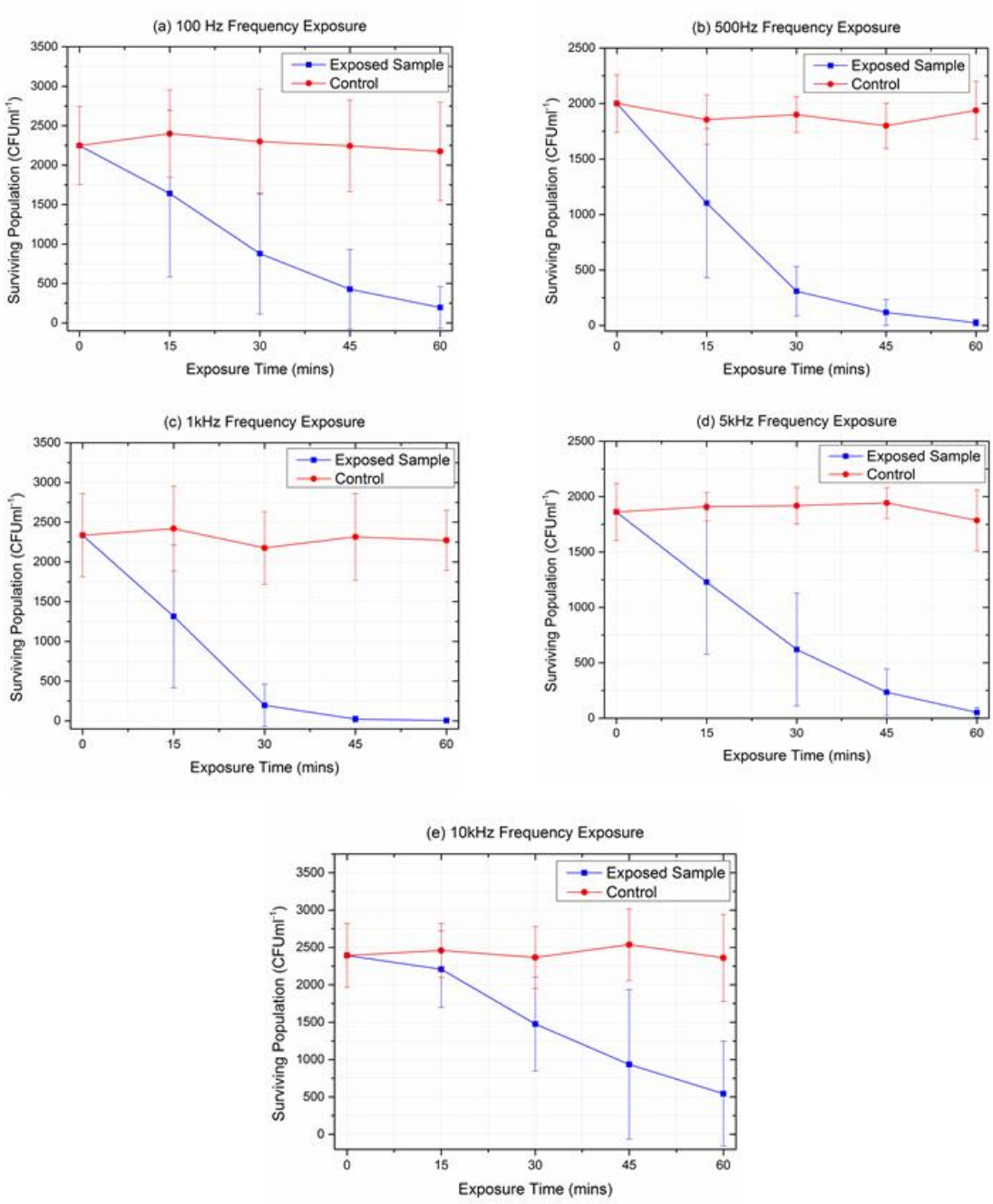

Figure 5.8: Graph demonstrating the bacterial inactivation achieved under pulsed 405 nm light at a 50% duty cycle across a range of 5 different frequencies. S. aureus populations in suspension over the course of a 1 hour exposure to 405 nm light at an average irradiance of 24 mWcm-2. Data points represent the mean values (n=6) of Surviving population ± SD, standard deviation. Lines are for visual guidance. (a) Results of the 100Hz Frequency exposure; (b) Results of the 500Hz Frequency exposure; (c) Results of the 1kHz Frequency exposure; (d) Results of the 5kHz Frequency exposure; and (e) Results of the 10kHz Frequency exposure.

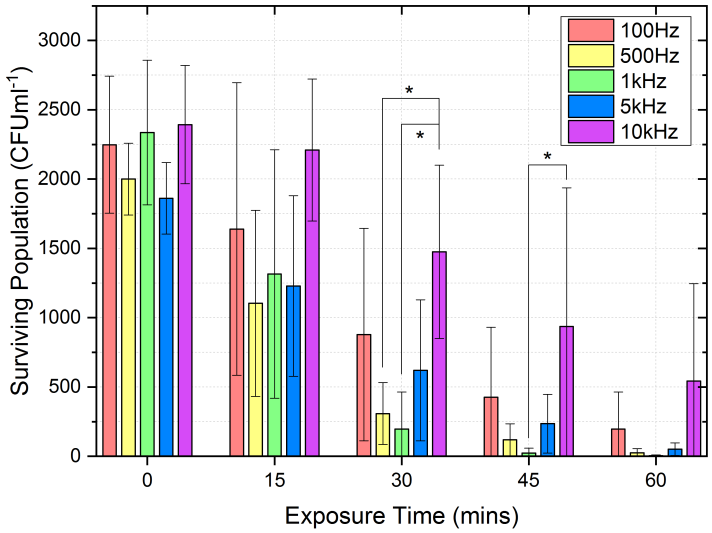

Figure 5.9: A comparison of the inactivation effects of 405-nm LED-light exposures with varying frequencies (100 Hz – 10 kHz) on bacterial suspensions of *S. aureus*. Each data point is a mean value (n≥6) ± SD, standard deviation. * indicates a significant difference ($p<0.05$).

Data in *Figure 5.8* shows that successful bacterial inactivation was achieved using all frequencies, and all show a significant difference ($p<0.05$) between the start and end populations. *Figure 5.8(a)* shows the 100 Hz frequency exposure results, which demonstrates a gradual decrease in population over the exposure time and approximately a 91% population reduction which is just a 1-$\log_{10}$ reduction. *Figure 5.8(b)* shows the 500 Hz experiment and demonstrates a similar downward trend over the exposure time however demonstrating a closer to a 98% reduction in population by the end – almost a 2-$\log_{10}$ reduction. *Figure 5.8(c)* illustrates the 1 kHz experimental results and the apparent best performance. This showed the same downward trend over the exposure time but demonstrated approximately a 99.8% reduction in bacterial population – almost a 3-$\log_{10}$ reduction in population. *Figure 5.8(d)* details the 5 kHz experiment and similarly downs a downward trend over the exposure time demonstrating a 97% population reduction, between a just under a 2-$\log_{10}$ reduction, from start to end. Finally, *Figure 5.8(e)* shows the results for the 10 kHz experiment which demonstrates the slowest and least inactivation. There is a downward trend although it appears slower than the other frequencies and across the same exposure time only demonstrates a reduction of 77% - which is less than a 1-$\log_{10}$ reduction.

There was a wide range of inactivation results with the 1 kHz experiment achieving the most inactivation by the end of the exposure showing almost 2.8-$\log_{10}$ reduction in population whilst the 10 kHz only demonstrated approximately a 0.65-$\log_{10}$ reduction over the same period with the same dose.

Statistically, there is no significant difference ($p \geq 0.05$, ANOVA) when comparing the bacterial inactivation achieved each of the specific time points at the 100 Hz, 500 Hz, 1 kHz and 5 kHz exposures. The 10 kHz exposure, however, shows statistically significant differences in the bacterial populations at the 30- and 45-minute time points, as illustrated on *Figure 5.9*.

Post-hoc analysis using the Tukey test showed that, after 30-minutes exposure, there was a significant difference between the inactivation at 1 kHz and 10 kHz ($p=0.002$), as well as between the inactivation at 500 Hz and 10 kHz ($p=0.0056$). At the 45-minute time point, the only significant difference in inactivation was found between 10 kHz and 1 kHz ($p=0.035$) with all other time points showing no significant differences ($p>0.05$) between the frequencies.

The non-exposed control samples appear to be consistent across the range of frequency experiments. Each shows no significant reduction from start point to end point ($p>0.05$). Additionally, when compared with each other, all the starting populations demonstrate no significant differences ($p>0.05$) and likewise all 60 minute time points, when compared, show no significant differences either ($p>0.05$).

The only differing result is that of the 10 kHz frequency, which appears to achieve a slightly lower level of inactivation across the 60 minute period (despite statistical analysis deeming no significant difference). Observably the 15-, 30- and 45-minute time points appear to have less kill than other frequencies – with statistical analysis showing significantly less kill than 1 kHz at the 30 and 45 minute time points and 500 Hz at the 30 minute time point, suggesting a possible lag in inactivation kinetics at 10 kHz.

Considering the inactivation mechanism, it was initially hypothesised that a critical number of photons must be absorbed within a specific timeframe to achieve

maximum production of the radicals necessary for inactivation. Building upon this theory, it was postulated that perhaps the pulses of light at 10 kHz (at a 50% duty cycle) with a pulse width of 50 μs are too short, resulting in reduced photon uptake by the intracellular porphyrins, non-optimal radical production and hence a reduced rate of inactivation. The second law of photochemistry (Stark-Einstein Law) however states that light absorbed need not necessarily result in a photochemical reaction, but if it does, only one photon is required for each molecule effected (Smith and Hanawalt, 1969, pp. 5). This suggests that each molecule only needs to absorb one photon of 405-nm light, and so the idea of reduced photon uptake per molecule causing non-optimal radical production seems less likely. However, if the assumption is made that more than one of the target porphyrin molecules are present inside the bacterial cells, it could be suggested that a certain number of these porphyrins must absorb photons to induce sufficient ROS production and associated oxidative damage, to cause complete inactivation of the bacterial cell, below which the bacterial cell can still survive or take a longer time to become inactivated. Hence, with a short pulse of photons, it may be the case that not enough porphyrins in some bacterial cells are being excited which could result in slower death of the cells or a reduced rate of inactivation, which is seen in the results displayed in *Figure 5.8* & *5.9*.

Although photons are discussed above the number of photons of flux density is an interesting note. For 405 nm light of 24 $mWcm^{-2}$ – the flux density of photons per cm^2 per second passing through the bacterial suspension would be approximately 1.17×10^{36}. This is an astronomical number of photons – and it is just to put the discussion point of single photons into context and could be of interest for future work if looking at or modelling photon interaction with microbial cells.

The start and end populations of the bacteria for the 10 kHz exposure appear to be higher than the other frequency end populations show no; statistical analysis of the end populations suggested however that over the full exposure period the inactivation achieved at 10 kHz was not significantly different ($p>0.05$) when

compared with the other frequencies. Additionally, when looking the inactivation kinetics, it appears that inactivation at the intermediate time points occurred at a slower rate. In the case of each frequency, the number of photons applied over the exposure time is the same in theory, given the dose for each of the different frequency exposures is constant; and so the only difference is the pulsing frequency, which in essence is the periods of 'on' and 'off' time the sample is exposed to. It could be that the shorter periods of photon exposure allow the bacterial cells to activate cellular defenses, which could slow down the rate of reaction possibly explaining the reduced rate of inactivation for the 10 kHz exposure. Again, further investigation would be required to confirm this theory, but the current results indicate that, for the most part, frequency appears to have little effect on inactivation.

Li (Li *et al.*, 2010) carried out similar experiments investigating pulsed UV-A LEDs and their inactivation effects on microbial biofilms. The experiments were carried out using biofilms of both *C. albicans* and *E. coli*, and the frequency range was from 0.1 Hz to 1 kHz and demonstrated that the inactivation rate significantly increased ($p<0.01$) with frequency up to 100 Hz – however the 1 kHz demonstrated a reversal in the trend. Results with *C. albicans* showed microbial inactivation of approximately 99.25% for the 100 Hz pulsed exposure, with the continuous exposure yielding approximately 94% inactivation. Similarly, *E. coli* biofilms showed bacterial inactivation of approximately 97% for the 100 Hz pulsed exposure, with the continuous exposure only achieving approximately a 90% inactivation. The present study however demonstrates a range of bacterial population reductions from approximately 77% to 99.8% across the 10^2-10^4 Hz frequency range, hinting at a possible lag in inactivation kinetics at the highest frequency. It demonstrates a similar trend, showing 91% reduction at 100 Hz, increasing to 98% reduction at 500Hz, increasing to the maximum of 99.8% reduction at 1 kHz, then reducing after 1 kHz to 97% reduction at 5 kHz and finally 77% reduction at 10 kHz. The same trend appears however the frequencies at which the maximum inactivation occurs is different. Additionally, statistical analysis showed no significant differences between

the final bacterial populations in the present study due to high levels of variability whereas the study by Li (Li *et al.,* 2010) demonstrated significant differences between the remaining populations. Again, the experiments are not directly comparable, given the difference in the frequency ranges used and the differing antimicrobial mechanism between 405 nm and UV light. The study by Li (Li *et al.*, 2010) however does suggest that frequency can have an effect, and although the statistic suggest that there is no significant difference – the number appears to suggest that there could be an effect and the study by Li (Li *et al.,* 2010) appears to concur.

The study by Wengraitis (Wengraitis *et al.*, 2012), which used UV-C LEDs, compared different duty cycles and frequencies and their effect on inactivation of *E. coli*. The authors found that varying frequencies in the range from 0.5 Hz to 100 Hz had a much less distinct effect on inactivation than that of the duty cycle. There was only a significant difference found between the 1 Hz and the 100 Hz experiments, with the 1 Hz demonstrating improved sensitivity when compare with the 100 Hz experiment. All other frequencies showed no significant difference. The trend appears to be a decrease in Sensitivity (author defines sensitivity as log kills per $mJcm^{-2}$ of irradiance) with an increase in frequency which is the opposite of the finding demonstrated by Li *et al.* – however, the statistical analysis only demonstrated one significant difference between the 1 Hz and 100 Hz exposure with the rest showing no significant difference, not unlike the present study, which in fact demonstrates no statistically significant difference between start and end.

The experimental results from Wengraitis (Wengraitis *et al.*, 2012) are not directly comparable the present study or the study undertaken by Li (Li *et al.,* 2010*),* not only because of the difference in wavelength of radiation used, but the difference in the frequency ranges used, organisms used and culture of said organisms. S. Wengraitis *et al.* (Wengraitis *et al.*, 2012) experimented with frequencies from 0.1-100 Hz and Li *et al.* (Li *et al.*, 2010) used 0.1-1000 Hz, with varying degrees of resolution. The frequencies in the present study were higher overall, spanning from 100 Hz – 10 kHz, and this range was chosen bearing in mind possible practical antimicrobial

applications. One of the main benefits of the use of 405-nm light for disinfection is that it can be used safely in the presence of humans and thus it would be desirable to design a system with comfort in mind, i.e. to not have a perceivable pulsing 405 nm light as would be apparent with the lower frequencies, but to have higher frequency pulsing which appeared continuous to the human eye.

5.2.3 INVESTIGATING THE EFFECTS OF VARYING EXPOSURE LENGTH AND DUTY CYCLE

As mentioned in *Section 5.2.4.3*, The design of these experiments was based on the experimental protocols used in the studies by both Li (Li *et al.*, 2010) and Wengraitis (Wengraitis *et al.*, 2012), which varied the microbial exposure times.

There is a consideration that over a longer exposure time, the damaging radicals produced by the photoexcitation process could have more time to interact with, and cause oxidation of, the exposed cells, thus over an extended period of time this could increase the overall inactivation achieved. It is for this reason that the general protocol for the experiments in this chapter was to ensure that all exposure times were kept constant to ensure fair comparison, however, this experiment was specifically set up in order to investigate this technical consideration. The experimental protocol was fixed to investigate the effect of applying the same dose, at the same peak irradiance with differing duty cycles and exposures times similar to that Li (Li *et al.*, 2010) and Wengraitis (Wengraitis *et al.*, 2012), in an effort to demonstrate any differences exposure time could have. As stated in *Section 5.2.4.3*, for these experiments, samples were taken at the start and end exposure points only. Results are shown below in *Tables 5.6* & *5.7*.

Table 5.6: Experimental results of the 20-80 minute exposure length experiments investigating the effects of the varying the length of exposure and duty cycle on the antimicrobial efficacy, with peak irradiance and dose kept constant at 30 $mWcm^{-2}$ and 36 Jcm^{-2}, respectively. Each population represents an average of 6 samples, n=6. Each of the four duty Cycles demonstrated a significant difference (P<0.05) between start and end population as denoted by *.

Duty Cycle (%)	Starting Population ±Std Dev ($CFUml^{-1}$)	Post-exposure Population ±Std Dev ($CFUml^{-1}$)	Percentage Reduction (%)	Exposure Time (min)
25	2075 ± 321	1128* ± 785	45.6	80
50	1830 ± 348	801* ± 785	56.2	40
75	1880 ± 366	1126* ± 859	40.1	27
100	2232 ± 178	412* ± 157	81.5	20

Table 5.7: The experimental results of the 30-120 minute exposure length experiments investigating the effects of the varying the length of exposure and duty cycle on the antimicrobial efficacy, with peak irradiance and dose kept constant at 30 $mWcm^{-2}$ and 54 Jcm^{-2}, respectively. Each population represents an average of 6 samples, n=6. Each of the four duty Cycles demonstrated a significant difference (P<0.05) between start and end population as denoted by *.

Duty Cycle (%)	Starting Population ±Std Dev ($CFUml^{-1}$)	Post-exposure Population ±Std Dev ($CFUml^{-1}$)	Percentage Reduction (%)	Exposure Time (min)
25	1710 ± 142	305* ± 346	82.2	120
50	1897 ± 141	125* ± 194	93.4	60
75	1872 ± 269	45* ± 70	97.6	40
100	2232 ± 178	117* ± 129	94.8	30

In both the 20-80 minute experiments and the 30-120 minute experiments – results detailed in *Table 5.6 & 5.7*, all of the post-exposure populations showed a significant reduction ($p<0.05$) in bacterial population when compared to the starting populations. There was a range of percentage reduction in bacterial population across the two sets of experiments ranging from 40.1% up to 97.6%.

In the 20-80 minute exposure experiment there is a large difference in the inactivation achieved with the 100% duty cycle, or continuous, for 20 minutes – this exposure achieved the maximum reduction in bacterial population of 81.5%. The other three pulsed duty cycles, 25%/50%/75%, all demonstrated inactivation levels much lower, with 75% duty demonstrating 40.1% reduction, less than half the percentage reduction of the continuous. The variation of results in these experiments was large leading to sizable standard deviations and thus the statistical analysis suggested no significant difference ($p>0.05$) between any of the post-exposure bacterial populations despite the differences in the averages between the continuous and the 3 pulsed experiments in terms of percentage reduction. These results appear to suggest that the pulsed exposures over a longer period are less effective in terms of antimicrobial efficacy than the continuous exposure over a shorter period. There are, however, sizable standard deviations on the pulsed exposure results so it is still unclear whether the conclusion that pulsing is less effective is entirely true – the statistical analysis seemed to suggest not. The non-exposed samples showed no significant difference ($p>0.05$) from the starting population.

This result contributed to the decision to repeat the experiment with longer exposure times in order to increase the bacterial inactivation achieved, and attempt to improve the consistency of results.

The 30-120 minute exposures all demonstrated a significant reduction in bacterial population from starting population to post-exposure population. In terms of percentage reduction, they also seem much more consistent with a smaller range of 15.4% - ranging from 82.2% up to 97.6% - much less than the 41.4% range in the 20-80 minute exposures. Additionally, the standard deviations in the 30-120 minute exposures are numerically smaller than that observed in the 20-80 minute exposures – so the results appear to be more consistent overall in terms of range on percentage reduction and variability. It is unclear why this is the case – perhaps that the dose being delivered in the case of the former experiments was inactivating to a shoulder point causing high levels of variation whereas the latter experiment applied a higher

dose bringing the populations down much closer to zero providing more consistent results across the board.

The highest reduction is observed with the 75% duty cycle for 40 minutes that demonstrates a 97.6% reduction in bacterial population. A close second is the continuous 100% duty cycle exposure for 30 minutes which demonstrates a 94.8% reduction followed by the 50% duty cycle and then the 25% duty cycle. Again, these results when analysed statistically show no significant difference ($p>0.05$) between any of the post-exposure bacterial populations. The non-exposed samples showed no significant difference ($p>0.05$) from the starting population.

These results seem to suggest that pulsing over a longer duration has little effect on the antimicrobial efficacy of the 405 nm light – suggesting that the dose is a more important factor than the duty cycle or exposure time. This being said – the results could vary with different levels of irradiance and much longer exposure times but these two experiments seem to suggest that the inactivation achieved is more dose dependent than time dependent. It would however to be interesting to apply a dose over very different exposure times - for instance 10 second and 30 minutes – and compare the results.

The main objective of these experiments was to evaluate any differences in the post exposure populations between the different exposure times/duty cycles. When compared, the post-exposure bacterial populations in both cases demonstrated no statistically significant difference ($p>0.05$) between any of the exposures, with the 25% duty cycle experiment being 4 times longer than the 100% duty cycle experiment. The results showed no significant difference in post exposure bacterial populations, suggesting no beneficial or detrimental effects in applying the same dose over different exposure times and duty cycles and indicate that dose ultimately appears to relate more closely with the amount of inactivation than exposure time.

The study by Li (Li *et al.*, 2010), investigated the effect different duty cycles for continuous and pulsed light, including exposure time variation to maintain a consistent dose. The results of the experiments demonstrated an improvement in

performance with pulsed UV-A when compared with continuous. For both *C. albicans* and *E. coli*, the antimicrobial efficacy increased directly with the duty cycle, with a 75% duty cycle showing the best inactivation. The experiment with *C. albicans* demonstrates an inactivation rate of 91.53% with the continuous exposure, but all of the pulsed exposures (25%/50%/75%) demonstrate an inactivation rate in excess of 99%. *E. coli* showed a similar improvement although not at the same level of inactivation with pulsed demonstrating excess of 90% inactivation and continuous lower than that. The exposure times were below five minutes so not comparable to the current study (*Section 5.2.3*) – due to the fact that UV-A is much more bactericidal than 405 nm light. The study by Li *et al.* (Li *et al.*, 2010), demonstrated clear advantage using pulsed UV-A over continuous with a higher inactivation rate achieved and suggests that with an increase in duty cycle the inactivation rate will also increase – which seem counter-initiative given that the 100% duty cycle is the lower level of inactivation rate.

The results do not agree with that of the finding in the experimental section however there are a sizable difference in the experiments – exposure time, wavelength of light, bacteria used – which could majorly impact the results.

A study by Wengraitis (Wengraitis *et al.*, 2012) also varied exposure time and dose, although it was noted in the study that the dose was altered because the exposure time would have been too long for the lower duty cycle. Due to this, the author used a measure called sensitivity, which is a measure of inactivation with respect to unit of dose. The results demonstrate, not necessarily more kill with the low duty cycles but more kill per unit of dose applied. These results therefore appear to contradict the results obtained in this study (*Section 5.2.3*), which suggest that inactivation is more dose dependent than based on exposure time of duty cycle. Again – the experiments are not directly comparable using different methods, bacteria, wavelength of light; however, they are more comparable to the next set of experiments, results discussed in *Section 5.3.4*.

5.2.4 INVESTIGATING PULSED-DELIVERED DOSE AND RESULTING BACTERIAL INACTIVATION

These experiments were performed in an effort to establish whether the bacterial inactivation was dose dependent under different pulsing conditions. There are studies (Murdoch *et al.*, 2012; Endarko *et al.*, 2012; Enwemeka *et al.*, 2008), that suggest the antimicrobial properties of 405 nm light appear to be dose dependent. No study thus far has looked at dose dependency under pulsed conditions, and this was the focus of the current experiment. This experiment kept all parameters, except the duty cycle, constant, which in turn directly impacted the dose applied to the bacterial sample. The hypothesis was that, assuming the antimicrobial effects of 405 nm light are not fully dose dependent, the duty cycle and dose are not directly proportional to the bacterial inactivation achieved and thus more efficient bacterial inactivation could be achieved through the application of pulsed 405 nm light opposed to continuous. The results are shown below in *Table 5.8.*

All four of the exposures demonstrate a significant reduction ($p<0.05$) between the starting populations and post-exposure populations. The percentage reductions range from 48.9% up to 98.9% and percentage reductions increase with the duty cycle from 25% up to 100% – and thus the dose, as expected. The continuous, or 100% duty cycle, demonstrated at 98.6% reduction in bacterial population and so for the 25% duty cycle, with 25% of the dose, the expectation would be 25% of the inactivation achieved if the reaction was dose dependent. The 25% duty cycle experiment however demonstrated a 48.9% reduction – just under 50% of the inactivation achieved by the continuous exposure but for 25% of the dose delivered. Similarly, the 50% duty cycle demonstrated a 70.8% reduction in bacterial population which is just over 70% of the inactivation achieved by the continuous exposure – and again for 50% of dose delivered. Furthermore the 75% duty cycle exposure demonstrated an 87.4% reduction in bacterial population, just over 88% of the inactivation achieved by the continuous exposure – for 75% of the dose delivered. The

results appear to contradict that of the earlier work in *Section 5.2.1 and 5.2.3* – which suggest there is an element of dose dependency to the 405 nm light inactivation. All unexposed sample showed no significant difference ($p>0.05$) when compared with the starting populations with all post exposure populations showing a significant difference ($p<0.05$) when compared with the starting populations.

An interesting addition had time allowed would have been to look at this experiment but instead of changing the duty cycle – apply the same dose across the range of duty cycles and do this for a number of doses to get a bigger picture of what might be happening.

Comparing the post-exposure bacterial populations statistically, results suggest a significant difference between the 25% duty cycle and the 100% duty cycle exposures ($p=0.00432$) and between the 25% duty cycle and the 75% duty cycle exposures ($p=0.02885$). However, there is no significant difference ($p>0.05$) between the 25%, 50% and 75% or between the 50%, 75% and 100% duty cycles.

In each of the pulsed cases the dose was directly related to the duty cycle, and the pulsed exposures, although demonstrated lower overall bacterial inactivation, demonstrated more inactivation per unit of dose delivered than the continuous exposure – with the inactivation per unit dose increasing with a decrease in duty cycle. This inactivation per unit dose is referred to in this study as optical efficiency – and the average optical efficiency of the 25% duty cycle exposure shows an increase of over 80% when compared with that of the 100% duty cycle exposure. Likewise, the other two pulsed exposure demonstrate an increase in optical efficiency.

Table 5.8: The experimental results showing the relation of a pulsed dose of 405 nm irradiation and the bacterial inactivation achieved. The power consumption is also provided, allowing a comparison of Optical Efficiency and Electrical Energy Consumption. Each experiment was carried out in triplicate with each starting population shown being an average of 3 values (n=3) with the standard deviation. [A]Average Optical Efficiency is the bacterial inactivation per unit of optical energy per cm^2 applied. [B]Average Electrical Energy Efficiency is the bacterial inactivation per unit of electrical energy expended. *Indicate post-exposure bacterial populations which were significantly different to the post-exposure population at 25% Duty Cycle ($p<0.05$).

Duty Cycle (%)	*Starting Population ± Std Dev ($CFUml^{-1}$)*	*Post-Exposure Population ± Std Dev ($CFUml^{-1}$)*	*Percentage Reduction (%)*	*Dose (Jcm^{-2})*	*Optical Efficiency[A] ($CFUml^{-1}/Jcm^{-2}$)*		*Energy Consumption (kJ)*	*Electrical Energy Efficiency[B] ($CFUml^{-1}kJ^{-1}$)*	
					Range	***Average***		***Range***	***Average***
25	*2272 ± 435*	*1161 ± 278*	*48.9*	*17.4*	*36.21-76.44*	*55.7*	*87.9*	*7.17-15.13*	*11.0*
50	*2246 ± 197*	*655 ± 879*	*70.8*	*34.8*	*4.60-63.74*	*41.9*	*112.8*	*1.42-19.66*	*12.9*
75	*2172 ± 152*	*273* ± 396*	*87.4*	*52.2*	*13.41-46.32*	*36.1*	*132.8*	*5.27-18.21*	*14.2*
100	*2167 ± 178*	*24* ± 34*	*98.9*	*69.6*	*29.02-33.04*	*30.4*	*174.0*	*11.60-13.22*	*12.2*

In terms of electrical power, the term electrical energy efficiency is used – which is bacterial reduction per unit of electrical energy. The continuous exposure used 174 kJ of electrical energy (measured using a wall plug power meter) and whilst the 25% duty cycle used 87.9 kJ which is approximately 51% of the electrical energy to achieve approximately 49% of the inactivation. In terms of electrical energy efficiency there is not much difference between the 25% duty cycle exposure and the continuous exposure – the pulsed exposure is marginally less efficient. The 50% duty cycle shows a slightly better electrical energy efficiency using 65% of the electrical energy used by the continuous and achieving an average of 70.8% of the inactivation. Finally, the 75% duty performed the best in terms of electrical energy efficiency. It used 132.8 kJ, approximately 76% of the electrical energy used by the continuous source, to achieve 87.4% of the continuous exposure. This is possibly due to the idea of a base power consumption. The circuit running at a 25% duty cycle will not simply use 25% of the electrical energy – there will be an amount of energy used regardless of the duty cycle and so 75% duty cycle makes the most of this delivering the highest dose (using the most energy) of the pulsed exposures and consequently achieving the highest bacterial inactivation of the pulsed exposures. Put another way, it combines the higher optical efficiencies when pulsing with the higher dose exploiting the most out of the base electrical energy.

The electrical readings do demonstrate that electrical energy efficiency can be improved by pulsing the LEDs however the higher duty cycle appears to provide the highest electrical energy efficiency.

Figures 5.10 (a) and *(b)* shows the change of fractional survival of bacterial populations with electrical energy and dose respectively.

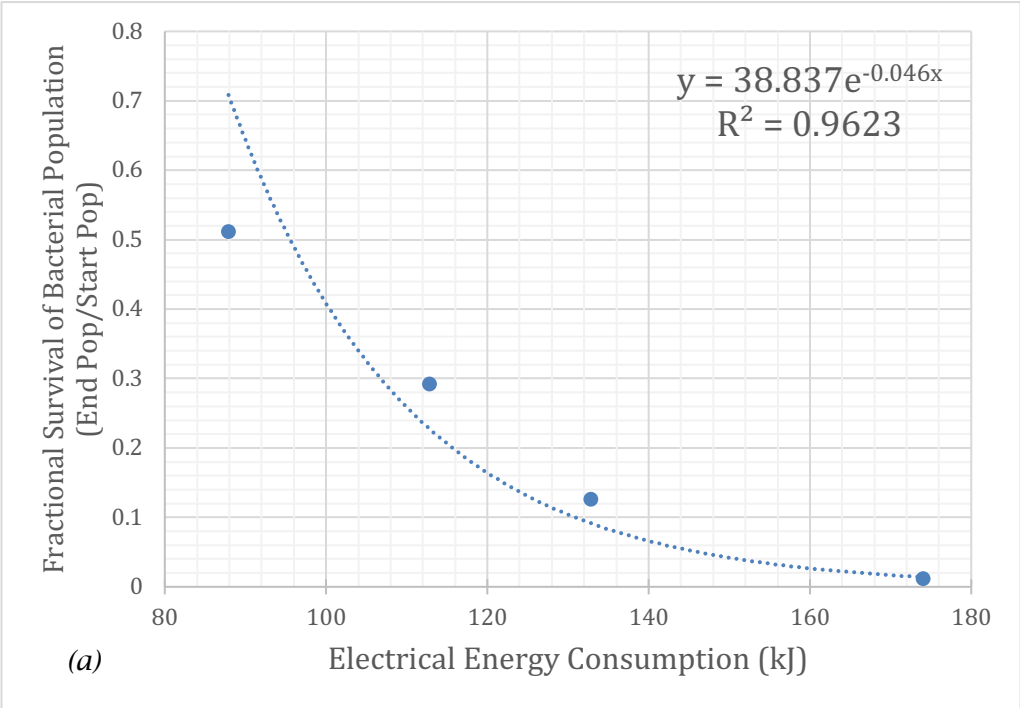

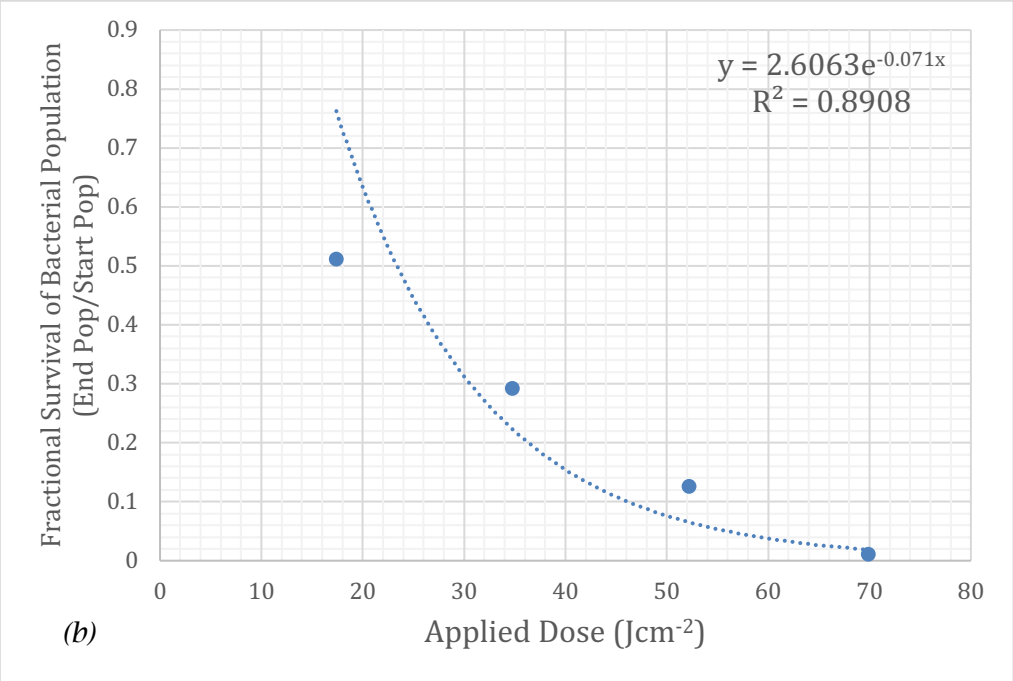

Figure 5.10: Graphs showing the fractional surviving bacterial population (results from *Table 5.8)* of *S. aureus* after exposure to 405 nm light and how it changes with (a) Electrical Energy and (b) Applied Dose of Optical Energy. The Solid lines are for visual guidance. The Broken lines demonstrate first order exponential trend lines - with the equations given on the graph – to obtain the inactivation rate constants for both electrical energy and applied dose.

Looking at *Figure 5.10(a)* and the equation is can be seen that from the trend line – there is an inactivation rate constant of 0.046 kJ^{-1} of electrical energy. Looking at the applied optical dose graph in *Figure 5.10(b)* – the trend line demonstrates an inactivation rate of 0.071 cm^2J^{-1} of applied dose. Comparing the inactivation rate of applied dose to that of *S. aureus* aerosols exposed to UV-C – the difference in the required dose becomes clearer. A study by Kim (Kim & Kang, 2018), demonstrated an approximate 6-log_{10} PFU/ml (Plaque Forming Units) reduction of *S. aureus* with an inactivation rate constant of 2.64 cm^2mJ^{-1}. As can be seen this when converted to equivalent units – the inactivation rate constant for 405 nm light is 71 cm^2mJ^{-1} compared with the 2.64 cm^2mJ^{-1} for UV-C. It is clear that UVC is more efficient at inactivation than 405 nm light. It should be noted that these rates are specific to these studies and these would vary between different experimental setups. Differences would be observed dependent on the medium of the organism e.g. suspension, seeded agar plate or aerosols, as well as the microbial organism used among other experimental parameters. However, the inactivation rate constants allow for comparison of UV and 405 nm light studies and should across the studies demonstrate the increased germicidal properties of UV when compared with 405 nm light.

Results demonstrated conclusive evidence showing that the antimicrobial efficacy of 405 nm light is not entirely dose dependent in all applications - and that pulsed application can lead to more efficient bacterial inactivation in terms of optical and electrical energy efficiencies. It may be the case that an element of optimization will be required between the optical efficiency and electrical energy efficiency to provide the most efficient means of inactivation give that the lowest duty cycle provides the highest optical efficiency but lowest electrical energy efficiency.

Initial experiments, in *Section 5.2.1*, altering peak irradiance and duty cycle simultaneously, showed no improvement in the antimicrobial efficacy, but this appears to contradict the final set of results shown in *Table 5.8.* These results may have been masked in initial experiments by the simultaneous change in peak

irradiance with duty cycle in order to keep the overall dose constant. Similarly, the experiments in *Section 5.2.3* demonstrated no improvement in efficiency but this may also have been masked by the different exposure times.

The results of these dose dependency experiments agree with those of Wengraitis (Wengraitis *et al.*, 2012), who also found an increase in both energy efficiency (synonymous with electrical energy efficiency in this study) and sensitivity (synonymous with optical efficiency). The two lower duty cycle exposures in the study by Wengraitis (Wengraitis *et al.*, 2012), of 10% and 25%, albeit with UV-C LED and not 405-nm light, showed higher efficiency in terms of electrical energy and optical energy. The lowest duty cycle showed the most efficient operation in terms of both efficiencies. The lowest duty cycle in this study (*Section 5.2.4*) was 25% and in terms of optical efficiency this was the most efficient, which agrees with the results found by Wengraitis (Wengraitis *et al.*, 2012), however the 75% duty cycle was found to be most efficient in terms of electrical energy efficiency which doesn't agree with the results found by Wengraitis (Wengraitis *et al.*, 2012). Again, due to slight differences in experimental methodology and the wavelength of light the results are not directly comparable but both studies do agree that improved efficiency is evident through pulsed delivery of light.

Additionally, a study by Li (Li *et al.*, 2010) did conclude that pulsed exposures, albeit using UV-A LEDs, resulted in more effective inactivation. These two studies (Wengraitis *et al.*, 2012; Li *et al.*, 2010) in tandem with this present study conclude that pulsed delivery of radiation, whether visible light or UV light, can demonstrate significant improvements in inactivation efficiencies.

As for the reason, neither the study by Li nor Wengraitis (Li *et al.,* 2010; Wengraitis *et al.,* 2012) has explicitly proposed a clear hypothesis as to why the pulsed light demonstrates higher efficiency. Both paper use different wavelengths of light so although both mechanisms attack cell DNA – UV-A generates ROS resulting in single-strand DNA breaks whilst UV-C causes direct DNA damage (Li *et al.*, 2010) – the reasons for pulsing being more effective in each case could be different. 405 nm

light however is thought to produce ROS through the excitation of porphyrin molecules within the cells. The ROS then likely causes oxidative damage to all components within the cell including the cell wall itself, as discussed in more detail in the literature review (*Section 3.5.3*). One possible explanation for the results in this study, showing more efficient pulsed 405 nm inactivation, is that there could be a delay in the inactivation mechanism, i.e. a period of time for enough radicals to be produced to cause enough cellar damage to render it inactivated. Assuming that there are multiple porphyrins capable of photon absorption per bacterial cell, there could be a point at which more photons being absorbed by the porphyrins in the bacterial cell would have little effect on the inactivation mechanism already in progress. Pulsing light with 'on/off' periods of exposure could be more efficient if this was the case, with optimal efficiency being achieved if the pulse width could be matched with the inactivation time constant. This would give the bacterial cells time to be inactivated and possibly allow for the photons to then reach other active bacterial cells that were perhaps shielded previously.

This idea also contributes to the thought that dose might not be the only factor in the inactivation efficacy and could explain why lower duty cycles show more efficient inactivation, in terms of both optical efficiencies and energy consumption. The 'off' period gives the absorption of light and generation of radicals time to occur and cause damage to the cells, and thus less photons are absorbed unnecessarily, i.e. without contributing to the inactivation process already in effect.

At the outset of the study, it was hypothesized that there may have been improved antimicrobial performance caused by the higher-irradiance pulses of light. A study carried out by Endarko (Endarko, 2011) using an array of 99 high powered 405 nm LEDs showed that, for the most part, the inactivation appears to be dose dependent. At the highest dose of 154.1 Jcm^{-2}, however, a significant difference between the varying irradiances was observed with the lower irradiance of 8.6 $mWcm^{-2}$ yielding less bacterial inactivation. In physical terms, higher irradiance does not affect the energy of the individual photons of light, but means that there will be more

photons per unit time reaching the sample. It seems intuitive that there will come a point at which the bacterial sample is saturated and cannot absorb any additional photons and thus the cumulative energy effect is lost; in other words, an increase in irradiance will have no additional inactivation effect. This would suggest that although there may be a range of irradiances through which the inactivation will be relatively dose dependent, inactivation may not always be fully dose dependent and the relationship between irradiance, dose and inactivation achieved will more than likely be a non-linear relationship.

5.3 CONCLUSIONS

This study has indicated that pulsing of 405-nm LED-light, whilst maintaining the same dose over the same period of time (i.e. altering the duty cycle and peak irradiance simultaneously), has no advantages over continuous 405-nm LED-light exposure in terms of antimicrobial efficacy, with all experiments demonstrating an approximate 2 $\log_{10}$ reduction over 2 hour exposures. In addition, the frequency of the pulsed 405-nm LED-light at a constant duty cycle of 50% appears to have little effect on the antimicrobial efficacy, with the exception of 10 kHz, which appeared to yield a difference in inactivation kinetics, but statistically showed the same level of inactivation at the end of the 60-minute exposure as other frequencies. Additionally, the extended exposure time appeared to have no effect, when the same dose is delivered across differing exposure times.

However, it appears that over the same exposure period with the same peak irradiance – the bacterial inactivation is not entirely dose-dependent and higher levels of efficiency - both in terms of power and bacterial inactivation - can be achieved by varying the duty cycle. The experiments demonstrated peak optical efficiency (bacterial inactivation per unit optical irradiance) at a 25% duty cycle – the lowest duty cycle – demonstrating almost an 80% increase in efficiency when compared with the continuous. Additionally, higher electrical energy efficiency (bacterial inactivation per unit electrical energy) was achieved at the highest pulsed duty cycle – 75%.

If these efficiency improvements are scaled up to a larger project – it could boast significant savings in electrical energy. More importantly – if pulsed 405 nm light can be used instead of continuous – with a significant enough level of inactivation – then the apparent level of 405 nm light could be reduced. This means that, pulsed at a 50% duty cycle, the 405 nm light would appear dimmer than a continuous 405 nm light output and could thus be blended into a white light more easily or could be more easily masked. A key issue with 405 nm light at present is that it is not aesthetically pleasant to work under; so, given the idea that the proposed use is for continuous disinfection over long periods of time – user acceptability will be a key issue.

Practically speaking, if these results can be scaled up, and the higher efficiencies can be achieved - with significant enough levels of inactivation under a pulsed light – then this could possibly provide a viable method of operation for 405 nm lighting to provide a more efficient commercial system with a higher level user acceptability.

CHAPTER 6
DEVELOPMENT OF A PULSED, BLENDED ANTIMICROBIAL WHITE LIGHT SOURCE:
PART I: PROTOTYPE DESIGN, BUILD & TESTING

6.0 OVERVIEW

This chapter will focus on the potential for pulsed 405 nm light to be used for the development of a pulsed blended white light for continuous environmental decontamination.

As discussed in *Section 2.5*, previous work by the ROLEST research group has involved the development of prototype systems which have utilized a combination of continuous 405 nm and white light (Bache *et al.*, 2012; Maclean *et al.*, 2010; Maclean *et al.*, 2013.); however, the optical output of these systems had limitations and required improvements to the blending in order to improve the aesthetic acceptability for continuous use within occupied environments (Maclean *et al.*, 2014). This chapter builds on the findings from the previous Chapters to investigate the design, build and testing of a small-scale blended white light prototype, which utilises pulsed width modulation in order to produce an improved optical blend whilst retaining good antimicrobial capabilities.

6.1 INTRODUCTION

As discussed, 405 nm light has proven to be effective for inactivating bacteria. UV light is still superior in terms of antimicrobial efficacy; however, it has several disadvantages when it comes to practical application. As discussed in *Section 2.4.2*, UV light is damaging to human tissue and so cannot be used in occupied rooms, with a secondary issue being that of reduced penetration. Light in the region of 405 nm addresses both of these issues. It can be used at doses that are not harmful to mammalian cells whilst being lethal to bacterial cells (Ramakrishnan *et al*, 2016), and the study by Ash (Ash *et al.,* 2017) concludes that an increasing wavelength

demonstrates higher levels of penetration – implying 405 nm light photons will penetrate more than shorter wavelength UV photons. These properties have led to 405 nm light being developed for continuous environmental decontamination applications, as commercialized by Kenall Lighting as mentioned in *Section 2.5.* Additionally, an American-based company Hubbell Lighting (IL, USA) has licensed the technology for application areas including the food processing industry (Hubbell Lighting Components, 2020).

In terms of its application for continuous decontamination, appropriate blending of the light is important. Despite the antimicrobial effects being achieved using violet light in the region of 405 nm, light of this output alone could not be used for continuous decontamination as it would not be aesthetically acceptable in occupied environments. Violet light has a very low colour rendering index (CRI) – a light quality described more in depth in *Section 6.4.2.1* - so if it is not appropriately blended with supplementary wavelengths of light, it can be uncomfortable to work under, and hard to conduct some clinical procedures such as finding patients veins and observing complexions that involve colour perception (Maclean *et al.*, 2014). Due to these reasons, for use as an environmental decontamination strategy in occupied environments, the violet light must either be used in a room already well illuminated with white lighting, or – as is the case with the existing prototypes such as the Kenall Indigo Clean systems – systems must have additional optical wavelength content (e.g. additional white lights or additional coloured LEDs) in order to produce a more balanced light output.

The work in this chapter investigates the potential to develop a blended antimicrobial white light using pulsed 405 nm LEDs with supplementary-pulsed red, green and yellow LEDs.

6.2 THE FUNDAMENTALS OF WHITE LIGHT

Light, or visible light, is a type of electromagnetic radiation with wavelength in the range of around 400-760 nm, which can be detected by the human eye (Sliney,

2016). The electromagnetic spectrum is illustrated in *Figure 6.1*, with the visible light region highlighted in the centre.

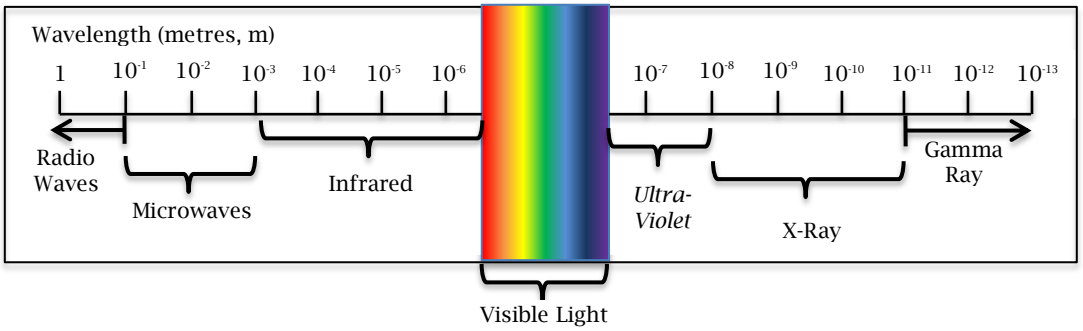

Figure 6.1: Illustration of the electromagnetic spectrum, detailing the type of radiation and the corresponding wavelength. ***Note: the visible light spectrum has been widened for illustrative purposes and so does not adhere to the scale.***

Wavelengths above and below the visible light region are types of radiation which humans cannot detect without the use of scientific equipment. Visible light spans the range of colours from red at the low frequency, longer wavelength end of the spectrum to violet at the high frequency, shorter wavelength end of the spectrum. Each wavelength in between has a corresponding colour associated. As in colour mixing – a mixture of different wavelength can give produce different colours. Most importantly however, a mixture of the colours across the full spectrum produces white light – which is a mixture of all colours (Zwinkels, 2015).

With this in mind – different compositions of wavelength will produce slightly different shades of white. Daylight is the most common association with white light and it contains a large spread of wavelength content from across the full spectrum from UV through to almost infrared (Hernández-Andrés *et al.,* 2001). Artificial or man-made white light however does not have the same appearance as day or sunlight – because they tend to have significantly less of a spread of wavelength content across the spectrum. An example white light LED spectrum is shown in *Figure 6.2*. As can be seen, in this particular LED, there is a peak in the violet portion of the spectrum, around 450 nm, and then a larger broader spread across the green-yellow-red portion of the spectrum with peak irradiance about 600 nm. This particular LED is classed as a cool light however it is on the low end of the temperature scale at 4000K. A warmer

white would have a smaller violet peak relative to the wavelength spread over the 500-700nm range. Conversely, the cooler the white – the higher the violet peak would be relative to the 500-700nm spread. The peaks and shapes vary with the LED. White LEDs are generally made in in two ways:

- Wavelength Conversion - White LEDs based on blue, violet or UV LEDs with a convertor (Phosphors, semiconductors, dyes) used to convert the light to longer wavelengths producing a mix of colours resembling white light. This can be done in a number of forms using a single blue, violet or UV LED with a number of different convertors creating a number of colours; or with blue, violet or UV LED and a red LED again with a single convertor or a number of convertors to create an array of colours. (Schubert, 2006).
- Colour Mixing Method – White LEDs contain multiple colours within the same LED module and so the blend of the colours can produce white light – e.g. blue and yellow; blue, green and red; or blue, cyan, green and red (Schubert, 2006).

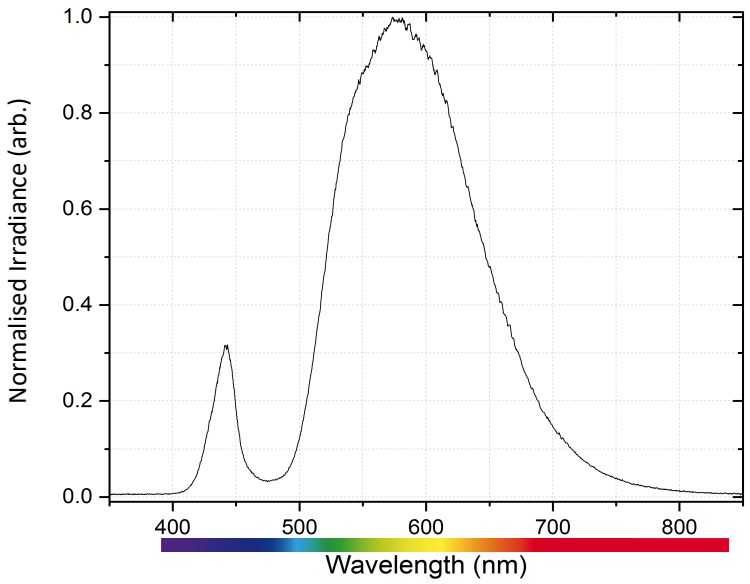

Figure 6.2: Spectrum of a typical cool white light (4000K) LED (Lumileds. Luxeon LXH7-PW40).

The wavelengths of light produced will then dictate the shade or type of white light produced. Depending on the means of producing white light and wavelengths produced – the shade of white achieved will be different.

The different shades of white LED output can be quantified by a term known as Colour Temperature. The colour temperature scale is shown in *Figure 6.3*.

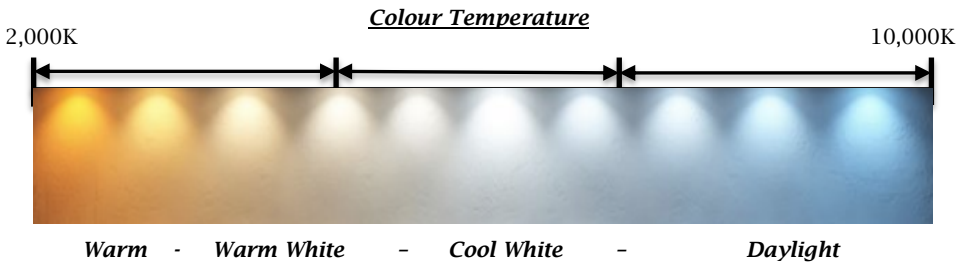

Figure 6.3: Illustration of the Colour Temperature Scale; the difference between so-called warm and cold whites; and which term corresponds to which colour temperature. Image Adapted from: https://illuminationsusa.com/cool-white-vs-warm-white-in-your-outdoor-lighting/

The spectrum starts at 2000K, which is a warm or warm white – the terms differ depending on which company or body is discussing them. If this is taken in reference to the spectrum in *Figure 6.2*, the warm and warm white (2000-3500K) will have more of the red and orange content compared to the violet – relatively speaking. As the colour temperature moves up, the violet or blue content increases in proportion as we move towards a cool white at about 4000-4500K, and finally daylight which is upwards of 6500K which has much more of blue tinge and thus more of the shorter blue/violet wavelength content relative to the longer wavelengths colours (Choudhury, 2014).

Each of the white lights has a different application, with the warmer lights suiting a bedroom, living room environment; the cooler whites for the kitchen or office – places where good lighting and visibility is required; and finally, daylight for more clinical or industrial environments.

The key point is that the white light is a mixture of wavelengths across the visible light spectrum and the relative irradiances of the wavelengths will define the shade of white that is achieved.

In this particular study the 405 nm light is the key component of the light – for the antimicrobial properties – so the challenge is to add supplementary wavelength content to produce a blend of white light with the control of the relative irradiances of these supplementary colours being done through pulsing.

6.3 Initial System Design of the Blended White Light Prototype

6.3.1 Introduction of the Concept

As mentioned, a major consideration when using 405 nm light for environmental disinfection is that 405 nm light alone can be uncomfortable to work under due to its violet colour and poor colour rendering index (CRI) – described in *Section 6.4.2.1*. Practically, the issue with 405 nm light is the narrow wavelength band; so supplementary wavelengths are required to produce a blend of white light more aesthetically pleasing.

The previous chapter's results demonstrated that pulsed operation of 405 nm light emitting diodes (LEDs) can provide more efficient disinfection, both in terms of electrical energy consumption and inactivation achieved per unit of optical energy expended. Results showed that with 405 nm light pulsed at a 50% duty cycle, a 70.8% reduction in bacterial population was demonstrated, which is just over 70% of the inactivation achieved by the continuous exposure – for 50% of dose delivered. The pulsed 50% dose means the 405 nm light will appear less intense, which in theory should make it easier to supplement with other colours and mask in a blended white light. **It is therefore of interest to investigate the potential for a range of pulsed LEDs, of differing wavelength, to be blended together to produce a white light, with the LEDs being controlled by pulsed width modulation (PWM).** The specific application being addressed in this study is that of continuous environmental decontamination and so aesthetics is an important point to address. The end goal would be the development of a light source which emits sufficient 405 nm light to inactivate problematic pathogens without posing risk to humans; whilst also containing supplementary wavelengths of light producing an aesthetically acceptable blended white light suitable for continuous environmental disinfection in occupied environments.

6.3.2 DESIGN OF THE BLENDED WHITE LIGHT PROTOTYPE

As mentioned, one of the main issues with using 405 nm light in occupied environments is that 405 nm light alone provides a poor CRI under which to work, and also results in a phosphorescence-like glow from white objects. Ideally, in a system that would provide additional room lighting, the amount of 405 nm light should be reduced to a point where the antimicrobial effects are still at a practical level, and it should be balanced by other wavelengths of light to aid colour blending and improve the visual aesthetics.

Previous studies have been carried out with 405 nm lighting designs incorporating varieties of cool and warm white LEDs in combination with the 405 nm light arrays (Anderson *et al.*, 2013; Maclean *et al.,* 2010; Bache *et al.,* 2012), however there are difficulties when trying to balance very intense 405 nm light with white light which already contains a significant blue/violet content. In an effort to combat this, the 405 nm light will be pulsed at a 50% duty cycle thus reducing its perceived brightness and theoretically making it easier to mask with other colours whilst maintaining antimicrobial effects.

The core idea of the system design in the present study was to use pulsed 405 nm LEDs alongside pulsed red, yellow and green LEDs in order to create a blended antimicrobial white light source. Pulsing was used to control the average irradiance of each of the individual colours, allowing for control over the overall blend of the 405 nm, red, yellow and green light, without having to change physical components or the number of each specific LED.

6.3.2.1 LEDs used in the design and build of the Prototype

Initial thoughts were to utilise the 3 primary colours red, green and blue (or in this case 405 nm): however, with LEDs in general having relatively narrow emission spectra it was decided that a fourth colour, yellow, would also be included in an effort to increase the spread of wavelengths that could be covered by the proposed blended source. The LEDs chosen are detailed in *Table 6.1*.

Table 6.1: Details of the LEDs selected for use in the initial design of the blended white light prototype.

Colour	Wavelength (nm)		Model	Number Used
	Peak	FWHM		
Red	617	20	Lumileds LXM2-PH01-0070	2
Yellow	593	20	Kingbright KADS-8072SY28Z4S	2
Green	530	30	Lumileds LXML-PM01-0090	2
Violet	405	12	Nichia NCSU276AT-U405	4

With the antimicrobial 405 nm light content being the most important it was decided that four 405 nm LEDs would be used, and two of each of the other three colours in the first instance. The LEDs were all surface mount components and thus had to be mounted onto small breakout PCBs for a number of reasons:

- making them a more manageable size to work with and to adhere in place on the heat sink;
- providing a contact for thermal conduction to a bigger heat sink, and;
- allowing for the easy connection of the source of driving power, with each of the boards having a positive and negative wire connected to the corresponding surface mount pads on the LEDs.

6.3.2.2 Power Supply for the Components of the Prototype

Each of the LEDs selected were chosen to run at roughly the same voltage, between 2.5-4.5V, and have varying current draws roughly from 200-1000 mA. It became clear upon inspection that a single lab power source would begin to struggle to power 10 LEDs some of which were drawing up to 600mA, and to use multiple power sources set at different levels for each branch of LEDs became quite cumbersome and inconvenient, so an alternative means of powering the LEDs was found. The idea was to use a single constant voltage source which would be able to provide enough current to power all the LEDs. An AC-DC power converter (Traco Power

TXM 075-105) was used, which converted mains 230 V down to a constant voltage level of 5 V, providing a maximum of 12 A current which was sufficient to power the LEDs. This came as a complete module and was connected to a standard UK wall plug to the 3 clips at the input (earth, live and neutral), and then the positive and negative wires to the output, which provided the power for the circuitry. This single constant voltage source, although solved and simplified the power issues, meant that resistance had to be altered in each circuit for the different coloured LEDs to provide the different levels of current required.

6.3.2.3 Microcontroller & Programming

One of the major differences in the prototype design was the introduction of a microcontroller for LED control opposed to the pulse generator used in Chapters 4 & 5. All prior experiments, described in Chapters 4 and 5, used a function generator to provide the TTL signal to control the duty cycle of the pulsing, however with the introduction of 3 additional colours of LED, which would all be pulsed at different duty cycles, 4 pulse generators would have been required opposed to a single microcontroller – so it was decided that a microcontroller would be used.

The microcontroller used was a Texas Instruments MSP430G2553, a 20-pin Plastic Dual Inline Package (PDIP), which could be (i) used with the MSP430 LaunchPad development board for programming; (ii) used on a breadboard for prototyping; and (iii) soldered to a circuit board for finalisation. It was a low power microcontroller operating between 1.8-3.6 V, which is where the first consideration had to be addressed. As discussed, the power source for the task was set to be a constant 5 V source and so a voltage regulator had to be used to reduce the voltage for the microcontroller. A regulator was sourced (ST electronics LD1117AV33) that would regulate 5 V down to 3.3 V for the microcontroller, and work with through hole package, TO-220.

When working with the microcontroller initially, and when programming, it was placed into the TI MSP430 LaunchPad development board, so when connected to the PC via USB, the board provided power to the relevant pins on the microcontroller

for it to function. However, when the microcontroller was moved to the breadboard for initial prototype of the circuitry, some of the pins had to be connected to the voltage source and to ground. Shown in *Figure 6.4* is the pin out schematic for the MSP430 microcontroller used and the pins that must be connected to voltage and ground for operation independent of the TI MSP430 LaunchPad development board.

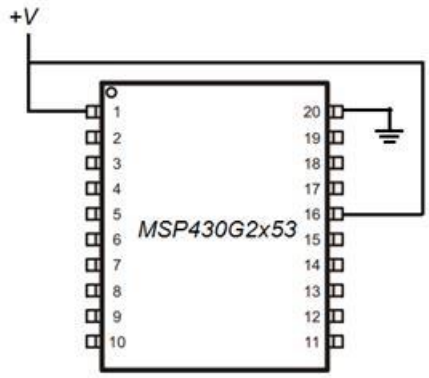

Figure 6.4: MSP430G2x53 microcontroller schematic showing the connections to voltage and ground required for operation independent of the TI MSP430 LaunchPad Development Board.

Pins 2-5 were set as the output pins and were set to output digital logic, either high or low: high being dependent on the input power which in this case was 3.3 V meaning that a high output for the microcontroller was around 3.3 V; and a low output was approximately zero. The microcontroller programming is detailed in *Section 6.3.2.6*, following details of the physical circuit design considerations, which were addressed.

6.3.2.4 Pulsing Circuit Design for the Prototype

The next step was to adapt the circuitry from the previous experiments in Chapter 4 – first described in *Section 4.3.1*, *Figure 4.11*. The concept was to use the same pulsing circuit however for this purpose it would need to be adapted for pulsing 10 LEDs at 4 different duty cycles at the same time. To do this, the circuit used in the previous experiments, shown below in *Figure 6.5*, was altered slightly and replicated for the four different LED colours and the multiple LEDs to be driven on each of the branches. The method for alteration and design is detailed below.

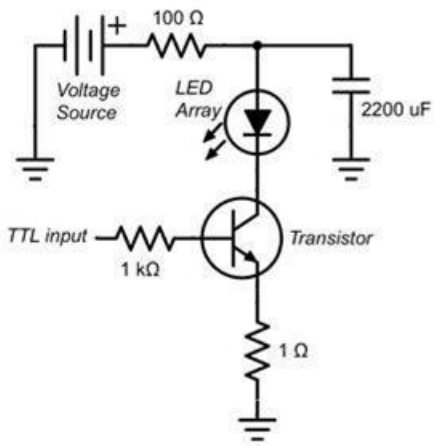

Figure 6.5: Circuit diagram of the initial pulsing circuit used for the proof of concept experiments in Chapter 4 & 5.

The 100 Ω resistor directly following the source in *Figure 6.5* was removed as each LED array would be paired with a specific LED. Additionally, the 1 Ω shunt resistor was removed as the measurement of the current was no longer required. The TTL input was to be provided now by a microcontroller, as discussed in *Section 6.3.2.3*, and so the resistor between the TTL input and the base of the transistor (STMicroelectronics BD239C) was reduced to a 330 Ω resistance as the voltage output of the microcontroller was lower than the output of the function generator used previously. The circuitry associated with the use of the microcontroller is detailed earlier in *Section 6.3.2.3*.

Each colour had a single transistor controlling the switching of multiple LEDs in that branch and each colour of LED had differing limiting resistors in order to control the current through each of the LEDs. The limiting resistor values were initially calculated using the I-V values quoted on the data sheets and displayed in *Table 6.2*. Using the values of rated current and voltage, the values of the accompanying limiting resistors were calculated as described below:

> *For example, the data sheet for the 405 nm LED quotes maximum current at* I_{MAX} *= 700 mA, and a typical forward voltage of* V_{LED} *= 3.55 V. In the branch, the LED and resistor are in series so the current is the same through both and the voltage is split; thus, with a source voltage of 5 V:*

$$V_{REISITOR} = V_{SOURCE} - V_{LED} = 5 - 3.55 = 1.45\ V$$

Forward current remains the same:

$$I_{MAX} = I_{RESISTOR}$$

Thus, using Ohm's Law, the resistor value can be calculated:

$$R = V_{RESISTOR} / I_{RESISITOR} = 1.45 / 0.7 = \underline{\mathbf{2.07\ \Omega}}$$

Resistors are generally available in specific set values so the closest available resistor was 2.7 Ω resistor. The other consideration was the power being drawn through the resistor and so the power through the resistor was calculated, as shown below:

$$P_{RESISTOR} = (I_{RESISTOR})^2 \times R = (0.7)^2 \times 2.7 = 1.323\ W$$

These calculations are based on the values from the data sheet, which are numerically indicative but not 100% accurate in practice – they do however give an idea of the magnitude of number. It was decided that higher power resistors would have to be sourced as anything over 1 W could cause overheating issues with standard sized resistors.

These calculations were carried out for each of the other 3 colours of LED with the results shown in *Table 6.2*. These values were a rough guide as a starting point to build the circuit with an element of protection, and so the LED resistor combinations were tested for each colour and the voltage and current assessed. As expected, the resistor values were a good initial estimate but had to be altered as some LEDs were drawing too much or too little current for the application. The assumptions made based on the initial calculations were that: the LEDs would be drawing the maximum current, which they were not – however this assumption was made in an attempt to make sure the resistor would be able to handle the maximum current draw; and secondly that the LEDs were operating at 25 ˚C – the LED would eventually be mounted on a heatsink but would not be actively cooled and so it was likely that the LEDs would

be operating at a higher temperature than 25 ˚C, but still within the rated operating temperature range (between approx. 10 ˚C and 100 ˚C).

Table 6.2: Initial values calculated for the resistors to accompany each colour of LED in the prototype circuitry. It also displays the associated power requirements for the operation of each LED in the prototype setup.

Colour	V_{LED} *(V)*	*I (mA)*	$V_{RESISITOR}$ *(V)*	*R (Ω)*	*Set Resistance Value (Ω)*	*P (W)*
Red	2.1	700	2.9	4.14	4.7	2.303
Yellow	2.5	350	2.5	7.14	8 (4.7 + 3.3)	0.98
Green	2.9	1000	2.1	2.1	2.7	2.7
405 nm	3.55	700	1.45	2.07	2.7	1.323

Each LED was linked in series with the resistor and powered by the 5 V power source and the current and voltage was measured in each case. Visually, the red LED appeared quite dull and the current input was much lower than expected so the resistor value had to be reduced. The other 3 colours of LEDs showed reverse behavior with quite high currents and felt noticeably hotter to the touch. For this reason, each of the resistances were increased. The final set of resistance values that were chosen are shown in *Table 6.3*.

Table 6.3: A comparison, for each colour of LED, of the calculated resistance values; the initial set values tested; and the finalised resistance values after testing.

Colour	*Initial Calculated Resistance (Ω)*	*Initial Set Resistance Value (Ω)*	*Final chosen Resistance Value (Ω)*
Red	4.14	4.7	**2.7**
Yellow	7.14	8 (4.7 + 3.3)	**8.9 (5.6 + 3.3)**
Green	2.1	2.7	**4.7**
405 nm	2.07	2.7	**5.6**

With the resistor values now validated, the full circuit could be designed with four branches containing each of the colours and the specified values of resistors and the transistor to control the pulsing. The full circuit diagram is shown in *Figure 6.6*.

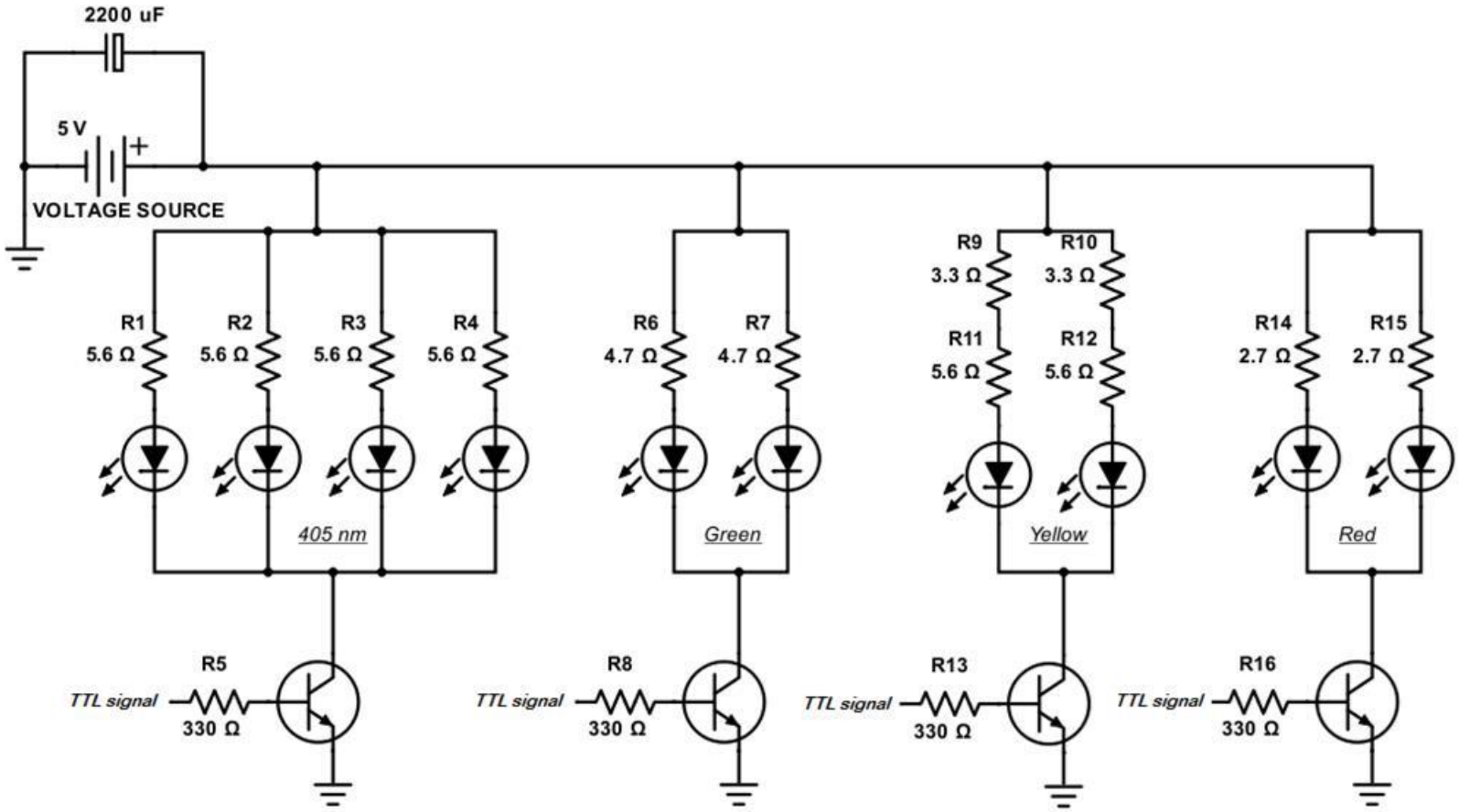

Figure 6.6: Full circuit diagram of the pulsing blended white light source prototype.

6.3.2.5 Component Placement and Arrangement of the Prototype

A single 405 nm LED is not capable of producing enough light for the current application of environmental decontamination; therefore, the initial system being developed was built using a number of individual sources (specified in *Table 6.1*):

- 4 × 405 nm LEDs,
- 2 × Red LEDs,
- 2 × Yellow LEDs, and
- 2 × Green LEDs

As each of the LED arrays varied in size depending on the PCB it was mounted on (footprints varying from approximately 1 cm^2 – 5 cm^2, as can be seen in *Figure 6.7(a)*), the arrangement of these LEDs had to be considered.

Firstly, to ensure adequate heat diversion, the LEDs were arranged and mounted on a heat sink. For this, the LEDs were mounted, with thermal adhesive on a square aluminium plate (220 mm × 220 mm), which had a central hole (∅50 mm) for the wire from the LEDs to be fed through as shown in *Figure 6.7(a)*. Secondly, the arrays needed to be positioned as closely together as possible to try to create a blended point source, although in this case it was difficult due to the footprints of the PCBs. The LEDs were placed and adhered, and the adhesive was left for 24-hr to make sure everything we firmly held in place.

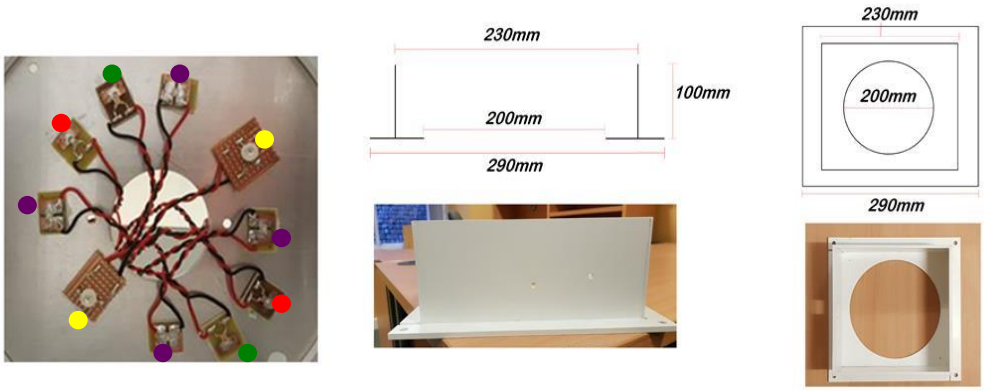

(a) *(b)* *(c)*

Figure 6.7: Pictures and drawings of the components of the prototype. (a) A close up view of the aluminium heat sink on which the LEDs are mounted (colour spots indicate the different colours of LED). Illustrations of dimensions and photos of the PVC housing unit for the blended white light prototype (b) Side view & (c) Top view. This aluminium plate in (a) is inserted into the PVC housing pictured in (b) & (c).

The plate was then mounted inside a polyvinyl chloride (PVC) housing unit shaped like a small ceiling tile. just slightly bigger that the heat sink plate (a depth of 100 mm and a single 200 mm diameter circular aperture) allowing the plate to slot in. All the dimensions are shown in *Figure 6.7(b) & (c).*

After the unit was designed and built and the LEDs all adhered in place, the heat sink, with LEDs attached, was initially placed into the housing unit straight to the bottom so that the LED were in line with the aperture, as can be seen in *Figure 6.8(b).* The unit itself was set up on a pair of adjustable jacks allowing for the height of the light unit to be adjusted throughout the experiments (shown in *Figure 6.8(a)*).

(a) *(b)*

Figure 6.8: Pictures of the fully assembled blended white light prototype. (a) Picture of the fully constructed prototype set up on a pair of jacks allowing for adjustable heights. (b) Underside picture showing the LEDs in line with the bottom of the housing unit and in the centre of the 200 mm aperture.

The extra depth of the housing enabled the aluminum plate to be mounted higher, away from the aperture so that lenses or diffusers could be included to aid with the blending of the colours. However, due to this being a small-scale proof-of-concept system, the optical output irradiance turned out to be too low to include a diffuser for improved blending and so was not included in the design at this stage.

6.3.2.6 Programming the Microcontroller

As mentioned, the microcontroller used was the Texas Instruments MSP430G2553 programmed in C++ (Using Code Composer Studio, CCSv8.3.1). The purpose of the microcontroller is to output four digital (high/low) PWM at the same time at the same frequency. The first step was to get a single pin to output a signal and then from there build up.

In microcontroller programming, there are built in timers that can be used however it was decided that a simpler method would be used. The solution used was involved waiting for a period of time through the use of a while loop as shown below:

```
While(x<20)
{ x++; }
```

The loop is conditional, based on the value of a variable x; While x is less than 20, the code in the brackets is carried out, which in this case is '*x++*', which means add 1 to the current value of x. Logically, if the variable x is initially declared to be zero, then after 20 iterations of the while loop, x will no longer be less than 20, so the statement is no longer true and the program now exits the while loop. This is a very short delay and this loop will take the same amount of time to be carried out every time so it can effectively be used as a timer.

The other conditional statement used the 'if statement', see the example below.

```
If (y==10) { *command }
```

Much like the while loop, the if statement is based on a variable, y in this case. If the variable y is equal to 10, then the code in the brackets will be run; otherwise if the statement is false and y does not equal 10, then the program will carry on past this statement.

These two elements make up the basis of the coding for the microcontroller using 'while' loops for waiting periods, incrementing variables each time which in turn multiply the waiting periods and using 'if' statements to decide when to set the pin outputs to HIGH or LOW, thus creating a periodic PWM signal.

Although there were more sophisticated way to code the microcontroller to complete this task, it was decided that the initial iteration of coding developed met the standard needed for the task, and so at this stage in the development, there would be no significant benefit in investing more time in the coding given it met all operational requires. Ideas on improvements however are included in the future work discussion.

6.4 Construction and Optical Tuning of the Blended White Light Prototype

6.4.1 Optical Tuning of the Prototype

Given the results of the previous chapter, which demonstrated that 405 nm light pulsed at a 50% duty cycle, achieved over 70% of the inactivation demonstrated by a continuous exposure, for 50% of the dose delivered; it was decided that each of the 4 colours would be pulsed at a 50% duty cycle in the first instance. In addition, a commercially available cool white spectrum was taken from a white LED (Lumileds, Luxeon LXH7-PW40) so that the spectra capture from the blended source prototype could be compared in order to tune the output of the blended white light prototype.

The optical output spectrum of the prototype was captured using the HR4000 spectrometer (Ocean optics, HR4000 spectrometer) and Ocean Optics software (Ocean Optic SpectraSuite), with the optical fibre clamped in place to capture the reflected light. The reason that reflected light was measured opposed to the direct source, was to ensure an accurate reading of the full light output. As mentioned earlier, the LEDs themselves were not able to be positioned close together due to the number of LEDs used, the size of the boards on which they were mounted, and the wiring which had

to be incorporated into the design. Therefore, pointing the optical fibre directly at the light source would not give an accurate read out of the proportional levels of each wavelength of light. For measurement, the surface under the light source was covered with white paper so that all light would be reflected equally, and the central point under the light was where the optical fibre was pointed. This is shown in *Figure 6.9*.

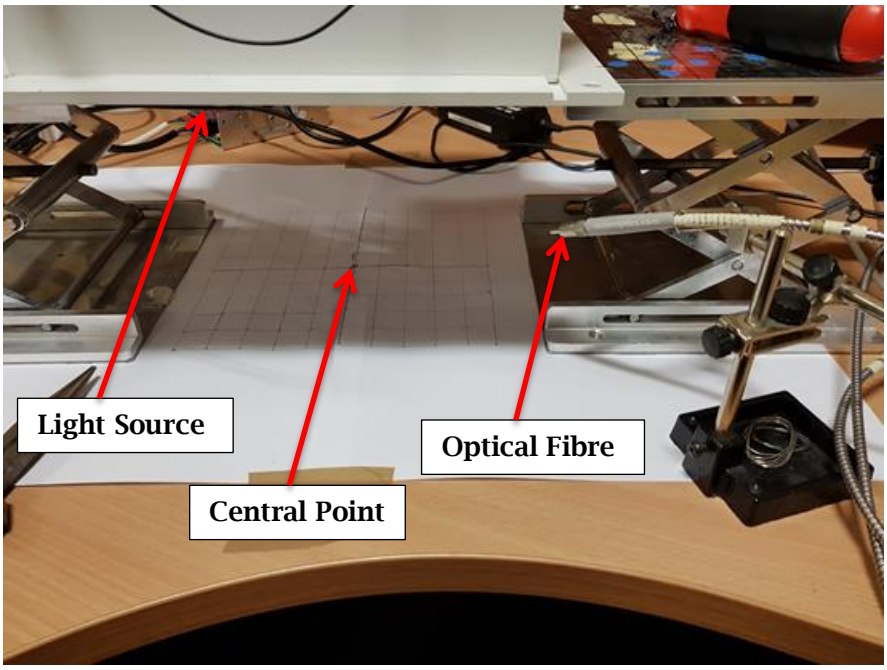

Figure 6.9: Demonstration of the setup used to measure the output spectra from the prototype light source showing the optical fibre from the spectrometer clamped in place pointed at the central point under the prototype.

The output spectrum of the white LED (Lumileds, Luxeon LXH7-PW40) was captured in the same manner, and then the magnitude of the irradiance was proportionally reduced using MATLAB (R2013b) to a magnitude similar to that of the prototype spectrum so that a useful comparison could be made of the shape of the spectra. A comparison of the spectra for the blended white prototype and the commercially-available white LED is shown in *Figure 6.10*.

The 3 spectra in *Figure 6.10* are quite different in terms of peaks and spread of wavelengths. The prototype and white LED source spectra show more similarities with a single violet peak (albeit at different wavelengths) and a spread across the 500-700 nm range. The fluorescent tube however demonstrates 2 violet peaks, a blue peak at

500 nm and then 2 large peaks at about 550 nm and 615 nm amid a selection of other peaks in the 500-700 nm range. All these different peaks are caused by the phosphor coating which convert the UV produced by the gas excitation into visible light peaks (Karlen *et al.,* 2012).

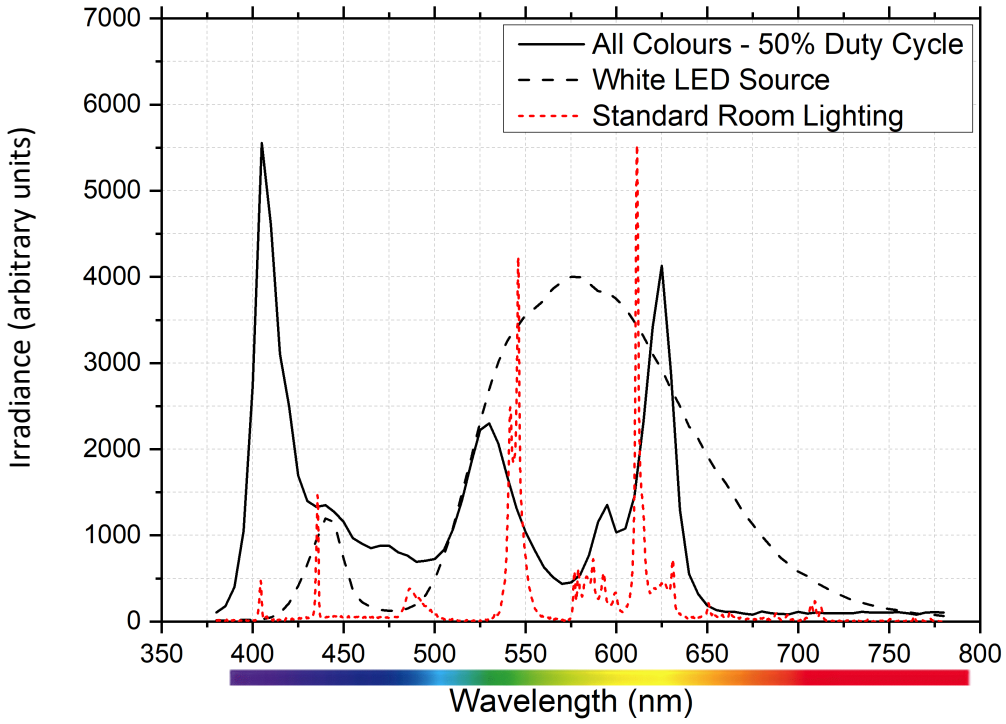

Figure 6.10: Spectral output of the prototype [405 nm, red, yellow, green @ 50% duty cycle], compared to the output of a standard cool white LED (Lumileds, Luxeon LXH7-PW40) and standard room lighting (fluorescent lamp).

In addition to taking a spectrum of each of the stages during the optical tuning process, photos were taken of an array of objects under the light source to visually document the differences in the colour rendering abilities. Items, with a range of different colours (including skin tone), were placed under the light and photographed using a smartphone camera (Samsung Galaxy S8). Photographs of these items, shown in *Figure 6.11*, were taken when illuminated using

(i) the prototype [all colours at 50% duty cycle] (spectrum in *Figure 6.10*);

(ii) the white LED (spectrum shown in *Figure 6.10*); and

(iii) standard room lighting (spectrum shown in *Figure 6.10).*

As can be seen in *Figure 6.11*, there is an observable difference between *Figure 6.11 (a), (b) & (c).* Due to the large 405 nm and 625nm peaks and the imperfect blend

and spacing of the coloured LEDs, *Figure 6.11(a)* appears to have very mixed purple/red hue – however the colours of the objects can be easily distinguished as there is a good spread of wavelength content.

Figure 6.11(b) is quite a crisp image – certainly a well-blended light source, however, does lack a warmth – particularly in the red and yellow colours, where they appear much darker and less vibrant when compared with that of *Figure 6.11(a)* and *(b).* Finally, as expected, the fluorescent tube (*Figure 6.11(c))* appears to provide the best quality of light, rendering all colours well and providing a very comfortable light under which to work.

The output of the blended white light has to then be tuned. This was carried out using this spectral comparison between the prototype and the white LED (*Figure 6.10),* and some visual observation i.e. observing how well true colours of an object were visual perceived under the blended white light output. For example the yellow/orange 590 nm peak of the source was much less than the equivalent wavelength content of the white LED source as can be seen in *Figure 6.10*. Additionally, the red content – specifically the 625 nm peak – was higher than the equivalent wavelength content of the white LED source. To tune the output, the irradiance of the LED producing the yellow/orange 590nm peak was increased in an attempt to match the white spectrum and conversely the irradiance of the LED producing the red 625nm peak was reduced to match the white light spectrum. The spectrum was then analysed after each change in irradiance to check the new peak levels of irradiance for each LED colour to compare with the white spectrum and to visually observe the difference in the light blend and how objects appeared under it.

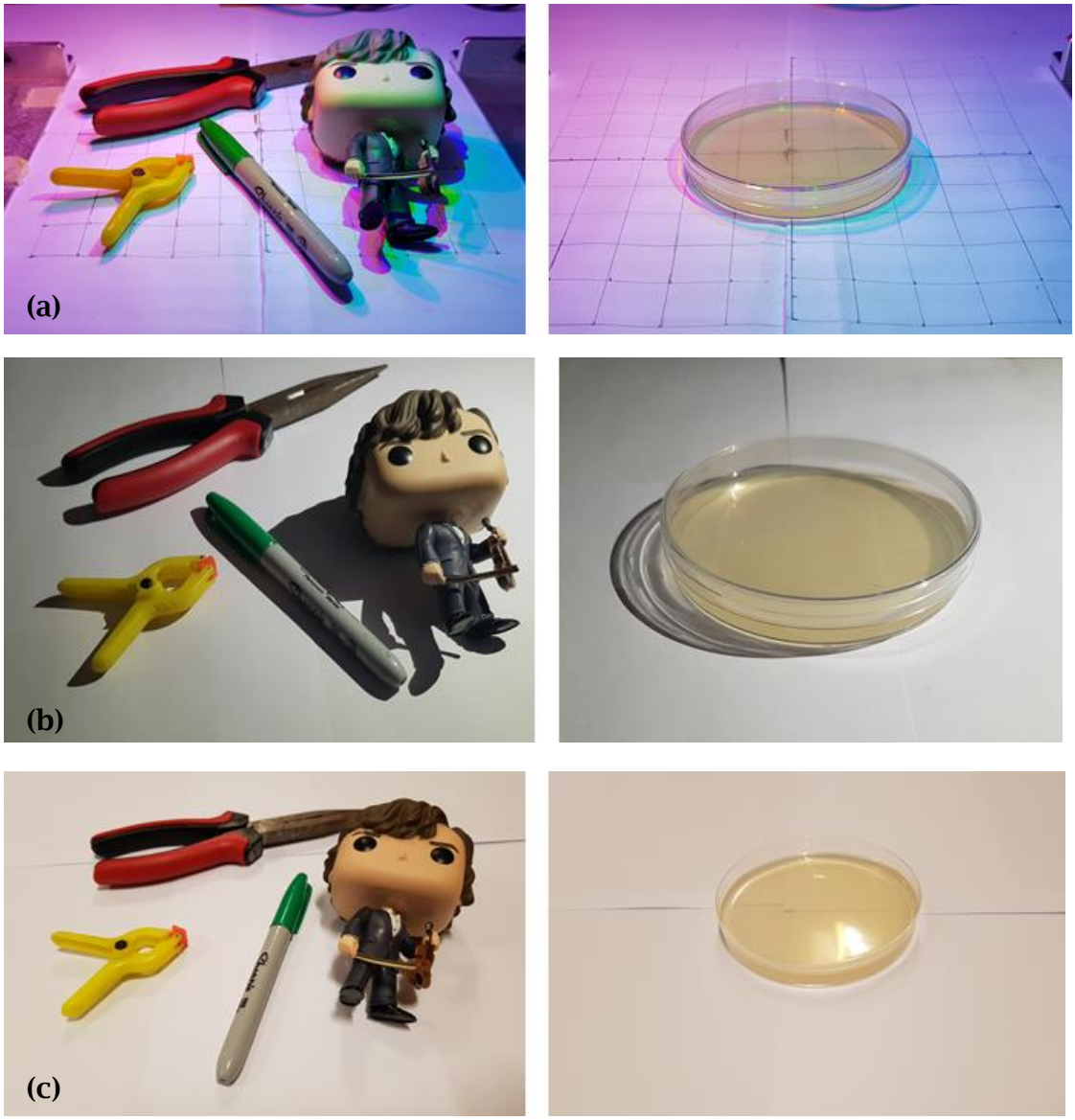

Figure 6.11: Various objects representing different colours under the illumination of (a) the prototype with all LEDs (405 nm, red, yellow, green) set at 50% duty cycle; (b) the white LED; and (c) standard room lighting. Images demonstrate the colour quality/colour rendering ability of the light sources

The first alteration to be made to the output was to the level of red light (600-650 nm). As can be seen from *Figure 6.12*, the red peak (approx. 625 nm) of the prototype when operating at 50% duty cycle is higher than that of the white LED spectrum so the duty cycle of the red LEDs was reduced from 50% and altered until the red peak matched that of the white LED comparison spectrum: the duty cycle for this was 33%. The spectrum of the prototype with the altered red is shown below in *Figure 6.12*, along with the colour comparison pictures in *Figure 6.13*.

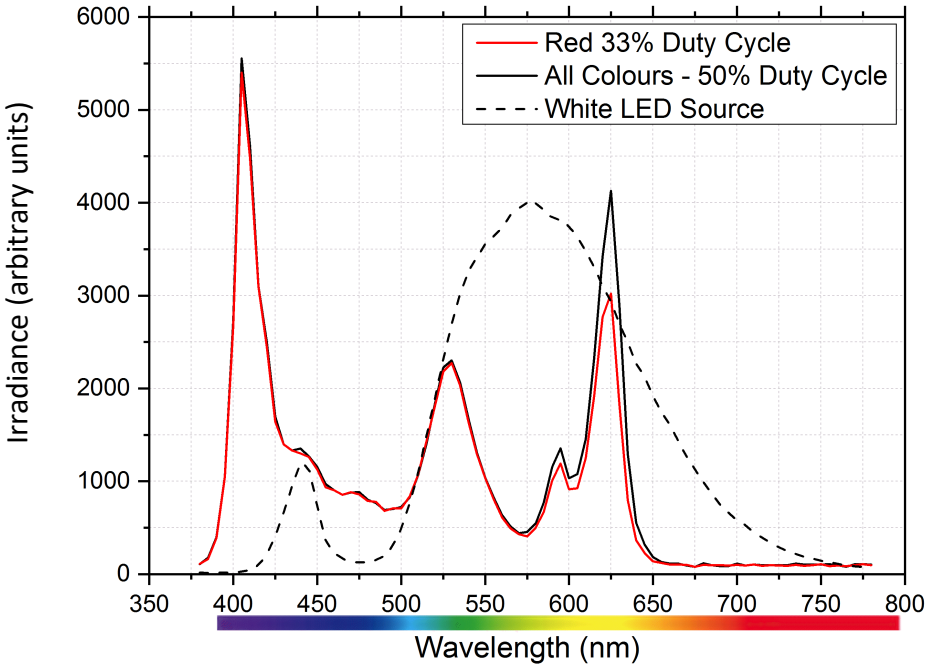

Figure 6.12: Spectral output of the prototype [red @ 33%; 405 nm, yellow, green @ 50% duty cycle], compared to the original output [all LEDs @50% duty cycle], and a standard cool white LED (Lumileds. Luxeon LXH7-PW40).

Figure 6.13: Various objects representing different colours under the illumination of the prototype [red LEDs @ 33%; 405 nm, yellow, green LEDs @ 50% duty cycle], demonstrating the colour quality/colour rendering ability of the prototype light source.

The green content (500-525 nm) produced was at a similar level to that of the white LED spectrum level, as can be seen in *Figure 6.12,* however after the 525 nm peak the content irradiance decreases whilst the white LED source content continues to increase. It was decided to boost the irradiance of the green LED slightly to try and find a balance with enough green content across the 500-550 nm range. The increase meant there was more of the 525-550 nm content with this upper tail reaching into the yellow region (575 – 610 nm) of wavelengths to fill out the gap between the green

(525 nm) and yellow (590 nm) peaks. As such, the duty cycle of the green LEDs was increased to 70%. The new spectrum of the prototype [red LEDs @ 33%; green LEDs @ 70%; 405 nm, yellow LEDs @ 50%] is shown in comparison with the original setting [all colours at 50% duty cycle], and the white LED in *Figure 6.14*, along with the colour comparison pictures in *Figure 6.15*.

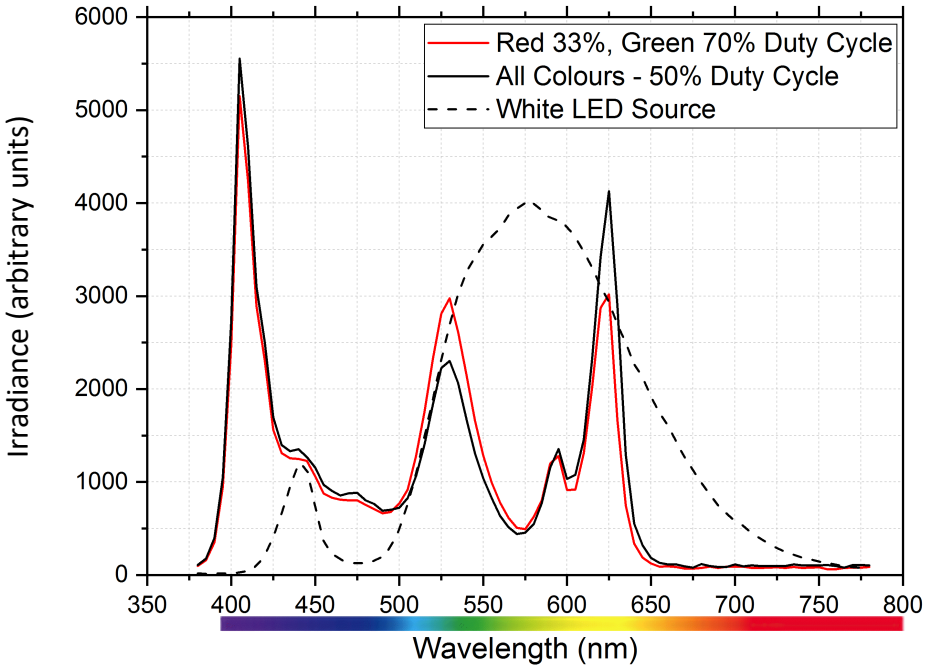

Figure 6.14: Spectral output of the prototype [red LEDs @ 33%; green LEDs @ 70%; 405 nm, yellow LEDs @ 50% duty cycle], compared to the original output [all LEDs @50% duty cycle], and a standard cool white LED (Lumileds, Luxeon LXH7-PW40).

Figure 6.15: Various objects representing different colours under the illumination of the prototype [red LEDs @ 33%; green LEDs @ 70%; 405 nm, yellow LEDs @ 50% duty cycle], demonstrating the colour quality/colour rendering ability of the prototype light source.

The final colour to be tuned was the yellow (575 - 610 nm) which was a suspected problem, as from the spectrum alone, it can be observed that in order for the yellow peak wavelength (590 nm) to reach that of the white LED spectrum level it would have to undergo somewhere in the region of a 2.5 fold increase. The yellow LED at maximum output, run continuously, or 100% duty cycle, would only be a 2-fold increase. In addition, running at 100% in the current setup with the selected resistors could cause heating problems. After some alteration of the yellow it was decided that the maximum that should be pulsed would be 80%, as the yellow content required would not be reached even at 100% therefore there would be no point in possibly damaging the prototype to still fall short in terms of yellow content. *Figure 6.16* and *Figure 6.17* show the final tuned spectrum of the prototype with the increased yellow content [red LEDs @ 33%; green LEDs @ 70%; yellow LEDs @ 80%; 405 nm LEDs @ 50% duty cycle], and the colour comparison pictures, respectively.

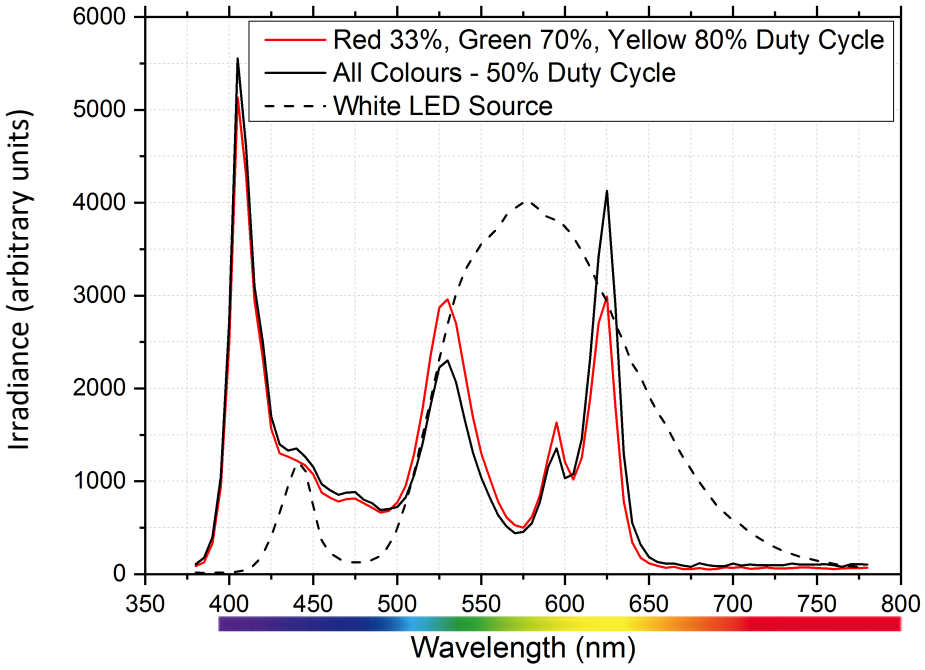

Figure 6.16: Spectral output of the prototype [red LEDs @ 33%; green LEDs @ 70%; yellow LEDs @ 80%; 405 nm LEDs @ 50% duty cycle], compared to the original output [all LEDs @50% duty cycle], and a standard cool white LED (Lumileds, Luxeon LXH7-PW40).

Figure 6.17: Various objects representing different colours under the illumination of the prototype [red LEDs @ 33%; green LEDs @ 70%; yellow LEDs @ 80%; 405 nm LEDs @ 50% duty cycle], demonstrating the colour quality/colour rendering ability of the prototype light source.

The final blend appeared to render colour well, having enough content in each part of the spectrum to produce a reasonably accurate representation of the true colours of the objects under the light. It can be seen however that the light output was not uniform across the area due to the spacing of the LEDs. This issue with spacing of the LEDs also produced coloured shadows as can be seen in all the pictures. Again this is an issue which could be solve by mounting the LEDs much closer together, ideally on the same PCB in a mixed array to create as close as possible to a single point source, which was unfortunately unfeasible in this developmental stage.

To provide a clearer idea of the improvement achieved through blending, the pictures have been arranged together in order for an easier comparison (*Figure 6.18)*. Although the final blend still has a hue of violet, the blend appears to be getting closer to a white, edging more on the cool-white side, most likely due to the content of violet and blue in the spectrum.

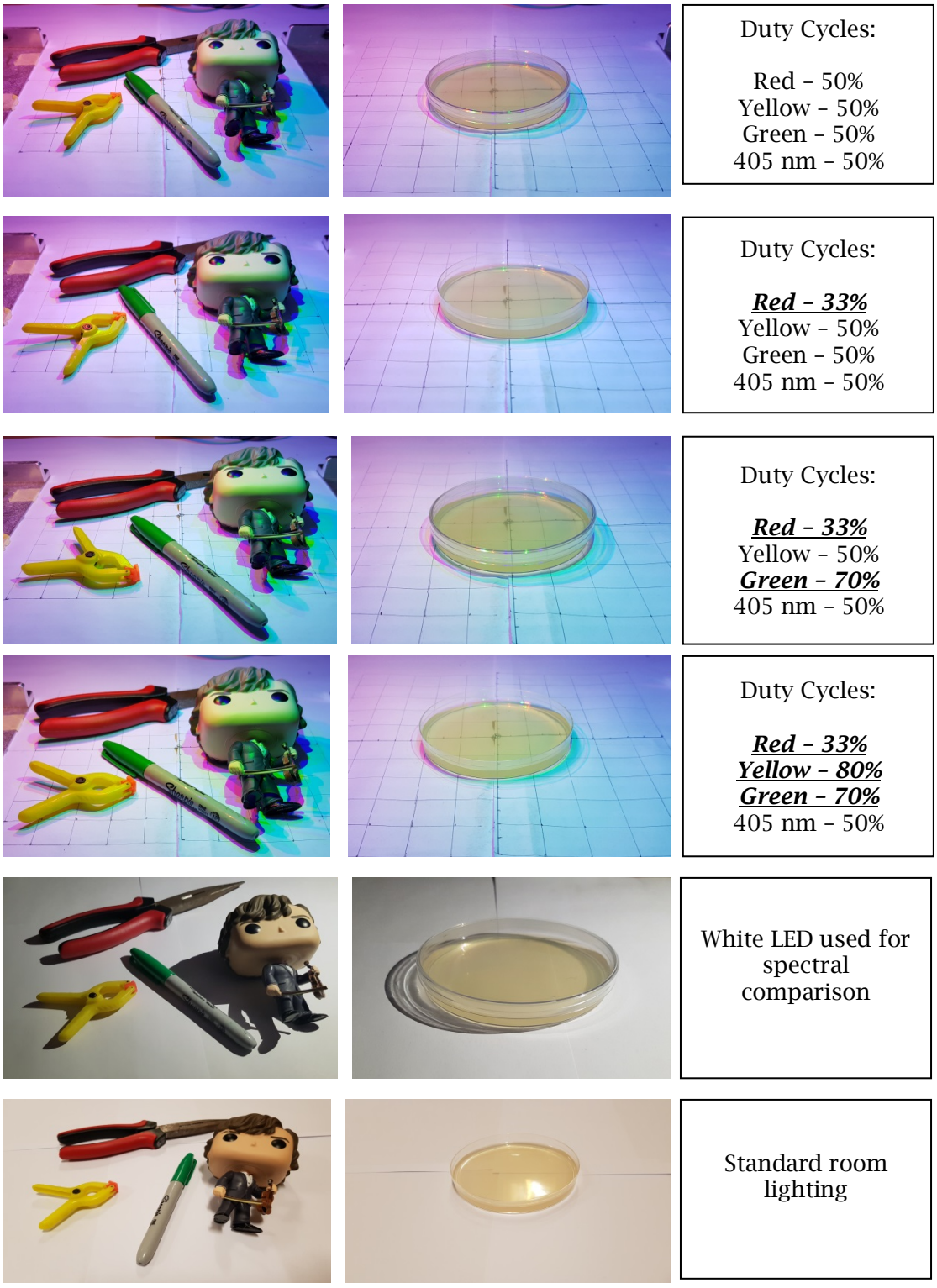

Figure 6.18: Comparison of various objects under the blended white light prototype at the 4 main iterations during the tuning process in addition to under standard room lighting and the white LED used for the spectral comparison.

Across the main 4 iterations of the optical tuning process – all colours are rendered well enough to be distinguishable unlike monochromatic light. As the iterations progress, the purple/red hue fades as the green and yellow content are increased and the red content decreased. The rendering of the skin tone of the figure appears to get worse – achieving more of a green hue as the tuning progressed. This was however due to the depth of the head – meaning that it was much closer to the green LED that was directly above it. In this case, although the skin tone appeared to be getting worse – this was due to the spacing between the LEDs – the spectral blend was actually getting closer to the example white LED spectrum – as demonstrated in the spectral comparisons.

In terms of the three other objects under the final optical blend, the colours appear better rendered with less of the purple/red hue, apparent in the initial blend, with the red, yellow and green colours standing out more than the initial blend. The spectral content of the blend appears to be enough to render these colours on par with the cool white LED – with the exception of the green hue on the figure due to the LED spacing. Neither the blended white light output or the cool white LED appear to render and be as comfortable as the standard room light.

6.4.2 Optical Analysis of the Prototype Tuning

6.4.2.1 Theory and Methods of Light Colour Analysis

All optical analysis was carried out using software called, NIST CQS version 7.4, created by Yoshi Ohno and Wendy Davis. It was kindly provided by Professor Robert Martin, Professor of Nanoscience in the Physics Department at the University of Strathclyde, Glasgow. This software analyses optical spectra and provides details on the quality of the colour of the light, providing values for measurements including:

- colour rendering index (CRI);
- colour quality scale (CQS);
- correlated colour temperature (CCT).

There are various ways of quantifying light, the most standard being power in Watts, however in this application where the colour and the quality of the blend of colour is of interest, a different quantity is required. One such measure is the **Correlated Colour Temperature (CCT)**. This relationship between temperature and perceived colour is derived from Planck's black-body radiator. Upon reaching a range of temperatures, the radiator emits visible wavelengths of light related to the temperature of the radiator. With an increasing temperature – the perceived glow of the radiator moves through red, orange, yellowish-white, white and ultimately a bluish white. The CCT value of a source is the temperature at which the perceived black-body radiator colour is closest to the white light source being measured. Hence – this is really only applicable for blends of light resembling white light and defines the appearance of white light sources (Schubert, 2006). It is measured in units of Kelvin, with commercially available white sources generally ranging from 2700K up to 8000K (Choudhury, 2014): with 2700-3000K quantifying a 'warm' white light source and 4000K+ quantifying a 'cool' white light. These bands and classifications are subject to change depending on what you read; however, these are broadly accurate with warm white having most red/orange content and cool white having more blue content than the warm whites (Choudhury, 2014).

A further measure of light output and the most widely used means of quantifying the rendering performance of light sources is known as the **Colour Rendering Index (CRI)** (Guo and Houser, 2004). CRI is an analysis based on 14 different colours, although only 8 are used for the overall CRI value. The ability of the light source to reproduce each of the colours, known as Ri, is measured and quantified and the difference between the colour measured and the ideal colour is mathematically calculated and scored out of 100 (Guo and Houser, 2004). An example screenshot if the output from the software used in this section is shown in *Figure 6.19*, where the 14 colours are shown.

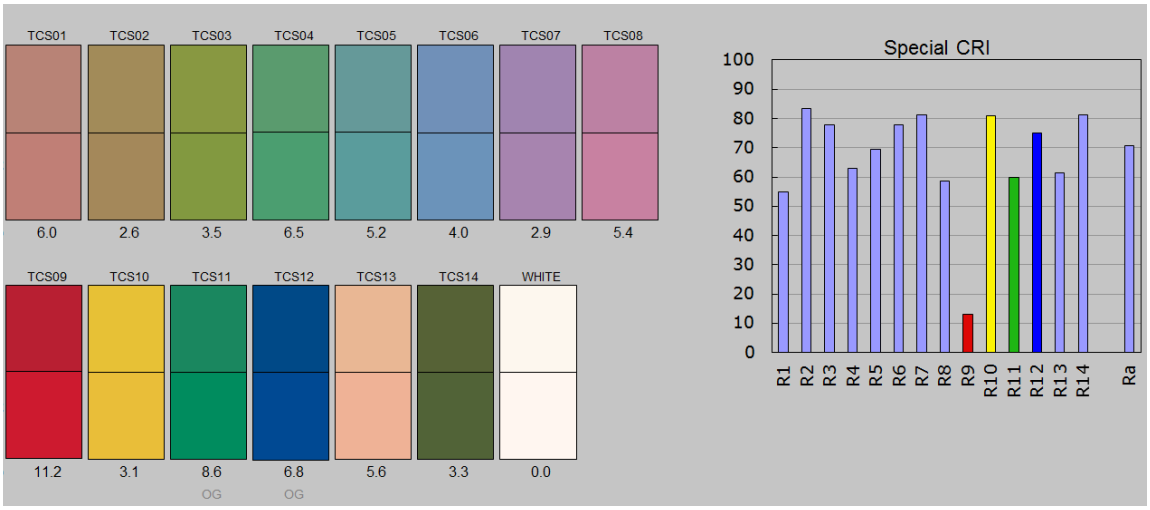

Figure 6.19: Screenshot from the NIST CQS software, illustrating the 14 colours that are analysed in the measure of colour rendering index (CRI). The R1-R14 labels on the Special CRI graph correspond to the TSC01-TSC14 colour boxes and likewise the Ra label corresponds to the White colour box.

Each colour is measured and then compared against a reference taken with an ideal light source for comparison. In *Figure 6.19*, the upper square for each colour shows the reference and the lower square shows the colour measured under the light source being tested. Each is given a score out of 100 as a measure of how close to the reference colour it is, and these are plotted in the 'Special CRI' graph to the right of *Figure 6.19*.

From R1 up to R8, an average is taken and this average constitutes the CRI value of the light source. The other values of R9 up to R14 are used for specific colour comparisons. CRI however is not a perfect measure of rendering ability with several issues, one being that the CRI average is an average of only these 8 representative colours (the real colour spectrum has a significant number of colours and shades), and secondly, the colours are pastels, with low chromatic saturation, opposed to saturated colours, which do not adequately span a range of standard object colours (Ohno, 2006; Davis and Ohno, 2009). CRI has been used since around the 1940s and despite the aforementioned issues, there is yet to be an overwhelming agreement on a replacement for this measure, so it is still commonly used.

One of the alternatives developed by the National Institute of Standards and Technology (NIST) is a concept called **Colour Quality Scale (CQS)**, analysed in the NIST

CQS software which was used. CQS tackles both of the issues raised previously about CRI. It is based on the same methods as CRI but uses 15 highly saturated colours as a comparison thus addressing issues with the number of colours and the pastel colours used for CRI (Davis and Ohno, 2010). Shown in *Figure 6.20* is a screenshot from the NIST CQS software showing the 15 colours used as reference.

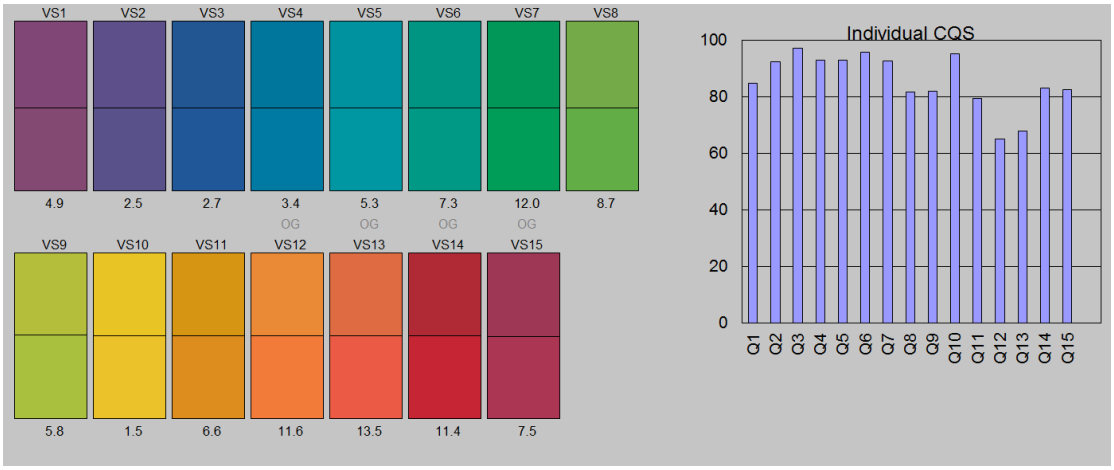

Figure 6.20: Screenshot from the NIST CQS software, illustrating the 15 colours that are analysed in the measure of colour quality scale (CQS). The Q1-Q15 labels on the Special CRI graph correspond to the VS1-VS15 colour boxes.

Calculations for CQS, as well as CRI, use the CIELAB colour space - a colour space specified by the International Commission on Illumination (CIE) in 1976 (CIE, 2007). As opposed to just taking an average of the performance of each colour as in CRI, which can hide certain colour shifts; CQS combines the colour with a Root-Mean Square (RMS) in an attempt to combat this issue. Again, as with CRI, CQS at the end gives a final value between 0-100. (Davis and Ohno, 2009; Davis and Ohno, 2010)

6.4.2.2 Analysis of Prototype Spectra

The analysis was carried out at all stages of the tuning process, with the main focus being on the initial output spectrum (all colours set at 50% duty cycle) and then the final tuned spectrum (red @ 33%; yellow @ 80%; green @ 70%; 405 nm @ 50% duty cycles). In analysis of the spectra using the NIST CQS software, a graph and accompanying bar graph are produced for both CRI and CQS. In each case the bar

graph displays the individual CRI and CQS values (R1-R14 and Q1-Q15 respectively). Additionally, the R and Q values are plotted in the CIELAB colour space along with reference points – which are the ideal individual values of CRI and CQS as illuminated from a source with overall CRI and CQS of 100. The reference points, shown in blue demonstrate what, under an ideal light source with an overall CRI and CQS of 100, the test-colour samples should be. The test points shown in red demonstrate the rendered sample colours under the test light source, allowing for comparison of how close the test-colour samples under the test light source and ideal light source are. This is done for the 14 colours used for CRI and the 15 different colours used for CQS. The accompanying bar graphs give a specific CRI or CQS value between 1 and 100 for each of the colour samples – so the closer the test and reference points of the colour space plot, the bigger the specific CRI or CQS value will be. The CIELAB colour space represents 3 dimensions – L, which is lightness and the axis a* an b* which chromaticity coordinates. The a* axis runs from +a which is more red to -a which is more green and the b* axis runs from +b which is yellow and -b which is more blue. This can be seen on the CIELAB colour space on which the reference and ideal colour point are plotted e.g. *Figure 6.22.*

Initially, the CRI of the initial prototype spectrum (all LEDs at 50% duty cycle) was considered. Shown in *Figure 6.21* is the CIELAB plot showing the test versus reference sample colours for CRI, and *Figure 6.22* shows the individual CRI values for the colour samples for the same spectrum.

It can be seen that the test colours in *Figure 6.21* are relatively close to the reference colours with the exception of a few indicating a good CRI and quality of light. *Figure 6.22* shows the individual breakdown of the CRI values with only the first 8 being averaged to give the CRI Ra value, which for this prototype was 67 out of a maximum score of 100, which is a good starting point.

The CQS value of was found to be 82, again with maximum 100, so the CQS actually rated the prototype output higher than CRI. Shown in *Figure 6.23* is the graph showing the test versus reference colour samples for CQS, along with the individual values for each colour in *Figure 6.24*.

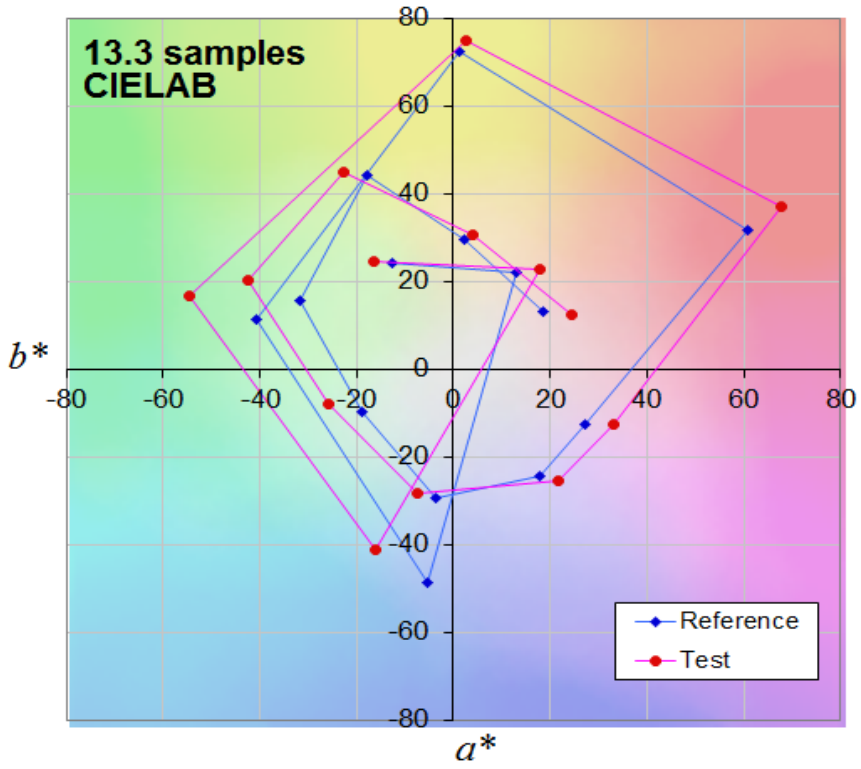

Figure 6.21: Comparison of the 14 CRI colour samples rendered under the blended white light prototype (all LEDs at 50% duty cycle) with the reference samples rendered under an ideal source i.e. a source with a CRI of 100. *NIST CQS program used for analysis.*

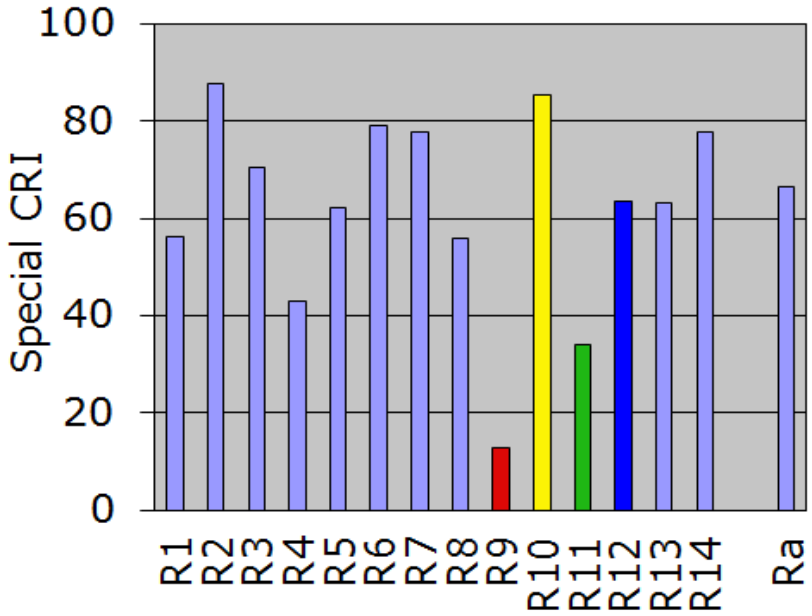

Figure 6.22: Bar Graph showing the 14 individual scores of CRI for each sample colour and the overall CRI value (Ra) – average of the first 8 R_i values – rendered under the blended white light prototype with all LED duty cycles at 50%. Graph demonstrates how the test light source renders colors with reference to the ideal light source, which would have special CRI values of 100 across the chart. *NIST CQS program used for analysis.*

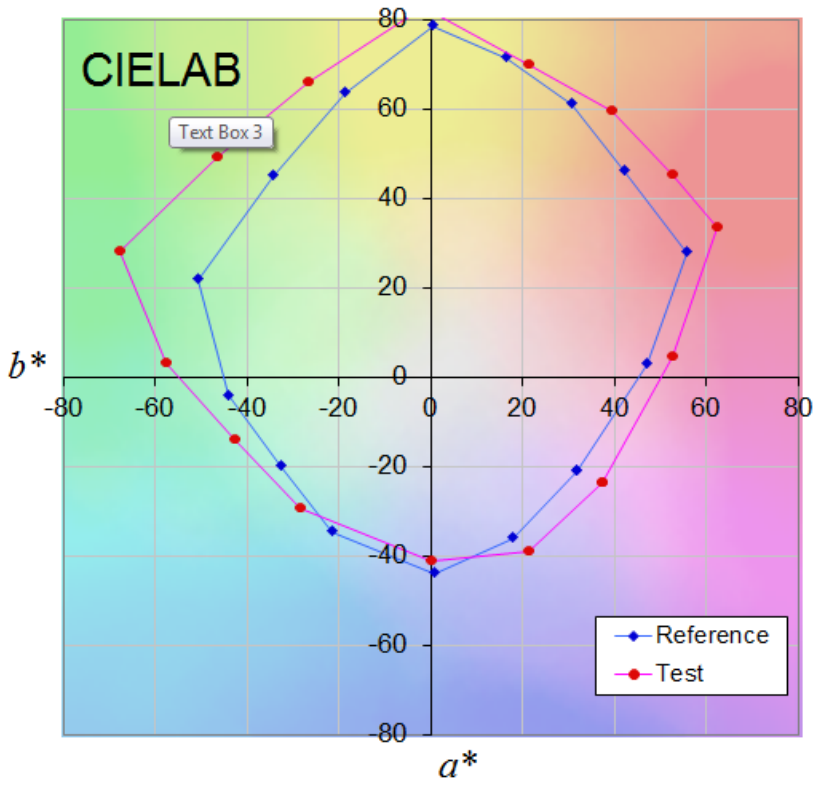

Figure 6.23: Comparison of the 15 CQS colour samples rendered under the blended white light prototype (all LEDs at 50% duty cycle) compared with the reference samples rendered under an ideal source. *NIST CQS program used for analysis.*

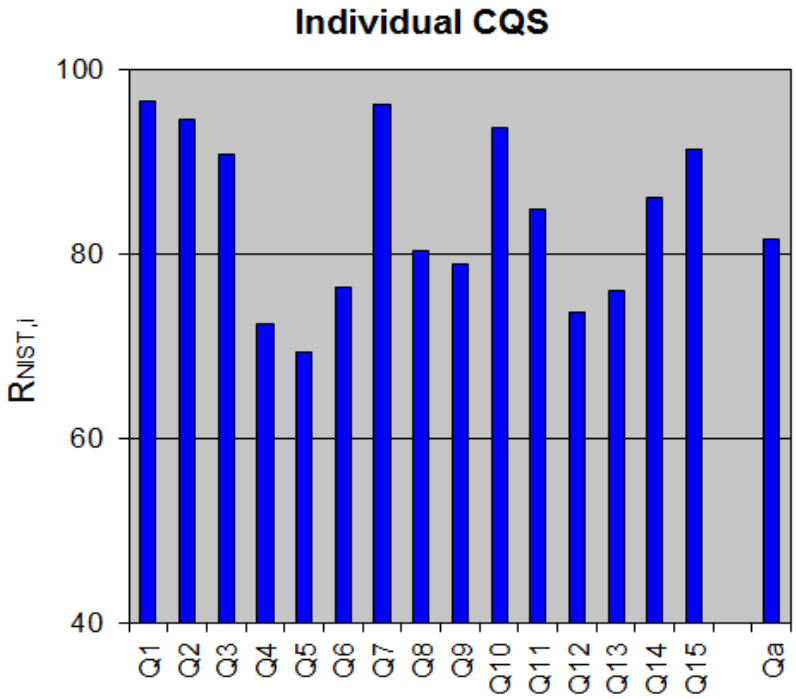

Figure 6.24: Bar graph showing the 15 individual scores of CQS for each of the colour samples with the average CQS value, Q_a – rendered under the blended white light prototype with all LED duty cycles at 50%. Graph demonstrates how the test light source renders colors with reference to the ideal light source, which would have $R_{NIST,i}$ values of 100 across the chart. *NIST CQS program used for analysis.*

As can be seen, most the colours match up well with a few samples scoring very highly - all values however are about 70+, with the average, Q_a, being over 82.

The next step was to analyse the blend of the final output spectrum (duty cycles: red–33%; yellow–80%; green-70%; 405 nm–50%), and compare the results. A side by side comparison of the CRI colour plot and graphs of the initial blend and the final tuned are shown blend in *Figure 6.25 & Figure 6.26*, respectively.

It can be clearly seen that there is a big improvement, between the test and reference colour samples. The majority of the test points plotted on the colour space in *Figure 6.25(b)* are more closely aligned with the ideal reference points. Furthermore, this is corroborated by the overall higher individual CRI values demonstrated on the graph shown in *Figure 6.26(b)* when compared with *Figure 6.26(a)*. The overall CRI value of the final blend is 82 so an increase of 15 in the overall CRI is observed between the initial and final blend, which demonstrated the successful development of a better blend of light through the PWM control.

The CQS showed much less of a numerical increase, increasing by only 1 from 82 with the initial blend to 83 for the final blend. Shown in *Figure 6.27 (a)* & *(b)* respectively, is a comparison of the two CIELAB CQS colour plots of the initial blend of the prototype and the final blend.

The results showed a closer match with the test and reference colour samples of the plot shown in *Figure 6.27* with the final blend than the initial and only a few improvements on the individual CQS scores shown in *Figure 6.28*. However when comparing both CRI and CQS there is a definite improvement in the quality of the light output making for a success in terms of the optical tuning process that was undertaken.

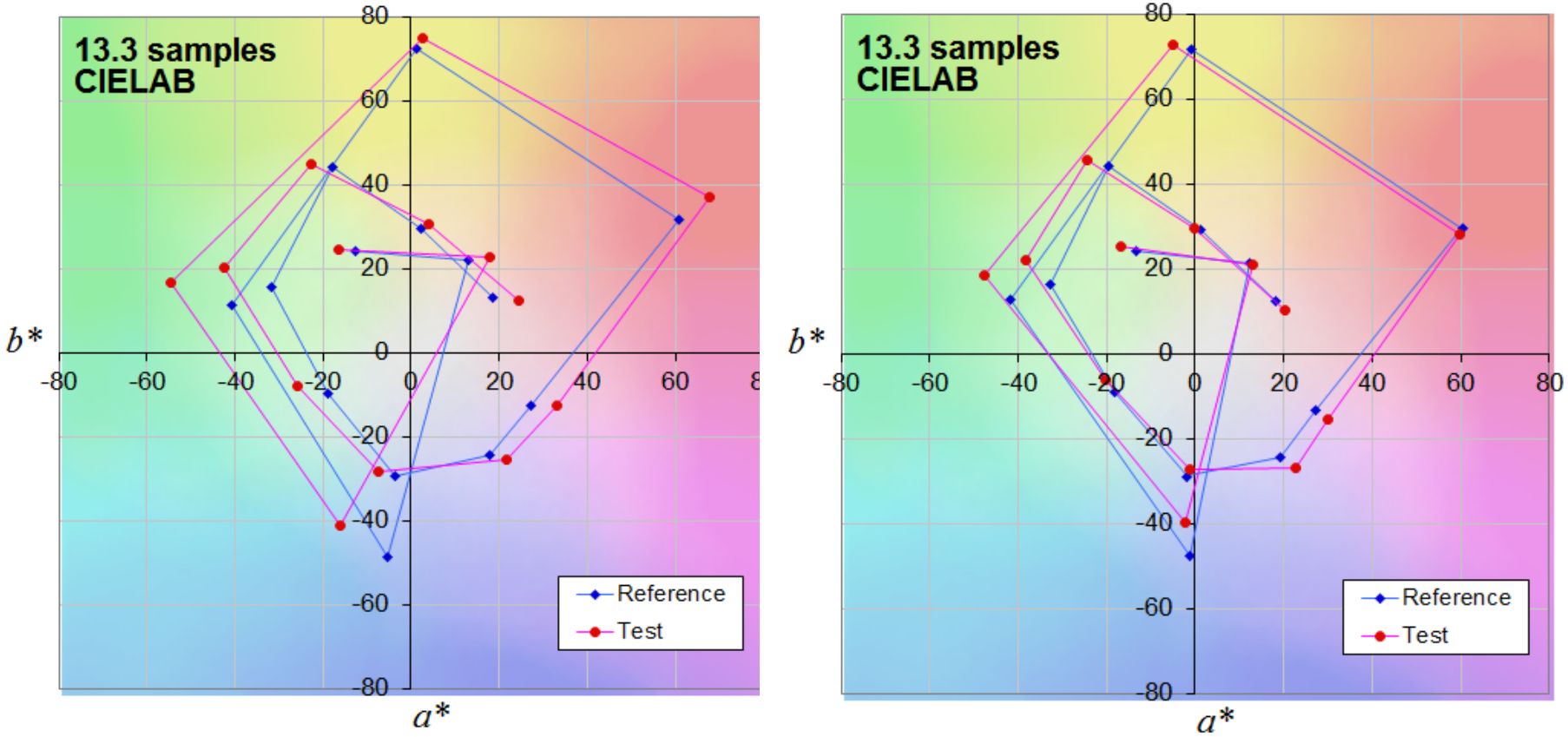

Figure 6.25: Comparison of the CIELAB CRI colour sample plots demonstrating the colour rendering ability of the light sources. (a) Initial blend of light with all colours at 50% duty cycle (b) Final tuned blend with red, yellow, green and 405 nm LEDs at duty cycles of 33%, 80%, 70% and 50% respectively.

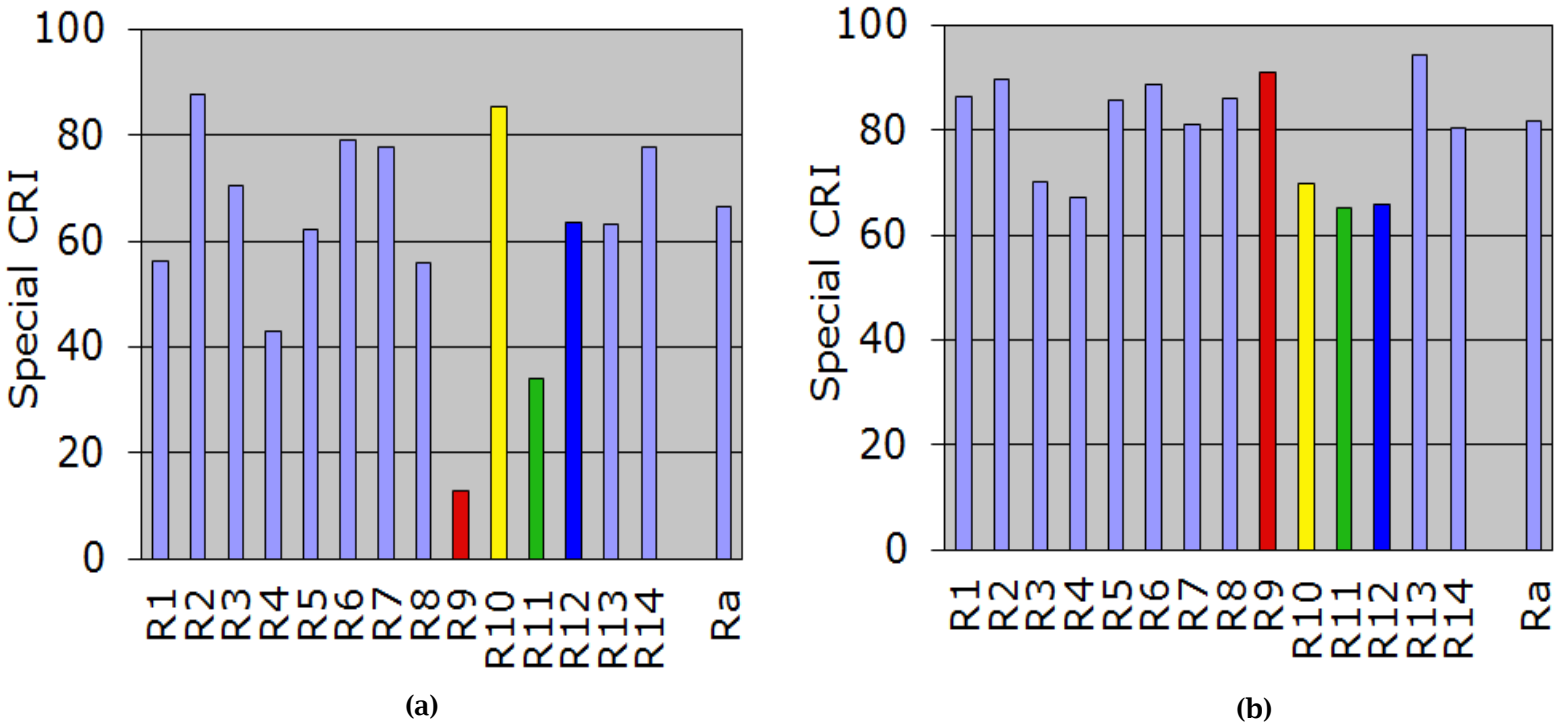

Figure 6.26: Comparison of the 15 Individual CRI values for each of the colour samples used for CRI analysis. (a) Initial blend of light with all colours at 50% duty cycle (b) Final tuned blend with red, yellow, green and 405 nm LEDs at duty cycles of 33%, 80%, 70% and 50% respectively.

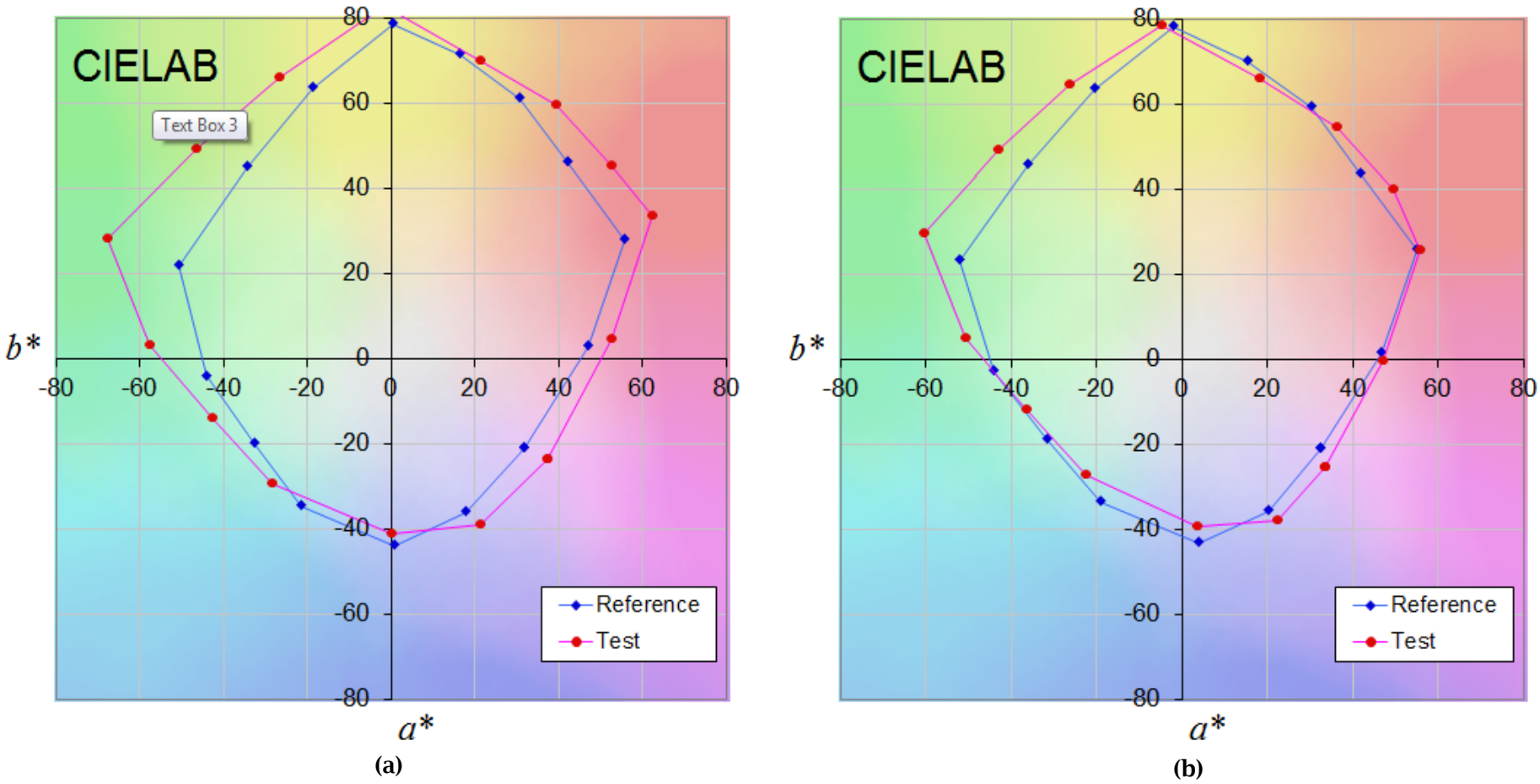

Figure 6.27: Comparison of the CIELAB CQS colour sample plots demonstrating the colour rendering ability of the light sources. (a) Initial blend of light with all colours at 50% duty cycle (b) Final tuned blend with red, yellow, green and 405 nm LEDs at duty cycles of 33%, 80%, 70% and 50% respectively.

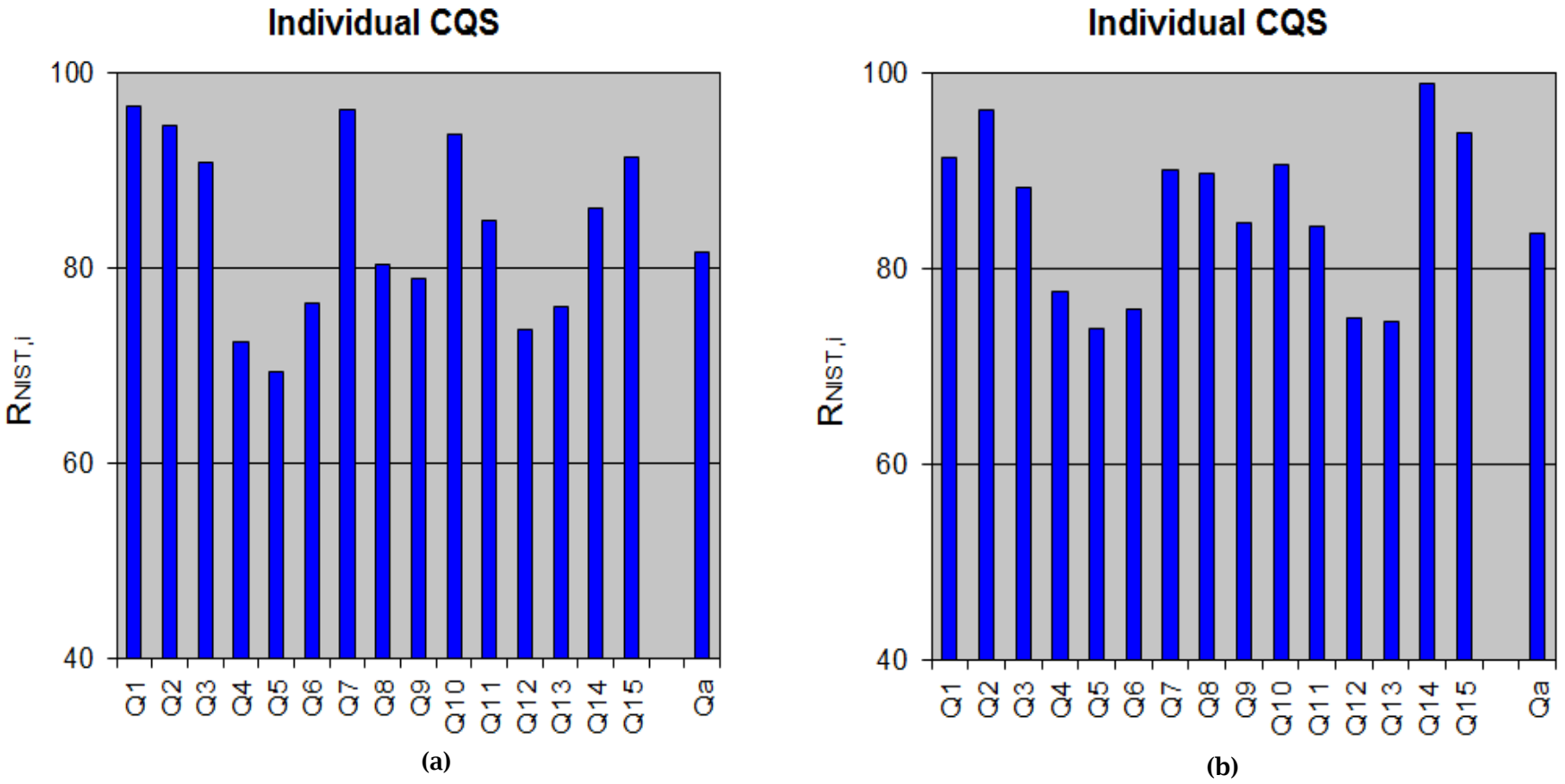

Figure 6.28: Comparison of the Individual CQS values for each of the colour samples used for CQS analysis. (a) Initial blend of light with all colours at 50% duty cycle (b) Final tuned blend with red, yellow, green and 405 nm LEDs at duty cycles of 33%, 80%, 70% and 50% respectively.

Analysis was also undertaken of the values of CRI, CQS and CCT for the intermediate stages of the tuning process in comparison to the initial and final blends. The values are shown in *Table 6.4*.

Table 6.4: Summary of the CRI, CQS & CCT for the four main stages in the optical tuning process of the blended prototype.

Duty Cycle Settings	*CRI*	*CQS*	*CCT (K)*
Initial: ***all LEDs = 50%***	67	82	4867
Altered Red Content: ***405 nm, yellow, green = 50%; red = 33%.***	74	83	6008
Altered Red & Green Content: ***405 nm, yellow = 50%; red = 33%; green = 70%***	81	83	5937
Final – Altered Red, Green & Yellow Content: ***405 nm = 50%; red = 33%; green = 70%; yellow = 80%***	82	83	5805

The results in *Table 6.4* show that the CRI improves incrementally thoughout the tuning process, however the CQS improves only between the first and second stages of tuning. The CCT increases from the intial CCT value, indicating that the blend is moving to a cooler blend of white light which is not nessecarily a problem unless it goes too far in that direction. The blend would come down to the application in the end – so it should be tailored to where the light is to be deployed. With warmer whites used for a more relaxed evironment and for clinical applications more of a cool white, perhaps about 4000K, since there will be a mix of patients residing for long periods but also staff working – so a balance between the two would be required.

Overall, on the basis of pulsing as the key concept, this chapter has involved a prototype system being designed, constructed, tested and optically tuned to achieve a better blend of white light. On the whole, the objective has been successfully achieved. The system operated as designed and the optical tuning demonstrated an

improvement in the quality of the blended of white light using PWM to control the LEDs output, acheving a substantial increase in the CRI value and an increase in the CQS value of the prototype. Chapter 7 will involve further development of this prototype, and comparison of these will be discussed in *Section 7.2* at the end of the next chapter. The next stage is to test the antimicrobial effects of the new prototype.

6.4.3 MICROBIOLOGICAL TESTING OF THE OPTICALLY TUNED BLENDED WHITE LIGHT PROTOTYPE

6.4.3.1 Experimental Methodology

With the prototype constructed, operational and tuned for the best achievable blend of wavelengths, the next step was to evaluate the antimicrobial effects. Bacteria were prepared as described in *Section 3.1.3.2*, and for all experiments, 100 µl 10^3 $CFUml^{-1}$ bacterial suspensions were pipetted and spread onto 50 mm diameter nutrient agar plates (Oxoid Ltd., UK). This sample volume provided a population density of approximately 250-350 CFU/plate, and was selected as a good representation of the typical levels of environmental contamination that can be collected from surfaces by contact plate sampling (Maclean *et al.*, 2010). Seeded plates (n=3) were positioned at a distance of 10 cm below the pulsed LED system (as shown in *Figure 6.29*) and exposed for increasing durations of time.

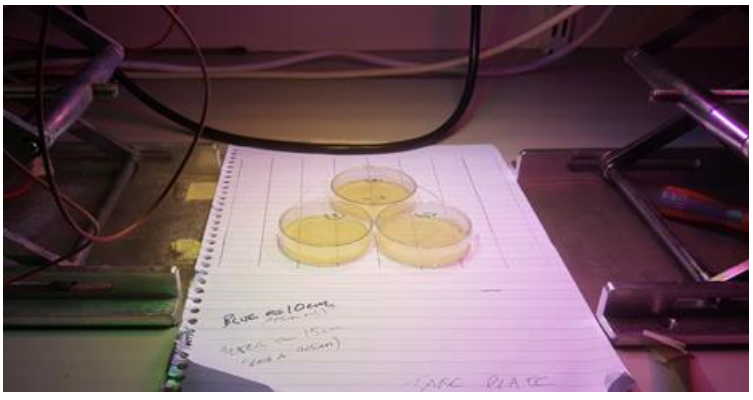

Figure 6.29: Picture demonstrating the placement and arrangement of the 3 agar plates, seeded with bacteria, under the light prototype being subject to the mixed blend of 405 nm and supplementary colours.

The irradiance measurements were taken 10cm under the light source, and the placement of the plates was selected such that the centre of each plate was illuminated with an average irradiance of approx. 1.5 $mWcm^{-2}$ 405 nm light (peak irradiance 3 $mWcm^{-2}$ pulsed at 50% duty cycle). Control samples were prepared which were exposed to standard laboratory lighting for the same durations. Post-exposure, all sample plates were incubated at 37 ˚C for 24 hours, and surviving populations were then enumerated, with results reported as CFU/plate. For statistical analysis, a one-way ANOVA was carried on the mean populations, with post-hoc Tukey tests where required (Origin Pro 2019b).

Using the final blended prototype (red–33%; yellow–80%; green-70%; 405 nm–50% duty cycles), three different light output settings were selected for exposure of bacterial samples. The microcontroller coding was altered in each case to switch different colours on and off, however all other parameters were kept the same (frequency, duty cycle and irradiance). The 3 different light outputs were:

1. All LEDs (red, yellow, green and 405 nm) ON: referred to as ***RYG-405 mix***
2. The 405 nm LEDs ON, with red, yellow and green LEDs switched OFF: referred to as ***405 alone***
3. Red, yellow and green LEDs ON and 405 nm LEDs OFF: referred to as ***RYG mix***

For these experiments, two species of bacteria were used: *Staphylococcus aureus,* a Gram-positive cocci; and *Pseudomonas aeruginosa,* a Gram-negative rod. Bacterial sample plates were exposed to each of the 3 different light outputs, for 15, 30, 45 and 60 minutes. Experiments were carried out in triplicate, with 3 sample plates exposed each time for each time point.

The optical emission spectrum of the *RYG-405 nm mix* is illustrated in *Figure 6.30(a)*. The *RYG mix* spectrum is the same but without the 405 nm peak, so no violet content, as Illustrated in *Figure 6.30(b)*: whilst the *405 nm alone* spectrum is just the

violet spread around the 405 nm peak with no other wavelength content as illustrated in *Figure 6.30(c)*.

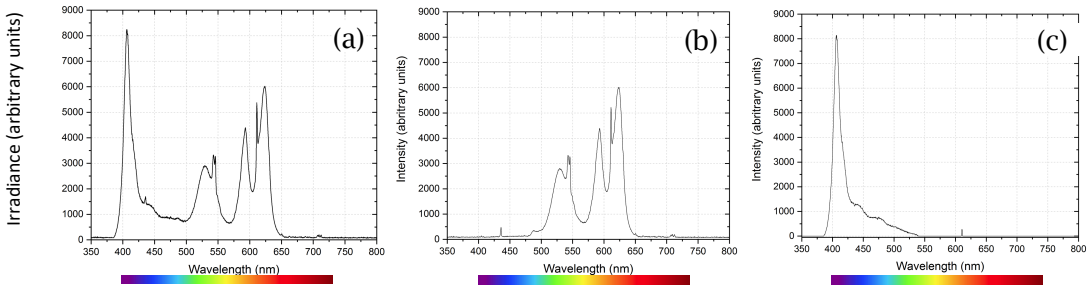

Figure 6.30: Spectra of the light output spectrum for each of the 3 setting for microbial testing. (a) *RYG-405 mix* (b) *RYG mix* (c) *405 alone.*

The irradiance of the *405 alone* was measured at the start and end of each exposure using the radiant optical power meter and, as stated, was measured at the centre of each plate to be an average of approximately 1.5 $mWcm^{-2}$ (which is a peak of approximately 3 $mWcm^{-2}$ due to it being pulsed at a 50% duty cycle). Based on the peak irradiance, this meant the plates were treated with doses of 1.35 Jcm^{-2} (15 min), 2.7 Jcm^{-2} (30 min), 4.05 Jcm^{-2} (45 min) and 5.4 Jcm^{-2} (60 min). The irradiance of the other 2 settings could not be accurately measured with the radiant optical power meter as it is not accurate for broadband light measurements. However, it was used to give an arbitrary reading of the irradiance at the beginning and end to make sure there was no change throughout the exposure and to make sure each exposure was subject to the same irradiance.

6.4.3.2 Experimental Results

The results of *S. aureus* and *P. aeruginosa* exposure to the *RYG-405 mix* are shown in *Figure 6.31*. All doses refer to the dose of 405 nm light content – not any of the other wavelengths of light.

In *Figure 6.31(a)*, the results for the *S. aureus* exposure to the *RYG-405 mix* are shown, and it can be observed that over the 60-minute exposure time (5.4 Jcm^{-2}) under the blended light source, the bacterial population underwent a relatively linear

reduction of approximately a 1.6-$\log_{10}$ across the 4 time points. The reduction of bacterial population was statistically significant when compared with the non-exposed populations from the 15-minute time point (P=0.006) right through to the 60-minute time point ($p=4.26\times10^{-5}$). A sizable observable reduction of 57% is demonstrated between the 15-minute (1.35 Jcm^{-2}) and the 30-minute time point (2.7 Jcm^{-2}). The total percentage reduction in surviving bacterial population after the 60-minute exposure is approximately 97%. The non-exposed population remained consistently between 300-400 CFU/plate.

Figure 6.31(b) displays the results of the *P. aeruginosa* exposure to the blended light, *RYG-405 mix*. Similar to the *S. aureus* exposure, the exposed bacterial populations demonstrate a significant reduction ($p\approx0.000$) over the 60-minute exposure (5.4 Jcm^{-2}) from approximately 370 CFU/plate down to less than approximately 2 CFU/plate (2.2-$\log_{10}$ /99.4% reduction). The population does not appear to drop until the 30-minute time point (2.7 Jcm^{-2}) where it drops in the region of 22% and statistical analysis confirmed a significant difference (p=0.03) between the exposed and non-exposed samples at 30-minutes exposure. The largest drop in population occurs between the 30- and 45-minute time points (2.7 Jcm^{-2} and 4.05 Jcm^{-2} respectively), and by 60-minutes (5.4 Jcm^{-2}) the surviving population is reduced to single-digit CFU/plate values. The non-exposed samples showed minimal variation over the course of the exposure – again remaining between 300-400 CFU/plate. This successfully demonstrates that the prototype works as a concept, in that the light quality has been improved and the blended unit can still inactivate bacteria successfully.

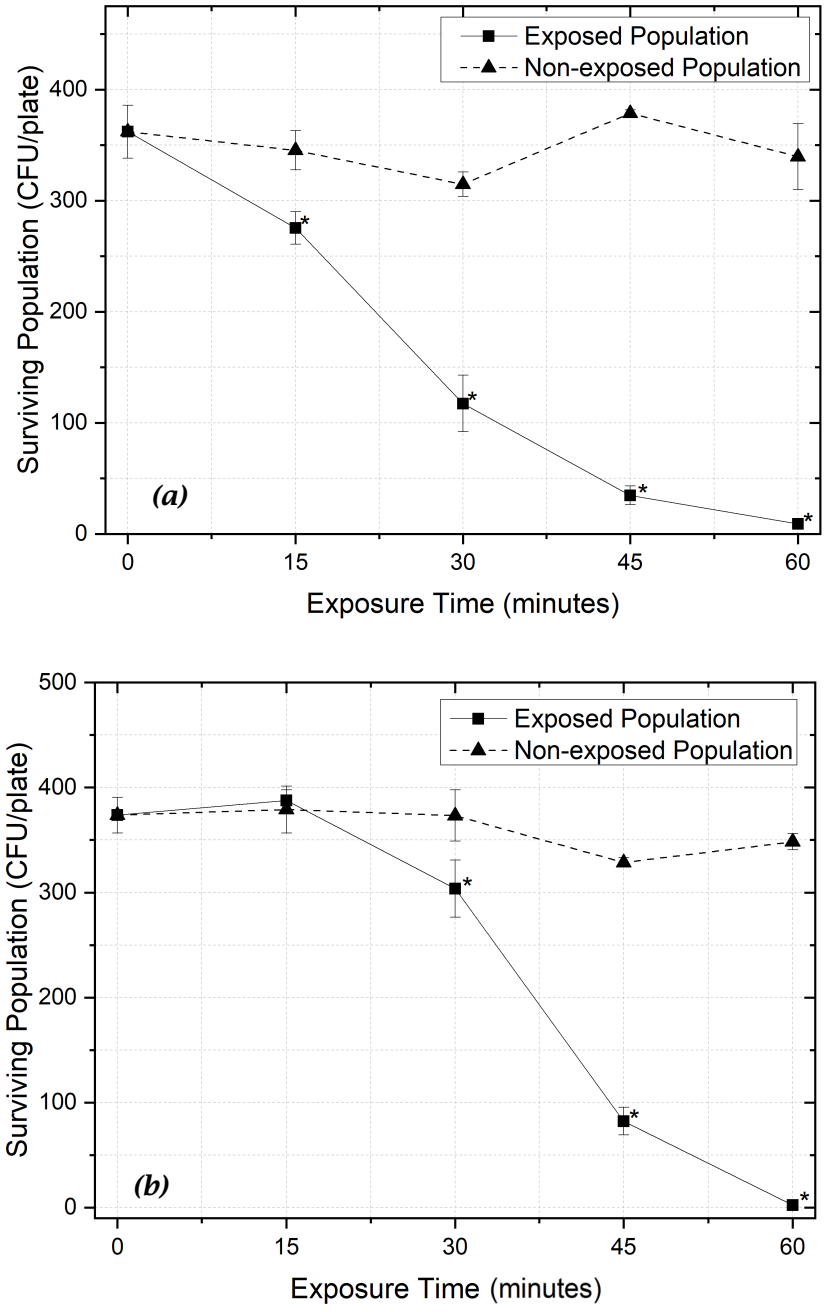

Figure 6.31: Inactivation of (a) *S. aureus* and (b) *P. aeruginosa* under the blended prototype set up to output *RYG-405 mix*. Exposures were carried out at 15-minute intervals with an average 405 nm light irradiance of approximately 1.5 mWcm^{-2} (peak irradiance being 3 mWcm^{-2}). Data points represent the mean values (n=3± SD) of surviving population. Lines are for visual guidance. * represents a significant difference compared with the equivalent control value ($p<0.05$).

In order to determine whether the supplementary colours provided any contribution to the antimicrobial efficacy, the next phase of investigation was to repeat the experiment using *405 alone*, and establish any possible difference in

performance. The results from the *405 alone* exposures for *S. aureus* and *P. aeruginosa* are shown in *Figure 6.32*.

When the plates seeded with *S. aureus* were exposed to the *405 alone* setting, shown in *Figure 6.32(a)*, it can be observed that over the 60-minute exposure time, the bacterial population shows a significant reduction ($p=3.72\times10^{-5}$), demonstrating a reduction of 99.6% / 2.4-$\log_{10}$ reduction over the 60-minute exposure (5.4 Jcm^{-2}). The bacterial population significantly drops by 22% after 15 minutes exposure (p=0.01). A mean drop of 45% was observed by 30 minutes (p=0.190) with a dose of 2.7 Jcm^{-2}, although there was a high degree of variation between the triplicate samples (highlighted by the error bars). By the 45-minute time point (4.05 Jcm^{-2}) the majority of the population had been inactivated (98.9% / 1.94-$\log_{10}$, reduction. The non-exposed samples remained consistent over the 60-minute exposure period.

Figure 6.32(b) shows the results of the *P. aeruginosa* exposure to the *405 alone* and similar to the results from the exposure to the *RYG-405 mix*, an overall downward trend over the 60-minute exposure time is observed. Over the full 60-minute exposure (5.4 Jcm^{-2}) there is a 1.77-$\log_{10}$ / 98.3% reduction ($p\approx0.000$) in the surviving population of the exposed samples compared to the non-exposed samples. Exposures of 15 and 30-minutes (1.35 Jcm^{-2} and 2.7 Jcm^{-2} respectively) showed no significant difference between the exposed and non-exposed populations (p=0.98 and p=0.13, respectively), however by 45-minutes exposure (4.05 Jcm^{-2}) a 0.7-$\log_{10}$ / 80.5% reduction in population was achieved ($p=1.145\times10^{-5}$).

When comparing the first two exposures from the *RYG-405 mix* and the *405 alone*, both the *S. aureus* and the *P. aeruginosa* demonstrate similar trends and almost identical levels of inactivation over the 60-minute exposure. Shown in *Figure 6.33* are the inactivation curves of *S. aureus* and *P. aeruginosa* comparing the *RYG-405 mix* exposure to the *405 alone* respectively for each organism. The data has been plotted as percentage surviving population to facilitate direct comparisons between the two experiments, and as can be seen from the graphs, the inactivation kinetics using the 2 settings follow very similar trends for each organism.

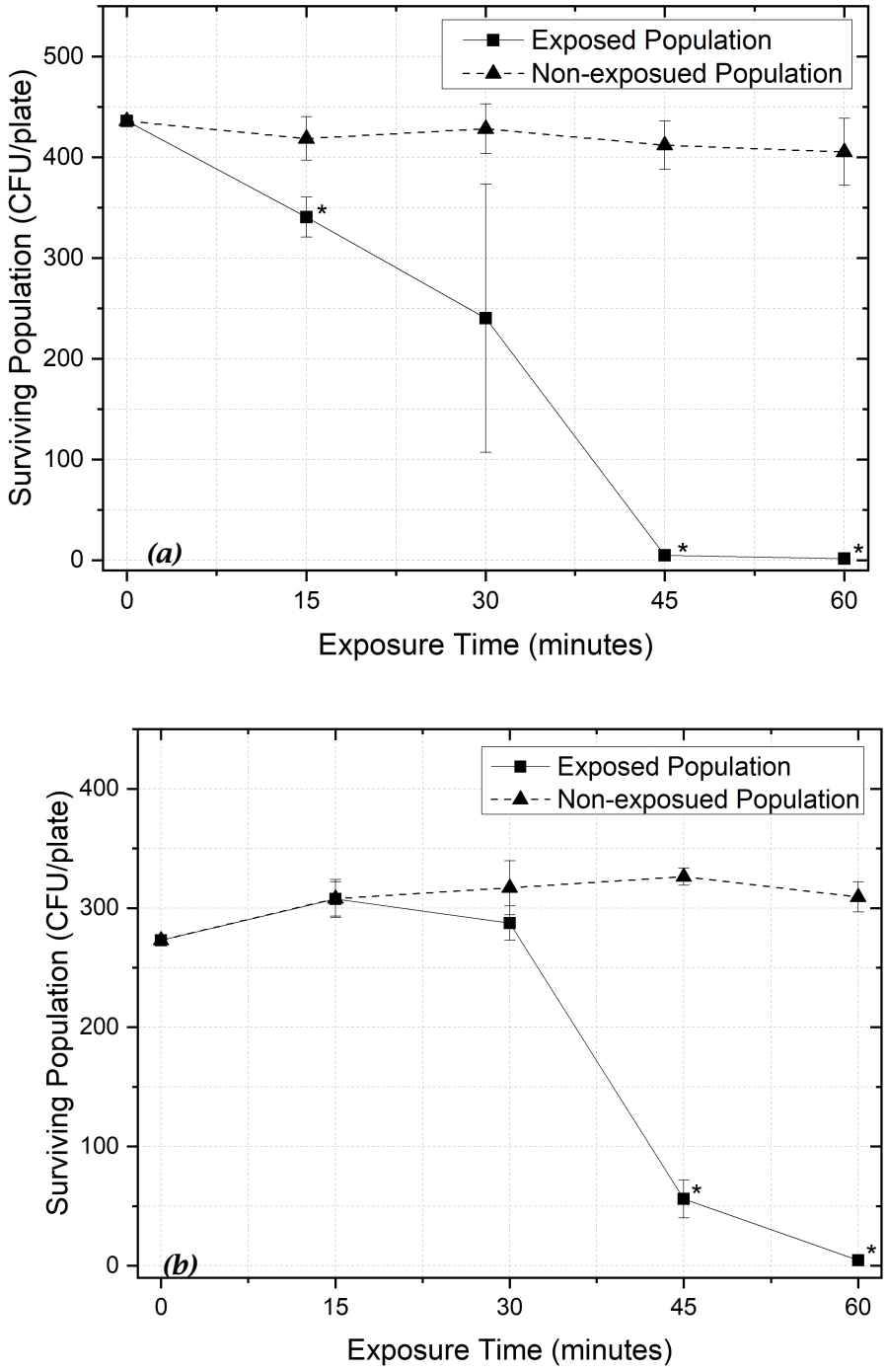

Figure 6.32: Inactivation of (a) *S. aureus* and (b) *P. aeruginosa* under the prototype set up to output *405 alone*. Exposures were carried out at 15-minute intervals with an average 405 nm light irradiance of approximately 1.5 mWcm^{-2} (peak irradiance being 3 mWcm^{-2}). Data points represent the mean values (n=3± SD) of surviving population. Lines are for visual guidance. * represents a significant difference compared with the equivalent control value ($p<0.05$).

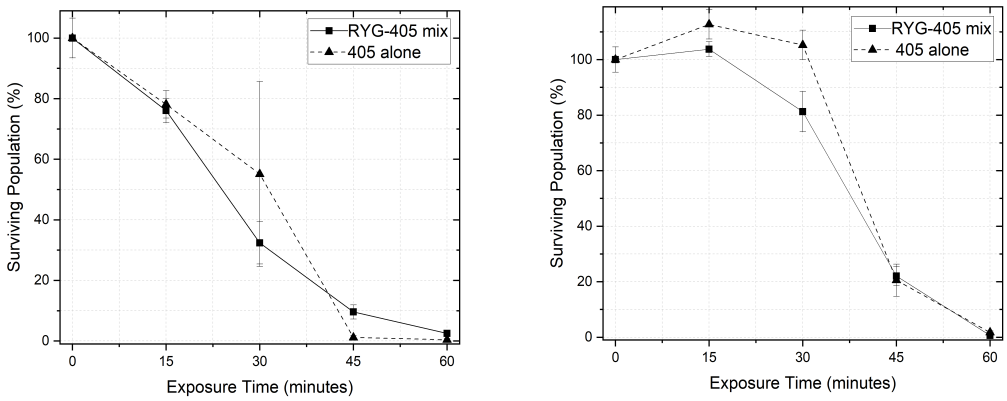

(a) *(b)*

Figure 6.33: Comparison of the inactivation curves after exposure to *RYG-405 mix* and *405 alone*. (a) Inactivation of *S.aureus* (b) Inactivation of *P. aeruginosa*. Data points represent the mean values (n=3± SD) of surviving population as a percentage of the average starting population. Lines are for visual guidance.

Finally, the bacterial contamination was exposed to the *RYG mix*: to evaluate the effects of the light source with only the supplementary colours, and no 405 nm light. Results for *S. aureus* and *P. aeruginosa* are shown in *Figure 6.34*.

For both organisms, exposure to *RYG-mix (Figure 6.34(a), 6.34(b))* caused no observable effects over the 60-minute period. Contamination levels remained consistent, and in both cases, statistical analysis showed there to be no significant difference ($p>0.05$) between any of the exposed and non-exposed sample populations at any given time point. These results demonstrate that the supplementary light has no significant effect, positive or negative, on the antimicrobial effects of the light source, and thus all inactivation is achieved through the photodynamic action of the 405 nm light.

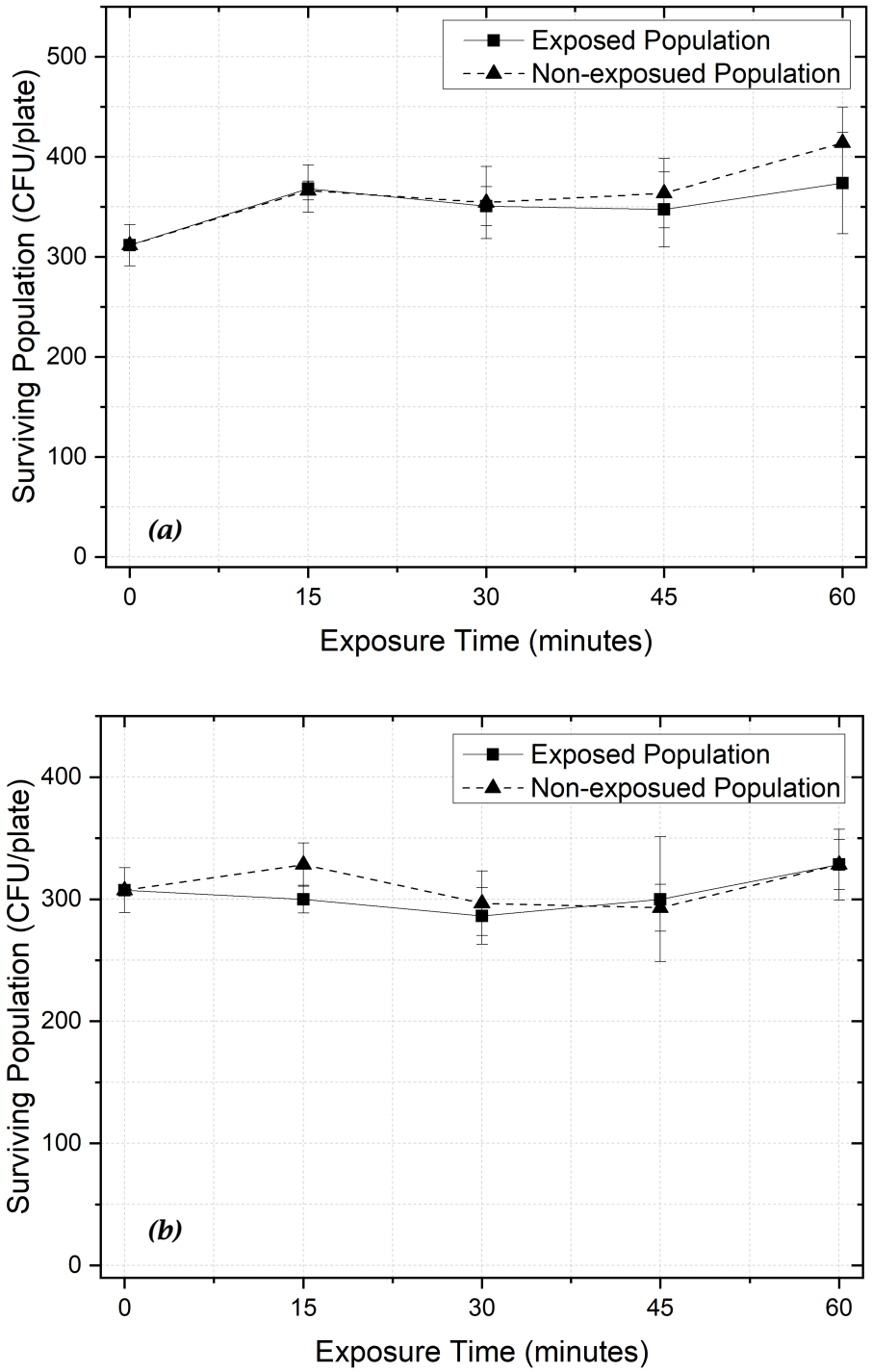

Figure 6.34: Inactivation of (a) *S. aureus* and (b) *P. aeruginosa* under the prototype set up to output *RYG mix*. Exposures were carried out at 15-minute intervals. Data points represent the mean values (n=3) of Surviving population ± SD, standard deviation. Lines are for visual guidance.

6.5 DISCUSSION

The prototype unit designed and built in this chapter shows promise for the concept. It demonstrated: the use of 405 nm light supplemented with other wavelengths to increase the quality of the light output – in terms of colour quality; the success in using PWM as a means to control the blend of wavelengths output from the unit; and finally, successful inactivation of two common hospital pathogens (*S. aureus* & *P. aeruginosa*). Along with the success however, various issues and questions regarding the concept arose and were highlighted during the process.

6.5.1 THERMAL DESIGN ISSUES

One of the big issues in working with LEDs in general is temperature. LEDs and LED arrays are sensitive to temperature, and with an increasing temperature the LED output irradiance drops (Schubert, 2006). Even in the initial stages of designing the surrounding circuitry for the LEDs, temperature came into play. When deciding upon which resistors to use in conjunction with the LEDs, the calculations were carried out initially, and then in practice the resistors had to be changed due to varying current draws and temperature. As temperature increases so does the I-V characteristic of the LED. This can cause increases in the current drawn by the LED and thus produce more heat, in turn causing more current to be drawn, leading to thermal runaway and component failure, if a constant current is not maintained. This design did not use a constant current driver – it was designed on a single constant voltage source with the current controlled by the LED characteristic and a resistor in each of the branches. The constant current driver wasn't employed because each LED, or array of LEDs, ran at a different current and so 4 drivers would have been required – additionally it wasn't known what current each LED would run at in practice so the constant voltage source was used instead. The use of constant current LED drivers however would be a sensible way to refine the design once all LEDs have been selected and proven to work. A constant current source or several could be incorporated into the design to avoid any issues with thermal runaway or overdraw of current.

The main source of heat in the system comes from the LEDs themselves as they produce heat along with light; so, the temperature has to be monitored and taken into account during the design process in order to control the operation and output of the LEDs. Small things like wear on electrical components could also affect the power drawn by the LED and so in a refined and future version of the prototype, a means of tuning the blend remotely via an interface could be a useful addition to the unit. The tuning function could also possibly be automated – creating a self-tuned blended LED. If the LED outputs were monitored by in-built photodiodes, then the microcontroller could alter the levels of each colour with reference to programmed preset levels. In any circumstance, it would be a useful addition to have control of the blend and light output of the unit after installation.

6.5.2 Aesthetics and Acceptability of Light Quality and Blending

Another issue relates to the aesthetics of the light – both in terms of the design and the light output produced. Addressing the former – there were issues which arose affecting how the unit looked. Ideally, the LEDs would be positioned very closely together and then the aperture covered with frosted glass or diffuser so that the light unit functions as a single non-point source of white light. In reality however, this was not achievable. The LEDs in the prototype build were mounted on individual PCBs to avoid any thermal build up during operation, which meant that the LEDs couldn't be arranged close together. Furthermore, because the LEDs did not output high irradiances of light, the aluminium panel was kept at its lowest position, closest to the aperture, so the output irradiance was sufficient for microbial inactivation. The inclusion of a diffuser or frosted glass panel for blending would require the LEDs to be moved further back from the aperture and further reduce the irradiance. Also, in terms of the diffuser or frosted glass, the distance between the diffuser and LEDs would have to be substantial enough to defocus the LED arrays to achieve a blended white non-point source light; so, the diffuser or frosted glass panel was excluded in this case due to the relatively low irradiances of the LEDs.

This meant that, from the underside of the current design, all the LEDs appeared as point sources of each colour, and as the unit is proposed to be mounted in the ceiling this is what would be readily seen. Ideally, the LED arrays would be mounted on a single PCB as close together as possible with a regular repeating pattern of colours – maybe groups of 4 colours at regular intervals depending of the thermal characteristics of the setup. Having the LEDs closer together may require some active cooling via a fan, or for example Peltier module as used in chapter 5 but would make blending much easier. With more of a modular approach to the LED placement i.e. an arrangement of 4 different colour LEDs together with a small footprint – a module, which could then be replicated to cover larger areas – the frosted glass or diffuser could then be incorporated to produce, visually, a much more blended white light.

As mentioned – there were issues with the light output as well as the design of the light unit. Due to the size of the LED PCBs, they could not be placed closely together - this meant that colour shadows were apparent under the light. Due to the light sources being relatively spaced out, each colour caused colour shadows depending on the position of the LEDs and the object, which would be unacceptable in a commercial design. This is a definite issue, which would have to be addressed in future iterations or designs. Again, the issue is with the LED sources being so far apart and the limited blending. This issue along with other issues, and possible solutions, will be further discussed in *Section 7.2*.

There was limited work carried out investigating the irradiance mapping due to the lack of blending and suitable equipment. The power meter, used for irradiance readings, is not suitable for broad spectrum light readings due to its wavelength sensitivity. The spectrometer used for capturing emission spectra used an optical fibre with a very small aperture for light capture which meant that pointing the optical fibre directly at the light source would give greatly varying readings depending on the position of the fibre. It is possible that the reflection spectra from a white piece of paper placed under the light unit could be measured – however there was no accurate way to align the optical fibre each time to sections of a grid under

the unit. For future analysis, more suitable optical capture equipment would be useful to look at the spread of wavelengths in the area under the unit. This would be more useful when the LEDs are positioned closer together and blended to a better extent than in the prototype built in this chapter.

Specifically referring to the prototype built – the yellow content was too low to match the level achieved by the white LED. The content between approximately 550-600 nm is lacking and so in the next design iteration this range of wavelengths should be filled out more. Ideally, an improvement would be to include an extra wavelength or several extra wavelengths of LED to ensure a more consistent spread of wavelengths across the spectrum. There will however be a compromise between how many colours can be included to better represent white light versus the space, circuitry, power requirements and cost of the unit.

During the measurements of the light output of the prototype, the spectra were captured using the spectrometer, normalised and input into the NIST Light Quality program, which provided analysis on the spectrum. The CCT, CRI and CQS were output and the CRI and CQS could not be calculated from the 405 nm spectrum alone because there was not enough of a spectral spread, so an improvement was demonstrated with the addition of supplementary colour allowing the program to analyse the spectra properly. The tuning process resulted in an improvement from 67 to 82 in CRI and 82 to 83 in CQS (data summarized in *Table 6.4*). Whilst this is useful in quantifying the quality and spread of wavelength content in the light output, it still gives no measure of how the light blends together. As can be seen from *Figure 6.9(b)* of the setup, the different coloured LEDs were clearly visible and although the light content was acceptable for rendering colours, the colour shadows were evident (*Figure 6.19)* partially due to a lack of blending. Future work would be to look at a way to quantify how blended a light source appears visually, opposed to just the content of the light. This is partially a subjective issue, as is a lot of the subject matter when it come to an acceptable and comfortable blend of light, so a possible option

for quantification of the blending and acceptability would be to use an opinion poll or panel for a spectrum of opinions on the acceptability of the light source.

6.5.3 Question of Scalability

There is also the question of scalability. With the current prototype, a good blend was produced and bacterial inactivation achieved, however the question remains as to whether this could be viably scaled up to provide room lighting with a useful level of 405 nm light content to disinfect the surrounding environment. A concern in scaling up, with the requirement for higher irradiance levels of 405 nm light and other LEDs, along with the control circuitry for pulsed operation, and appropriate thermal management, is the question as to whether the power requirements would be too high for the developed unit to be financially viable. Again, these issues are hard to address on the small-scale system currently developed. The fact that 405 nm technology has proved to be effective for reducing environmental bacterial contaminants (Bache *et al.,* 2012; Maclean *et al.*, 2010; Maclean *et al.*, 2013), and the technology has been successfully commercialised by Kenall Lighting and Hubbell Lighting, suggests that the concept of using pulsed control to produce a blended white light prototype could be developed into a viable system.

6.5.4 Consideration of Safety

As the application of an antimicrobial blended visible light system is towards decontamination of occupied environments, such as hospital wards, an important topic to be addressed is the optical safety of the unit. The wavelength ranges and associated injury that can be caused by optical radiation was detailed in *Section 2.6.* The pulsed light in this prototype consists of 405 nm peak light content pulsed at 50% duty cycle and the peak irradiance of the light would be the same magnitude as an equivalent continuous unit. However, if it was decided to use a higher peak irradiance to enable the use of reduced duty cycles in a future iteration, the threshold limit value would have to be investigated so as to avoid the blue light hazard

associated with blue/violet light. Additionally, the threshold limit value (TLV) for the supplementary colours would also have to be assessed if the prototype was scaled up to ensure it was within any photothermal or photochemical injury limits.

Work by Endarko (Endarko, 2011) carried out TLV calculations for the HINS-light EDS unit investigating what was a safe level of optical radiation to have constant exposure to. The main concern was to ensure that the levels of 405 nm light emitted by the EDS were within ICNIPR guidelines (ICNIRP, 1997). The EDS output at 405 nm was an irradiance of 0.32 $mWcm^{-2}$ at a distance of 200 cm from the source, and this resulted in an effective light radiance value less than the 10 $mWcm^{-2}sr^{-1}$ TLV, with a normal healthy eye being subject to the range of 4-8% of the TLV. Similarly, the study by Endarko (2011) demonstrated that the light levels generated by the EDS also satisfied safety requirements for the UV, UV-A and retinal thermal hazards.

The prototype constructed in this chapter demonstrates a peak irradiance of 3 $mWcm^{-2}$ at a distance of 10 cm. As demonstrated in *Equation 6.1,* the irradiance of radiation follows the inverse square law i.e. with every unit of distance further away from a point source, the irradiance drops by the unit of distance squared (Voudoukis and Oikonomidis, 2017).

$$I_y = \frac{I_x}{D^2} \qquad \textit{Equation 6.1}$$

Where I_x *is the irradiance in* $mWcm^{-2}$ *at a distance* x *in cm;* D *is the distance from the source as a multiple of* x*; and* I_y *is the irradiance in* $mWcm^{-2}$ *at the new distance, the product of* D *and* x*. With this being the case, if the prototype generates 3* $mWcm^{-2}$ *at a distance of 10 cm, then the irradiance at 200 cm would be*

$$I_y = \frac{3}{(20)^2} = \frac{3}{400} = \mathbf{7.5 \times 10^{-3}\ mWcm^{-2}}$$

This substantially lower than the optical output deemed safe for exposure by Endarko (Endarko, 2011), however upon scale up, safety considerations would again have to be addressed.

The microbial experiments carried out demonstrated significant ($p<0.05$) inactivation with the *405 alone* exposure and the *RYG-405 mix* exposure. The average 405 nm irradiance at the centre of each of the agar exposure plates was 1.5 $mWcm^{-2}$ (or a peak irradiance of 3 $mWcm^{-2}$). This however would be hard to achieve for instance in a hospital room, specifically if the light was mounted in the ceiling over 2m from the floor. To achieve this irradiance level across all surfaces, the irradiance would have to be very high and would be particularly high at eye level - likely exceeding the TLV. It is likely, upon scaling up, the irradiances would be lower than that used in the experiments in this chapter – similar to previous HINS-EDS unit levels for example around 0.32 $mWcm^{-2}$ at a distance of 200 cm, as documented by Endarko (Endarko 2011). The inactivation rate would be slower, however clinical studies by Bache and Maclean (Bache *et al.,* 2012; Maclean *et al.,* 2010; Maclean *et al.,* 2013) demonstrate successful environmental decontamination at these levels – and they adhere to all safety guidelines discussed in *Section 2.6.* A more in-depth comparison of systems and the inactivation kinetics with the published studies using the HINS-EDS unit and the prototypes build in this and the subsequent chapter will be discussed at the end of the next chapter, in *Section 7.2.*

The prototype would have to be sizably scaled up to partial or full room decontamination levels before the issues discussed in this section, along with safety parameters, could be adequately realised and properly investigated.

6.6 CONCLUSION

The goal of designing and building a prototype antimicrobial-pulsed blended white light unit was achieved. With the results from Chapter 5 demonstrating a higher efficacy, in terms of inactivation per optical dose delivered, with a pulsed optical dose delivery, the starting point for the prototype development in this chapter was to build

the design around the pulsing concept using the 50% duty cycle – so as to achieve the increased antimicrobial efficacy as demonstrated in Chapter 5. The pulsed 405 nm light was supplemented with pulsed red, yellow and green content demonstrating an observable improvement in the light quality in terms of how it rendered colours. The pulsing was crucial in the optical tuning process. It allowed for the content of each colour, i.e. the output of each LED, to be controlled using the microcontroller. The pulse width was changed in order to control the colour content in the prototype and made the tuning process much simpler.

Additionally – as demonstrated in Chapter 5 – the pulsed 405 nm light can produce comparable levels of antimicrobial activity as continuous – and so the 405 nm light was pulsed at 50% thus making the 405 nm content visually less intense whilst still maintaining a higher peak irradiance. An apparent less intense 405 nm is then easier to blend with other colours to produce the white light objective. The CRI and CQS values were greatly increased when the supplementary colours were added – and using PWM to tune the supplementary colour composition, the CRI and CQS values were further improved.

Furthermore, the light unit was a success in terms of antimicrobial activity. Whilst demonstrating a higher CRI and CQS – a better quality of light – the light output from the unit demonstrated significant bacterial inactivation of both *S. aureus* and *P. aeruginosa.* The unit demonstrated over 97% inactivation of both strains of bacteria, subject to an average 405 nm light irradiance of 1.5 $mWcm^{-2}$ (Peak 405 nm irradiance of 3 $mWcm^{-2}$) over a 60-minute exposure time at a distance of 10 cm from the unit.

The results demonstrated that the concept of the pulsed blended light unit was a success – there is however much development still required before pulsed, blended systems are viable for environmental decontamination. To this end, there are a number of key issues that should be addressed, both in terms of this prototype and the general concept, including:

- for this prototype, the amount of yellow wavelength content needs to be increased in order to improve the overall optical blend;
- in general, the aesthetics of the unit must be addressed – the LEDs must be arranged closer together, with a diffuser incorporated to improve blending and achieve a single source light unit; and;
- finally, is the design or concept scalable? – In terms of size, light output, power requirements, cost and antimicrobial efficacy.

Some of these aspects will be investigated and expanded upon in the next chapter.

CHAPTER 7
DEVELOPMENT OF A PULSED, BLENDED ANTIMICROBIAL LIGHT WHITE SOURCE:
PART II: SCALE-UP & OPTIMISATION

7.0 OVERVIEW

This chapter will build on the prototype design developed in Chapter 6. Of the three point on which to expand in detail at the end of Chapter 6 – two of the issues will be addressed in this chapter: improving the spectral content of the light, in particular the yellow content; and investigating how a scaled up version of the design compares in terms of performance and viability.

7.1 THE REDESIGN OF THE BLENDED WHITE LIGHT UNIT

The light unit designed and built in Chapter 6 successfully demonstrated that, under pulsed control, antimicrobial 405 nm light can be supplemented with other wavelengths of light to improve the quality of the overall light output, in terms of colour quality and rendering ability, with relative wavelength irradiances controlled via PWM. As mentioned, the work of this chapter investigates the potential to scale up this prototype, and addresses technical challenges including optimizing the blend of the optical output and assessing antimicrobial performance.

7.1.1 DESIGN OF THE SCALED-UP PROTOTYPE LIGHT UNIT

From here onwards the prototype light unit developed in Chapter 6 will be referred to as the ***Mk I unit*** and the redesigned prototype in this chapter will be referred to as the ***Mk II unit***.

The first issue to be addressed in the *Mk II unit* was to increase the yellow component of the output spectrum. Amber Lumileds LUXEON Rebel LEDs (LXML-PL01-0040) were selected for this purpose as they had a peak wavelength in the region of 590 nm ± 5.5nm. The resistors used for these new amber LEDs were 3.3 Ω and 5.6 Ω

used in series for a total resistance of 8.9 Ω, the same as that used with the Kingbright yellow LEDs in the *Mk I unit*.

For the scale-up, it was decided that the *Mk I unit* would be supplemented with more LEDs (rather than building a separate unit) in order to increase the optical output. The full electronic setup was replicated, with the number of each LED doubled, with the exception of the yellows which remained at 2 but were supplemented with 4 × amber LEDs. A full list and details of the LEDs used are in *Table 7.1.*

Table 7.1: Details of the LEDs selected for use in the scaled-up design of the blended white light prototype – Mk II unit.

Colour	Wavelength (nm)		Model	Number Used
	Peak	FWHM		
Red	617	28	Lumileds LXM2-PH01-0070	4
Yellow	593	20	Kingbright KADS-8072SY28Z4S	2
Amber	590	10	Lumileds LXML-PL01-0040	4
Green	530	30	Lumileds LXML-PM01-0090	4
Violet	405	12	Nichia NCSU276AT-U405	8

The first ring of LEDs, as arranged in the *Mk I unit*, was supplemented in the *Mk II unit*. A second ring of LEDs was adhered around LEDs from the *Mk I unit* spreading the different colours as much as possible and attempting to keep the LEDs as close together as possible – however, due to the sizable footprint of the PCBs on which the LEDs were mounted, the LEDs were further apart than the ideal scenario. Ideally, the LEDs would be as small and close together as possible so as the different LEDs are indiscernible and to create a perceived point source – this is however difficult to achieve.

The full setup and arrangement of the LEDs for the *Mk II unit* is shown in *Figure 7.1*. As can be seen from the picture, the wiring in particular became quite sizable and awkward so for any real scale up of the design, the LEDs would need to be mounted together on a single custom PCB which would allow them to be placed closer together and avoid the amount of wiring seen in *Figure 7.1*.

The *Mk I unit* circuitry was left as it was, and an almost identical circuit was fabricated for the new ring of supplementary LEDs (as illustrated in *Figure 7.1)*. The only difference with the *Mk II unit* circuitry was that there were 4 parallel branches instead of two in the yellow/amber section of the circuitry. The *Mk II unit* circuitry was controlled by a second identical microcontroller to control the second ring of LEDs. This meant that the LEDs were most likely not all synchronized in their pulsing but the duty cycles and irradiances would all be identical so this issue was not a major problem for the purposes of this study. It was decided that both microcontrollers would be loaded with exactly the same code – meaning each colour of LED in both rings would be pulsed at the same duty cycle.

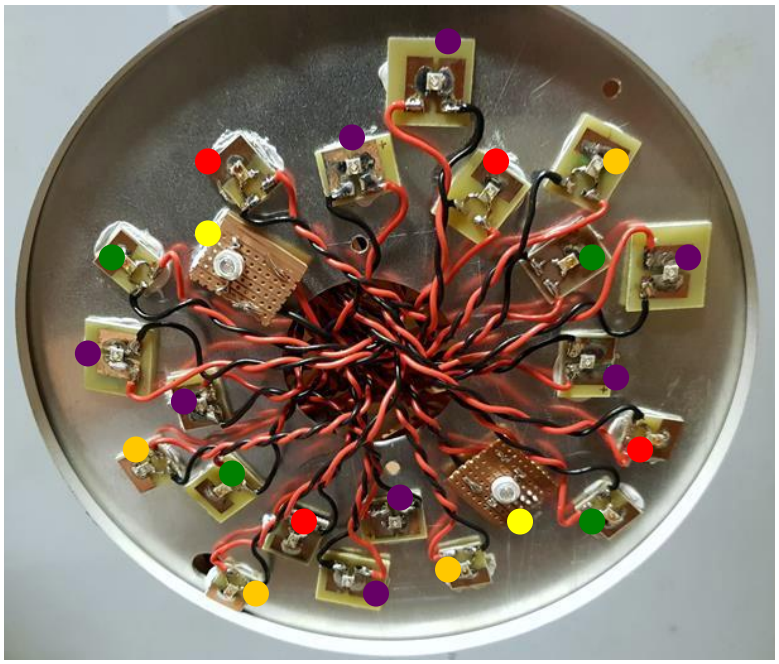

Figure 7.1: Picture of the arrangement of the LEDs after the integration of the second set of LEDs for the redesigned *Mk II* unit as seen from the underside of the unit through the 200 mm aperture (colour spots indicate the LED colours).

7.1.2 Optical Tuning of the Mk II Unit

As with the *Mk I unit*, the duty cycles had to be altered to find the optimal blend, as close to white light as possible. It was decided that with the new amber LEDs and the doubling up of the rest of LEDs with different spacing and positions, that the

tuning process would be re-evaluated, beginning again with all colours set at a 50% duty cycle. Shown in *Figure 7.2* is the spectral output of the *Mk II unit* with all colours set at 50% duty cycle compared with that of the standard white LED (Lumileds, Luxeon LXH7-PW40). Visual images demonstrating the colours rendered under the *Mk II unit* at this setting are shown in *Figure 7.3*.

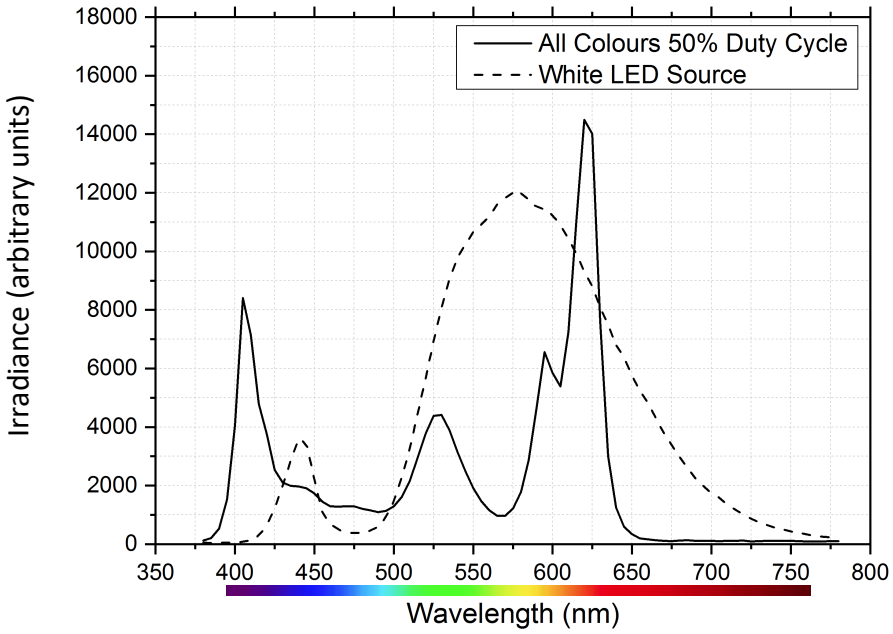

Figure 7.2: The spectral output of the *Mk II* unit [all colours @ 50% duty cycle] compared with the spectrum of a standard cool white LED (Lumileds, Luxeon LXH7-PW40).

Figure 7.3: Various objects representing different colours under illumination by the *Mk II unit* [all colours @ 50% duty cycle], demonstrating the colour quality or colour rendering ability of the light source.

As before, there is still a purple hue about the picture. However, the colours appear to be rendered quite well – with the skin tone looking quite natural. It was

observed that the red peak was too high – in comparison to the white LED spectrum - as can be seen in *Figure 7.2*, so this was incrementally reduced until it matched that of the white LED spectrum. The duty cycle eventually settled upon was 33%, the same as that used in the *Mk I unit*. The spectral comparison and picture showing the new light output are shown in *Figure 7.4* & *Figure 7.5*, respectively.

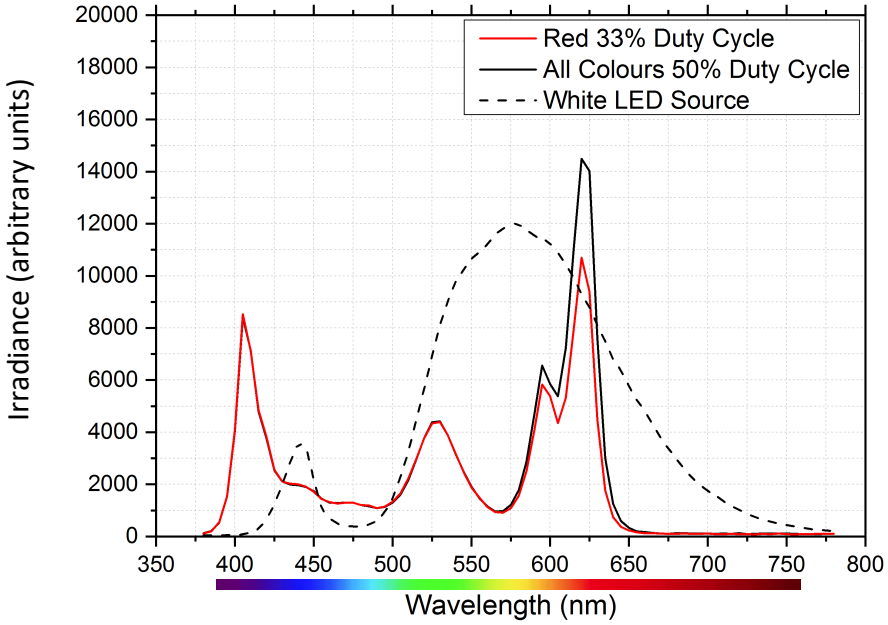

Figure 7.4: Spectral output of the *Mk II unit* [red LEDs @ 33%; green, yellow/amber, 405 nm LEDs @ 50% duty cycle], compared to the initial *Mk II unit* output [all LEDs @50% duty cycle], and a standard cool white LED (Lumileds, Luxeon LXH7-PW40).The red LEDs have been reduced to 33% duty cycle to better match the output of the white LED.

Figure 7.5: Various objects representing different colours under illumination by the *Mk II unit* [red LEDs @33%; 405 nm, yellow/amber and green LEDs @ 50% duty cycle], demonstrating the colour quality or colour rendering ability of the light source.

It can be seen, that the red peak of the prototype output is a little higher than that of the white LED spectrum after the duty cycle was reduced. The red LED was kept a little higher in an effort to maintain an extra portion of yellow wavelength content on the lower tail of the spectral spread. As can be seen from the comparison graph in *Figure 7.4*, as with a reduction in the red level, the yellow also reduces. With the issue of too little yellow content in the *Mk I unit*, it was decided that an extra portion of yellow content would be a justifiable reason to have a slightly higher red peak.

The next change was the green light, which was at too low a level. The green was incrementally increased until it matched the level of the white light spectrum. The duty cycle decided upon was 70% duty cycle. The spectral comparison and picture showing the new light output are shown in *Figure 7.6* & *Figure 7.7*, respectively.

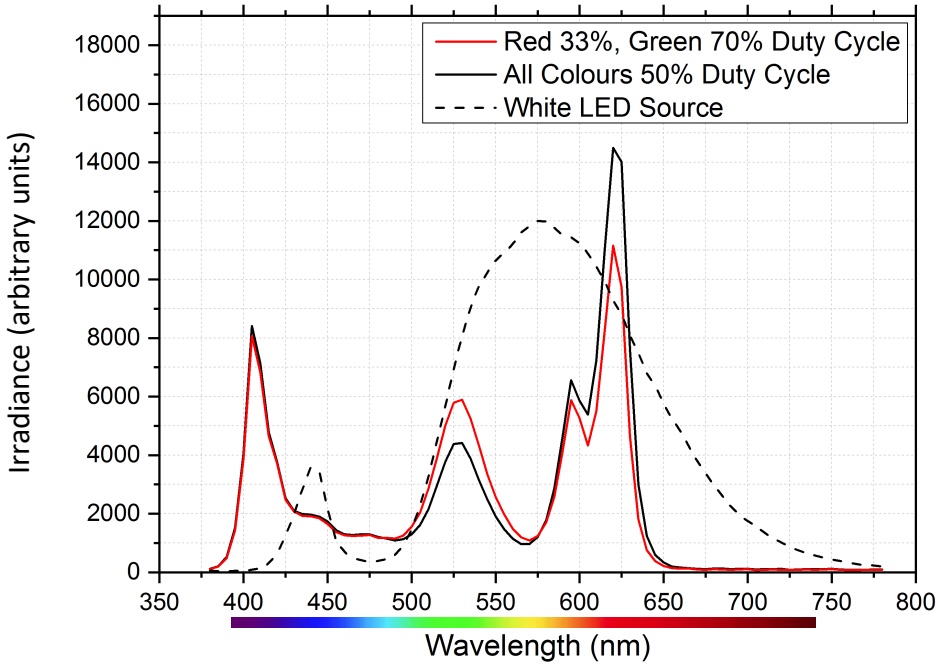

Figure 7.6: Spectral output of the *Mk II unit* [red LEDs @ 33%; green LEDs @ 70%; yellow/amber, 405 nm LEDs @ 50% duty cycle], compared to the initial *Mk II unit* output [all LEDs @50% duty cycle], and a standard cool white LED (Lumileds, Luxeon LXH7-PW40).The green LEDs have been increased to 70% duty cycle to match the output of the white LED.

Figure 7.7: Various objects representing different colours under illumination by the *Mk II unit* [red LEDs @33%, green LEDs @ 70%; yellow/amber, 405 nm LEDs @ 50% duty cycle], demonstrating the colour quality or colour rendering ability of the light source.

Unfortunately, at this stage it could be foreseen again that the yellow/amber content would be lacking. The amber LEDs (Lumiled LXML-PL01-0040) were selected to match the Lumiled brand of the other coloured LEDs, and it was hoped the performance, of the other coloured LEDs. With the red peak at approximately 620nm and the green peak approximately 525nm – the central peak to fill the spectral was estimated about 570nm. At the time of sourcing the LEDs for the *Mk II unit,* due to availability, the amber LEDs – which have a peak of 590nm and a FWHM of 20nm – were selected. The intention was that the tail on either side of the 590nm peak would give a 20nm spread at half irradiance, and theoretically fill the spectral gap.

With only the yellow/amber LEDs left to adjust and both at 50% duty cycle, the peak was about 6000 arbitrary units of irradiance and it had to be increased to almost 12000 arbitrary units of irradiance so to raise it to a level comparable with the white LED (see *Figure 7.6*). As discussed before (*Section 6.4.1*) the maximum duty cycle that can be used is approximately 80%, in order to keep the temperature down and ensure safe operation. However, the yellow/amber LEDs were incrementally increased in an effort to see how close the yellow content could be matched to that of the white LED spectrum. It was increased to the maximum, at a duty cycle of 80%, and the spectral comparison and picture showing the new light output are shown in *Figure 7.8* & *Figure 7.9*, respectively.

Unfortunately, the level of yellow content couldn't be increased enough to match that of the white LED spectrum: the yellow appears to be a limitation in the

current system. On *Figure 7.8* there is only a small observable increase in the yellow/amber peak from *Figure 7.6*. The peaks of the original yellow LEDs (Kingbright KADS-8072SY28Z4S) at 593nm and the amber (Lumiled LXML-PL01-0040) at 590nm were so close that it is hard to discern the new peak from the addition of the 4 new amber LEDs. The new amber LEDs, much like the original yellow LEDs, performed worse than expected and as such the yellow content and in general wavelength content around 570nm mark was insufficient. The yellow LEDs in future iterations would have to be chosen and tested very carefully in order to ensure optimal output and wavelength spread.

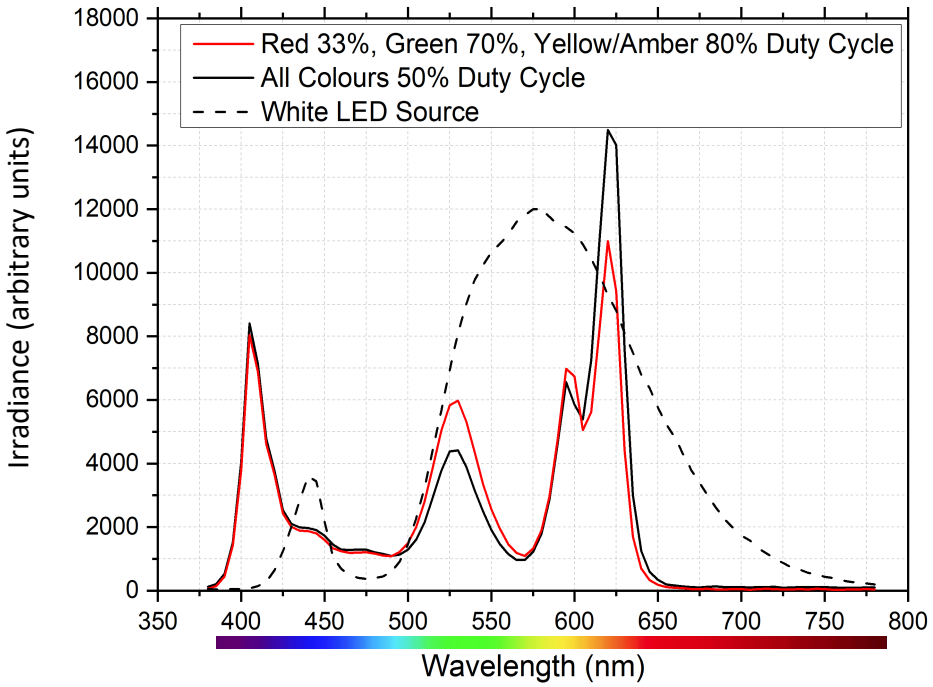

Figure 7.8: Spectral output of the *Mk II unit* [red LEDs @ 33%; green LEDs @70%; yellow/amber LEDs @ 80%; 405 nm LEDs @ 50% duty cycle], compared to the initial *Mk II unit* output [all LEDs @50% duty cycle], and a standard cool white LED (Lumileds, Luxeon LXH7-PW40).

Figure 7.9: Various objects representing different colours under illumination by the *Mk II unit* [red LEDs @33%; green LEDs @ 70%; yellow/amber LEDs @ 80%; 405 nm LEDs @ 50% duty cycle], demonstrating the colour quality or colour rendering ability of the light source.

Nevertheless, the final blended output of the *Mk II unit* appeared to be successful in rendering colours, as can be seen in *Figure 7.9*, and showed an improvement from the initial untuned output (all LEDs @50% duty cycle) and indeed a major aesthetical improvement from the 405 nm light alone (*Figure 7.10*).

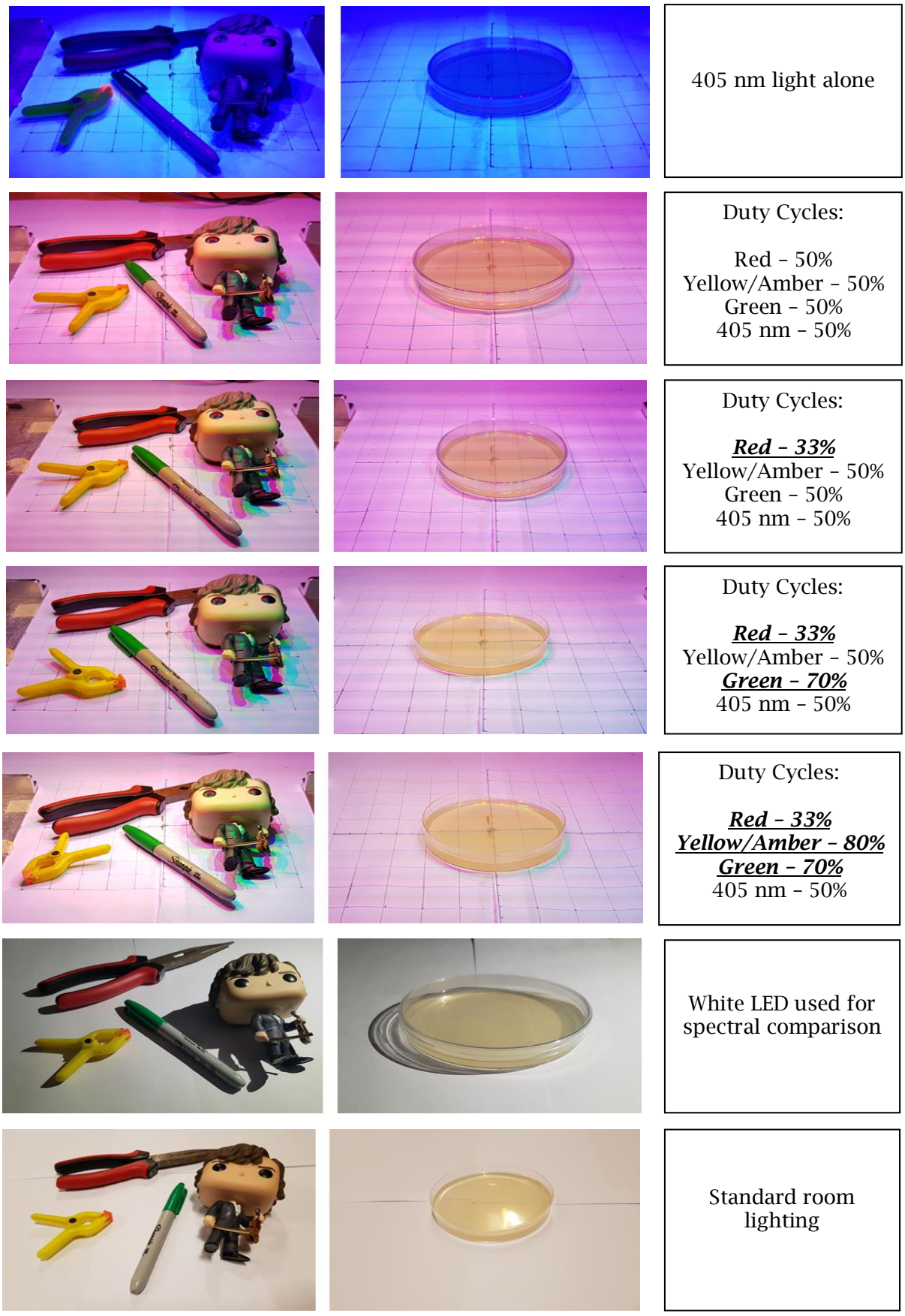

Figure 7.10: Comparison of various objects under the *Mk II unit* at the 4 main iterations during the tuning process (tuning in bold and underlined), and under 405 nm light alone, standard room lighting and the white LED used for the spectral comparison.

As in Chapter 6, with the initial blend (all LEDs at a 50% duty cycle), there is a purple hue about the light output. This however reduced observably as the irradiance of each colour of LED was tuned, with the final blend demonstrating a bright source which renders all of the colours remarkably well – despite the issues of LED spacing in the prototype. Even the skin tone of the figure is better than in the same image of the final blend of the *Mk I unit* (*Figure 6.18*), which had a green hue due to the LED spacing. The additional LEDs appear to have provided a much more consistent blend of colours over the full areas – although the figure still demonstrated colour shadows due to the LED spacing which is not ideal. These observations of course are subjective; however, I would suggest that the final blend of the *Mk II unit* provides a brighter and better blend of light, rendering the colours more naturally and with more vibrance and depth than the final blend of the *Mk I unit*, shown for comparative purposes in *Figure 7.11.*

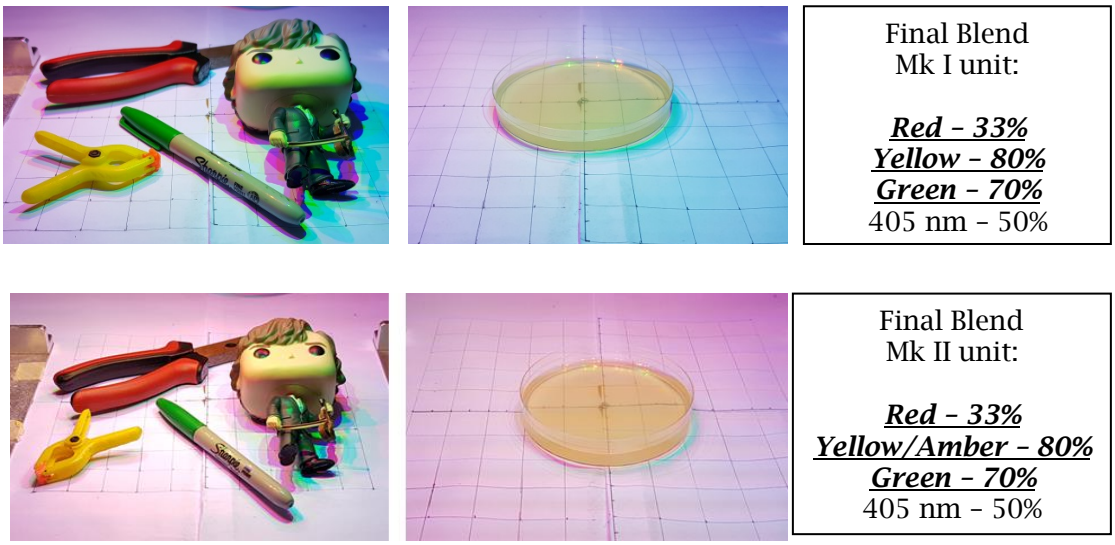

Figure 7.11: Comparison of various objects under the final blend of the *Mk I unit* and *Mk II unit* after the optical tuning process.

As can be seen, there is still a hue of violet in both although it has been significantly reduced from the initial 50% duty cycle blend. This could be improved by increasing the irradiances of the supplementary colours to balance out the violet content and with some improved blending – through the use of a diffuser and spacing the LEDs closer together.

7.1.3 Optical Analysis of the Mk II unit after Optical Tuning

The optical analysis of the Mk II unit was carried out at the same 4 tuning settings (as shown in *Figure 7.10*) but this section will focus on the initial output spectrum [all colours set at 50% duty cycle] and the final tuned spectrum [red LEDs @ 33%; green LEDs @70%; yellow, amber LEDs @ 80%; 405 nm LEDs @ 50% duty cycle] looking at the overall improvement. *Section 6.4.2.2* provides detail of how to interpret the plots. Initially, the CRI was considered. The CIELAB plot showing the test versus reference sample colours for CRI and the individual CRI values for the colour samples for the initial 50% duty cycle output, is shown in *Figure 7.12* & *Figure 7.13*, respectively.

It can be seen that the test colours in *Figure 7.12* are relatively close to the reference colours with the exception of a few samples in the blue green quadrant, indicating a good CRI and quality of light. *Figure 7.13* shows the individual breakdown of the CRI values with only the first 8 being averaged to give the CRI Ra value, which for the *Mk II unit* [all LEDs @50% duty cycle], was 69. At 69 this *Mk II unit* CRI was slightly better than that of the initial CRI of the *Mk I unit* [all LEDs @50% duty cycle], which was 67 (as detailed in *Table 6.4*). As mentioned, the problematic sample colours in the CIELAB colour plot were in the blue green quadrant, and this is reflected in the low R11 and R12 which can be seen on *Figure 7.13.*

The CQS for the *Mk II unit* [all LEDs @50% duty cycle] is much lower in this case than the initial measurement of the *Mk I unit* [all LEDs @ 50% duty cycle], with the *Mk II unit* demonstrating a CQS value of 73 opposed to the initial CQS value of 82 for the *Mk I unit* (as detailed in *Table 6.4*). However, the prototype was still to be tuned so it was not problematic that, at that initial setting, the CQS was much lower than *Mk I unit*. Shown in *Figure 7.14* & *Figure 7.15* show the test versus reference colour samples for CQS along with the individual values for each colour, respectively.

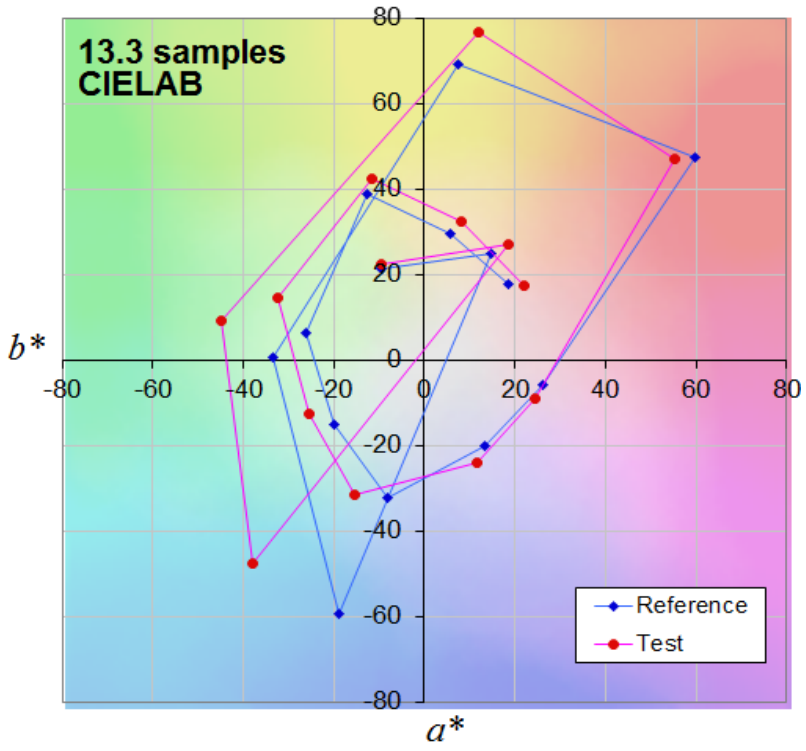

Figure 7.12: Comparison of the CRI colour samples rendered under the *Mk II unit* (all LEDs at 50% duty cycle) with the reference samples rendered under an ideal source i.e. a source with a CRI of 100. *NIST CQS program used for analysis.*

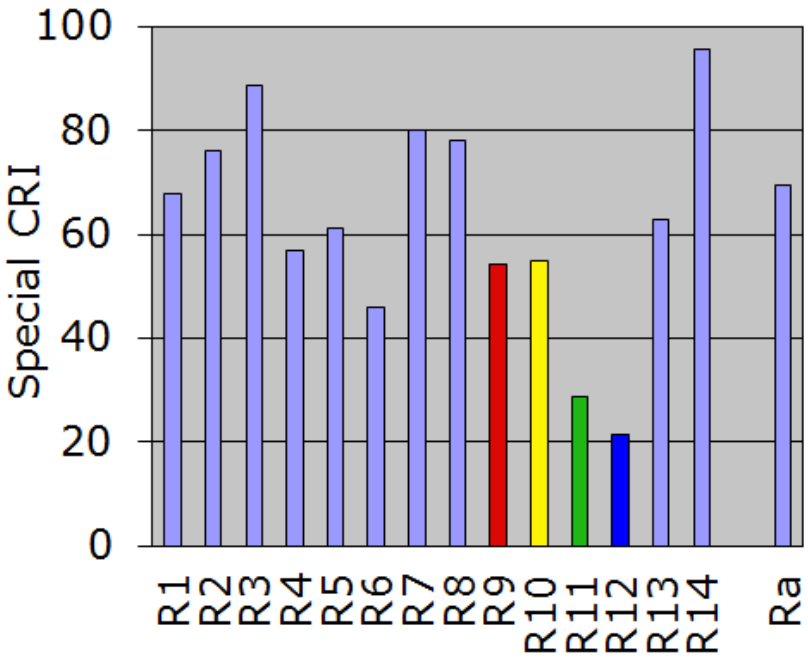

Figure 7.13: Bar graph showing the individual scores of CRI for each sample colour and the overall CRI value (Ra) – average of the first 8 R_i values– rendered under the *Mk II unit* with all LED duty cycles at 50%. Graph demonstrates how the *Mk II unit* renders colors with reference to the ideal light source, which would have special CRI values of 100 across the chart. *NIST CQS program used for analysis.*

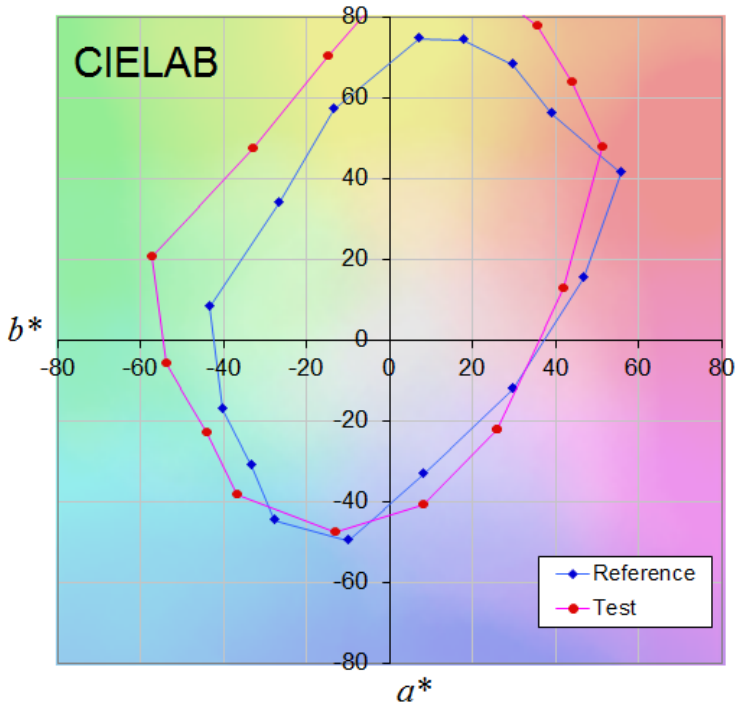

Figure 7.14: Comparison of the CQS colour samples rendered under the *Mk II unit* (all LEDs at 50% duty cycle) compared with the reference samples rendered under an ideal source i.e. a source with a CQS of 100. *NIST CQS program used for analysis.*

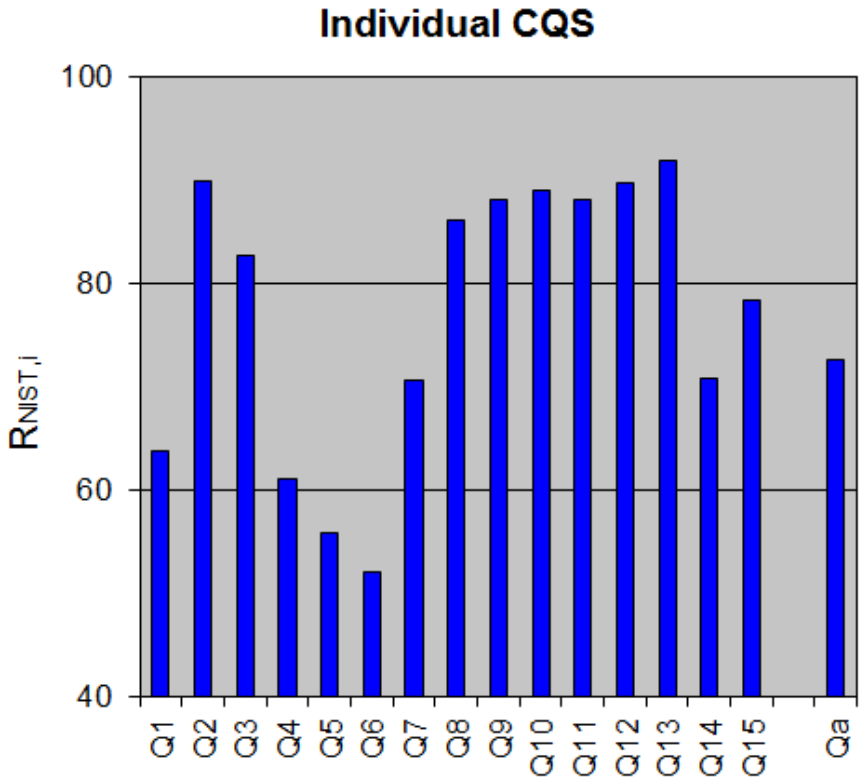

Figure 7.15: Bar graph showing the individual scores of CQS for each of the colour samples with the average CQS value, Q_a – rendered under the *Mk II unit* with all LED duty cycles at 50%. Graph demonstrates how the *Mk II unit* renders colors with reference to the ideal light source, which would have $R_{NIST,i}$ values of 100 across the chart. *NIST CQS program used for analysis.*

As can be seen in *Figure 7.14*, the colours matched up well in the lower 2 quadrants of the CIELAB CQS plot however the upper half of the CIELAB CQS plot demonstrated quite a bit of deviation in the test and reference colours. Again, this still had to be tuned so the aim was to resolve these deviations in colour samples.

As mentioned, the *Mk II* unit LEDs were all initially set at a duty cycle of 50%. The full prototype was then tuned as described in *Section 7.1.2.* Optical analysis of the initial [all LEDs @ 50% duty cycle] and final blended output spectrum [red @ 33%, green @ 70%; yellow/amber @ 80%; 405 nm @ 50%] was then conducted. A side-by-side comparison of the CIELAB CRI colour plot and graphs of the initial blend and the final tuned blend are shown in *Figure 7.16* & *Figure 7.17*, respectively.

The tuning process resulted in a visible improvement: the light output's test and reference colour samples matched much more closely on the CIELAB CRI plots in *Figure 7.16.* Moreover, the individual CRI values for the final blend, shown in *Figure 7.17,* are almost all higher than the initial blend of the *Mk II unit* [all LEDs @ 50% duty cycle), with the lowest 44 opposed to the lowest of 20 in the initial blend. The overall CRI value of the final blend is 81, so an increase of 12 in the overall CRI is observed between the initial and final blend, which demonstrates a resounding success in the tuning process creating a better blend of light content. The final blend of the *Mk II unit* however has a CRI of 81 whilst the final blend of the *Mk I unit* had a CRI of 82. This is not much of a difference and it is unclear why this is the case; a possibility is that underperforming yellow, and now underperforming ambers, have reduced the content around the 590nm peak relative to the other wavelengths. In any case – an overall CRI value above 80 falls in the same range as fluorescent lights, as well as trichromatic and phosphor based white LEDs (Schubert, 2006), so this would be an accepted CRI if the blending aesthetics issue was solved and a sufficient scale was achieved.

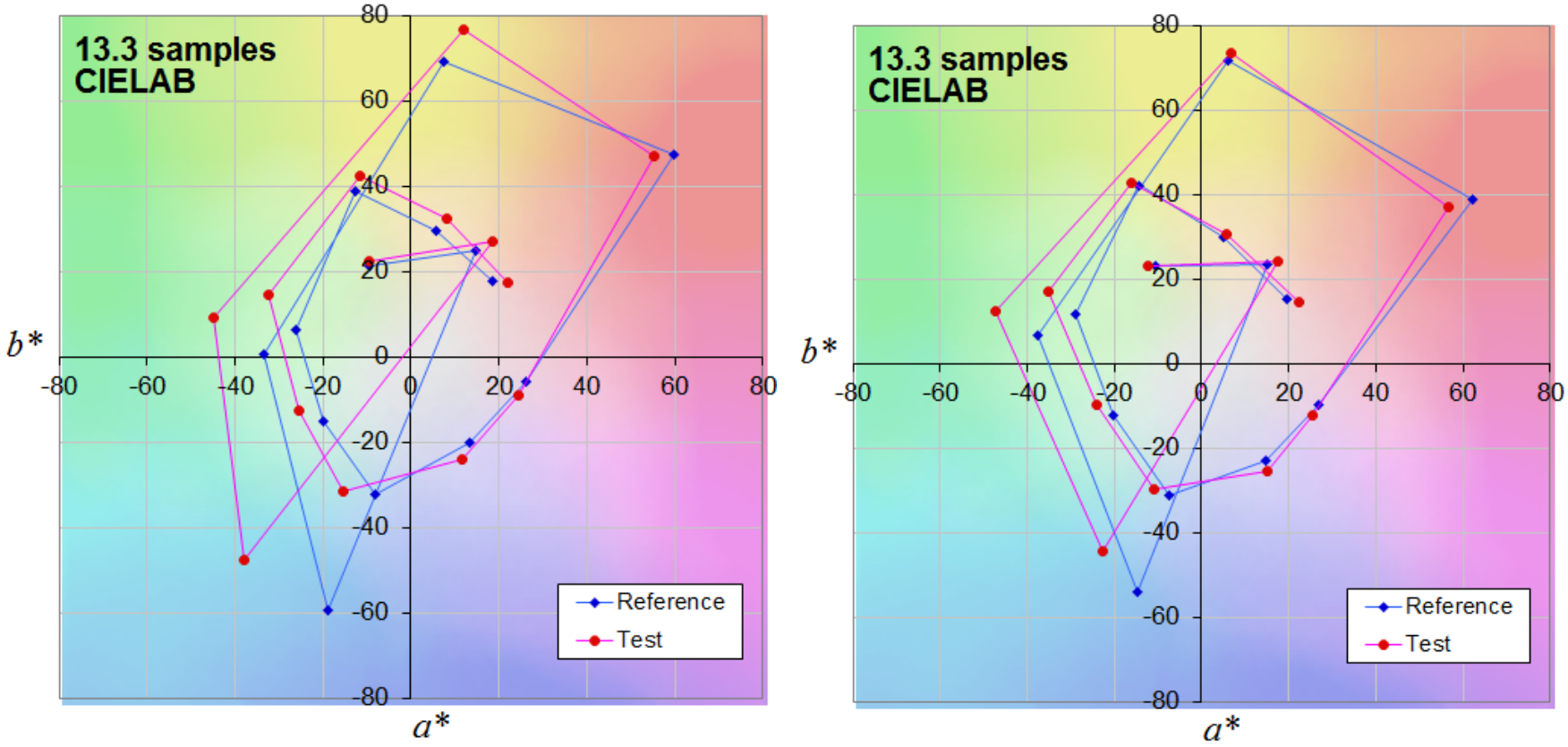

Figure 7.16: Comparison of the CIELAB CRI colour sample plots demonstrating the colour rendering ability of the initial and final blended *MK II units*. (a) Initial blend of light [all colours at 50% duty cycle] (b) Final tuned blend [red @ 33%, green @ 70%; yellow/amber @ 80%; 405 nm @ 50% duty cycle].

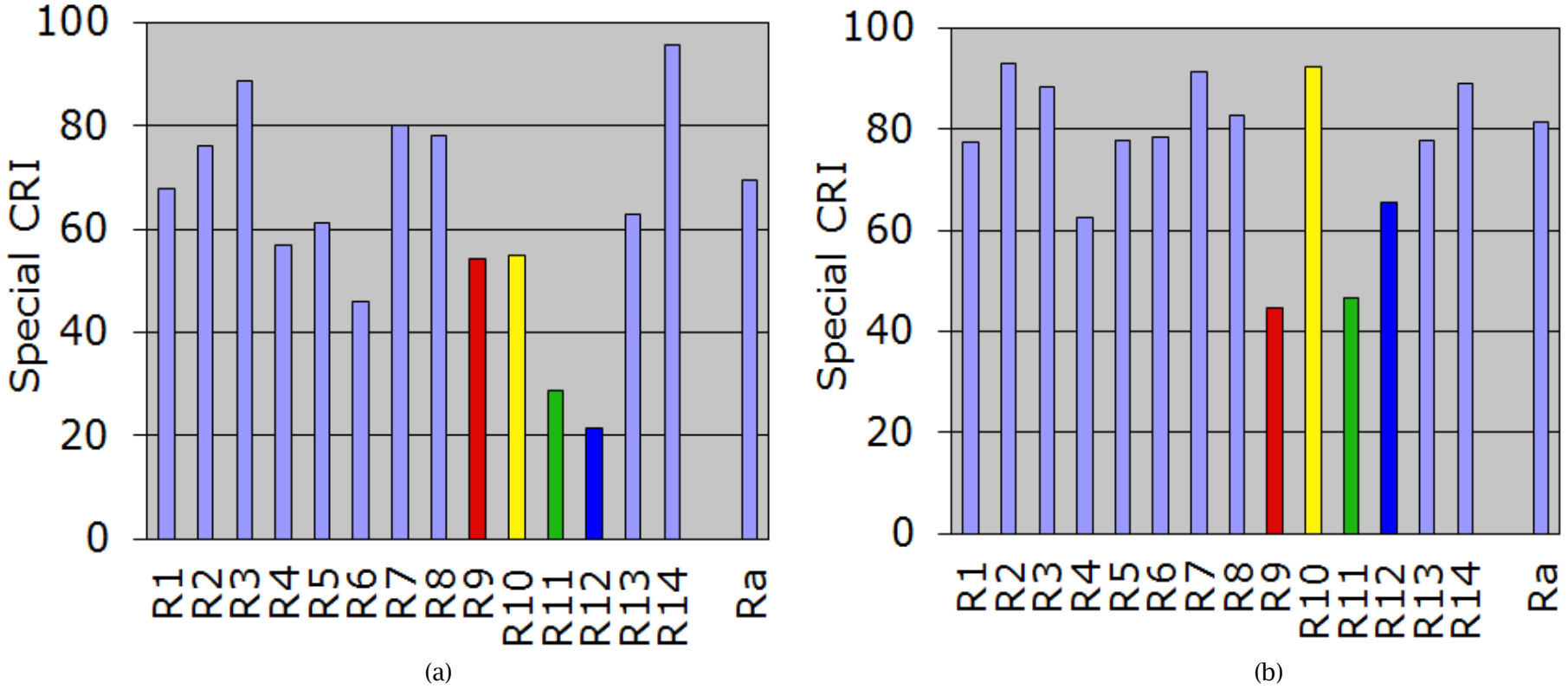

Figure 7.17: Comparison of the Individual CRI values for each of the colour samples used for CRI analysis of the initial and final blended *Mk II units*. (a) Initial blend of light [all colours at 50% duty cycle] (b) Final tuned blend [red @ 33%, green @ 70%; yellow/amber @ 80%; 405 nm @ 50% duty cycle].

The CQS showed a sizable increase, increasing by 9, from 73 with the initial blend to 82 for the final blend. Shown in *Figure 7.*18 *(a)* & *(b)* respectively, is a comparison of the two CIELAB CQS colour plots of the initial blend and the final blend of the *Mk II unit*. Similar to the CRI, the CQS value of 83 of the final blend of the *Mk I unit* is slightly higher than that of the final blend of the *Mk II unit*, which had a CQS of 82. Again, the assumption is that the minor difference is due to the difference in the relative levels of the 405 nm peak and its accompanying tails on either side compared with the levels of other wavelength content.

The results showed a closer match with the test and reference colour samples of the plot, shown in *Figure 7.18,* with the final blend than the initial; and only a few improvements on the individual CQS scores, as shown in *Figure 7.19*. However, when comparing both CRI and CQS there is a definite improvement in the quality of the light output from the initial blend to the final blend making for a success in terms of the optical tuning process that was undertaken.

As with the *Mk I* prototype, the final part of the optical analysis that was undertaken was to look at the values of CRI, CQS and CCT for four stages of the tuning process. These are shown in *Table 7.2*.

Table 7.2: Summary of the CRI, CQS & CCT at the four main stages in the optical tuning process of the *Mk II unit*.

	CRI	*CQS*	*CCT (K)*
Initial blend [all LEDs @ 50% duty cycle]	69	73	2372
Altered Red Content [Red @ 33%; Green, Yellow/Amber, 405 nm @ 50%]	76	80	2977
Altered Red & Green Content [Red @ 33%; Green @70%; Yellow/Amber, 405 nm @ 50%]	81	81	3458
Final blend – Altered Red, Green & Yellow Content [Red @ 33%; Green @ 70%; Yellow/Amber @ 80%; 405 nm @ 50%]	81	82	3312

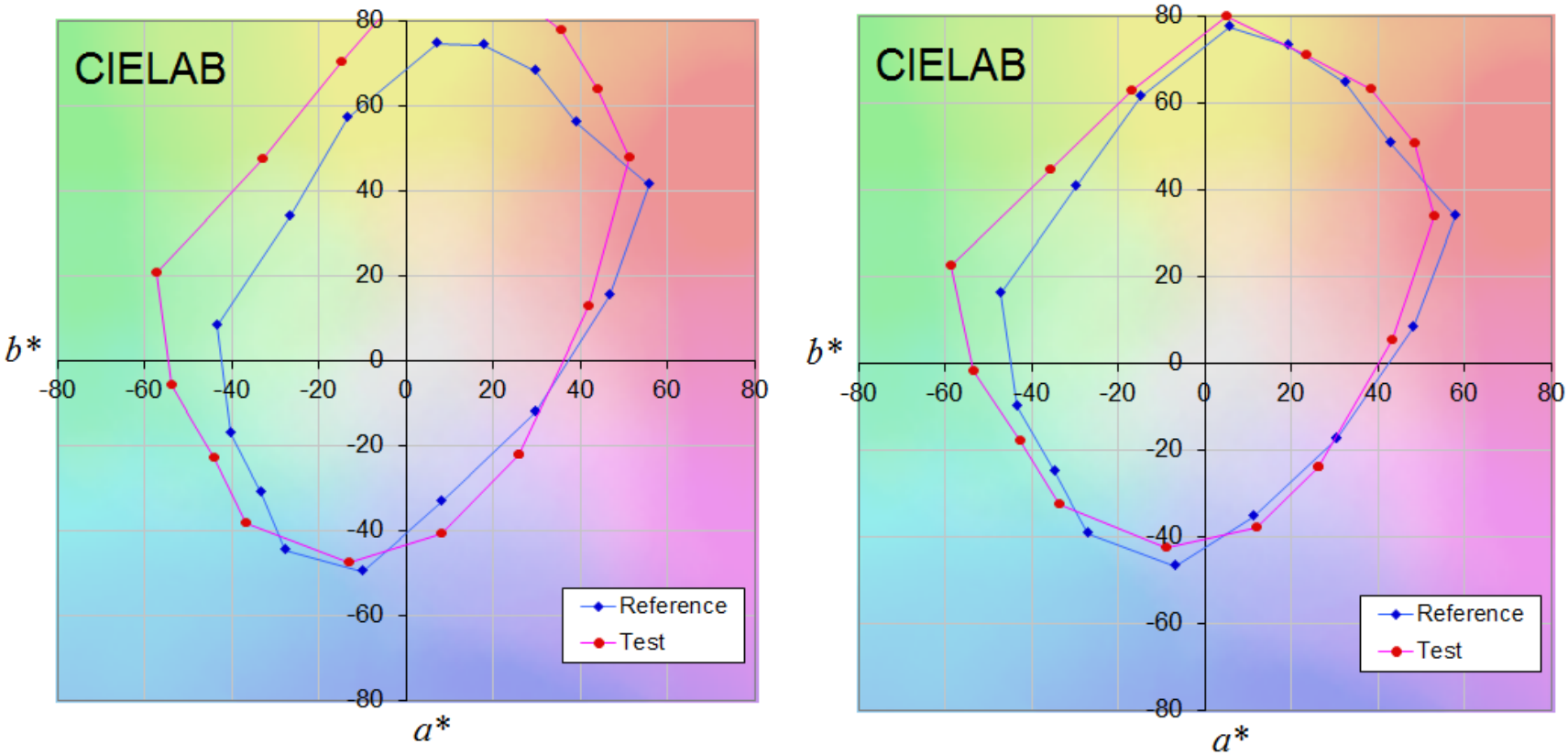

Figure 7.18: Comparison of the CIELAB CQS colour sample plots demonstrating the colour quality of the initial and final blended *Mk II* unit. (a) Initial blend of light [all colours at 50% duty cycle] (b) Final tuned blend [red @ 33%, green @ 70%; yellow/amber @ 80%; 405 nm @ 50% duty cycle].

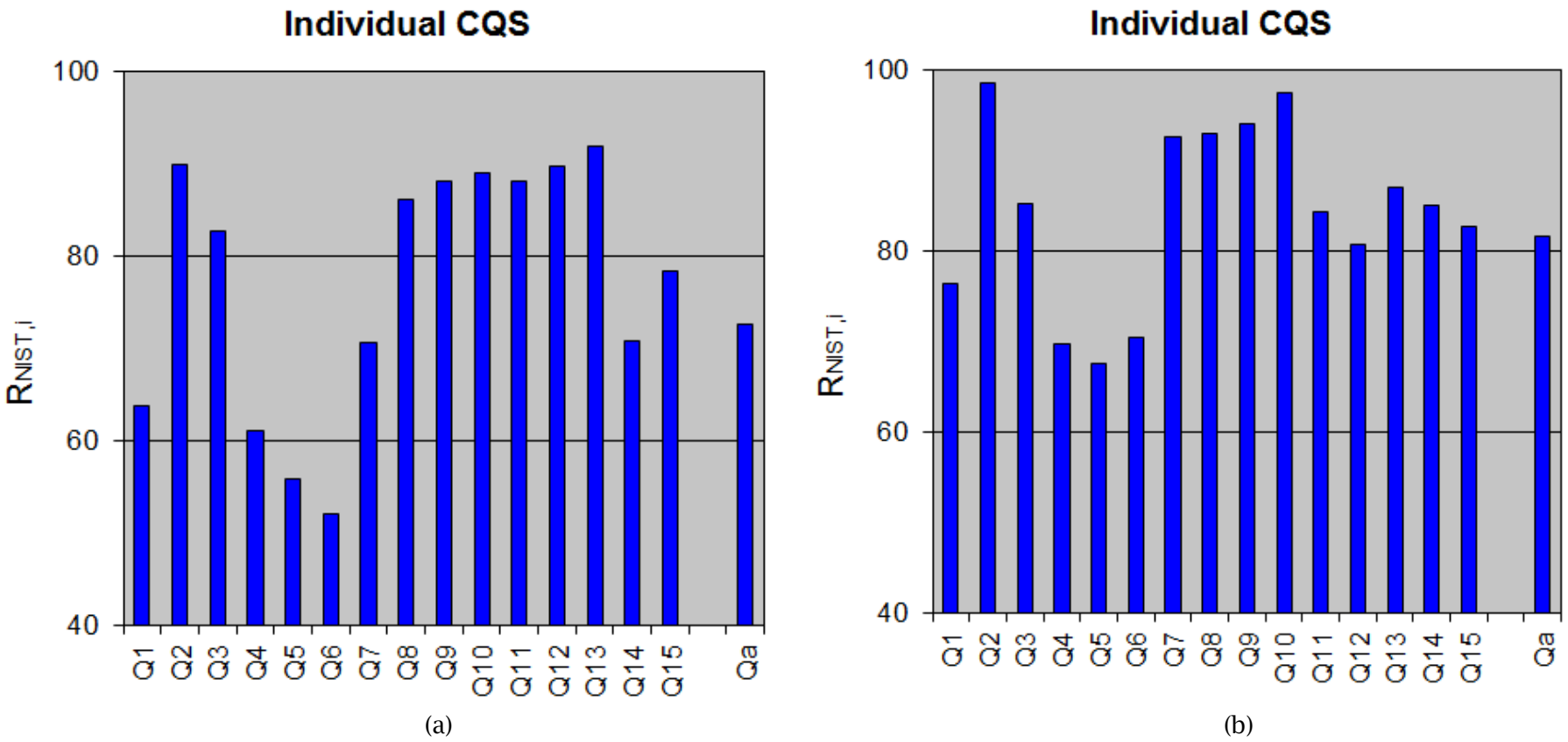

Figure 7.19: Comparison of the Individual CQS values for each of the colour samples used for CQS analysis of the initial and final blended *Mk II unit*. (a) Initial blend of light [all colours at 50% duty cycle] (b) Final tuned blend [red @ 33%, green @ 70%; yellow/amber @ 80%; 405 nm @ 50% duty cycle].

It is demonstrated in *Table 7.2* that as the CRI improves incrementally thoughout the process, so does the CQS. The CCT increases indicating that the blend is moving from a warmer white blend of light to a cooler blend.

Overall, the optical tuning has been demonstrated to be a success, acheving a substantial increase in the CRI value of the *Mk II unit* and an increase in the CQS value. The next stage in the process was to re-assess the antimicrobial effectiveness of the system and look at the difference in efficacy with the increase in the number of LEDs, and consequently the increase in output irradiance.

7.1.4 MICROBIOLOGICAL TESTING OF THE REDESIGNED AND MK II UNIT

The results in S*ection 6.3.3* confirmed that the antimicrobial effects of the small-scale prototype were caused by the 405 nm light LEDs only, with the other colours purely contributing to the blending of the system. Therefore, in order to validate the antimicrobial efficacy of the scaled-up system, testing focused on exposures using the 405 nm light alone. As before, two strains of bacteria were used; *S. aureus* and *P. aeruginosa.* The experiments were conducted with the bacterial sample plates positioned at a distance of 10 cm from the light unit (as with the small-scale *Mk I unit*), and the seeded plates were subject to an average measured irradiance of approximately 2.2 $mWcm^{-2}$ of 405 nm light (a peak irradiance of 4.4 $mWcm^{-2}$). Based on the peak irradiance, this meant the plates were treated with doses of 1.98 Jcm^{-2} (15 min), 3.96 Jcm^{-2} (30 min), 5.94 Jcm^{-2} (45 min) and 7.92 Jcm^{-2} (60 min). The distance between the light unit and sample plates was then increased to 15cm, where plates were exposed to the same irradiance as the prototype in Chapter 6: ~1.5 $mWcm^{-2}$ of 405 nm light (a peak irradiance of 3 $mWcm^{-2}$, giving a maximum applied dose of 5.4 Jcm^{-2} at 60 minutes). The distance of 15 cm was chosen as it provided the same irradiance levels as a 10 cm distance with the Mk I unit and it was thought that these experiments would tie together the scale up results with the Mk I results. Ideally, a larger distance would have been tested – however this would have required much

longer exposures at lower irradiances and would have required different experimental apparatus for suspending the light source at 1 m or perhaps 2 m above the bacterial samples, so 15 cm was decided upon. Future work however should almost definitely increase the distance further for future experiments.

The graphs showing the inactivation of *S. aureus* and *P. aeruginosa* after exposure to the *Mk II unit* at a distance of 10cm are shown in *Figure 7.20*.

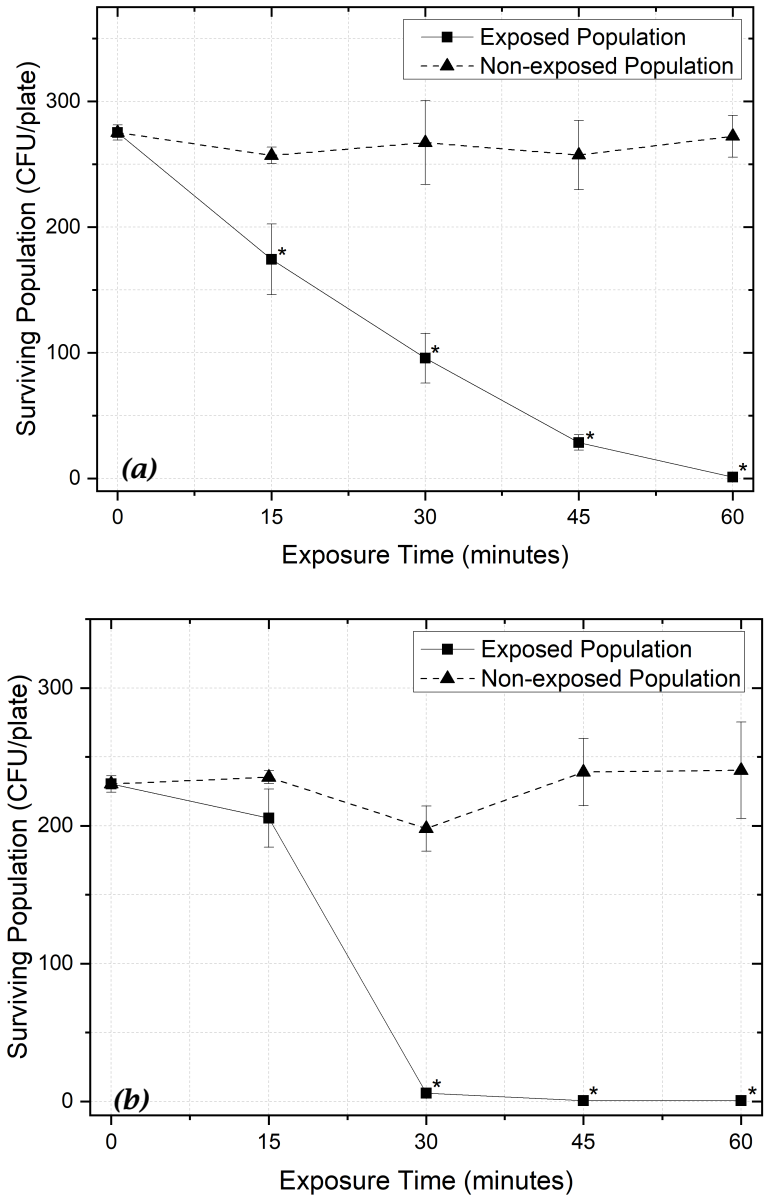

Figure 7.20: Inactivation of (a) *S. aureus* and (b) *P. aeruginosa* on agar surfaces by exposure to the *Mk II unit* at a distance of 10 cm, and an average irradiance of 2.2 mWcm^{-2} (peak irradiance 4.4 mWcm^{-2}) 405 nm light. Data points represent mean values (n=3± SD). Lines are for visual guidance. * represents a significant difference compared with the equivalent control value (P<0.05).

For *S. aureus* (*Figure 7.20a),* the bacterial population followed a downwards linear trend, demonstrating a significant 36.7% / 0.2-$\log_{10}$ reduction (p=0.0076) by 15-minutes (1.98 Jcm^{-2}) exposure. A 2.44-$\log_{10}$ / 99.6% reduction in bacterial population was achieved by the 60-minute exposure time, dropping to an average of 1 CFU/plate.

In the case of *P. aeruginosa* (*Figure 7.20b),* only a 10.8% reduction (p=0.076) was observed after 15 minutes. By 30 minutes (3.96 Jcm^{-2}), the majority of the seeded contamination had been inactivated, with a significant 97.4% / 1.58-$\log_{10}$ reduction ($p=3.57\times10^{-5}$). By 60 minutes (7.92 Jcm^{-2}), a 2.58-$\log_{10}$ / 99.7% reduction was observed.

To compare the *Mk I* and *Mk II* unit's inactivation efficacy, the bacterial populations were converted to percentages, and the kinetics shown in *Figure 7.21.*

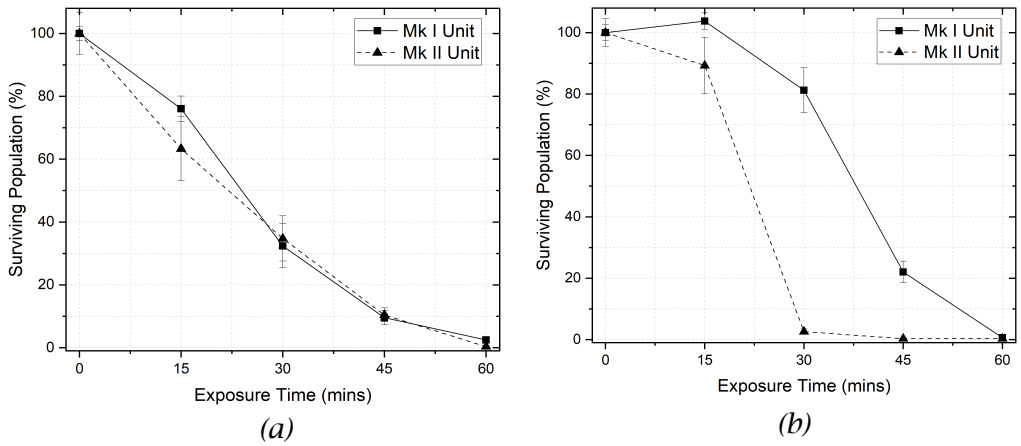

Figure 7.21: Comparison of the inactivation of (a) *S. aureus* and (b) *P. aeruginosa* exposed to the *Mk I unit* at 1.5 $mWcm^{-2}$ (Peak 3 $mWcm^{-2}$; max dose of 5.4 Jcm^{-2}) and the *Mk II unit* at 2.2 $mWcm^{-2}$ (Peak 4.4 $mWcm^{-2}$; max dose of 7.92 Jcm^{-2}) 405 nm light, at a height of 10cm. Data points represent the percentage mean values (n=3±SD) of surviving population relative to the starting populations. Lines are for visual guidance.

The *S. aureus* inactivation curves in *Figure 7.21(a)* demonstrate very similar kinetics. This suggests that over the 60-minute exposure – the inactivation of the *S. aureus* was not affected by the 0.7 $mWcm^{-2}$ increase in average 405 nm irradiance.

For *P. aeruginosa* however (*Figure 7.21(b)*), the *Mk II unit* appears to achieve faster inactivation than the *Mk I unit*, with the majority of the bacteria inactivated by 30 minutes, compared to 45-60 minutes with the *Mk I unit.*

The next stage was to increase the distance between the light source and the bacterial samples to 15 cm, giving an average irradiance of ~1.5 $mWcm^{-2}$ (the same as that of the *Mk I unit* at a 10cm distance). *Figure 7.22* shows the inactivation of *S. aureus* and *P. aeruginosa* after exposure to *Mk II unit* at a distance of 15cm. *S. aureus* (*Figure 7.22a)* demonstrated a relatively linear reduction over the 60 minute period (5.4 Jcm^{-2}), with a 1.21-log_{10} / 93.8% reduction in bacterial population. *P. aeruginosa* (*Figure 7.22b)* also demonstrated successful inactivation, albeit at a slightly faster rate, with a 1.32-log_{10} / 95.3% reduction after 45 minutes exposure (4.05 Jcm^{-2}).

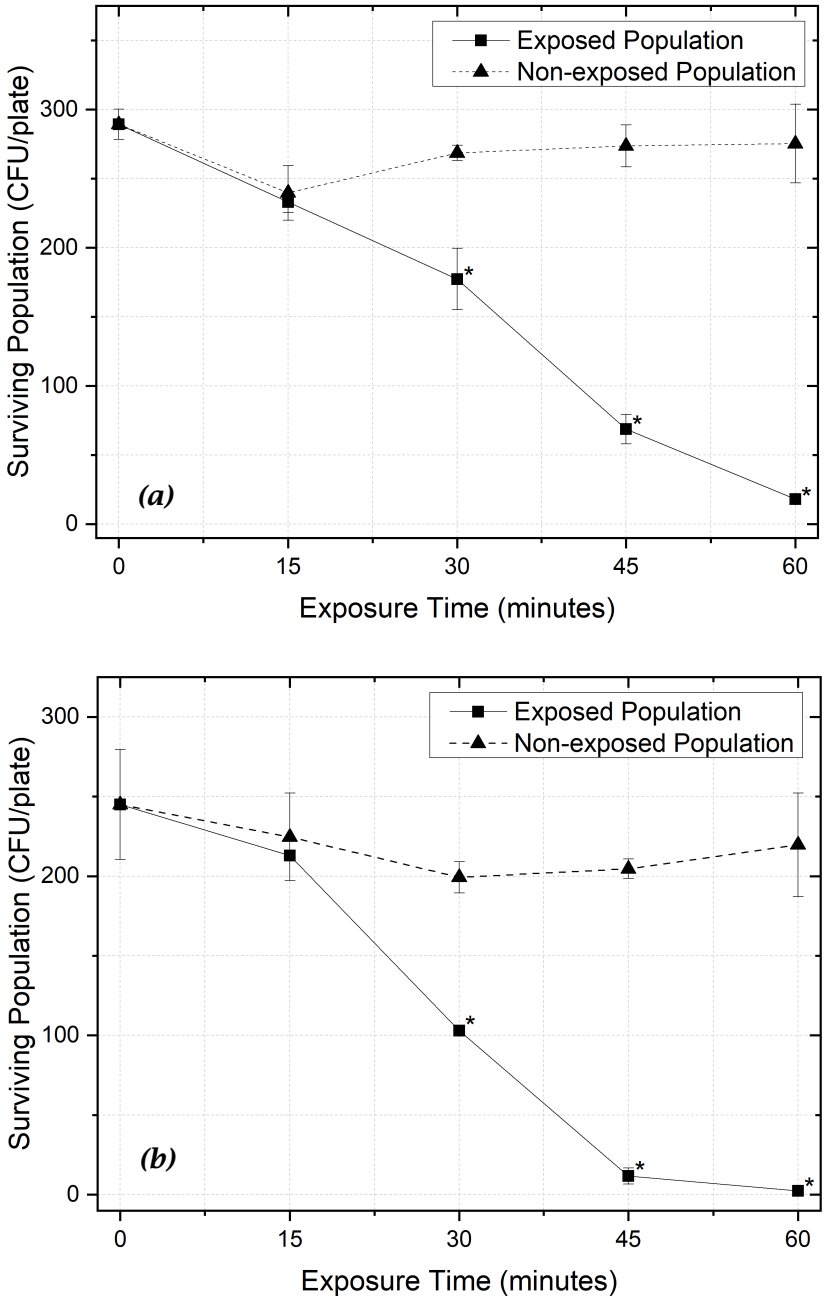

Figure 7.22: Inactivation of (a) *S. aureus* and (b) *P. aeruginosa* on agar surfaces by exposure to the Mk II unit at a distance of 15 cm and an average of 1.5 mWcm^{-2} (peak irradiance 3 mWcm^{-2}) 405 nm light. Data points represent mean values (n=3± SD). Lines are for visual guidance. * represents a significant difference compared with the control value ($p<0.05$).

The *Mk II unit* at both 10 cm and 15 cm demonstrated successful inactivation of both species of bacteria. A further point of interest was to assess whether the exposures at heights of 10cm and 15cm from the *Mk II unit* demonstrated any

statistical difference in the rate of inactivation. Shown in *Figure 7.23* are the comparative inactivation curves at the two height settings.

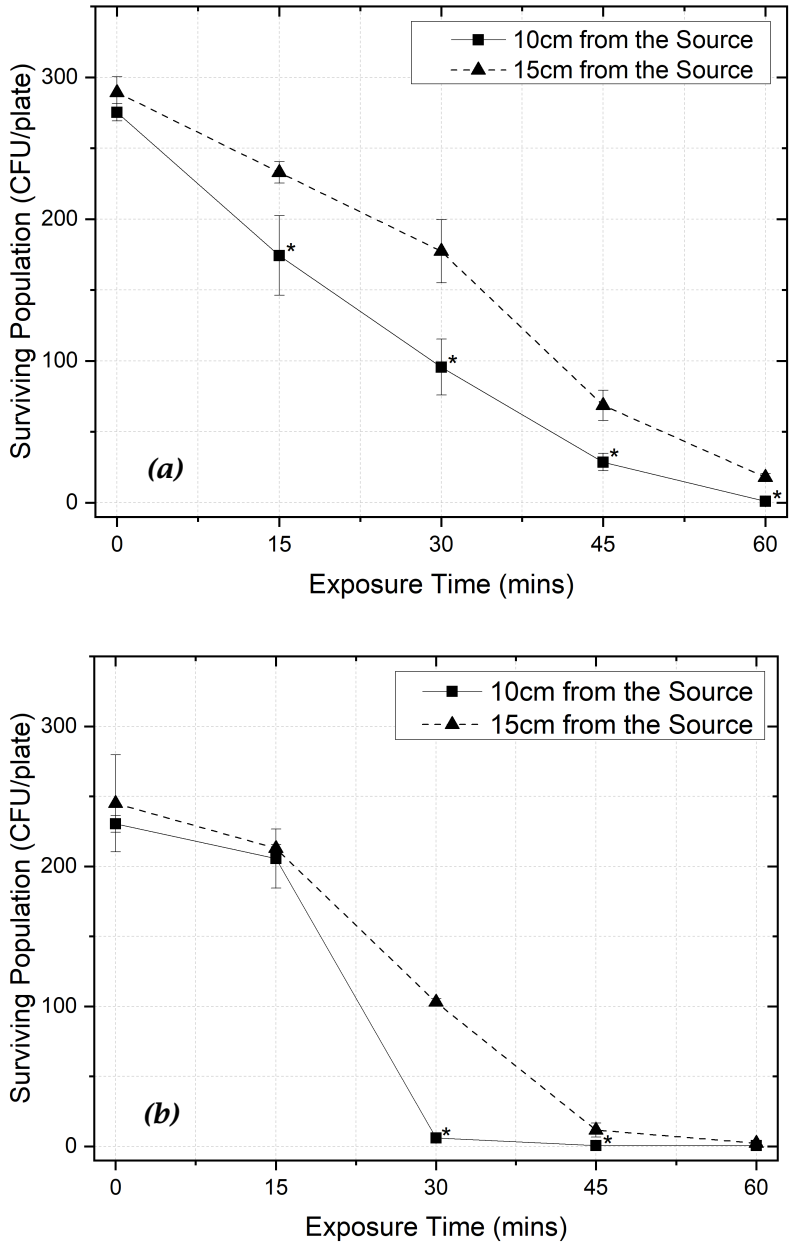

Figure 7.23: Inactivation of (a) *S. aureus* and (b) *P. aeruginosa* at distances of 10cm and 15cm from the *Mk II unit*. Sample plates were subject to 405 nm light at 2.2 mWcm^{-2} and 1.5 mWcm^{-2} irradiance (peak irradiance being 4.4 mWcm^{-2} and 3 mWcm^{-2}, respectively). Data points represent the mean values (n=3± SD). Lines are for visual guidance. * represents a significant difference compared with the value at the same time point from the 15cm exposure ($p<0.05$).

In the case of *S. aureus* (*Figure 7.23a*) the inactivation kinetics are similar, demonstrating a relatively linear reduction with time. However the trends demonstrate significant differences at each of the time points ($p<0.05$), with the

biggest observable difference being at 30 minutes where the population of the 10 cm exposure is 54% of that of the 15 cm exposure (p=0.0089). The results suggest that the 10cm exposure, i.e. the higher irradiance exposure, demonstrates a significantly quicker inactivation. The peak irradiance of the 10 cm exposure is almost 50% higher than the peak irradiance of the 15 cm exposure - from 3 $mWcm^{-2}$ up to 4.4 $mWcm^{-2}$. Similar results are shown for *P. aeruginosa* (*Figure 7.23b)*, with significantly enhanced inactivation at the 30-minute point ($p=9.08\times10^{-7}$): 97.4% reduction at 10cm compared to 75.8% at 15cm distance. Overall, the results demonstrate that the higher irradiance exposure, the faster inactivation of the organisms.

7.2 DISCUSSION

The scaled up *Mk II unit*, like the *Mk I unit*, demonstrated successful inactivation of both *S. aureus* and *P. aeruginosa* on agar plates. Both units supplemented the pulsed 405 nm light with other colours, produced by pulsed LEDs, to produce a better quality of light. The subsequent discussion sections will:

- Compare the *Mk I* and *Mk II* units
- Relate the *Mk II unit* performance with other EDS studies
- Discuss design and performance issues of the pulsed prototype.

7.2.1 COMPARISON OF THE MK I AND MK II UNITS

Both iterations of the prototype met the main objectives of the project – to create an antimicrobial blended light source controlled by pulsed width modulation (PWM). Another important element for consideration when developing a light source is the irradiance profile, or irradiance spread, on surfaces below the light source. Shown in *Figure 7.24* and *Figure 7.25* are the irradiance profiles of the 405 nm light output of the *Mk I unit* and *Mk II unit*, respectively, at a height of 10 cm. Unfortunately, due to the optical measurement equipment (Power meter and

photodiode, *Section 3.2.1*) not allowing accurate measurement of broadband light sources, these profiles focus on the 405 nm light output rather than the full blended spectrum, but are being presented here to support general discussion.

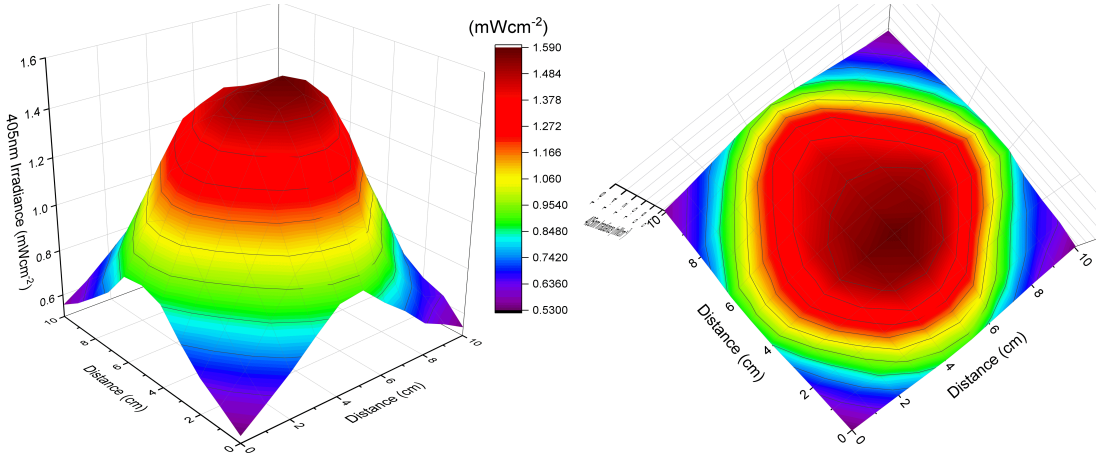

(a) *(b)*

Figure 7.24: Irradiance profile of 405 nm light under the *Mk I unit* at a distance of 10cm, (a) Side on surface plot (b) Aerial view of surface plot.

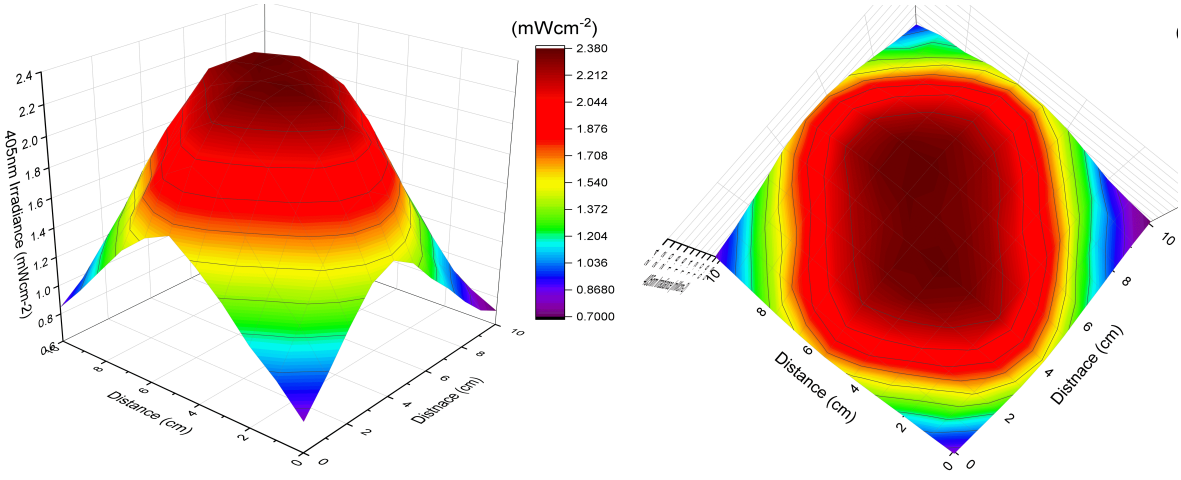

(a) *(b)*

Figure 7.25: Irradiance profile of 405 nm light under the *Mk II unit* at a distance of 10cm, (a) Side on surface plot (b) Aerial view of surface plot.

Both irradiance profiles demonstrate a relatively normal distribution. As can be seen, the *Mk II unit* with double the number of LEDs, has about 30% higher peak than the *Mk I unit* – however it can be seen more clearly from the aerial views in *Figure*

7.24(b) and *Figure 7.25(b)* that the *Mk II unit* irradiance profile has a higher spread demonstrating a higher irradiance over a larger area.

An additional comparison of interest is the inactivation kinetics achieved with the *Mk I unit* at 10 cm and the *Mk II unit* at 15 cm – which both exposed samples to an irradiance of 1.5 $mWcm^{-2}$ (peak irradiance of 3 $mWcm^{-2}$). Shown in *Figure 7.26* is the inactivation curves of *S. aureus* using the two units. The results demonstrate relatively similar kinetics, although the inactivation rate at 30 minute using the *Mk I unit* was better. Generally, both units demonstrated >90% inactivation by 60 minute exposure, with the *Mk I unit* performing marginally better demonstrating a 97.5% reduction compared to the Mk II unit's 93.8% reduction.

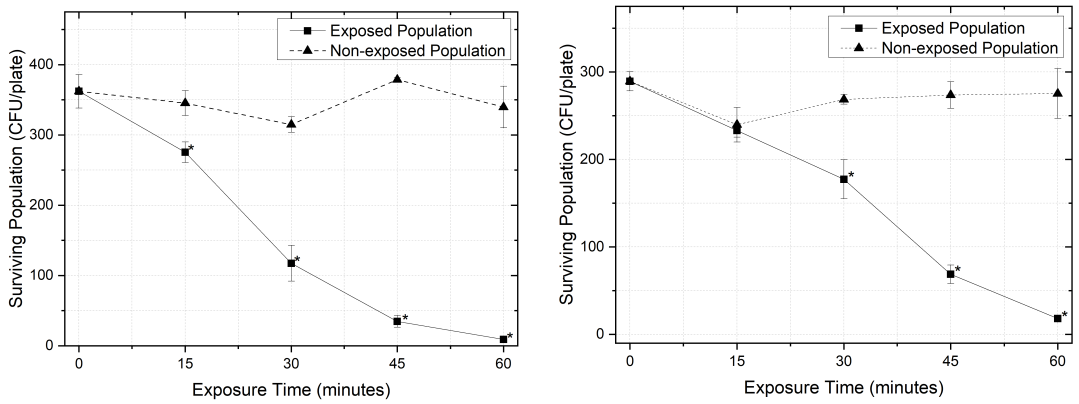

Figure 7.26: Comparison of the Inactivation of *S. aureus* under (a) the *Mk I unit* at 10 cm and (b) the *Mk II unit* at 15 cm – both of which had an irradiance of 1.5 $mWcm^{-2}$, or a peak irradiance of 3 $mWcm^{-2}$.

In the case of *P. aeruginosa* (*Figure 7.27)* both units again demonstrated fairly similar inactivation kinetics, with again the biggest difference being at the 30 minute period, however in this case it was the *Mk II unit* which had the greater reduction. In terms of inactivation achieved for the same dose delivered at 60 minutes – both units demonstrated an inactivation of over 99%, with the *Mk I unit* technically performing marginally better demonstrating a 99.4% reduction compared to the *Mk II unit's* 99.1% reduction.

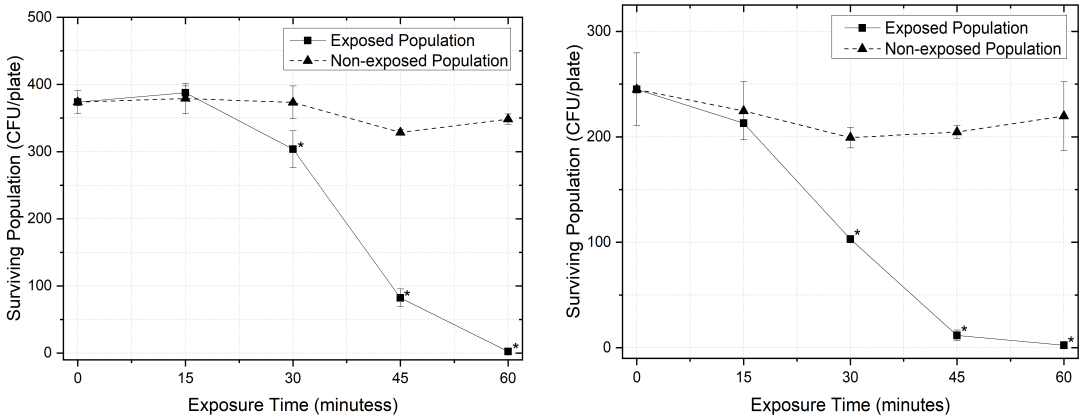

Figure 7.27: Comparison of the Inactivation of *P. aeruginosa* under (a) the *Mk I unit* at 10 cm and (b) the *Mk II unit* at 15 cm – both of which had an irradiance of 1.5 mWcm^{-2}, or a peak irradiance of 3 mWcm^{-2}.

In both cases – although the Mk II performed marginally better, the margins were very small and suggest very little difference between the two prototypes. This was to be expected given the small difference in irradiance from an average of 1.5 mWcm^{-2} to 2.2 mWcm^{-2}. For both strains of bacteria, the inactivation kinetics demonstrated similar trends but with slight differences, as would be expected with different experimental setups. In terms of the inactivation – the levels of irradiance were the same and as such the population reductions over the 60-minute exposure time were also similar. Unfortunately, due to the variation in the starting populations of each of the tests, statistical analysis could not to be carried out. Referring back to the differences observed at the 30 minute point in both *Figure 7.26* and *Figure 7.27*, the differences observed at this mid-point are not unusual, and inactivation kinetics in other publications have demonstrated similar variability in replicates that are on this downward slope. The reason for this is due to the mechanism of action. Typical 405 nm light inactivation curves tend to show a degree of plateau/slow inactivation at the start, due to the fact that there needs to be the build-up of sufficient ROS (and subsequent cell damage) before lethal damage, and downwards trends in the population are observed. Once this downward trend begins, this is the point in the

kinetics where the greatest deviation in results can be observed (Maclean *et al.,* 2009; Endarko *et al.,* 2012).

Overall, the experiment has successfully demonstrated that the Mk II unit was capable of producing the same levels of irradiance at a greater distance and achieving comparable levels of bacterial inactivation a greater distance, so with respect to this, the scale up to the *Mk II unit* was successful.

7.2.2 COMPARISON OF RESULTS TO OTHER EDS STUDIES

As discussed in *Section 2.4*, research at The Robertson Trust Laboratory for Sterilisation Technologies (ROLEST) developed the 405 nm light Environmental Decontamination System (EDS), and there have been a number of model prototypes which have been developed and tested as part of the research programme. The work of this present study differs in that the prototypes being developed have used PWM to control the optical output and blending. It is therefore of interest to compare the efficacy of the pulsed prototypes with those of the previous research studies, the main ones being by Endarko (2011) and Bache (2013). For analysis, the results from the *Mk II unit* exposures at 10 cm for inactivation of *S. aureus* in this study will be compared with similar experiments by Bache (using *S. aureus* and *P. aeruginosa*) and Endarko (using *S. aureus*) - albeit, these studies used larger scale EDS prototypes, and greater exposure distances.

In the study by Bache (Bache, 2013) *S. aureus* was subject to a 405 nm irradiance of 0.5 $mWcm^{-2}$ at a distance of 156 cm from the HINS-light EDS. The organism was subject to various exposure lengths from 1 to 7 hours with starting populations of between 120-200 CFU/plate. Sizable tailing of the inactivation occurred after 6-hour so this point will be used for comparison. After 6-hours exposure, a dose of 10.8 Jcm^{-2} was delivered resulting in a 90% reduction in the *S. aureus* populations. The inactivation demonstrated a relatively steady reduction over the 6-hour period.

The study by Endarko (Endarko, 2011) exposed *S. aureus* to 405 nm irradiation, this time at an irradiance of 0.17 $mWcm^{-2}$ at a distance of 120 cm from the HINS-light

EDS up to 9 hours, with starting populations of between 175-200 CFU/plate. Sizable tailing of the inactivation occurred after the 6-hour time point so this point is used for comparison. Over the 9-hour exposure there was a 90% reduction in the *S. aureus* populations was seen after 6-hours, with a dose of 3.67 Jcm^{-2} delivered. Like the study by Bache (Bache, 2013), the kinetics demonstrate a steady decline over the exposure duration.

The results of the *Mk II unit* as well as the two studies detailed above are summarised in *Table 7.3.*

Table 7.3: Table comparing the results of this study using the Mk II pulsed unit for inactivation of *S. aureus*, to those of previous studies by Endarko (2011) and Bache (2013) which used continuous prototype EDS units.

Author of Study	*Exposure time* ***(hrs)***	*Average Irradiance* ***($mWcm^{-2}$)***	*Dose Delivered* ***(Jcm^{-2})***	*Distance from Source* ***(cm)***	*Population reduction* ***(% CFU/plate)***
Bache	6	0.5	10.8	156	90
Endarko	6	0.17	3.67	120	90
Gillespie	1	2.2 (4.4 *peak)*	7.92	10	99.6

It is difficult to compare the studies given the significant variables between the present work and that by Endarko and Bache, however it is of interest to look at any trends that can be identified. Both Endarko's and Bache's inactivation was subject to sizable tailing of the inactivation after 6-hours of exposure so these point will be compared. The irradiance in Endarko's work is about 40% of Bache's, and the dose is about 34% of that used in Bache's work – however both demonstrate about a 90% reduction in *S. aureus* populations. The *Mk II unit* used a much shorter exposure at a much higher average irradiance of 2.2 $mWcm^{-2}$ (Peak – 4.4 $mWcm^{-2}$ @ 50% duty cycle) however the dose is in between the other two studies yet yields a higher inactivation of 99.6% compared with both. It could be argued that a lower irradiance is more

efficient in terms of inactivation per unit of optical energy comparing Endarko's dose to Bache's dose. Each study achieves 90% reduction over the same exposure time but with Endarko's irradiance and dose approximately one third of Bache's – it appears that lower irradiance is more efficient when it comes to bacterial inactivation. The *Mk II* results however use a higher irradiance over a much shorter time (1 hour compared to 6 hours) delivering an overall lower dose than Bache – achieving a higher inactivation level suggesting a higher irradiance is more efficient. It is also of interest to note that a 90% inactivation with the Mk II unit comparable to that of Bach and Endarko is more likely achieved at 45 minutes exposures so at a reduced dose closer to 6 Jcm^{-2}. In this case, Endarko with the lowest irradiance and dose achieves the most efficient inactivation with the Mk II unit higher irradiance, shorter exposure coming in second. A comparison of results suggest that lower irradiance could provide more efficient bacterial inactivation – however, over the 60 minutes the shorter higher intensity exposure achieved a much higher level of inactivation so the answer to the question of better efficiency at higher or lower irradiance levels remains unclear.

There are always many variations between studies however what can be inferred is that the inactivation is not entirely dictated by the dose delivered. The length of exposure and level of irradiance clearly have an impact too.

Bache also carried out a similar exposure with *P. aeruginosa* (250-300 CFU/plate) using the HINS-light EDS again with a 0.5 $mWcm^{-2}$ irradiance at a distance of 156 cm for up to 7 hours. Within 4 hrs, the population had reduced by 90% - with a delivered dose of 7.2 Jcm^{-2}. Comparing this with the *Mk II unit*, again the exposure time was much shorter at 1 hr; the irradiance was higher at 2.2 $mWcm^{-2}$; however the doses were comparable this time with the *Mk II unit* dose delivered being 7.92 Jcm^{-2}. The inactivation achieved however by the Mk II unit was 99.7% compared with Bache's 90% for the same dose. Comparing these two studies again demonstrate more efficient inactivation at a higher irradiance although perhaps to a lesser extent given the doses are much closer this time. Either way, it again supports the theory that the

inactivation is not entirely dictated by the dose delivered, but irradiance levels and exposure time have an impact.

All three studies demonstrate successful inactivation across a range of relatively low irradiances and with varying exposure times. The results further strengthen the idea that a system based on this technology would undoubtedly reduce environmental decontamination and could assist with the problem of HAIs plaguing the health system.

7.2.3 Design and Performance Issues

The scale up to the pulsed control *Mk II unit* was a demonstrable success and in terms of achievements, the unit:

- generated levels of 405 nm light high enough to demonstrate inactivation of both *S. aureus* and *P. aeruginosa*.
- generated a higher irradiance of 405 nm light, with an average of 2.2 $mWcm^{-2}$ at the plate positions compared to 1.5 $mWcm^{-2}$ with the *Mk I unit.*
- demonstrated comparable levels of inactivation to the *Mk I unit*, with >90% reduction for *S. aureus* and >99% reduction for *P. aeruginosa* at an increased distance of 15 cm (compared to 10 cm).
- generated a similar blend of light content, with CRI and CQS values of 81 and 82, respectively, compared with the values of 82 and 83 for *Mk I.*

7.2.3.1 Underperformance of the Yellow/Amber LEDs

There was, and still remain, some issues with the design and the first to be addressed is that of the spectral gap in the 550-600 nm region – i.e. the yellow/amber issue. When inspecting the final tune output spectrum of the *Mk II unit* (*Figure 7.8*) there is a clear dip between the 550-600 nm region. Work in this chapter attempted to rectify this issue of the low yellow content during the scale-up, however, although

improved slightly, was not solved. The 4 new yellow/amber LEDs were introduced in an effort to combat the lack of content in the 550-600 nm region since the yellows underperformed in the *Mk I unit*. For this reason, 4 new amber LEDs (590 nm peak) were added during the development of the *Mk II unit* with only 2 extra red and green LEDs to supplement the *Mk I unit's* LEDs. Upon inspection, a slightly lower wavelength closer to 570 nm might have been a better choice to fill out the spectral gap. However, at the time it was decided that the company Lumileds produced the red and green LEDs, which were performing well, so the decision was made to stick with that brand and when it came to availability the amber 590 nm peak LEDs were chosen. It should be noted – that had they produced a high enough irradiance or if more LEDs had been added, they would most likely have sufficiently filled the spectral gap. Given the spectral spread of the amber LEDs – there would have been wavelength content on either side of the 590 nm peak would fill out gap; and this could have been improved if required by increasing the green (525 nm peak) with the upper tail providing content up to about 570 nm. In the future design process – the output of each LED would have to investigated closely and the relative peak irradiances tested along with the FWHM to determine whether the spread and irradiances required can be achieved before building the different colour LEDs into a system.

7.2.3.2 Possible Addition of Additional Supplementary Wavelengths

A further idea of interest would be to design a system with a larger spread of different coloured LEDs so as to provide the ability to produce a wider spread of wavelengths and provide more control over the blend of light created. There are a variety of complications that come with using multiple coloured LEDs to produce white. There are trichromatic and tetrachromatic LEDs available but there is a difficulty when designing them. The three big issues are (i) uniform spatial light mixing and distribution, (ii) maintaining a white colour point, and (iii) thermal management (Muthu *et al.*, 2002). The idea of more colour would certainly increase the complexity of the system however this would be a way to increase the CRI of the

Mk II unit and create a light source with an overall higher level of customisation and function. There would however need to be consideration as to how many different colours of LED would be included. Ideally, the system would have the capacity to produce every wavelength of light, to provide the ultimate blend of light and the ultimate level of control over the blend - this however is completely unfeasible. There is a compromise to be found between the number of different coloured LEDs and the added functionality or benefits it brings to the system.

7.2.3.3 Consideration of LED Spacing & Placement

The scale up in terms of size, involved doubling the number of Red, Green and 405 nm LEDs and 4 additional amber LEDs were added. As in the *Mk I unit* in Chapter 6, the LEDs were all mounted on individual PCBs and so again the problem remained that the LEDs could not be mounted as close together as would be ideal. The *Mk II unit* had more than double the number of LEDs than the *Mk I unit* and so the LEDs were spread out much more than was ideal. This meant that although the number of LEDs was more than doubled, the output irradiance was not, due to the physical spacing apart of the LEDs. As discussed in Chapter 6, the LED spacing and arrangement would need to be addressed in the next scaled up prototype. A means of doing this would be to design, for instance, a PCB as a replicable module. A custom designed PCB would facilitate the surface-mounting of LEDs much closer together in an array – in the simplest iteration, just one of each colour. This PCB would be much closer to a point source emitting the full range of wavelengths and these modules could then be replicated and even if the modules were spaced out, it would certainly improve the colour shadow problems.

Moving the LEDs closer together could however raise different issues too. As light sources, LEDs are very compact, efficient and can produce high irradiances of light output – however with these high irradiances come high temperatures. High temperature fluctuations can cause a decrease in the band gap of the semiconductor and lead to wavelength shift (Muthu *et al.*, 2002). Additionally, with a temperature

increase comes a decrease in the optical output of the LEDs (Schubert, 2006). This on top of the spread of performance of different LEDs and the effects of age (which can reduce output by up to 50%) (Muthu *et al.*, 2002) means that trying to keep the three or four LED outputs at the same wavelength and irradiance with uniform light distribution is a very challenging task and in general would require some kind of feedback control. Trichromatic and tetrachromatic LEDs however have the ability of producing light with high output irradiance and CRI values up to 89 and 95 respectively so although they come with challenges, they can produce very high quality light (Lei et al., 2007).

An extension of this idea of trying to create a point source would be the inclusion of some blending element whilst not having the LEDs too close as to cause thermal issues. This would either be some type of lens-diffuser setup, frosted glass, or some physical element such that the individual colours of LEDs are masked and the translucence of the blending element makes the module of 4 individual colours appear as a single white point source. The acceptability of a blend of light can be a subjective quantity - different people can have differing perceptions of what their ideal light output looks like – however with CRI and CQS, the light quality can be quantified and compared with other light source competitors. With LED technology offering a more customizable source in terms of wavelength content, there is a large body of research currently looking at the effects of different type of warm and cool whites, as well as the effects of certain wavelengths on human health and behaviour (Correa, 2016). The issues of colour, quality and brightness of light can have significant effects on aspects such as alertness; cognitive performance; how well people can relax; sleep patterns, and other bodily function (Cajochen, 2007; Gabel *et al.*, 2015; Blume *et al.*, 2019). Future work would have to include focus groups to gauge the acceptability and the preferences of individuals and groups of different composition of light output.

7.2.3.4 Comparison to Alternative Light Sources

On the topic of light quality, the CRI and CQS demonstrated an improvement over the tuning process but fell just shy of the final *Mk I unit* values, by just 1 in each case. The CRI value of both the *Mk I* and *Mk II units*, 82 and 82 respectively, are comparable to that of LED light bulbs on the market (Philips, 2019). The halogen and fluorescent tube lighting provide CRI values from as low as about 50 right up to 100 (Guo and Houser, 2004), so in terms of CRI values for standard lighting, the prototypes are acceptable, the problem lies in the actual blending of the prototypes albeit there should always be a push for better CRI. In *Table 7.4* are some example CRI value ranges for different light sources.

Table 7.4: Table of typical CRI value ranges for common light sources. (Adapted from Schubert, 2006)

Light Source	***Colour Rending Index (CRI)***
Sunlight	100
Tungsten (W) filament incandescent light	100
Fluorescent light	60-95
Trichromatic white LED	60-95
Phosphor based LED	55-95
Mercury (Hg) vapour light coated with phosphor	50

When compared to theses other sources, the CRI value above 80 achieved by the *Mk I* and *Mk II* pulsed prototypes would be an acceptable standard of CRI – with some commercial fluorescent lights and LEDs producing similar if not lower values of CRI. This then means the blending, aesthetics and scale up would be the main focus when taking the prototype forward.

7.2.3.5 Considerations for Scale Up & Discussion of Commercialised 405 nm light Decontamination Systems

In respect of future work regarding the *Mk II* prototype, the colour blend for aesthetics could be improved, and work towards eradicating the colour shadows would be key areas of focus. Although in this study the decision was made to use 3 colours spaced throughout the spectrum to supplement the 405 nm light –this is not the only way to achieve a blended light. An interesting alternative to supplementary coloured LEDs is to supplement with white LEDs. This would require less blending than that of 4 different colours, however it would be important to get the correct balance of 405 nm light to white, in order for the overall light output to be an acceptable shade of white. The continuous HINS-light EDS prototypes used in previous studies (Bache *et al.,* 2012; Maclean *et al.,* 2010; Maclean *et al.,* 2013) used white LEDs to supplement the 405 nm LEDs. These lighting units investigated the use of cool, neutral and warm white LEDs to achieve the best balance possible, and the resulting units produced an acceptable blended output when used in combination with existing lighting, as was the case in those studies. For use of the system as the primary light source in a room, further adjustments to the blend were required in order to produce a comfortable output (as was involved in the development of the commercial Indigo-Clean product by Kenall). Investigating the potential for pulsed control of white LEDs in combination with the pulsed 405 nm LEDs would be an interesting way forward. It would be useful to compare pulsed units built using supplementary coloured LEDs, as in this study, and supplementary warm white LEDs as done in previous iterations of the HINS light system (Endarko, 2011) to investigate differences in (i) blend and wavelength content; (ii) efficiency in terms of power, size and cost requirements; and (iii) general design and aesthetics.

Upon further redesign of a scale up, safety considerations would have to be addressed. In this study general optical safety considerations were outlined in *Section 2.6*, detailing the types of injury which can be sustained with different wavelengths

of light, and the idea of Threshold Limit Values (TLV) for different wavelengths of light. Specific safety analysis of the previous EDS units (Anderson *et al.*, 2013; Endarko, 2011; Bache, 2013), which produced approx. 0.2 – 0.5 $mWcm^{-2}$ at a distance of 200 cm, confirmed the output of the units to be below the TLV for the different safety considerations. The prototype developed in this study, which uses pulsed operation, and any future pulsed control designs, must also fall within these limits. As discussed in *Section 6.5* the irradiance levels being used in this study peak at 4.4 $mWcm^{-2}$, which although higher than 0.5 $mWcm^{-2}$, is only 10 cm from the source, not 200 cm as with the previous continuous control, large scale prototypes. Nonetheless, moving forward and scaling up the concept further, safety would have to be a significant consideration to ensure any final design is fit-for-purpose.

As discussed in *Section 2.3.2*, Kenall Lighting (Kanall.com, 2019), a US lighting manufacturer, licensed the technology from the University of Strathclyde, and have launched a commercial lighting product range using 405 nm light. A number of their products, including the surgical and procedure room light, have the option to switch between two modes – so called 'Indigo Disinfection', or 'White Disinfection' mode shown in *Figure 7.28 (a)* and *(b)* respectively.

(a) *(b)*

Figure 7.28: Photographs of the Indigo Clean system, from Kenall, in patient rooms in (a) Indigo Disinfection mode and (b) White Disinfection mode. Images taken from: https://kenall.com/Indigo-Clean/Continuous/Procedure-Rooms

White disinfection is where the white light in the unit is on to balance out the 405 nm light providing a comfortable level of white light when visual acuity is essential. Indigo disinfection uses a higher level of 405 nm light with the white lights turned off and is typically used in rooms during unoccupied times (e.g. overnight) (Kenall.com, 2019). Hubbell Lighting, who have also licensed the technology from the University, have produced a range of 405 nm based disinfection lighting products, again with a range of operational modes: continuous disinfection mode which is 405 nm light blended with white; a high irradiance mode for higher level of disinfection; and alternate mode in which 405 nm light or white can be individually switched on and used for disinfection or just lighting (Hubbell Lighting Components, 2020).

Both companies have successfully developed products using 405 nm light with supplementary white light, which demonstrates that viable systems based on this technology can be built. With this in mind – if the results in Chapter 5 which demonstrated pulsing can provide more efficient inactivation (in terms of the amount of optical energy resulting in inactivation) when compared with continuous, if pulsed control could be implemented in a commercial sized system it could potentially lead to higher levels of optical and electrical energy efficiency. Additionally, if the *Mk II* concept could be further developed it may lead to the potential development of a multipurpose continuous environmental disinfection light product in which the colour of the blend of light could be controlled and altered for different times of the day, applications and environments.

7.3 CONCLUSION

The work of this Chapter, and that of Chapter 6, builds on the results demonstrated in Chapter 5, which showed that 405 nm light can be pulsed at a lower duty cycle and thus the average irradiance will be lower and will appear less bright than the peak irradiance whilst maintaining the same levels of inactivation. Chapters 6 and 7 investigated whether by using pulsed 405 nm light, the level of 405 nm light

would appear lower whilst maintaining the inactivation achieved with continuous 405 nm light, making it easier to blend with supplementary colours in order to produce a blended white light. The pulsed prototypes developed in Chapters 6 and 7 have successfully achieved this and conclude that a pulsed blended white light unit with antimicrobial properties could be a viable option for continuous environmental decontamination applications. The results showed that, the addition of supplementary pulsed red, yellow and green light does not affect, either negatively or positively, the antimicrobial properties of the pulsed 405 nm light. In addition to this, the optical output of the *Mk I & Mk II* pulsed circuit LED systems was, based on CRI measurements, comparable to commercially available white light sources. This means the aesthetics of the lights can be improved by the addition of the supplementary colours without any interference to the environmental decontamination objective – however a sizable redesign of the concept would be required for the scaled up system to be a viable option for commercial environmental decontamination.

CHAPTER 8
CONCLUSIONS & FUTURE WORK

8.0 OVERVIEW

This chapter will reaffirm the problem and motivation for this body of research and summarise the conclusions of each chapter. Suggestions will also be provided for future areas of investigation which will build upon the outcomes of this study.

The main motivation for this work is the issue of infection control. Unfortunately, with infection levels on the rise and new problematic pathogens, e.g. MRSA, resistant to antibiotics and with the ability to remain viable on dry surfaces for long periods (Boyce, 2007), the need for new technologies to combat this is very much of interest. 405 nm light has demonstrated significant antimicrobial efficacy for environmental decontamination (Maclean *et al.*, 2010; Maclean *et al.,* 2013; Bache *et al.*, 2012) but as discussed in *Section 2.4*, it is important to ensure that the 405 nm light is appropriately blended with white light to ensure that the output of the lighting system is aesthetically acceptable due to its major advantage being the fact that it can be used safely in occupied environments. Based on this technical consideration, the main objectives of this study were to investigate whether pulsed 405 nm provided any advantages over continuous 405 nm light in terms of antimicrobial efficacy and/or energy efficiency, and whether a viable mixed antimicrobial white light prototype (containing pulsed 405 nm light) could be designed and created for continuous environmental decontamination.

Overall, this study demonstrated the first evidence of increased efficiency in terms of electrical & optical energy using pulsed 405nm LEDs when compared with continuous for antimicrobial applications. The study demonstrated the use of pulsed 405 nm LEDs to facilitate the blending of a blended white light source with supplementary colours for improved user acceptability. Finally, the study output a successful prototype of a pulsed blended white antimicrobial light system -

demonstrating successful bacterial inactivation; an improvement in colour quality after the tuning process; and providing the basis for a novel pulsed commercial system which could provide continuous environmental decontamination in populated clinical accommodation.

8.1 Optical Characteristics of Pulsing LEDs

8.1.1 Summary of Key Findings

The work of Chapter 4 was designed to gain familiarity with the operational considerations for pulsing LEDs and investigating the means to control the pulsing of LEDs. The first and foremost output of this chapter was the pulsing circuit which was decided upon and then used as a basis for the remainder of experiments in this study.

The main conclusions from the chapter were to do with the effects of pulsing, operating bulk temperature (as LED junction temperature is very difficult to measure) and input current on the LED optical output. Temperature was demonstrated to be a significant variable when working with LEDs – with high temperatures causing a drop in optical output as well as the threat of component failure when the temperature rises. The study looks at how temperature and input current affect the position of the LED output spectra in terms of wavelength as well as the FWHM, which is a measure of the width of the spectra, again in terms of wavelength. Across the temperature range and input current range investigated (within rated values), both the position and width of the spectra demonstrated some variation across the ranges – however no drastic variation - at most showing <5% change in values.

Operating temperature however was demonstrated to have detrimental effects on the peak optical output of the LEDs. When pulsed, there is a cool-down time between the 'on' periods of the LED, which allow the LED to operate at a cooler temperature. The results showed that, given the same level of input current, the

continuous current demonstrated a measurably lower peak irradiance at the output than with any of the pulsed LED runs. These results detailed in *Section 4.3.4.2*, demonstrated that with an increasing input current and no temperature control – effectively a rising temperature – the difference in peak optical output between the pulsed and continuous driven LEDs became more and more apparent. Specifically, the lower duty cycles demonstrated the highest peak optical output consistently across the range of input currents.

The input current is generally related to the temperature and with a higher input current, the temperature tends to increase and thus LED performance suffers in terms of efficiency. Combatting this drop in efficiency can be achieved to an extent by controlling the temperature. The final conclusion is that temperature must be monitored and controlled during experiments because it can have serious effects on the irradiance of light output from the LED.

Each LED temperature was measured over a range of input currents to look at how variable the output was with temperature fluctuations to decide on how much temperature control was required i.e. passive using just a heat sink or more active using a Peltier module, heatsink and fan combination. Additionally, the build and testing of the pulsing circuits provided a useful means of deciding on the pulsing circuit to use for the subsequent sections of the study allowing the most concise and appropriate version of the circuitry for the experiments to be chosen. This also provided a chance to further understand the circuit's operation so that upon future builds, any troubleshooting or faults could be dealt with.

A further finding from the testing of the circuits with LEDs was the LED behaviour under pulsing. A particularly useful finding was the temperature differences under different levels of pulsing – and again this highlighted for future experiments that the LEDs had to be rigorously checked in terms of how much the LED output fluctuated with the temperature before use in experiments to ensure consistency in the LED performance. Additionally, the work provided and idea of rise and fall times for the pulse on and off the LEDs and thus an idea of the highest

frequency which the LEDs could be pulsed at. This allowed some practical experience in how to measure this and meant the frequency parameters for the frequency sweep in chapter 5 could be set within an appropriate range.

8.2 Pulsed 405 nm LEDs – Proof of Concept

8.2.1 Summary of Key Findings

The proof-of-concept work of Chapter 5 investigated the use of pulsed 405 nm light and its effects on the antimicrobial efficacy and energy efficiency compared to continuous 405 nm light. The experiments varied the peak irradiance, duty cycle, frequency of the pulsing; exposure length and dose delivered; and looked at the effects on the antimicrobial efficacy and energy efficiency of the 405 nm light in each case.

Initial experiments were carried out across a range of different irradiances, varying the duty cycle and peak irradiance, whilst maintaining a constant dose and exposure time. The experiments showed no significant difference in the antimicrobial effect between the experiments, suggesting that the method of delivery of the same dose over the same time appears to have no effects, either beneficially or detrimentally, on the antimicrobial action. However, with the change in both peak irradiance and duty cycle at the same time, there is a possibility that effects could be masked because the nature of the experiment requires altering two variables simultaneously.

Subsequent experiments looked at whether the frequency of the pulsing had any effect on the antimicrobial efficacy of the 405 nm light. Experimental data demonstrated very little change in the antimicrobial properties across a range of frequencies from 100Hz – 10kHz. At the highest frequency there a slight drop in antimicrobial efficacy but only when compared with some of the lower frequency experiments. The evidence from this study though suggests that frequency has very

little effect on the antimicrobial efficacy of the 405 nm light – however with the scope in terms of the small number of frequency intervals, the single length of exposure, the same irradiance levels, the same organisms among many other variables used throughout the experiments, that is not to say frequency has no effect.

Exposure time was examined, looking at exposures with the same peak irradiance, varying the duty cycle and exposure time to maintain a constant dose, to investigate any effects of longer or shorter exposures on the antimicrobial efficacy of the 405 nm light. The experiments showed apparent differences in terms of average percentage reduction; however, when the errors were taken in account and the statistical analysis undertaken, results demonstrated that the length of exposure from varying from 30 minutes to 120 minutes (with the same dose but varying duty cycles from 100% to 25% respectively) had no effect either way on the antimicrobial efficacy of the 405 nm light. This however is not to say that this will hold true over much longer or shorter periods of exposure. The difference in exposure time between 30 and 120 minutes could be too small to see a difference – however comparing 40 minutes at 90% duty cycle and 360 minutes at 10% duty cycles may demonstrate different results. Future work should look across a wider range of exposure times and duty cycles – maintaining the same dose - to investigate any possible changes in the antimicrobial effect.

The key conclusion taken from the proof on concept work was that the 405 nm light induce inactivation may not be an entirely dose-dependent action. The experiments kept exposure time and peak irradiance the same whilst altering the duty cycle, which proportionally altered the applied dose. The experimental evidence showed that the antimicrobial action is not entirely dose dependent. The 25% duty cycle exposure, which was 25% of the dose of the continuous exposure demonstrated almost 50% of the bacterial inactivation achieved by the continuous exposure with 4x the dose. Additionally, the 50% and 75% duty cycle runs showed no significant difference ($p>0.05$) when compared with the continuous exposure with the two

pulsed exposures, 50% and 75%, demonstrating improved bactericidal efficiency in terms of dose delivered compared with the continuous exposure.

These results suggest that, in this case, the antimicrobial action is not entirely dose dependent and the inactivation could be more dependent on the peak irradiance and length of exposure opposed to a purely dose dependent reaction. This in turn leads to the further conclusion suggesting that pulsing LEDs could lead to a more energy efficient means of bacterial inactivation - in addition to an apparent lower irradiance of 405 nm light producing comparable bacterial inactivation.

8.2.2 FUTURE WORK

There is a wide range of subsequent experiments that could be carried out building on this proof-of-concept work. Throughout the experiments the duty cycles used were 25%, 50% and 75%, however it would be interesting to investigate intermediate duty cycles: and specifically lower duty cycles since the results seemed to suggest that the optical efficiency was the best at the lowest 25% duty cycle, so it could be of interest to establish if better efficiencies continue to be obtained at even lower duty cycles.

Additionally, the maximum irradiance used was 30 $mWcm^{-2}$ throughout the study. This was done with the application of continuous environmental decontamination in mind, so high irradiance light was thought to be of less interest under that practical context. However it would be of interest to repeat the experiments at lower and higher irradiances in an effort to see if the results found at the irradiances used in this study hold true at higher and lower irradiances. These experiments could also reveal any effects on the efficiency – for instance, do different levels of irradiance provide more efficient inactivation in terms of the overall dose delivered?

An interesting experiment would be to look at comparing very high irradiance short pulses of 405 nm light, for instance 100 $mWcm^{-2}$ at a 5% duty cycle, with lower

irradiance longer pulses, e.g. 5.3 $mWcm^{-2}$ at a 95% duty cycle – which would result in the same dose delivered but in very different ways. Frequency might also be altered such that you have a rapidly repeating high irradiance short pulse compared with a much lower irradiance longer pulse at a smaller frequency. This could reveal more about pulsing and how more extreme variations in the delivery of pulsed 405 nm light affects the inactivation properties of the light.

Furthermore, given the results of more efficient (in terms of energy efficiency) bacterial inactivation with pulsed light and some of the discussed hypotheses on what might be happening (*Section 5.2*), a more in-depth investigation of the effect of frequency could be of interest. In one of the hypotheses (discussed in *Section 5.2.4*) – the idea of a 'saturation point' is introduced. The inactivation mechanism of 405 nm light involves the endogenous porphyrins within pathogens absorbing 405 nm light and causing excitation of these porphyrin molecules resulting in the production of radical oxygen species. These radicals cause damage to cellular components and the cell wall and can lead to cell death. The 'saturation point' is the point at which a cell absorbs a photon, or enough photons, which will result in cell death – however photons can still be absorbed by this already dying cell with no extra effect. If this is case, then burst of photons allowing time for the cells undergo the inactivation process could possibly result in improved antimicrobial efficacy. Thus – if this is the case there could prove to be an optimal frequency or duty cycle or pulse width for the most efficiency inactivation in terms of energy efficiency.

Additionally, although the study results demonstrated more efficient kill in terms of optical and electrical energy consumed per CFU of bacteria inactivated, this was a single peak irradiance, frequency and exposure time so it would certainly be of interest to repeat these experiments at higher irradiances; a range of different frequencies; and varying lengths of exposure time in an effort to investigate whether the apparent increase in efficiencies are apparent under different conditions.

A final note is that of investigating first order inactivation kinetics more – it was briefly touched upon and used in the results in *Section 5.2.4*, however with more

iterations using a wider array of different parameters, it could prove a very useful means of comparison and highlighting any key differences in results.

8.3 PULSED ANTIMICROBIAL BLENDED WHITE LIGHT

8.3.1 SUMMARY OF KEY FINDINGS

Chapters 6 and 7 focused on the development of a blended pulsed white antimicrobial light source containing antimicrobial levels of 405 nm light. Continuing the theme of pulsing and applying it to the use of 405 nm light for environmental decontamination was the starting point of Chapters 6 & 7. With a demonstrated improvement in optical efficiency and electrical efficiency from Chapter 5, the idea was that pulsing could be used to exploit these improved efficiencies also incorporating the use of pulsing as a control element.

Building upon the previous HINS-light systems developed within ROLEST, the concept of combining 3 supplementary colours (red, green and yellow/amber) with the 405 nm light and using pulse width modulation as a control mechanism was the key idea for the new system – to create a pulsed blended antimicrobial white light source.

The pulsing circuits work from Chapter 4 provided the base for the circuit design in Chapter 5 and likewise drawing from both chapters, the circuitry in Chapters 6 & 7 had to be redesigned such that each colour of LED could be pulsed at different duty cycles with the added complexity of multiple LEDs of each colour. The first major output was the design, build and test of the pulsing circuitry for the lighting unit – which was subsequently replicated and amended for Chapter 7.

Upon build and testing it became apparent that the wavelength content of the output from the *Mk I unit* was much improved compared with 405 nm light alone however the aesthetics and blending of the different coloured LEDs required attention and the yellow LEDs underperformed results in a partial spectral gap in the

overall *Mk I unit's* spectrum. The spectrometer (HR4000, Ocean Optics, UK) and analysis software (NIST CQS version 7.4) was used to investigate the light quality in terms of CCT, CRI and CQS. The system was tuned with the duty cycles of each colour changed to control the content of each colour in the overall blend. The quality of light improved as can be seen from the picture examples and the CRI and CQS values in Chapter 6 and was a definite improvement over the 405 nm light alone.

The CRI and CQS values of the final tuned *Mk I unit* were 82 and 83 respectively which are comparable to white light sources on the market - e.g. fluorescent, trichromatic LEDs and phosphor based LEDs – which all range from about 60-95 in terms of CRI (Schubert, 2006). The blending however was an issue which was hard to address due to a combination of the physical spacing of the LEDs and the low irradiance output. The LEDs were required to be positioned more closely together to generate something more akin to a point source and a blending element such as frosted glass or a diffuser would be required to adequately blend the colour together – however all the wavelength content was present to create a blend.

The *Mk I unit* was subsequently scaled up to the *Mk II unit* and demonstrated higher irradiances a comparable quality of light in terms of CRI and CQS, as well as visual inspection. The yellow LED issue was addressed by added more yellow LEDs relative to the colours however the yellow LEDs persisted in underperforming despite their increase number resulting in more of a spectral gap around the yellow region that hoped. The tuning process was successful in improving the quality of the light as in the *Mk I unit* – both visually and in terms of CRI and CQS demonstrating an increase from 69 and 73 to 81 and 82 respectively. It remained that the predominant issue with both prototypes was that of blending – not of light quality.

The blending issues was further compounded by the addition of more LEDs albeit placed as close together as possible. It was realised that to address this problem in a more effective manner, the PCBs upon which the LEDs were mounted would require a complete redesign to a smaller size or possibly mount multiple on the one PCB. Either way, the placement and design of the LED PCBs would require a more

rigorous plan in terms of physical arrangement bearing in mind the issues which arose in the development of the *Mk I* and *Mk II units* in this study.

The *Mk II unit* however did provide a higher output irradiance as planned, however again with the LED physical spreading it was not double that of the *Mk I unit*. It did however demonstrate the same levels of 405 nm light at 1.5x the distance demonstrating a successful scale up in term of irradiance.

In terms of the antimicrobial efficacy, the *Mk I unit* designed and built, practically speaking, worked and the pulsed 405 nm light supplemented with other colours demonstrated over 90% reductions of both *S. aureus* and *P. aeruginosa* populations. It was also demonstrated that the supplementary colours had no effect either positively or negatively on the antimicrobial action of the *Mk I unit* as intended.

The *Mk II unit* as discussed provided the same levels of irradiance at 1.5x the distance of the *Mk I* unit – and as such at the original height of 10 cm had a higher irradiance and demonstrated a quicker inactivation in both *S. aureus* and *P. aeruginosa*. This was a demonstrated success in the scale up. Furthermore, the *Mk II unit* demonstrated a comparable level of inactivation of *S. aureus* and *P. aeruginosa* at the 15cm distance when compared with the *Mk I unit* at 10cm again demonstrating a successful scale in this respect.

Overall, between the two iterations of the prototype, the concept was shown to have promise demonstrating a successful inactivation of pathogens and a comparable quality of light in terms of CRI to that of some white light sources. The blending remained the issue. However, further development and testing of the prototype could lead to a viable system for lighting and environmental decontamination.

8.3.2 FUTURE WORK

The scale up would be a clear element upon which to build for future work. Although the work in this study suggests a good basis from which to start and the technology has been demonstrated to be viable by commercial companies, Kenall Lighting and Hubbell Lighting. The system designed in this study must be further

scaled up to light levels in which ceiling mounted lights, for instance would produce enough 405 nm light to result in a significant of disinfection. Practically speaking, power requirements will be a key consideration in the viability of any blended white prototype. Therefore, in theory, if the LEDs are pulsed on and off, then the electrical energy consumption should be lower than that of a continuous blended light system. Future work could investigate the optimal duty cycle and pulsed operation for most efficient bacterial inactivation in terms of electrical energy and investigate whether it would be viable to run the system continuously considering the potential energy draw it would consume.

An additional consideration is the spread of wavelengths of light across the spectrum. The white LED spectrum has a contiguous spread from green through to red, which is theoretically what is required to blend white light. Ideally, more LEDs across of a variety of wavelengths would have been used to create a fuller spectrum closer to a white blend but this isn't practical, so it was decided on four LEDs spread across the spectrum – given that some tetrachromatic LEDs can produce CRI values of up to 95 (Lei et al., 2007). Again, further study into the acceptability of what spread of wavelengths would provide adequate quality of light is required. This area in terms of the perfect blend of white is a current hot topic particularly with the emergence of LEDs and the customisation option that accompany it, so it is of interest to note that there is no industry standard on the perfect blend as it is such a subjective concept.

A major aspect of future development is the blending work. The LEDs in this study were too spaced apart due to the size of the PCBs, heating issues among other design issues. Future work would look at getting the LEDs colours as close together as possible more akin to a single point light source. Possibly look at a modular design as discussed in *Section 7.2.3* with small replicable module of 4 or 5 LEDs placed on custom PCBs, in order to achieve something closer to a point source from which all wavelength content comes from. Subsequent research would then look at the use of diffusers or frosted glass to mask the individual coloured LEDs when looking up at

the light, so as to create what would appear as a large white source opposed to many different coloured individual LEDs.

8.4 Overall Study Conclusion

From the outset, the overall aim of this study was to investigate the use of pulsed 405 nm light for environmental decontamination. The study investigated the different approaches to pulsing in terms of circuitry and reaffirmed LED behaviour under pulsed operating conditions.

Upon investigation of pulsed 405 nm LEDs specifically, a wide variety of parameters were investigated, including peak irradiance, pulsing frequency, duty cycles and exposure time, and how they effected the antimicrobial action of the 405 nm light in terms of optical energy, electrical energy used, antimicrobial efficacy and whether the 405 nm light acted in dose dependent manner. One of the key finding from these experiments was the increase in optical efficiency (defined as the amount of inactivation in $CFUml^{-1}$ per unit of optical energy in Jcm^{-2}), the improved electrical efficiency (defined as the amount of inactivation in $CFUml^{-1}$ per unit of electrical energy in J) when using pulsed 405 nm light. Whilst changing the duty cycle, and proportionally the dose, higher optical and electrical efficiencies were found with the optical efficiency demonstrating an inverse relationship with the duty cycles – with the maximum optical efficiency found at the lowest 25% duty cycle. Electrical efficiency did not demonstrate a clear trend however did offer an increase level of efficiency at 2 of the 3 pulsing regimes when compared with continuous 405 nm exposures. This provided a novel output from the study, and future work could expanded this to investigate this anomaly in terms of both how the trends appear and the cause of the increased efficiency.

Building on these improved optical and electrical efficiencies, pulsed 405 nm light was incorporated into the concept of the HINS-light EDS developed by ROLEST. The key objective was to develop a blended white light which would blend 3

supplementary wavelengths with 405 nm light maintaining the antimicrobial action. The core concept of pulsing was used a method to control the blend of the 4 colours and, using measures of colour quality such as CRI and CQS, the output of the system could be tuned to provide a better quality of output whilst still maintaining a useful antimicrobial level of 405 nm light.

Overall, the prototype developed in this study demonstrates a good colour quality, which in terms of CRI can be compared with white sources on the market, whilst still providing antimicrobial action from the 405 nm light content. The study demonstrates an encouraging foundation for the concept of a pulsed, blended antimicrobial white light source, and with further research and development this could provide the basis for a tunable lighting technology for continuous environmental decontamination.

REFERENCES

Allegranzi, B. and Pittet, D. (2009). Role of hand hygiene in healthcare-associated infection prevention. *Journal of Hospital Infection*, 73(4), pp.305-315.

Amin, R., Bhayana, B., Hamblin, M. and Dai, T. (2016). Antimicrobial blue light inactivation of *Pseudomonas aeruginosa* by photo-excitation of endogenous porphyrins: In vitro and in vivo studies. *Lasers in Surgery and Medicine*, 48(5), pp.562-568.

Anderson JG, Maclean M, Woolsey GA, MacGregor SJ. Optical Device for the Environmental Control of Pathogenic Bacteria. European Patent number 2211914 (granted 2014); USA – Patent number 8,398,264 (granted 2013).

Ash, C., Dubec, M., Donne, K. and Bashford, T. (2017). Effect of wavelength and beam width on penetration in light-tissue interaction using computational methods. *Lasers in Medical Science*, 32(8), pp.1909-1918.

Aslam, B., Wang, W., Arshad, M., Khurshid, M., Muzammil, S., Rasool, M., Nisar, M., Alvi, R., Aslam, M., Qamar, M., Salamat, M. and Baloch, Z. (2018). Antibiotic resistance: a rundown of a global crisis. *Infection and Drug Resistance*, Volume 11, pp.1645-1658.

Atkins, P., De_Paula, J. and Friedman, R., 2014. Physical Chemistry. Oxford: Oxford University Press.

Bache, S., Maclean, M., MacGregor, S., Anderson, J., Gettinby, G., Coia, J. and Taggart, I. (2012). Clinical studies of the High-Irradiance Narrow-Spectrum light Environmental Decontamination System (HINS-light EDS), for continuous disinfection in the burn unit inpatient and outpatient settings. *Burns*, 38(1), pp.69-76.

Bache, S.E. (2013). *Clinical evaluation of the HINS-light EDS for the continuous light based decontamination of the burns unit inpatient and outpatient settings*. Ph.D. thesis, University of Strathclyde.

Barneck, M., Rhodes, N., de la Presa, M., Allen, J., Poursaid, A., Nourian, M., Firpo, M. and Langell, J. (2016). Violet 405-nm light: a novel therapeutic agent against common pathogenic bacteria. *Journal of Surgical Research*, 206(2), pp.316-324.

Beczkowski, S. and Munk-Nielsen, S. (2010). Led spectral and power characteristics under hybrid PWM/AM dimming strategy. *2010 IEEE Energy Conversion Congress and Exposition*.

Bedrosian, T. and Nelson, R., 2017. Timing of light exposure affects mood and brain circuits. *Translational Psychiatry*, 7(1), pp.e1017-e1017.

Behar-Cohen, F., Martinsons, C., Viénot, F., Zissis, G., Barlier-Salsi, A., Cesarini, J., Enouf, O., Garcia, M., Picaud, S. and Attia, D., 2011. Light-emitting diodes (LED) for domestic lighting: Any risks for the eye?. *Progress in Retinal and Eye Research*, 30(4), pp.239-257.

Bioquell (2015). *Hydrogen peroxide automated room decontamination: vapour vs. aerosol systems*. Bioquell, UK. [online] Available at: https://www.bioquell.com/wpcontent/uploads/2017/07/Aerosol_white_paper.pdf [Accessed on 30 Jan 20].

Blume, C., Garbazza, C. and Spitschan, M., 2019. Effects of light on human circadian rhythms, sleep and mood. *Somnologie*, 23(3), pp.147-156.

Boer, H., van Elzelingen-Dekker, C., van Rheenen-Verberg, C. and Spanjaard, L. (2006). Use of Gaseous Ozone for Eradication of Methicillin-Resistant Staphylococcus aureus From the Home Environment of a Colonized Hospital Employee. *Infection Control & Hospital Epidemiology*, 27(10), pp.1120-1122.

Bohrerova, Z., Shemer, H., Lantis, R., Impellitteri, C. and Linden, K. (2008). Comparative disinfection efficiency of pulsed and continuous-wave UV irradiation technologies. *Water Research*, 42(12), pp.2975-2982.

Boyce, J. (2016). Modern technologies for improving cleaning and disinfection of environmental surfaces in hospitals. *Antimicrobial Resistance & Infection Control*, 5(1).

Boyce, J., Havill, N., Otter, J. and Adams, N. (2007). Widespread Environmental Contamination Associated With Patients With Diarrhea and Methicillin-Resistant Staphylococcus aureus Colonization of the Gastrointestinal Tract. *Infection Control & Hospital Epidemiology*, 28(10), pp.1142-1147.

Boyce, J.M. (2007). Environmental contamination makes an important contribution to hospital infection. *Journal of Hospital Infection,* 65(S2), pp.50-54.

Bullough, J., 2000. The Blue-Light Hazard: A Review. *Journal of the Illuminating Engineering Society*, 29(2), pp.6-14.

Bullough, J., Bierman, A. and Rea, M., 2017. Evaluating the blue-light hazard from solid state lighting. *International Journal of Occupational Safety and Ergonomics*, 25(2), pp.311-320.

Cajochen, C., 2007. Alerting effects of light. *Sleep Medicine Reviews*, 11(6), pp.453-464.

Chang, J., Ossoff, S., Lobe, D., Dorfman, M., Dumais, C., Qualls, R. and Johnson, J. (1985). UV inactivation of pathogenic and indicator microorganisms. *Applied and Environmental Microbiology*, 49(6), pp.1361-1365.

Chen, H., Xie, Z., Jin, X., Luo, C., You, C., Tang, Y., Chen, D., Li, Z. and Fan, X. (2012). TiO_2 and N-Doped TiO_2 Induced Photocatalytic Inactivation of Staphylococcus aureus under 405 nm LED Blue Light Irradiation. *International Journal of Photoenergy*, 2012, pp.1-5.

Choudhury, A. (2014). *Principles of colour and appearance measurement*. Oxford: Woodhead Publishing.

Clordisys.com. (2014). *Products | Minidox-M*. [online] Available at: https://www.clordisys.com/minidoxm.php [Accessed 11 Feb. 2020].

Cole, M., Clayton, H. & Martin, K. (2015). Solid-state lighting: The new normal in lighting. *IEEE Transactions on Industry Applications*, 51(1), pp.109–119.

Conlon-Bingham, G., Aldeyab, M., Kearney, M., Scott, M., Baldwin, N. and McElnay, J. (2015). Reduction in the incidence of hospital-acquired MRSA following the introduction of a chlorine dioxide 275 ppm based disinfecting agent in a district general hospital. *European Journal of Hospital Pharmacy*, 23(1), pp.28-32.

Correa, Á., Barba, A. and Padilla, F., 2016. Light Effects on Behavioural Performance Depend on the Individual State of Vigilance. *PLOS ONE*, 11(11), p.e0164945.

Crabtree, A., Mercer, G., Horan, R., Grant, S., Tan, T. and Buxton, J. (2013). A qualitative study of the perceived effects of blue lights in washrooms on people who use injection drugs. *Harm Reduction Journal*, 10(1), p.22.

Dai, T., Gupta, A., Huang, Y., Sherwood, M., Murray, C., Vrahas, M., Kielian, T. and Hamblin, M. (2013B). Blue Light Eliminates Community-Acquired Methicillin-Resistant Staphylococcus aureus in Infected Mouse Skin Abrasions. *Photomedicine and Laser Surgery*, 31(11), pp.531-538.

Dai, T., Gupta, A., Huang, Y., Yin, R., Murray, C., Vrahas, M., Sherwood, M., Tegos, G. and Hamblin, M. (2013A). Blue Light Rescues Mice from Potentially Fatal Pseudomonas aeruginosa Burn Infection: Efficacy, Safety, and Mechanism of Action. *Antimicrobial Agents and Chemotherapy*, 57(3), pp.1238-1245.

Dai, T., Gupta, A., Murray, C., Vrahas, M., Tegos, G. and Hamblin, M. (2012). Blue light for infectious diseases: Propionibacterium acnes, Helicobacter pylori, and beyond?. *Drug Resistance Updates*, 15(4), pp.223-236.

Dai, T., Tegos, G. P., Zhiyentayev, T., Mylonakis, E. and Hamblin, M.R. (2010). Photodynamic Therapy for Methicillin-Resistant Staphylococcus aureus Infection in a Mouse Skin Abrasion Model. *Laser Surg Med*, 42(1), pp.1-14.

Dancer, S. (2009). The role of environmental cleaning in the control of hospital-acquired infection. *Journal of Hospital Infection*, 73(4), pp.378-385.

Dancer, S. (2014). Controlling Hospital-Acquired Infection: Focus on the Role of the Environment and New Technologies for Decontamination. *Clinical Microbiology Reviews*, 27(4), pp.665-690.

Davies, A., Pottage, T., Bennett, A. and Walker, J. (2011). Gaseous and air decontamination technologies for Clostridium difficile in the healthcare environment. *Journal of Hospital Infection*, 77(3), pp.199-203.

Davis, W. and Ohno, Y. (2009). Approaches to color rendering measurement. *Journal of Modern Optics*, 56(13), pp.1412-1419.

Davis, W. and Ohno, Y. (2010). Color quality scale. *Optical Engineering*, 49(3), p.033602.

Denton, M., Wilcox, M., Parnell, P., Green, D., Keer, V., Hawkey, P., Evans, I. and Murphy, P., 2004. Role of environmental cleaning in controlling an outbreak of Acinetobacter baumannii on a neurosurgical intensive care unit. *Journal of Hospital Infection*, 56(2), pp.106-110.

Ducel, G., Fabry, J. and Nicolle, L. (2002). Prevention of hospital-acquired infections. Geneva: World Health Organization.

Duckro, A. (2005). Transfer of Vancomycin-Resistant Enterococci via Health Care Worker Hands. *Archives of Internal Medicine*, 165(3), p.302.

Elmnasser, N., Ritz, M., Leroi, F., Orange, N., Bakhrouf, A. and Federighi, M. (2007). Bacterial inactivation using pulsed light. *Acta Alimentaria*, 36(3), pp.373-380.

Endarko, (2011). *Optimisation of ultra-violet and visible light based technologies for disinfection applications in clinical and other environments*. Ph.D. thesis, University of Strathclyde.

Endarko, E., Maclean, M., Timoshkin, I., MacGregor, S. and Anderson, J., 2012. High-Irradiance 405 nm Light Inactivation of Listeria monocytogenes. *Photochemistry and Photobiology*, 88(5), pp.1280-1286.

Enwemeka, C., Williams, D., Hollosi, S., Yens, D. and Enwemeka, S. (2008). Visible 405 nm SLD light photo-destroys methicillin-resistant Staphylococcus aureus (MRSA) in vitro. *Lasers in Surgery and Medicine*, 40(10), pp.734-737.

European Centre for Disease Prevention and Control. (2012). List of microorganisms. [online] Available at: https://www.ecdc.europa.eu/en/healthcare-associated-infections-acute-care-hospitals/database/microorganisms-and-antimicrobial-resistance/list [Accessed 21 Jan. 2020].

Falagas, M., Thomaidis, P., Kotsantis, I., Sgouros, K., Samonis, G. and Karageorgopoulos, D. (2011). Airborne hydrogen peroxide for disinfection of the hospital environment and infection control: a systematic review. *Journal of Hospital Infection*, 78(3), pp.171-177.

Fernstrom, A. and Goldblatt, M. (2013). Aerobiology and Its Role in the Transmission of Infectious Diseases. *Journal of Pathogens*, 2013, pp.1-13.

Fu, T., Gent, P. and Kumar, V. (2012). Efficacy, efficiency and safety aspects of hydrogen peroxide vapour and aerosolized hydrogen peroxide room disinfection systems. *Journal of Hospital Infection*, 80(3), pp.199-205.

Gabel, V., Maire, M., Reichert, C., Chellappa, S., Schmidt, C., Hommes, V., Cajochen, C. and Viola, A., 2015. Dawn simulation light impacts on different cognitive domains under sleep restriction. *Behavioural Brain Research*, 281, pp.258-266.

Garvey, M., Rabbitt, D., Stocca, A. and Rowan, N. (2014). Pulsed ultraviolet light inactivation of *Pseudomonas aeruginosa* and *Staphylococcus aureus* biofilms. Water and Environmental Journal, 29, pp.36-42.

Gayral, B. (2017). LEDs for lighting: Basic physics and prospects for energy savings. *Comptes Rendus Physique*, 18(7-8), pp.453-461.

Gebreyohannes, G., Nyerere, A., Bii, C. and Sbhatu, D., 2019. Challenges of intervention, treatment, and antibiotic resistance of biofilm-forming microorganisms. *Heliyon*, 5(8), p.e02192.

Gillespie, J., Maclean, M., Given, M., Wilson, M., Judd, M., Timoshkin, I. and MacGregor, S. (2017). Efficacy of Pulsed 405-nm Light-Emitting Diodes for Antimicrobial Photodynamic Inactivation: Effects of Irradiance, Frequency, and Duty Cycle. *Photomedicine and Laser Surgery*, 35(3), pp.150-156.

Guffey, J. and Wilborn, J. (2006). In Vitro Bactericidal Effects of 405-nm and 470-nm Blue Light. *Photomedicine and Laser Surgery*, 24(6), pp.684-688.

Guo, X. and Houser, K. (2004). A review of colour rendering indices and their application to commercial light sources. *Lighting Research & Technology*, 36(3), pp.183-197.

Hall, L., Otter, J., Chewins, J. and Wengenack, N. (2007). Use of Hydrogen Peroxide Vapor for Deactivation of Mycobacterium tuberculosis in a Biological Safety Cabinet and a Room. *Journal of Clinical Microbiology*, 45(3), pp.810-815.

Halstead, F., Hadis, M., Marley, N., Brock, K., Milward, M., Cooper, P., Oppenheim, B. and Palin, W. (2019). Violet Light Arrays at 405 Nanometers Exert Enhanced Antimicrobial Activity for Photodisinfection of Monomicrobial Nosocomial Biofilms. *Applied and Environmental Microbiology*, 85(21).

Halstead, F., Thwaite, J., Burt, R., Laws, T., Raguse, M., Moeller, R., Webber, M. and Oppenheim, B. (2016). Antibacterial Activity of Blue Light against Nosocomial Wound Pathogens Growing Planktonically and as Mature Biofilms. *Applied and Environmental Microbiology*, 82(13), pp.4006-4016.

Hamblin, M. and Hasan, T. (2004). Photodynamic therapy: a new antimicrobial approach to infectious disease?. *Photochemical & Photobiological Sciences*, 3(5), p.436.

Haque, M., Sartelli, M., McKimm, J. and Abu Bakar, M. (2018). Health care-associated infections - an overview. *Infection and Drug Resistance*, Volume 11, pp.2321-2333.

Hayden, M., Blom, D., Lyle, E., Moore, C. and Weinstein, R. (2008). Risk of Hand or Glove Contamination After Contact With Patients Colonized With Vancomycin-Resistant Enterococcus or the Colonized Patients' Environment. *Infection Control & Hospital Epidemiology*, 29(2), pp.149-154.

Hernández-Andrés, J., Romero, J., Nieves, J. and Lee, R. (2001). Color and spectral analysis of daylight in southern Europe. *Journal of the Optical Society of America A*, 18(6), p.1325.

Holc, K., Marona, Ł., Czernecki, R., Boćkowski, M., Suski, T., Najda, S. and Perlin, P. (2010). Temperature dependence of superluminescence in InGaN-based superluminescent light emitting diode structures. *Journal of Applied Physics*, 108(1), p.013110.

Holmdahl, T., Lanbeck, P., Wullt, M. and Walder, M. (2011). A Head-to-Head Comparison of Hydrogen Peroxide Vapor and Aerosol Room Decontamination Systems. *Infection Control & Hospital Epidemiology*, 32(9), pp.831-836.

Hönes, K., Stangl, F., Sift, M. and Hessling, M. (2015) Visible optical radiation generates bactericidal effect applicable for inactivation of health care associated germs demonstrated by inactivation of E. coli and B. subtilis using 405-nm and 460-nm light emitting diodes. *Proc. SPIE 9540, Novel Biophotonics Techniques and Applications III*, 95400T.

Hope, C., Hindley, J., Khan, Z., de Josselin de Jong, E. and Higham, S. (2013). Lethal photosensitization of Porphyromonas gingivalis by their endogenous porphyrins under anaerobic conditions: An in vitro study. *Photodiagnosis and Photodynamic Therapy*, 10(4), pp.677-682.

Horan, T., Andrus, M. and Dudeck, M. (2008). CDC/NHSN surveillance definition of health care–associated infection and criteria for specific types of infections in the acute care setting. *American Journal of Infection Control,* 36(5), pp.309-332.

Hubbell Lighting Components. (2020). Hubbell Lighting. [online] Available at: https://www.hubbell.com/hubbelllightingci/en/spectraclean [Accessed 3 Mar. 2020].

Integral-led.com. *Warm white or Cool white? | Integral LED*. [online] Available at: https://integral-led.com/education/warm-white-or-cool-white [Accessed 5 Mar. 2020].

International Commission of Non-Ionising Radiation Protection (ICNIRP). (1997). Guidelines on limits of exposure to broad-band incoherent optical radiation (0.38-3 μm). *Health Physics*, 73(3), pp.539-554.

Irving, D., Lamprou, D., Maclean, M., MacGregor, S., Anderson, J. and Grant, M. (2016). A comparison study of the degradative effects and safety implications of UVC and 405 nm germicidal light sources for endoscope storage. *Polymer Degradation and Stability*, 133, pp.249-254.

Jinadatha, C., Villamaria, F., Restrepo, M., Ganachari-Mallappa, N., Liao, I., Stock, E., Copeland, L. and Zeber, J. (2015). Is the pulsed xenon ultraviolet light no-touch disinfection system effective on methicillin-resistant Staphylococcus aureus in the absence of manual cleaning?. *American Journal of Infection Control*, 43(8), pp.878-881.

Johnston, C., Cooper, L., Ruby, W., Carroll, K., Cosgrove, S. and Perl, T. (2006). Epidemiology of Community-Acquired Methicillin-Resistant Staphylococcus aures Skin Infections Among Healthcare Workers in an Outpatient Clinic. *Infection Control & Hospital Epidemiology*, 27(10), pp.1133-1136.

Karlen, M., Benya, J. and Spangler, C. (2012). *Lighting Design Basics*. 2nd edition. Hoboken, NJ, USA: John Wiley & Sons.

Kenall.com. (2019). *Indigo-Clean*. [online] Available at: https://kenall.com/Indigo-Clean [Accessed 23 Nov. 2019].

Keppens, A., Ryckaert, W., Deconinck, G. and Hanselaer, P. (2010). Modeling high power light-emitting diode spectra and their variation with junction temperature. *Journal of Applied Physics*, 108(4), p.043104.

Khan, H., Baig, F. and Mehboob, R. (2017). Nosocomial Infections: Epidemiology, prevention, control and surveillance. *Asian Pacific Journal of Tropical Biomedicine*, 7(5), pp.478-482.

Kim, D. and Kang, D. (2018). UVC LED Irradiation Effectively Inactivates Aerosolized Viruses, Bacteria, and Fungi in a Chamber-Type Air Disinfection System. *Applied and Environmental Microbiology*, 84(17).

Kim, M. and Yuk, H. (2016). Antibacterial Mechanism of 405-Nanometer Light-Emitting Diode against Salmonella at Refrigeration Temperature. *Applied and Environmental Microbiology*, 83(5).

Kim, M., Mikš-Krajnik, M., Kumar, A. and Yuk, H. (2016). Inactivation by 405 ± 5 nm light emitting diode on Escherichia coli O157:H7, Salmonella Typhimurium, and Shigella sonnei under refrigerated condition might be due to the loss of membrane integrity. *Food Control*, 59, pp.99-107.

Kim, S., Kim, D. and Kang, D. (2015). Using UVC Light-Emitting Diodes at Wavelengths of 266 to 279 Nanometers To Inactivate Foodborne Pathogens and Pasteurize Sliced Cheese. *Applied and Environmental Microbiology*, 82(1), pp.11-17.

Kowalski, W. (2014). *Ultraviolet Germicidal Irradiation Handbook: UVGI for air and surface disinfection.* Berlin: Springer Berlin.

Lei, Z., Xia, G., Ting, L., Xiaoling, G., Qiao Ming, L. and Guangdi, S. (2007). Color rendering and luminous efficacy of trichromatic and tetrachromatic LED-based white LEDs. *Microelectronics Journal*, 38(1), pp.1-6.

Li, J., Hirota, K., Yumoto, H., Matsuo, T., Miyake, Y. and Ichikawa, T. (2010). Enhanced germicidal effects of pulsed UV-LED irradiation on biofilms. *Journal of Applied Microbiology*, 109(6), pp.2183-2190.

Lin, Y., Gao, Y., Lu, Y., Zhu, L., Zhang, Y. and Chen, Z. (2012). Study of temperature sensitive optical parameters and junction temperature determination of light-emitting diodes. *Applied Physics Letters*, 100(20), p.202108.

Linley, E., Denyer, S., McDonnell, G., Simons, C. and Maillard, J. (2012). Use of hydrogen peroxide as a biocide: new consideration of its mechanisms of biocidal action. *Journal of Antimicrobial Chemotherapy*, 67(7), pp.1589-1596.

Livingston, S., Cadnum, J., Benner, K. and Donskey, C. (2020). Efficacy of an ultraviolet-A lighting system for continuous decontamination of health care–associated pathogens on surfaces. *American Journal of Infection Control*, 48(3), pp.337-339.

Lowe, J., Gibbs, S., Iwen, P., Smith, P. and Hewlett, A. (2013). Impact of Chlorine Dioxide Gas Sterilization on Nosocomial Organism Viability in a Hospital Room. *International Journal of Environmental Research and Public Health*, 10(6), pp.2596-2605.

Lukšienė, Z. (2003). Photodynamic therapy: mechanism of action and ways to improve the efficiency of treatment. *Medicina,* 39(12), pp.1137-1150.

Luksiene, Z., Gudelis, V., Buchovec, I. and Raudeliuniene, J. (2007). Advanced high-power pulsed light device to decontaminate food from pathogens: effects on Salmonella typhimurium viability in vitro. *Journal of Applied Microbiology*, 103(5), pp.1545-1552.

Mackley, A., Baker, C. and Bate, A. (2018). Raisingstandard of infection prevention and control in the NHS. *House of Commons Library, Debate pack,* Number CDP-2018-0116. [online] Available at: http://researchbriefings.files.parliament.uk/documents/CDP-2018-0116/CDP-2018-0116.pdf [Accessed 21 Jan. 2020].

Maclean, M., (2006). *An Investigation into the Light Inactivation of Medically Important Microorganisms.* Ph.D. thesis, University of Strathclyde.

Maclean, M., Anderson, J., MacGregor, S., White, T. and Atreya, C. (2016). A New Proof of Concept in Bacterial Reduction: Antimicrobial Action of Violet Light (405 nm) in Ex Vivo Stored Plasma. *Journal of Blood Transfusion*, 2016, pp.1-11.

Maclean, M., Booth, M., Anderson, J., MacGregor, S., Woolsey, G., Coia, J., Hamilton, K. and Gettinby, G. (2013). Continuous decontamination of an intensive care isolation room during patient occupancy using 405 nm light technology. *Journal of Infection Prevention*, 14(5), pp.176-181.

Maclean, M., MacGregor, S., Anderson, J. and Woolsey, G. (2008). High-irradiance narrow-spectrum light inactivation and wavelength sensitivity of *Staphylococcus aureus*. *FEMS Microbiology Letters*, 285(2), pp.227-232.

Maclean, M., MacGregor, S., Anderson, J. and Woolsey, G. (2009). Inactivation of Bacterial Pathogens following Exposure to Light from a 405-Nanometer Light-Emitting Diode Array. *Applied and Environmental Microbiology*, 75(7), pp.1932-1937.

Maclean, M., MacGregor, S., Anderson, J., Woolsey, G., Coia, J., Hamilton, K., Taggart, I., Watson, S., Thakker, B. and Gettinby, G. (2010). Environmental decontamination of a hospital isolation room using high-irradiance narrow-spectrum light. *Journal of Hospital Infection*, 76(3), pp.247-251.

Maclean, M., McKenzie, K., Anderson, J., Gettinby, G. and MacGregor, S. (2014). 405 nm light technology for the inactivation of pathogens and its potential role for environmental disinfection and infection control. *Journal of Hospital Infection*, 88(1), pp.1-11.

Maclean, M., Murdoch, L., Lani, M., MacGregor, S., Anderson, J. and Woolsey, G. (2008B). Photoinactivation and Photoreactivation Responses by Bacterial Pathogens after Exposure to Pulsed UV-Light. *2008 IEEE International Power Modulators and High-Voltage Conference*.

Maclean, M., Murdoch, L., MacGregor, S. and Anderson, J. (2013B). Sporicidal Effects of High-Irradiance 405 nm Visible Light on Endospore-Forming Bacteria. *Photochemistry and Photobiology*, 89(1), pp.120-126.

Masaoka, T., Kubota, Y., Namiuchi, S., Takubo, T., Ueda, T., Shibata, H., Nakamura, H., Yoshitake, J., Yamayoshi, T., Doi, H. and Kamiki, T. (1982). Ozone decontamination of bioclean rooms. *Applied and Environmental Microbiology*, 43(3), pp.509-513.

McCord, J., Prewitt, M., Dyakova, E., Mookerjee, S. and Otter, J. (2016). Reduction in Clostridium difficile infection associated with the introduction of hydrogen peroxide vapour automated room disinfection. *Journal of Hospital Infection*, 94(2), pp.185-187.

McDonald, K., Curry, R., Clevenger, T., Unklesbay, K., Eisenstark, A., Golden, J. and Morgan, R. (2000). A comparison of pulsed and continuous ultraviolet light sources for the decontamination of surfaces. *IEEE Transactions on Plasma Science*, 28(5), pp.1581-1587.

McDonald, R., Gupta, S., Maclean, M., Ramakrishnan, P., Anderson, J., MacGregor, S., Meek, R. and Grant, M. (2013). 405 nm light exposure of osteoblasts and inactivation of bacterial isolates from arthroplasty patients: potential for new disinfection applications?. *European Cells and Materials*, 25, pp.204-214.

McDonald, R., MacGregor, S., Anderson, J., Maclean, M. and Grant, M. (2011). Effect of 405-nm high-irradiance narrow-spectrum light on fibroblast-populated collagen lattices: an in vitro model of wound healing. *Journal of Biomedical Optics*, 16(4), p.048003.

McKenzie, K., (2014). *Inactivation of foodborne pathogenic and spoilage microorganisms by 405 nm light : an investigation into potential decontamination applications.* Ph.D. thesis, University of Strathclyde.

McKenzie, K., Maclean, M., Timoshkin, I., Endarko, E., MacGregor, S. and Anderson, J. (2013). Photoinactivation of Bacteria Attached to Glass and Acrylic Surfaces by 405 nm Light: Potential Application for Biofilm Decontamination. *Photochemistry and Photobiology*, 89(4), pp.927-935.

McKenzie, K., Maclean, M., Timoshkin, I., MacGregor, S. and Anderson, J. (2014). Enhanced inactivation of Escherichia coli and Listeria monocytogenes by exposure to 405 nm light under sub-lethal temperature, salt and acid stress conditions. *International Journal of Food Microbiology*, 170, pp.91-98.

Mediland.com. (2019). *Hyper Light*. [online] Available at: https://www.mediland.com.tw/mediland/pages_en/product_info.aspx?aid=155 [Accessed 14 Feb. 2020].

Meena, M., Swapnil, P., Barupal, T., and Sharma, K., 2019. A Review on Infectious Pathogens and Mode of Transmission. *Journal of Plant Pathology & Microbiology,* 10(1), pp.1-4.

Memarzadeh, F., Olmsted, R. and Bartley, J. (2010). Applications of ultraviolet germicidal irradiation disinfection in health care facilities: Effective adjunct, but not stand-alone technology. *American Journal of Infection Control*, 38(5), pp.S13-S24.

Miller, R., Simmons, S., Dale, C., Stachowiak, J. and Stibich, M. (2015). Utilization and impact of a pulsed-xenon ultraviolet room disinfection system and multidisciplinary care team on Clostridium difficile in a long-term acute care facility. *American Journal of Infection Control*, 43(12), pp.1350-1353.

Mitchell, B., Digney, W., Locket, P. and Dancer, S. (2014). Controlling methicillin-resistant Staphylococcus aureus(MRSA) in a hospital and the role of hydrogen peroxide decontamination: an interrupted time series analysis. *BMJ Open*, 4(4), p.e004522.

Montazeri, N., Manuel, C., Moorman, E., Khatiwada, J., Williams, L. and Jaykus, L. (2017). Virucidal Activity of Fogged Chlorine Dioxide- and Hydrogen Peroxide-Based Disinfectants against Human Norovirus and Its Surrogate, Feline Calicivirus, on Hard-to-Reach Surfaces. *Frontiers in Microbiology*, 8, pp.1-9.

Moorhead, S., Maclean, M., Coia, J., MacGregor, S. and Anderson, J. (2016). Synergistic efficacy of 405 nm light and chlorinated disinfectants for the enhanced decontamination of Clostridium difficile spores. *Anaerobe*, 37, pp.72-77.

Murdoch, L., Maclean, M., Endarko, E., MacGregor, S. and Anderson, J. (2012). Bactericidal Effects of 405 nm Light Exposure Demonstrated by Inactivation of *Escherichia, Salmonella, Shigella, Listeria*, and *Mycobacterium* Species in Liquid Suspensions and on Exposed Surfaces. *The Scientific World Journal*, 2012, pp.1-8.

Murdoch, L., McKenzie, K., Maclean, M., MacGregor, S. and Anderson, J. (2013). Lethal effects of high-irradiance violet 405-nm light on Saccharomyces cerevisiae, Candida albicans, and on dormant and germinating spores of Aspergillus niger. *Fungal Biology*, 117(7-8), pp.519-527.

Murray, B., Ohmine, S., Tomer, D., Jensen, K., Johnson, F., Kirsi, J., Robison, R. and O'Neill, K. (2008). Virion disruption by ozone-mediated reactive oxygen species. *Journal of Virological Methods*, 153(1), pp.74-77.

Murrell, L. (2018). [online] Kenall.com. Available at: https://kenall.com/Kenall-Files/Product-Files/Literature/Maury-Poster-Study_casestudy.pdf [Accessed 26 Feb. 2020].

Murrell, L., Hamilton, E., Johnson, H. and Spencer, M. (2019). Influence of a visible-light continuous environmental disinfection system on microbial contamination and surgical site infections in an orthopedic operating room. *American Journal of Infection Control*, 47(7), pp.804-810.

Muthu, S., Schuurmans, F. and Pashley, M. (2002). Red, green, and blue LED based white light generation: Issues and Control. In: *Conference Record of the 2002 IEEE Industry Applications Conference. 37th IAS Annual Meeting (Cat. No.02CH37344)*. Pittsburgh, PA, USA: IEEE, pp.327-333.

Neamen, D. A. (2012). *Semiconductor Physics and Devices: Basic Principles*. 4th Edition. New York: McGraw-Hill.

NHS Greater Glasgow and Clyde. (2016) Infection Prevention and Control Manual, 2016. NHS GGC, Glasgow, UK. Available from: http://www.nhsggc.org.uk/your-health/infection- prevention-and-control/prevention-and-control-of-infection-manual-policies-sops-guidelines/ [Accessed March 2019]

NHS, Health Protection Scotland. (2016B). Routine and terminal cleaning of isolation rooms and cohort areas in healthcare settings, and terminal cleaning of wards following outbreaks or increased incidence of infection [online] Available at: https://hpspubsrepo.blob.core.windows.net/hps-website/nss/1941/documents/1_clean-isolation-cohort-lr-v1.0.pdf [Accesed 29 Jan 2020].

NHS, Health Protection Scotland. (2017). Healthcare Associated Infection Annual Report 2017. HPS, Glasgow, UK. [online] Available at: https://hpspubsrepo.blob.core.windows.net/hps-website/nss/2402/documents/1_HAI-Annual-Report-2017.pdf [Accessed 21 Jan. 2020].

NHS, Health Protection Scotland. (2017B). Roles & Responsibilities for Reusable Patient Care Equipment and Environmental Decontamination. Health Protection Scotland, Glasgow, UK. [online] Available at: https://hpspubsrepo.blob.core.windows.net/hps-website/nss/2346/documents/1_Roles%20and%20Responsibilities%20Reusable%20Patient%20Care%20Equipment%202017-12-21.pdf [Accessed 29 Jan. 2020].

NHS, Health Protection Scotland. (2018). National Infection Prevention and Control Manual: Chapter 2 - Transmission Based Precautions (TBPs). [online] Available at: http://www.nipcm.hps.scot.nhs.uk/chapter-2-transmission-based-precautions-tbps/#a1090 [Accessed 29 Jan. 2020].

NHS, Health Protection Scotland. (2019) Healthcare Associated Infection Annual Report 2018. Health Protection Scotland, Glasgow, UK. [online] Available at: https://hpspubsrepo.blob.core.windows.net/hps-website/nss/2776/documents/1_HAI-Annual-Report-2018-final-v1%201.pdf [Accessed 24 Jan 2020]

Nyangaresi, P., Qin, Y., Chen, G., Zhang, B., Lu, Y. and Shen, L. (2018). Effects of single and combined UV-LEDs on inactivation and subsequent reactivation of E. coli in water disinfection. *Water Research*, 147, pp.331-341.

O'Donoghue, B., NicAogáin, K., Bennett, C., Conneely, A., Tiensuu, T., Johansson, J. and O'Byrne, C. (2016). Blue-Light Inhibition of Listeria monocytogenes Growth Is Mediated by Reactive Oxygen Species and Is Influenced by σBand the Blue-Light Sensor Lmo0799. *Applied and Environmental Microbiology*, 82(13), pp.4017-4027.

OECD/EU (2016), Health at a Glance: Europe 2016 – State of Health in the EU Cycle, OECD Publishing, Paris.[online] Available at: http://dx.doi.org/10.1787/9789264265592-en [Accessed 21 Jan. 2020].

Ohno, Y. (2006). Optical metrology for LEDs and solid state lighting. *Fifth Symposium Optics in Industry, Proceedings of SPIE Vol. 6046, 604625-1.*

Osha.gov. (1991). *Sampling and Analytical Methods | Determination of Chlorine Dioxide in Workplace Atmospheres | Occupational Safety and Health Administration*. [online] Available at: https://www.osha.gov/dts/sltc/methods/inorganic/id202/id202.html [Accessed 11 Feb. 2020].

Otter, J., Yezli, S., Perl, T., Barbut, F. and French, G. (2013). The role of 'no-touch' automated room disinfection systems in infection prevention and control. *Journal of Hospital Infection*, 83(1), pp.1-13.

Passaretti, C., Otter, J., Reich, N., Myers, J., Shepard, J., Ross, T., Carroll, K., Lipsett, P. and Perl, T. (2012). An Evaluation of Environmental Decontamination With Hydrogen Peroxide Vapor for Reducing the Risk of Patient Acquisition of Multidrug-Resistant Organisms. *Clinical Infectious Diseases*, 56(1), pp.27-35.

Philips (2019). *Quality of LED lighting*. [online] Philips Lighting. Available at: https://www.lighting.philips.co.uk/consumer/led-lights/quality-of-light-led-lighting [Accessed 23 Nov. 2019].

Pittet, D., Hugonnet, S., Harbarth, S., Mourouga, P., Sauvan, V., Touveneau, S. and Perneger, T. (2000). Effectiveness of a hospital-wide programme to improve compliance with hand hygiene. *The Lancet*, 356(9238), pp.1307-1312.

Ramakrishnan, P., Maclean, M., MacGregor, S., Anderson, J. and Grant, M. (2014). Differential sensitivity of osteoblasts and bacterial pathogens to 405-nm light highlighting potential for decontamination applications in orthopedic surgery. *Journal of Biomedical Optics*, 19(10), p.105001.

Ramakrishnan, P., Maclean, M., MacGregor, S., Anderson, J. and Grant, M. (2016). Cytotoxic responses to 405 nm light exposure in mammalian and bacterial cells: Involvement of reactive oxygen species. *Toxicology in Vitro*, 33, pp.54-62.

Ramm, L., Siani, H., Wesgate, R. and Maillard, J. (2015). Pathogen transfer and high variability in pathogen removal by detergent wipes. *American Journal of Infection Control*, 43(7), pp.724-728.

Randle, J., Arthur, A. and Vaughan, N. (2010). Twenty-four-hour observational study of hospital hand hygiene compliance. *Journal of Hospital Infection*, 76(3), pp.252-255.

Reed, N. (2010). The History of Ultraviolet Germicidal Irradiation for Air Disinfection. *Public Health Reports*, 125(1), pp.15-27.

Rhodes, N., de la Presa, M., Barneck, M., Poursaid, A., Firpo, M. and Langell, J. (2016). Violet 405 nm light: A novel therapeutic agent against β-lactam-resistant Escherichia coli. *Lasers in Surgery and Medicine*, 48(3), pp.311-317.

Rutala, W. and Weber, D. (2013). Disinfectants used for environmental disinfection and new room decontamination technology. *American Journal of Infection Control*, 41(5), pp.S36-S41.

Santos, A., Oliveira, V., Baptista, I., Henriques, I., Gomes, N., Almeida, A., Correia, A. and Cunha, Â. (2012). Wavelength dependence of biological damage induced by UV radiation on bacteria. *Archives of Microbiology*, 195(1), pp.63-74.

Schanda, J. (2007). *Colorimetry: Understanding the CIE System*. John Wiley & Sons, pp.207-208.

Schubert, E. F. (2006). Light-Emitting Diodes. 2nd Edition. New York: Cambridge University Press.

Senawiratne, J., Chatterjee, A., Detchprohm, T., Zhao, W., Li, Y., Zhu, M., Xia, Y., Li, X., Plawsky, J., Wetzel, C. (2010). Junction temperature, spectral shift, and efficiency in GaInN-based blue and green light emitting diodes. *Thin Solid Films*, Volume 518 (6), pp. 1732-1736.

Sergent, A., Slekovec, C., Pauchot, J., Jeunet, L., Bertrand, X., Hocquet, D., Pazart, L. and Talon, D. (2012). Bacterial contamination of the hospital environment during wound dressing change. *Orthopaedics & Traumatology: Surgery & Research*, 98(4), pp.441-445.

Sharma, M. and Hudson, J. (2008). Ozone gas is an effective and practical antibacterial agent. *American Journal of Infection Control*, 36(8), pp.559-563.

Shkirman, S., Solov'ev, K., Kachura, T., Arabei, S. and Skakovskii, E. (1999). Interpretation of the soret band of porphyrins based on the polarization spectrum of N-methyltetraphenylporphin fluorescence. *Journal of Applied Spectroscopy*, 66(1), pp.68-75.

Siegel, J., Rhinehart, E., Jackson, M. and Chiarello, L. (2007). 2007 Guideline for Isolation Precautions: Preventing Transmission of Infectious Agents in Health Care Settings. *American Journal of Infection Control*, 35(10), pp.S65-S164.

Sliney, D. (2016). What is light? The visible spectrum and beyond. *Eye*, 30(2), pp.222-229.

Smith, K. and Hanawalt, P. (1969). Molecular photobiology. New York: Academic Press.

Stibich, M., Stachowiak, J., Tanner, B., Berkheiser, M., Moore, L., Raad, I. and Chemaly, R. (2011). Evaluation of a Pulsed-Xenon Ultraviolet Room Disinfection Device for Impact on Hospital Operations and Microbial Reduction. *Infection Control & Hospital Epidemiology*, 32(3), pp.286-288.

Tomb, R., Maclean, M., Coia, J., Graham, E., McDonald, M., Atreya, C., MacGregor, S. and Anderson, J. (2016). New Proof-of-Concept in Viral Inactivation: Virucidal Efficacy of 405 nm Light Against Feline Calicivirus as a Model for Norovirus Decontamination. *Food and Environmental Virology*, 9(2), pp.159-167.

Tomb, R., Maclean, M., Herron, P., Hoskisson, P., MacGregor, S. and Anderson, J. (2014). Inactivation of Streptomycesphage ϕC31 by 405 nm light. *Bacteriophage*, 4(3), p.e32129.

Tomb, R.M. (2017). *Antimicrobial 405 nm light for clinical decontamination: Investigation of the antiviral efficacy and potential for bacterial tolerance*. Glasgow: University of Strathclyde.

Tomb, R.M., (2017). *Antimicrobial 405 nm light for clinical decontamination: Investigation of the antiviral efficacy and potential for bacterial tolerance*. Ph.D. thesis, University of Strathclyde.

Trevisan, A., Piovesan, S., Leonardi, A., Bertocco, M., Nicolosi, P., Pelizzo, M. and Angelini, A. (2006). Unusual High Exposure to Ultraviolet-C Radiation. *Photochemistry and Photobiology*, 82(4), p.1077.

Tuchina, E. and Tuchin, V. (2009). Low-irradiance LED (625 and 405 nm) and laser (805 nm) killing of Propionibacterium acnes and Staphylococcus epidermidis. *Mechanisms for Low-Light Therapy IV*.

Veerabadran, S. and Parkinson, I. (2010). Cleaning, disinfection and sterilization of equipment. *Anaesthesia & Intensive Care Medicine*, 11(11), pp.451-454.

Vianna, P., Dale, C., Simmons, S., Stibich, M. and Licitra, C. (2016). Impact of pulsed xenon ultraviolet light on hospital-acquired infection rates in a community hospital. *American Journal of Infection Control*, 44(3), pp.299-303.

Voudoukis, N. and Oikonomidis, S. (2017). Inverse square law for light and radiation: A unifying educational approach. *European Journal of Engineering Research and Science*, 2(11), p.23.

Wainwright, M. (1998). Photodynamic antimicrobial chemotherapy (PACT). *Journal of Antimicrobial Chemotherapy*, 42(1), pp.13-28.

Wells, W.F. (1934). On air-borne infection: study II. Droplets and droplet nuclei. *American Journal of Epidemiology*, 20(3), pp. 611–618

Wengraitis, S., McCubbin, P., Wade, M., Biggs, T., Hall, S., Williams, L. and Zulich, A. (2012). Pulsed UV-C Disinfection of *Escherichia coli* With Light-Emitting Diodes, Emitted at Various Repetition Rates and Duty Cycles. *Photochemistry and Photobiology*, 89(1), pp.127-131.

WHO. (2018A). Antimicrobial resistance. [online] Available at: https://www.who.int/news-room/fact-sheets/detail/antimicrobial-resistance [Accessed 22 Jan. 2020].

WHO. (2018B). Antibiotic resistance. [online] Available at: https://www.who.int/news-room/fact-sheets/detail/antibiotic-resistance [Accessed 22 Jan. 2020].

Willert, C., Stasicki, B., Klinner, J. and Moessner, S. (2010). Pulsed operation of high-power light emitting diodes for imaging flow velocimetry. *Measurement Science and Technology*, 21(7), p.075402.

World Health Organization. (2020). The burden of health care-associated infection worldwide. [online] Available at: https://www.who.int/infection-prevention/publications/burden_hcai/en/ [Accessed 21 Jan. 2020].

World Health Organization. (2020). *Ultraviolet radiation and health*. [online] Available at: http://www.who.int/uv/uv_and_health/en/ [Accessed 11 Feb. 2020].

Wren, M., Rollins, M., Jeanes, A., Hall, T., Coën, P. and Gant, V. (2008). Removing bacteria from hospital surfaces: a laboratory comparison of ultramicrofibre and standard cloths. *Journal of Hospital Infection*, 70(3), pp.265-271.

Yang, J., Wu, U., Tai, H. and Sheng, W. (2019). Effectiveness of an ultraviolet-C disinfection system for reduction of healthcare-associated pathogens. *Journal of Microbiology, Immunology and Infection*, 52(3), pp.487-493.

Yeap, J., Kaur, S., Lou, F., DiCaprio, E., Morgan, M., Linton, R. and Li, J. (2015). Inactivation Kinetics and Mechanism of a Human Norovirus Surrogate on Stainless Steel Coupons via Chlorine Dioxide Gas. *Applied and Environmental Microbiology*, 82(1), pp.116-123.

Yousif, E. and Haddad, R. (2013). Photodegradation and photostabilization of polymers, especially polystyrene: review. *SpringerPlus*, 2(1).

Zhang, S., Hao, Z., Zhang, L., Pan, G., Wu, H., Zhang, X., Luo, Y., Zhang, L., Zhao, H. and Zhang, J. (2018). Efficient Blue-emitting Phosphor SrLu2O4:Ce3+ with High Thermal Stability for Near Ultraviolet (~400 nm) LED-Chip based White LEDs. *Scientific Reports*, 8(1).

Zhang, Y., Zhu, Y., Chen, J., Wang, Y., Sherwood, M., Murray, C., Vrahas, M., Hooper, D., Hamblin, M. and Dai, T. (2016). Antimicrobial blue light inactivation of Candida albicans: In vitroandin vivostudies. *Virulence*, 7(5), pp.536-545.

Zhang, Y., Zhu, Y., Gupta, A., Huang, Y., Murray, C., Vrahas, M., Sherwood, M., Baer, D., Hamblin, M. and Dai, T. (2014). Antimicrobial Blue Light Therapy for Multidrug-Resistant Acinetobacter baumannii Infection in a Mouse Burn Model: Implications for Prophylaxis and Treatment of Combat-related Wound Infections. *Journal of Infectious Diseases*, 209(12), pp.1963-1971.

Zhu, H., Kochevar, I., Behlau, I., Zhao, J., Wang, F., Wang, Y., Sun, X., Hamblin, M. and Dai, T. (2017). Antimicrobial Blue Light Therapy for Infectious Keratitis: Ex Vivo and In Vivo Studies. *Investigative Opthalmology & Visual Science*, 58(1), pp.586.

Zwinkels, J.C. (2015) 'Light, Electromagnetic Spectrum' in Luo, M.R., (ed.) *Encyclopedia of Color Science and Technology,* Springer Science+Business Media, New York, pp 1-8.

APPENDIX A: PUBLICATIONS

JOURNAL PUBLICATIONS

Gillespie JB, M Maclean, MJ Given, M Wilson, M Judd, IV Timoshkin, JG Anderson, SJ MacGregor (2017). Pulsed 405-nm LEDs for disinfection applications: effects of irradiance, frequency and duty cycle. *Photomed Laser Surg*, 35(3): 150-156. DOI: 10.1089/pho.2016.4179.

CONFERENCE PROCEEDINGS

Gillespie JB, M Maclean, MP Wilson, MJ Given, SJ MacGregor (2017). Development of an antimicrobial blended white LED system containing pulsed 405 nm LEDs for decontamination applications. Proc. SPIE 10056, Design and Quality for Biomedical Technologies X, 100560Y (March 14, 2017); doi:10.1117/12.2250539

CONFERENCE PRESENTATIONS

Gillespie JB, M Maclean, MJ Given, MP Wilson, SJ MacGregor. Development of an antimicrobial blended white LED system containing pulsed 405-nm LEDs for decontamination applications. SPIE BiOS 2017, 28 January – 2 February 2017, San Francisco, United States.

Gillespie JB, Maclean M, Given MJ, Wilson MP, MacGregor SJ. Investigating the use of pulsed RYGB LEDs to create a blended white light for antimicrobial applications. Photon16, 5-8 September 2016, Leeds, UK
https://cdn.eventsforce.net/files/ef-q5vmtsq56tk6/website/610/posters.pdf